



FAKULTÄT FÜR VERFAHRENS-  
UND SYSTEMTECHNIK

# Contributions to develop enantioselective chromatographic processes

Dissertation  
for the award of the degree

Doktoringenieurin (Dr.-Ing.)

by M.Sc. Ivana Mutavdžin

Date of birth: 4 July 1987, in: Pančevo, Serbia

accepted by the Faculty of Process and Systems Engineering  
of the Otto-von-Guericke-University of Magdeburg

Committee: Prof. Dr. rer. nat. Dieter Schinzer (Chairman)  
Prof. Dr.-Ing. Andreas Seidel-Morgenstern (Reviewer)  
PhD P.Eng. Mladen Eić (Reviewer)  
Prof. Dr.-Ing. Dieter Bathen (Reviewer)

Submitted on: 30 June 2017

Graduation Colloquium on: 24 November 2017



## Acknowledgements

This dissertation is the result of research work performed at Max Planck Institute for Dynamics of Complex Technical Systems, Magdeburg, Germany, in the group “Physical and Chemical Foundations of Process Engineering” (PCG).

First of all, I would like to express my deep gratitude to my supervisor, Prof. Andreas Seidel-Morgenstern, for giving me the opportunity to become a member of his team. His continuous support, guidance, patience and motivating optimism have been giving the right direction to my research work, from the starting point until its finalization. Further thanks I owe to Prof. Mladen Eić, for his guidelines during our collaboration, and to Prof. Dieter Bathen, both of them for showing interest in my work and being referees of this thesis.

I am especially thankful for the cooperation with Thomas Munkelt (Otto von Guericke University, Magdeburg, Germany), for sharing with me his experimental expertise and knowledge and for the fruitful discussions during our work on the same project. The financial support of the project by DFG (Priority Programme SPP1570) is gratefully acknowledged. Moreover I would like to thank our collaboration partners Prof. D. Enke and Dr. C. Chmelik (University Leipzig).

During my whole PhD time, I was very glad for being part of International Max Planck Research School (IMPRS) and grateful, not only for their funding, but also for the help of the coordinators, as well as the opportunity of attending numerous workshops and meeting wonderful people.

Great gratitude I owe to Prof. Menka Petkovska from University of Belgrade, for her teaching during my studies, advice and giving me the chance to come to Magdeburg for the first time. Throughout my research, I have highly appreciated the valuable remarks of my colleagues, especially Hector Rubiera and Francisco Santos da Silva, as well as the technical support of Jacqueline Kaufmann at the lab work. I am also thankful for all the help of the secretaries, IT department, librarians and the administration.

I feel extremely fortunate and grateful that the life in Magdeburg has allowed me to get to know amazing people and make precious friendships. I wanted to thank my PCG group for creating kind atmosphere and turning the working time into enjoyable moments. Special thanks go to Emilija, for her friendship and numerous hours of motivating discussions and fun time. Also to Kasia and Francisco, my best travel companions, to Bettina, Thiane, Giang (and Linh) and all PCG-lunch-group members. I am very happy for meeting Sabine, Philipp, Susann and Georg, for the sporty and relaxing events, enjoyable “IMPRSiVe” lunches and their efforts in improving my German language. It was always nice to meet with our Yugoslavian group, Dijana and Pawel, Emilija and her family, Mima, Samanta and Rene, Petar, Milena, and to share the same “being far from home” experiences.

Finally, my deepest thanks go to my family, for never-ending encouragement and understanding. Without their love and support, I would not have been the person I am. Thank you for everything!

Magdeburg, July 2017

Ivana Mutavdžin

## Abstract

Separation of enantiomers of medically relevant substances represents an important and challenging task. Still a larger number of drugs are produced and used as racemic mixtures, containing both enantiomers in equal amounts. One such example are fluorinated volatile anaesthetics isoflurane and desflurane, which are investigated in this work. Although many preliminary studies reported different pharmacological and toxicological effects of two enantiomers of these substances, they are still applied in the racemic form during surgeries. To investigate their effect further, larger amounts of single enantiomers are required.

The main task of this thesis was to develop a procedure for the production of pure enantiomers of isoflurane and desflurane using gas chromatographic separation. For this a suitable cyclodextrin-based selector, developed in preliminary works, could be exploited. While the processes in the liquid phase have been widely investigated and known, preparative gas chromatography is still not present at great extent in the research and application. Another chiral system (bicalutamide enantioseparation using liquid chromatography) was additionally examined by experiments and simulations. This system served to better understand separation phenomena and as a reference system to provide validation of some of the procedures developed.

To properly analyse adsorption processes and for their design and optimization, it is essential to know the adsorption isotherms. One of the goals of this study was to provide understanding of the process thermodynamics by quantifying the adsorption isotherms. It starts with testing two dynamic methods that can be applied for isotherm determination in chiral systems. One is the known peak-fitting method, which was analysed for the application on the investigated systems, while the other method is newly developed extension of the elution by characteristic point that was here derived for a binary mixture.

Subsequently, the gas-chromatographic process was simulated using thermodynamic data for the applied cyclodextrin stationary phase. The simulation study was conducted in order to identify the operating parameters which would provide the highest possible production of the pure enantiomers. The performance of larger columns was investigated by simple scale-up relations. Finally, also a capture step was described for isolating the pure components and storing them after the separation in non-selective columns. Some of the predictions were experimentally confirmed in an accompanying project. In addition, the enantioseparation using a continuous multi-column pressure swing adsorption process was theoretically studied and compared in terms of productivity to the batch gas chromatography.

Experimental data acquired in a parallel project, show that the here developed simple theoretical concept together with the determined adsorption isotherms can be successfully applied to describe gas chromatography processes for diluted systems. It was demonstrated that it is feasible to produce enough amounts of pure enantiomers of anaesthetic gases, which are essential for performing further medical tests.

## Zusammenfassung

Die Trennung von medizinisch relevanten Enantiomeren ist eine wichtige und herausfordernde Aufgabe. Immer noch wird die Mehrheit der Medikamente als racemisches Gemisch, das beide Enantiomere in gleichen Mengen beinhaltet, produziert und angewandt. Ein Beispiel für solche Medikamente sind die flurhaltigen und flüchtigen Anästhetika Isofluran und Desfluran. Obwohl viele Studien bereits belegen, dass die Enantiomere von diesen Substanzen unterschiedliche pharmakologische und toxikologische Wirkungen besitzen, werden sie immer noch als Racemat während einer Operation verabreicht. Um deren Effekte weiter studieren zu können, werden größere Mengen der einzelnen Enantiomere benötigt.

Das Hauptziel dieser Arbeit war es, einen Prozess, der auf der gaschromatographischen Trennung basiert, für die Herstellung der reinen Enantiomere von Isofluran und Desfluran zu entwickeln. Dafür wurde ein geeigneter Cyclodextrin-basierter Selektor, der in vorangegangenen Arbeiten entwickelt wurde, benutzt. Während dieser Prozess für die flüssige Phase bereits ausführlich untersucht und beschrieben ist, findet die präparative Gaschromatographie bis heute immer noch keine breite Anwendung. Ein zweites chirales Trennproblem, die Trennung der Enantiomere von Bicalutamid mittels Flüssigchromatographie, wurde zusätzlich mit Experimenten und Simulationsstudien untersucht und diente dem besseren Verständnis der Trennphänomene. Außerdem wurde es als Referenzsystem verwendet, um einige der entwickelten Prozessschritte zu validieren.

Um Adsorptionsprozesse zu analysieren, auszulegen und zu optimieren, ist es notwendig, die Adsorptionsisothermen zu bestimmen. Eines der Ziele dieser Arbeit war es, durch die Quantifizierung der Adsorptionsisothermen den Ablauf der Prozesse zu verstehen. Als erstes werden zwei dynamische Methoden, mit denen Isothermen von chiralen Systemen bestimmt werden können, getestet. Eine dieser Methoden ist die bekannte Chromatogramm-Anpassungsmethode, welche für beide in dieser Arbeit untersuchten Systeme angewandt wurde. Die andere Methode basiert auf einer Erweiterung der Methode der Auswertung disperser Fronten, welche hier für ein binäres Gemisch neu entwickelt wurde.

Aufbauend auf der Kenntnis der Isothermen wurde der gaschromatographische Prozess für das angewendete Cyclodextrin-Derivat simuliert. Die Simulationsstudien wurden genutzt, um die Betriebsbedingungen zu bestimmen, die es erlauben möglichst viel reine Enantiomere zu produzieren. Die Möglichkeit größerer Säulen zu verwenden, wurde mit Hilfe einfacher Scale-Up-Relationen untersucht. Schließlich wurde ein „Auffang-Schritt“ für die Isolierung und Lagerung der reinen Komponenten in nicht selektiven Säulen beschrieben. Einige Vorhersagen wurden im Rahmen einer Kooperation experimentell validiert. Zusätzlich wurde die Enantiomerentrennung mit dem kontinuierlichen Mehrsäulen-Druckwechseladsorptionsprozess (PSA) theoretisch erforscht und mit der Batch-Gaschromatographie bezüglich der erreichbaren Produktivitäten verglichen.

Experimentelle Daten, die in einem parallel durchgeführten Projekt erzeugt wurden, zeigten, dass der entwickelten Prozessmodelle in Verbindung mit den ermittelten thermodynamischen Daten erfolgreich für die Beschreibung des gaschromatographischen Prozesses angewendet werden können. Es wird gezeigt, dass mit dem Batch-Prozess ausreichende Mengen reiner Enantiomere anästhetischer Gase, die für die Durchführung weiterer klinischer Tests erforderlich sind, produziert werden können.



# Table of Contents

|          |   |           |
|----------|---|-----------|
| <b>1</b> | <b>Introduction .....</b>   | <b>1</b>  |
| 1.1      | Pairs of enantiomers .....  | 1         |
| 1.2      | Chromatographic separation .....  | 4         |
| 1.3      | Objectives and structure of the thesis .....  | 5         |
| <br>     |   |           |
| <b>2</b> | <b>Fundamentals of chromatographic separation .....</b>   | <b>11</b> |
| 2.1      | Model parameters and relations .....  | 11        |
| 2.2      | Mathematical models of chromatographic columns .....  | 14        |
| 2.2.1    | Ideal model .....   | 16        |
| 2.2.2    | Equilibrium dispersive model .....  | 17        |
| 2.2.3    | Transport dispersive model .....  | 17        |
| 2.2.4    | General rate model .....  | 18        |
| 2.3      | Chromatographic processes in the gas phase .....  | 18        |
| 2.4      | Adsorption isotherms .....  | 20        |
| 2.4.1    | General types of adsorption isotherms .....   | 21        |
| 2.4.2    | Methods to experimentally determine adsorption isotherms .....  | 23        |
| 2.5      | Continuous multi-column chromatographic processes .....   | 29        |
| 2.5.1    | Simulated moving bed (SMB) process .....  | 29        |
| 2.5.2    | Pressure swing adsorption (PSA) process .....   | 32        |
| <br>     |   |           |
| <b>3</b> | <b>Derivation of specific methods for determining the adsorption isotherms .....</b>  | <b>43</b> |
| 3.1      | Development of extended elution by characteristic point method (ECP) for<br>estimating competitive Langmuir isotherms ..... | 44        |
| 3.1.1    | Well-known ECP for single component adsorption isotherms .....  | 44        |
| 3.1.2    | New extension of the elution by characteristic point method .....   | 46        |
| 3.2      | Analysis of the peak-fitting method for racemic mixtures .....  | 51        |
| <br>     |   |           |
| <b>4</b> | <b>Simplified concept for performance analysis, scale-up and product capture .....</b>                                      | <b>55</b> |
| 4.1      | Process performance analysis .....  | 55        |
| 4.2      | Chromatographic column scale-up .....   | 60        |
| 4.3      | External capture of products after the separation .....   | 62        |
| 4.3.1    | Sizing of the capture columns .....   | 66        |

|          |   |            |
|----------|---|------------|
| <b>5</b> | <b>Investigated substances.....</b>   | <b>73</b>  |
| 5.1      | Bicalutamide .....  | 73         |
| 5.1.1    | Previous provisions of pure bicalutamide enantiomers .....  | 74         |
| 5.2      | Fluorinated volatile anaesthetics .....   | 75         |
| 5.2.1    | Different effects of isoflurane and desflurane enantiomers .....  | 77         |
| 5.2.2    | Previous separations of isoflurane and desflurane enantiomers .....   | 78         |
| <b>6</b> | <b>Experiments, models and simulations of the separation processes .....</b>                                  | <b>85</b>  |
| 6.1      | Experimental part .....   | 85         |
| 6.1.1    | Separation of the enantiomers of bicalutamide .....   | 85         |
| 6.1.2    | Separation of the enantiomers of anaesthetic gases .....  | 91         |
| 6.2      | Modelling and simulation studies .....  | 96         |
| 6.2.1    | Models and parameters used for description of the processes .....   | 96         |
| 6.2.2    | Solutions of the system of equations .....  | 97         |
| 6.2.3    | Simulation software .....   | 97         |
| <b>7</b> | <b>Determination of adsorption isotherm parameters (only racemic mixtures available) .....</b>                | <b>99</b>  |
| 7.1      | Binary-mixture ECP method .....   | 99         |
| 7.1.1    | Preliminary systematic simulation study for evaluating the binary-mixture ECP method .....                    | 99         |
| 7.1.2    | Estimation of the adsorption isotherms of the investigated substances with the binary-mixture ECP method..... | 108        |
| 7.2      | Peak-fitting method.....  | 110        |
| 7.2.1    | Peak-fitting method representation and validation using bicalutamide .....                                    | 110        |
| 7.2.2    | Peak-fitting method application for isoflurane and desflurane .....   | 113        |
| 7.3      | Summary and discussion .....  | 115        |
| <b>8</b> | <b>Design and evaluation of the enantiomer production process.....</b>  | <b>117</b> |
| 8.1      | Process performance of repetitive-injection separation .....  | 118        |
| 8.1.1    | Process performance of bicalutamide enantioseparation .....   | 118        |
| 8.1.2    | Process performance of isoflurane and desflurane enantioseparation .....                                      | 122        |
| 8.2      | Scale-up of the batch HPLC and GC processes.....  | 131        |
| 8.2.1    | Scale-up for bicalutamide enantioseparation.....  | 131        |
| 8.2.2    | Scale-up for isoflurane and desflurane enantioseparation .....  | 133        |
| 8.3      | Design of the product capture process for desflurane .....  | 138        |



|  |            |
|--|------------|
| 8.4 Continuous enantioseparation using a PSA process .....   | 140        |
| 8.5 Summary and discussion .....   | 148        |
| <b>9 Conclusions.....</b>  | <b>151</b> |
| <b>References.....</b>   | <b>155</b> |
| <b>Appendix .....</b>  | <b>165</b> |
| A. Derivation of the overall and component mass balance equations for a pressure swing adsorption process.....                               | 165        |
| B. Derivation of the equations for the new binary-mixture ECP method from the analytical solution of the ideal model of chromatography ..... | 169        |
| <b>List of symbols.....</b>  | <b>173</b> |
| <b>List of Tables .....</b>  | <b>181</b> |
| <b>List of Figures.....</b>  | <b>185</b> |
| <b>Curriculum Vitae .....</b>  | <b>193</b> |



# 1 Introduction

The broad field of medication production is characterized by fast development and requires constant improvements and investigations. Especially sensitive is the class of chiral drugs, where the active substance (one enantiomer) is always confronted to an opponent, which has the same physical and chemical properties, while in most cases it provides a different effect in biological systems. The number of chiral compounds used not only in pharmaceutical industry, but for example, as part of agrichemicals, flavours and fragrances, has been increasing over the past years. As a consequence, also the demand for pure enantiomers is growing rapidly.

One of the ways to produce pure enantiomers is enantioselective synthesis. Principally it is a very complex process, since in most cases the regular synthesis leads to the production of a mixture containing both of enantiomers. Therefore much more applied are different separation methods. Preparative chromatography is one of the most important techniques available to separate enantiomers. Due to the large number of available stationary phases, nowadays almost every chiral separation problem can be solved in this way.

## 1.1 Pairs of enantiomers

Optically active substances – also called chiral – are an important class of compounds. These substances always exist in two forms named enantiomers. More additional forms are possible if compound has more than one chiral centre. The presence of a chiral centre in the molecule causes chiral behaviour of the substance. This centre is an asymmetric atom, most often carbon that has four different substituent groups connected to it. A schematic representation of such two molecules is given in Figure 1.1. Due to the described structure, molecules of enantiomers represent non-superimposable mirror images of one another. A mixture of two opposite enantiomers in equal proportions (50:50 %) is called racemic mixture or racemate and shows no optical activity.

Since the molecular and structural formula of both enantiomers is the same, these compounds have identical physico-chemical properties, except for their ability to rotate plane-polarized light in the opposite direction by equal amounts. Another important difference between enantiomers of the same compound is the way how they interact with other substances in living organisms. There are different possible ways how two enantiomers used as medicines can relate to each other:

1. Both enantiomers have similar desired effect;
2. Both enantiomers are effective, but one reduces the action of the other;

3. One enantiomer is active and the other does not exhibit any activity;
4. Two enantiomers have completely different positive activities;
5. One enantiomer has a wanted effect, while the other is toxic (this case belongs to the case 4. and represents its more severe form).

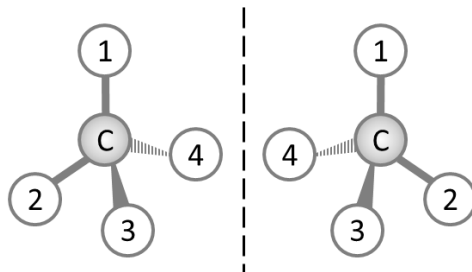


Figure 1.1. Spatial representation of molecules of enantiomers: C - chiral centre (mostly carbon atom), 1,2,3,4 - different groups attached to the centre.

There are three ways of enantiomer nomenclature that are used in the literature: (+)-/(-)-, D-/L- and R-/S- nomenclature. According to the (+)-/(-)- classification, the enantiomers which turn the plane of polarized light beam in a clockwise direction (viewed facing the oncoming light) are designated as dextrorotatory and are given the symbol (+)-. The enantiomers that turn the plane in the opposite direction are laevorotatory and have the sign (-)- [1]. The nomenclature D-/L- [2, 3] denotes the compounds with the same relative configuration like (+)-glyceraldehyde as D-enantiomers (*dexter*, Latin: right, favourable), and those with the relative configuration of (-)-glyceraldehyde as L (*laevus*, Latin: left, sinistral). R-/S- nomenclature [1, 4] describes the three-dimensional arrangement of the groups around the chiral centre. The groups are ranked in decreasing order of priority. The atom with the highest atomic number gets the highest priority and the atom with the lowest atomic number has the lowest priority (in Figure 1.1. the group 1 has the highest priority and the group 4 – the lowest). Then, molecule should be turned so that the group with the lowest rank is behind the asymmetric atom. If the progression from group 1 to group 3 is clockwise, the configuration is named R-enantiomer (*rectus*, Latin: righteous, straight) and if the progression is counter-clockwise, then it is S-enantiomer (*sinister*, Latin: left, wrong), as shown in Figure 1.2. Within this thesis the R-/S- classification will be used.

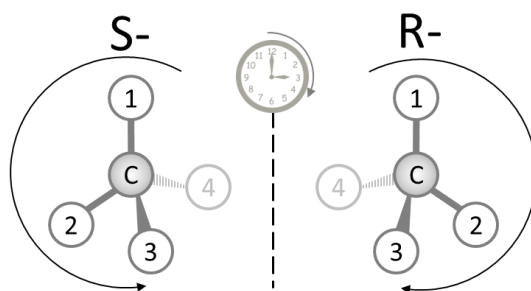


Figure 1.2. Determination of R- and S- configuration of enantiomers. The arrows around the molecules show the direction of decreasing priority (from 1 to 3) of the groups attached to the chiral centre (C).

The phenomenon of chirality was for the first time described in 1848 by Pasteur [5], who revealed, by studying many natural compounds, that one substance can appear in more crystalline forms showing different properties. The detailed explanation of this behaviour was provided later, in 1874 by two independent works of van't Hof and LeBel. They discovered that optical activity is caused by the existence of an asymmetric carbon atom. After this, chirality has started to receive more serious attention. During the 20<sup>th</sup> century, a large number of new drugs, including extensively chiral compounds, was developed, so that by the end of the century, more than a half of all used medicines was based on chiral molecules [6]. With the time, the number of racemates present in the drugs has started to decrease owing to findings which showed that single enantiomers can very often exhibit different pharmacological and especially toxicological effects. Some of these discoveries were made before, but some after the start of the drug introduction to the market [7]. Consequently, in 1992 the American Food and Drug Administration (FDA) issued a policy about development of chiral drugs [8]. According to it, majority of clinical substances should be marketed in the form of just one enantiomer – the active one. With this, development of the procedures to produce single enantiomers has received an increased interest.

There are numerous available methods for obtaining pure enantiomers [9]. In general, they could be classified in three groups: asymmetric synthesis, chiral pool synthesis and separation of racemic mixtures (Figure 1.3).

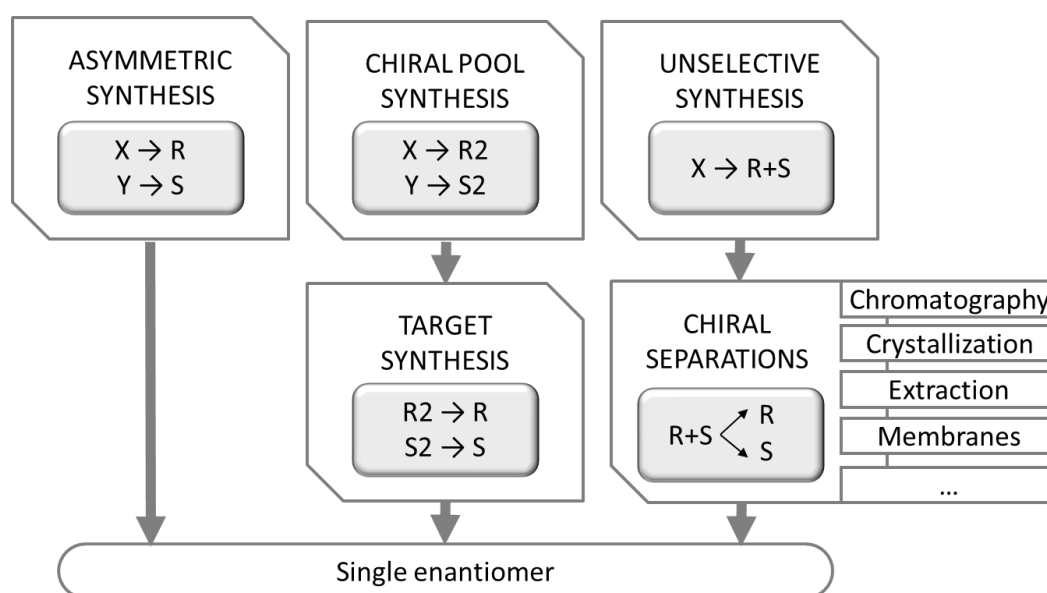


Figure 1.3. Some of the ways to produce single enantiomers (R and S represent single target enantiomers, R2 and S2 are intermediate enantiomers, and X and Y include one or more starting non-chiral substance(s)).

Asymmetric synthesis represents the production of just one target enantiomer. It is the most direct way, but very often complicated or even not possible to perform. Chiral pool synthesis [9] refers to the production of certain chiral molecules or fragments that can be easier synthesized as single enantiomers than the target chiral substances. Then, in the consequent step (further chemical reaction), from such precursor-enantiomer one can obtain the wanted

enantiopure substance. However, in the most of the cases, the synthesis is unselective and leads to the production of racemic mixtures, which should afterwards be separated into single enantiomers. Several methods have been developed for this purpose. Some of them are: chiral chromatography, crystallization, extraction, membrane separation, diastereomeric salt resolution etc.

## 1.2 Chromatographic separation

One of the most important techniques available for separation of racemates is preparative chromatography [10, 11]. In general, chromatography is used for separating mixtures and for analysis of the composition of substances. This technique can provide highly efficient separation of very similar compounds, which is one of the main reasons why there is increasing interest in its application in the research area, as well as in the industrial production. Chromatographic methods are very expensive and their implementation therefore requires a careful optimization of all the operating conditions.

Separation in a chromatographic column is based on selective adsorption of components in the mixture. The mixture (in our case, racemate) is firstly dissolved in a proper solvent. The solution is then injected into the eluent stream that passes through a chromatographic column and is called mobile phase. The column is packed with the stationary phase – specific porous medium chosen in the way that different components from the mixture have different affinities to it. Therefore various constituents of the mixture travel at different speeds through the column, which causes them to separate. Less adsorbed components travel faster and leave the column after shorter time (retention time) than the stronger adsorbed ones. A representation of a chromatographic process is illustrated in Figure 1.4. For chiral separations, the stationary phase normally consists of a solid support made of porous silica and of a functional part that provides separation. This are usually derivatised cellulose-, amylose- and antibiotic molecules, which have large number of chiral centres and can therefore provide selective interactions with single enantiomers [9].

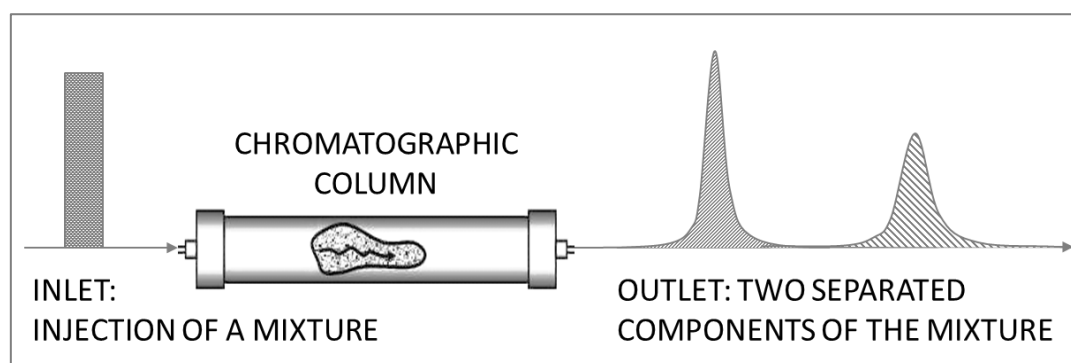


Figure 1.4. Chromatographic separation of a binary mixture. At the column inlet the narrow rectangular pulse of the mixture is injected resulting at the outlet in dispersed peaks of the two separated substances.

Chromatography can be preparative or analytical. The purpose of preparative chromatography is to separate the components of a mixture for their further use, while analytical chromatography is done for measuring the relative proportions of components in a mixture and generally operates with smaller amounts of substances. Depending on the mobile phase, there are three types of chromatography:

1. Gas chromatography (GC)
2. Liquid chromatography (LC or HPLC – high performance liquid chromatography)
3. Supercritical fluid chromatography (SFC).

Computer simulations of a chromatographic process are an important issue in order to optimize the separation without investing into expensive experimental work. Data that one must obtain beforehand include determining the system and column dead volumes, characterization of the column in terms of porosity and efficiency, as well as calculation of the adsorption isotherm parameters. Adsorption isotherms give the relation between concentrations in the mobile and stationary phase. For most cases they can be determined only experimentally and this, when working with chiral systems, could be a difficult task. Most of the developed methods require pure components for the experimentation, and single enantiomers are usually not easy to provide or it might be very costly to use them just for testing experiments. Because of this reason there is a tendency to develop methods for estimating competitive adsorption isotherms (isotherms of components in a mixture) of enantiomers which would use only the racemate as a starting material. That is one of the tasks in this work.

Beside simple batch chromatographic separations, also a variety of processes that provide continuous operation has been developed over the years. The most commonly used are simulated moving bed (SMB) and pressure swing adsorption (PSA) [10, 12, 13]. SMB process represents a simulation of a counter-current movement of the stationary and mobile phase. This is managed by exploiting columns connected in series with port switching between them. The conventional case is a 4-zone SMB with two inlet and two outlet ports, but many other variations of the process have been described. SMB can be employed for liquid systems, as well as for gas-phase and supercritical fluid separations. Gas mixtures can also be successfully separated by means of a PSA process. It is based on changing the total pressure in the column in order to first enhance the adsorption and then to ease the desorption of certain components in the mixture. It may be operated with one or more columns in parallel, and with different number of operation steps. Basic case would be a single column with four elementary steps.

### **1.3 Objectives and structure of the thesis**

The main objective of this thesis refers to the design of a process for producing pure enantiomers of specific medically significant substances, namely fluorinated anaesthetic gases, what gives a potential for improving anaesthesia and has practical application in the

field of medicine. This part of the work is done under the DFG (Deutsche Forschungsgemeinschaft) Priority Programme “SPP1570: Porous Media with Defined Porous Structure in Chemical Engineering - Modelling, Applications, Synthesis.” We have been working on the specific project “Separation of mixtures of chiral volatile anaesthetics via modified porous glasses,” which belongs to the SPP1570 programme and comprises the investigation of the enantioseparation of two anaesthetic gases using a gas-chromatographic process. The complete project is divided in two subprojects, denoted here as I and II. Subproject I represents the basis of this thesis. It is mostly focused on theoretical and conceptual investigations, while Subproject II is experimentally oriented.

Subproject I of the mentioned SPP1570 Project is performed by the author of this thesis. The main task was to provide the understanding and planning of the separation process by investigating the basics of chromatography (GC and HPLC). The largest part of that investigation is done in the area of process thermodynamics, i.e. adsorption isotherm determination. In brief, it includes the suggestion and analysis of the process model, estimation of the parameters from a few starting experiments (done in the Subproject II) and simulations of the separation process with the goal to improve it and to maximize the production rate of the pure components. As it is the topic of this thesis, the more detailed description of Subproject I will be given in the later paragraphs.

Subproject II is performed by Thomas Munkelt at Otto von Guericke University in Magdeburg, Germany. It includes, first the investigation of the suitable adsorbents and separation columns, based on the outcomes of preliminary research done in this area, and then synthesis of the chiral selector and preparation of the stationary phase, the starting GC experiments, as well as the work on later experiments with improved parameters, which should provide significant amounts of pure enantiomers of the anaesthetics and serve at the same time as validation of the process behaviour predicted by the simulations (done as part of Subproject I).

These two subprojects were conducted in parallel with an intensive collaboration. Subproject I is completely presented in this thesis, while the results of Subproject II will be described in the upcoming doctoral thesis of Thomas Munkelt [14]. The joint research between the subprojects was organized in the way that in Subproject I the experimental data from Subproject II were used and then the analysis of the separation and further design of the enantiomer production process were studied by simulation tests. The obtained results were transferred to Subproject II to be used for planning the new improved experiments and for the confirmation of the predictions. The final production of pure enantiomers still needs to be done as part of Subproject II. Since in this thesis the data and some of the outcomes from the parallel subproject will be mentioned, they are always referred as “SPP1570 Subproject II” or only shortly “Subproject II”.



In order to solve the task of Subproject I, it is needed to characterize and analyse the complete chromatographic separation process. For that purpose, two chiral systems were studied. The first one is defined by the goals of the described SPP1570 Project and represents the separation of enantiomers of two fluorinated anaesthetic gases, namely isoflurane and desflurane. These substances were studied theoretically using batch gas chromatography (GC), as well as a continuous multi-step pressure swing adsorption (PSA). Since the processes conducted in the gaseous phase are more complicated and in general not so well described as those in the liquid phase, there was first another system introduced in this work, which served as a reference and provided better understanding of the separation process and especially its thermodynamics. This separation problem is the enantioseparation of bicalutamide using liquid chromatography (HPLC). Bicalutamide was chosen based on its accessibility in our laboratories and on available previous research [15-18]. The advantage of using it lays in the fact that, unlike for the anaesthetics, there is access to pure enantiomers, which eases the testing of the described methods.

In this thesis firstly the possibilities to estimate adsorption isotherms using two methods were discussed. An extension of the elution by characteristic point (ECP) for a binary mixture was here developed and analysed. In addition the peak-fitting method was examined and applied for estimation of the isotherm parameters. The data were further used to evaluate the process performance and to optimize the separation. Improvement of the process using larger-diameter columns was also investigated and the procedure of capturing and isolating the pure enantiomers was presented.

One of the ideas of this work was to investigate the procedure for simple and fast analysis of a gas chromatographic process when the studied systems are diluted, as it is the case for the anaesthetic gases. In general, the description of the processes occurring in the gas phase requires larger number of parameters and therefore more time, more experimental work and computational effort for formulating and solving the involved relations. In this work the simpler equations are applied in the calculation procedure and afterwards the predictions were experimentally validated.

This study is mainly based on simulation studies. Own experiments in order to get the necessary data were performed in this thesis project only for bicalutamide, while for the anaesthetics they were done as part of the parallel Subproject II. As mentioned above, Subproject II also includes the validation experiments for the batch separation of the both anaesthetics.

The summary of the structure of the whole study is presented in the scheme given in Figure 1.5. It lists the processes that were investigated and the methods applied for providing a deeper understanding of chromatographic enantioseparation.

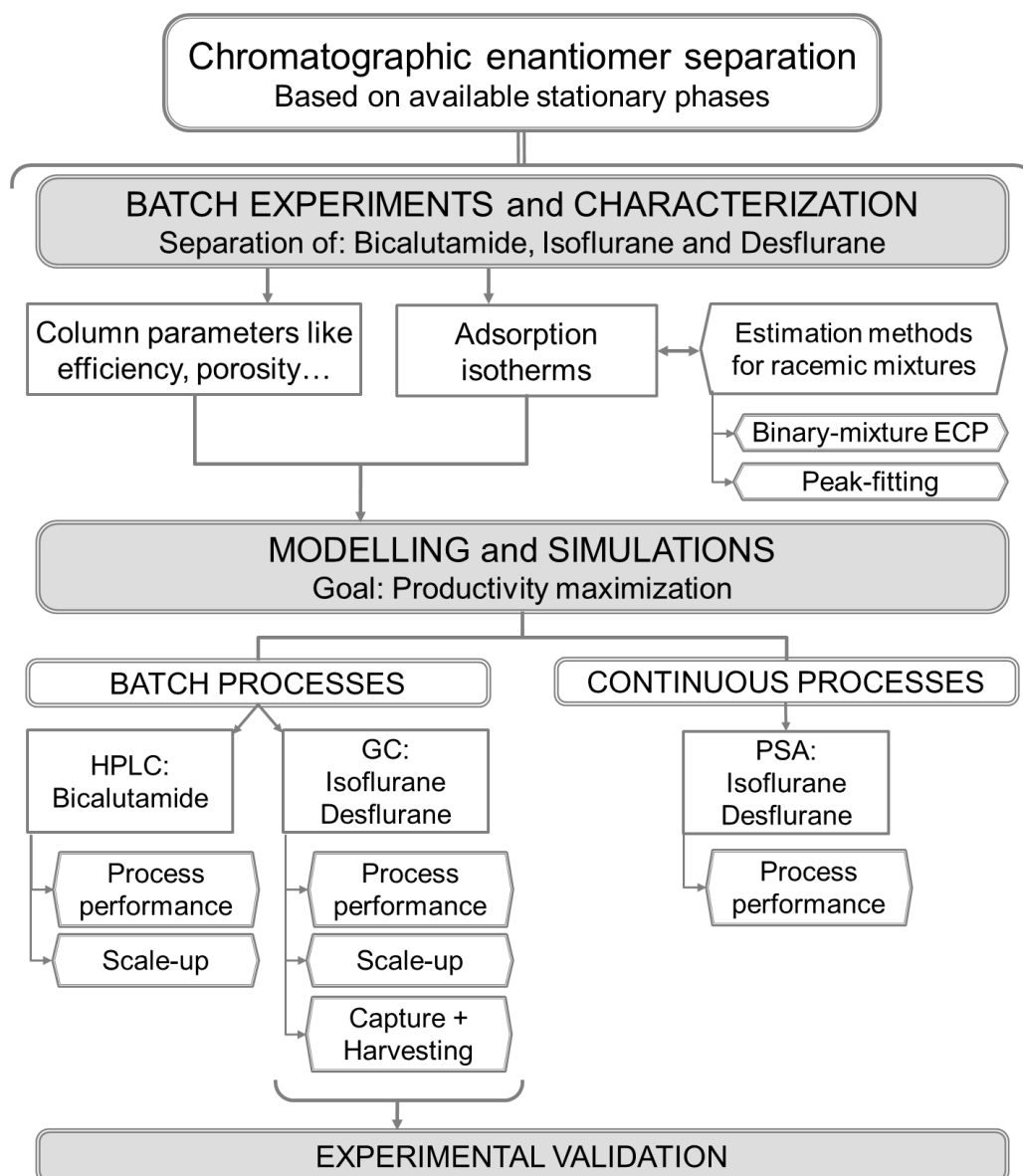


Figure 1.5. Schematic overview of the study presented in this thesis, including the investigated substances and processes performed for their analysis and chromatographic separation.

This work is divided into 9 chapters. Chapter 2 gives the basic laws and models that describe a chromatographic process, together with the description of the parameters needed for that purpose. The most important parameters are the adsorption isotherms and thus some space is taken for their explanation and the overview of different methods to determine them. The model equations that are presented are first given for liquid chromatography and then different terms were discussed and adapted for the use in the gaseous systems. At the end the basic concepts of more advanced continuous processes, simulated moving bed (SMB) and pressure swing adsorption (PSA), are presented. PSA process is applied in this work and is therefore explained in more details and characterized by giving the most common model equations, while SMB is just briefly described since it was used for the previous enantioseparations of the anaesthetic gases as well as for bicalutamide, but it was not elaborated in this work.

Chapter 3 gives the theoretical derivation of two methods for fast determination of adsorption isotherms of enantiomers, when only racemic mixture and no pure components are available for experimentation. The first of the methods is an extension of the ECP method derived in the frame of this work for a system of two components with Langmuir isotherms. The other method is the known peak-fitting method, which is here only examined and adapted for the application in the case when no pure enantiomers can be found.

Chapter 4 describes the simple methodology established in this thesis for the complete analysis of a gas chromatographic system. The procedure starts with adsorption isotherm determination described in Chapter 3 and is followed by process performance estimation and parametric study in order to provide the maximal productivity of the pure products. The column scale-up is discussed as well, using simple rules. Finally, an overview of the complete production process is given. It couples the previously described separation with the capture of the pure components in the non-selective columns, in order to produce concentrated streams, which will further provide easier storage procedure.

In Chapter 5 the substances which are used for examinations in this work are described. The properties of bicalutamide, isoflurane and desflurane are given, as well as the overview of the studies that dealt with different medical effect of the single enantiomers. Also the research on the previous work on the enantioseparation of bicalutamide and the fluorinated anaesthetics is presented.

Chapter 6 gives the data regarding the experimental and simulation work done in this thesis, explains the procedures used for measuring the adsorption isotherms and other parameters and the ways of providing data for process analysis using the simulation studies. Moreover, this chapter shows the results of the performed experiments.

Chapters 7 and 8 give the results of the simulation studies and experimental validation of the proposed procedures. In Chapter 7 the outcomes related to the theory presented in Chapter 3 are shown. The new binary-mixture ECP method and the peak-fitting method were applied for determination of the adsorption isotherm parameters. By using these parameters, the enantioseparation process of bicalutamide and fluorinated anaesthetics was simulated and analysed, which is presented in Chapter 8. It shows the results of the theory described in Chapter 4. The study on productivity maximization, GC column scale-up, design of the capture process and finally the separation using PSA can be found in this chapter.

All the results and findings are summarized in Chapter 9, with general conclusions and suggested directions for future work on this topic.



## 2 Fundamentals of chromatographic separation

Since the beginning of the 20<sup>th</sup> century, when chromatography was discovered [19], it started to develop and gain increasing attention, as a method for successful separation and purification of components in mixtures. Chromatography is a complex process, which is influenced by many different effects. A mobile phase with one or more solutes flows through the column filled with porous particles. Components diffuse in and out of the particles and interact with the stationary phase. Since the separation in the column depends on many factors, for its proper description and modelling, it is necessary to take into account fluid dynamics, mass transfer phenomena and equilibrium thermodynamics [10, 11, 20].

In this chapter the theoretical side of chromatographic processes will be presented. At the beginning, in the section 2.1, the basic details of the process are explained along with the most important parameters used for modelling and analysis. The following section (2.2) lists the most common models used for describing the separation in a chromatographic column. The laws and relations mentioned in both sections 2.1 and 2.2 are given for liquid chromatography, which is better known, as it has been extensively investigated and described in the literature. Since in this thesis the processes in the gaseous phase are also examined, the section 2.3 gives details on how the common laws for LC can be modified and applied for the gas-phase processes. More detailed equations used for GC are presented later in the chapter (section 2.5.2). Section 2.4 gives the insight into adsorption isotherms, which are the most important relations for chromatographic processes. At the end, in the section 2.5, two continuous chromatographic processes are introduced: simulated moving bed and pressure swing adsorption.

### 2.1 Model parameters and relations

Before starting with description of mathematical modelling of a chromatographic process, it is useful to provide explanation of some fundamental relations and the crucial parameters.

One of the basic characteristics of a chromatographic separation is the retention time ( $t_R$ ), which represents the position of the component peak in the chromatogram. It shows the time that a solute  $i$  ( $i = 1, 2, \dots, n$ , where  $n$  is the number of components) resides in the system. For a two-component mixture an example of chromatogram is given in Figure 2.1. Retention times of two substances ( $t_{R1}$  and  $t_{R2}$ ) are marked, as well as the dead time ( $t_0$ ). Dead time is the retention time of a non-adsorbing species, also called the column hold-up time. Since retention time includes the time that the solute spends in the mobile and the stationary phase, it is defined as following:

$$t_{R,i} = t_0 \left( 1 + \frac{1-\varepsilon}{\varepsilon} H_i \right) \quad (2.1)$$

where  $H_i$  represents the Henry constant (described later in section 2.4) and  $\varepsilon$  is the total column porosity. This equation is derived from the equilibrium theory (ideal model of chromatography), explained later in the section 2.2.1 (eq. (2.14)).

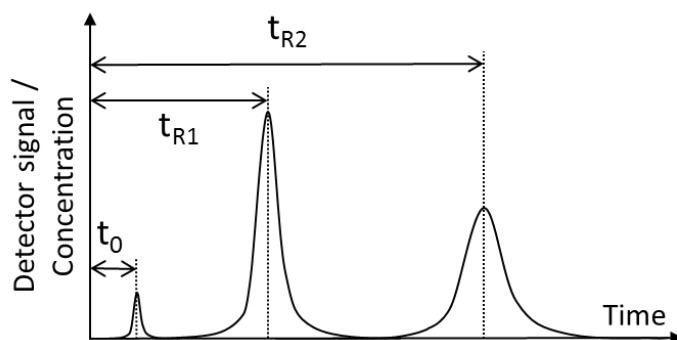


Figure 2.1. A typical chromatogram of a binary mixture with marked retention times of both components ( $t_{R1}$  – for the first eluting component and  $t_{R2}$  – for the second eluting component) and the dead time ( $t_0$ ).

The retention time of a non-adsorbed compound can be defined as:

$$t_0 = \frac{L}{u} = \frac{\varepsilon V}{Q} \quad (2.2)$$

In this equation,  $L$  is the column length,  $V$  its total volume,  $Q$  the volumetric flowrate and  $u$  interstitial linear mobile phase velocity, as expressed in eq. (2.3) and (2.4), where  $d$  is the column inner diameter:

$$V = L(d^2\pi/4) \quad (2.3)$$

$$u = \frac{Q}{\varepsilon(d^2\pi/4)} \quad (2.4)$$

Total column porosity ( $\varepsilon$ ) is defined as the fraction of total void volume of the column, which means the volume available for the fluid phase ( $V_f$ ) divided by the total column volume ( $V$ ):

$$\varepsilon = V_f/V \quad (2.5)$$

In practice  $V_f$  is calculated from the retention time of small amount of an unretained substance ( $t_0$ ):

$$V_f = t_0 Q \quad (2.6)$$

Very often also a ratio between the volume of the solid phase ( $V_s$ ) and the volume available for fluid phase ( $V_f$ ), is used. It is called phase ratio ( $F$ ):

$$F = V_s/V_f = (1 - \varepsilon)/\varepsilon \quad (2.7)$$

Total porosity consists of the external porosity ( $\varepsilon_e$ ), which is the space between the particles with respect to the total column volume, and internal porosity ( $\varepsilon_i$ ) – the empty space inside the particles (pores) with respect to the total column volume [10, 11], as shown in the following equations:

$$\varepsilon = \varepsilon_e + \varepsilon_i \quad (2.8)$$

$$\varepsilon_e = (V - V_p)/V \quad (2.9)$$

$$\varepsilon_i = \frac{V_{pore}}{V} = \frac{\varepsilon_p V_p}{V} = \frac{\varepsilon_p (1 - \varepsilon_e)V}{V} = \varepsilon_p (1 - \varepsilon_e) \quad (2.10)$$

In these equations  $V_p$  stands for the volume of all the particles (total particle volume),  $V_{pore}$  for the volume of all the pores in the particles (total pore volume) and  $\varepsilon_p$  for the particle porosity (pore volume with respect to the total particle volume). All the mentioned volumes are schematically represented in Figure 2.2.

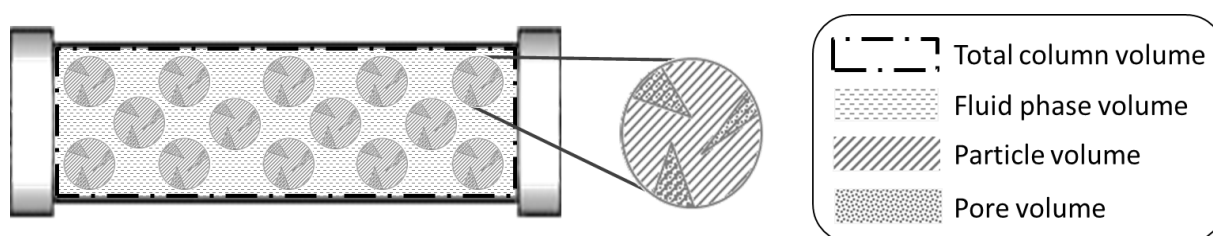


Figure 2.2. Scheme of a chromatographic column with marked different volumes used for defining porosity.

Another important factor for chromatographic separation is column efficiency, often expressed as the number of theoretical plates ( $NTP$ ). For different substances and columns the efficiency can vary in great extent.  $NTP$  can be determined using the elution profile when very small amount of substances is injected, providing that the isotherms are in the linear range and that the peak (or peaks) have symmetric Gaussian shape:

$$NTP_i = L/HETP_i \cong 5.54(t_{R,i} / w_{1/2,i})^2 \quad (2.11)$$

The term  $HEPT_i$  is height equivalent to a theoretical plate for component  $i$  and  $w_{1/2,i}$  is the peak width at its half-height. The value of the  $HETP$  for a chosen system is changing with the mobile phase velocity. This dependency is described by van Deemter equation [11, 21]:

$$HETP = A + B/u + Cu \quad (2.12)$$

where  $A$  shows the eddy diffusion contribution,  $B$  the band broadening due to axial diffusion and  $C$  the mass transfer kinetics. The parameter  $A$  reflects the packing quality (it has lower values for the well packed columns) and does not depend on velocity, while the parameter  $B$  decreases with increasing velocity. The effect of all the terms is presented in Figure 2.3. It can be observed that the total curve has a minimum which corresponds to the maximal column efficiency and determines the mobile phase velocity that provides this optimum. However, to obtain higher process performance, preparative separations are usually performed at higher speed than this optimal one, providing less efficiency on one hand, but shorter retention times on the other hand.

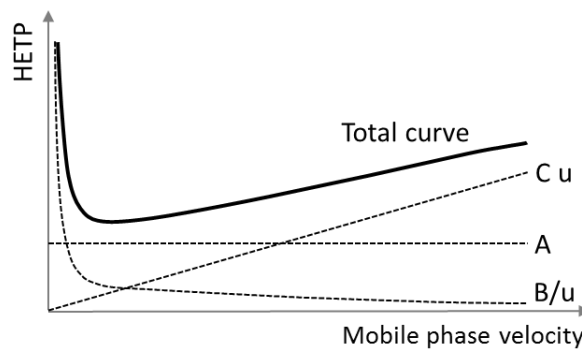


Figure 2.3. Van Deemter curve (denoted as Total curve) with effects of single terms used in van Deemter equation (2.12).

The column efficiency is related to dispersive effects, like axial dispersion and mass transfer resistances. In the chromatographic models very often apparent dispersion coefficient is used [10, 11]. It includes all band broadening effects like molecular, eddy and flow diffusion and non-equilibrium effects. Apparent dispersion coefficient ( $D_{app}$ ) can be calculated from the column number of theoretical plates ( $NTP$ ):

$$-D_{app} = \frac{Lu}{2NTP} \quad (2.13)$$

For the mass transfer resistance, a lumped form ( $k_m$ ) is mostly used and is calculated from the kinetic equation (eq. (2.21)), described in the section 2.2.3.

## 2.2 Mathematical models of chromatographic columns

To describe a chromatographic process, one could use different models [10-12] based on material, energy and momentum balances together with relations that define the



thermodynamic equilibrium between the adsorbent and the components being adsorbed. The models consist typically of one-dimensional mass balances. Frequently the following assumptions are used as well [10]:

- The adsorbent is homogeneous;
- Stationary phase consists of spherical particles that have constant diameter;
- Radial distributions are considered negligible;
- The eluent is non-adsorbable;
- There is no convection inside the particles;
- Fluid density and viscosity are constant (for liquid chromatography);
- The process is isothermal (for liquid chromatography).

The models that are more frequently applied, take into account some of the effects like convection, dispersion, mass transfer from the bulk fluid phase to the boundary layer of the adsorbent particle, pore diffusion, diffusion along the surface of the solid phase, adsorption kinetics etc. Based on the effects that are considered and on their type, there are various models developed. Some of them are:

- General rate model;
- Transport dispersive model;
- Equilibrium dispersive model;
- Ideal model.

The effects that these models include are given in Table 2.1, while the further details can be found in the following text.

Table 2.1. Different models used for describing a chromatographic process with the effects that they take into account.

|   | General rate model               | Transport dispersive model | Equilibrium dispersive model | Ideal model |
|---|----------------------------------|----------------------------|------------------------------|-------------|
| Convection                                      | ✓                                | ✓                          | ✓                            | ✓           |
| Adsorption equilibrium                          | ✓                                | ✓                          | ✓                            | ✓           |
| Dispersion                                      | ✓                                | ✓                          | ✓                            |             |
| Mass transfer resistance                        | ✓                                | ✓                          |                              |             |
| Adsorption kinetics                             | ✓                                |                            |                              |             |
| Mass transfer in the liquid film / in the pores | (at least one of the parameters) |                            |                              |             |
| Surface diffusion                               |                                  |                            |                              |             |

Here firstly the models will be presented in the form that is used for liquid chromatography and which is commonly known and established in the literature. Later, in the section 2.3 the laws that apply for the gaseous phase will be given and the needed modifications of the models will be discussed.

### 2.2.1 Ideal model

The simplest model to describe a chromatographic process is the ideal model (IM). It neglects all the dispersion and mass transfer effects, taking into account only convective transport and adsorption equilibrium (thermodynamics). The model assumes an instantaneous and permanently established local equilibrium between the mobile and stationary phase. Thanks to the model simplicity, it was possible to derive its analytical solutions [11]. More about these solutions can be found in Chapter 3, section 3.1. The other advantages lie in the fact that it can serve as a powerful tool to describe important phenomena in chromatography. Profound analysis of this model was done in [22, 23]. The mass balance can be expressed with the following equation:

$$\frac{\partial c_i}{\partial t} + \frac{1-\varepsilon}{\varepsilon} \cdot \frac{\partial q_i^*}{\partial t} + u \frac{\partial c_i}{\partial z} = 0, \quad i = 1, 2, \dots, n \quad (2.14)$$

where  $c$  stands for the concentration in the mobile phase,  $q^*$  for the equilibrium concentration in the stationary phase (expressed by adsorption isotherm, section 2.4),  $t$  for the time coordinate, and  $z$  for the space coordinate. The velocity  $u$  is assumed to be constant.

To solve the model, one needs to specify initial and boundary conditions. Initial conditions describe the state of the column when the experiment starts ( $t = 0$ ), when the column is filled with mobile phase with certain concentration ( $c_i^0$ ) of the compounds that can be adsorbed:

$$c_i(z, t = 0) = c_i^0 \quad (2.15)$$

Very often the column is unloaded, so the mobile phase does not contain any adsorbing substance and therefore  $c_i^0 = 0$ . Boundary condition at the column inlet ( $z = 0$ ) are defined as follows:

$$\begin{aligned} c_i(z = 0, t) &= c_i^{inj}(t), & \text{for } 0 < t \leq t_{inj} \\ c_i(z = 0, t) &= 0, & \text{for } t > t_{inj} \end{aligned} \quad (2.16)$$

where  $c_i^{inj}(t)$  is the injection profile introduced at the column and  $t_{inj}$  the injection time.

### 2.2.2 Equilibrium dispersive model

According to the equilibrium-dispersive model (EDM) there is permanent equilibrium between the mobile and the stationary phase, and all band broadening effects are lumped into the apparent dispersion coefficient ( $D_{app}$ , eq. (2.13)). The mass balance equation for EDM differs from the one for IM just by including the dispersion term, as showed in the following equation:

$$\frac{\partial c_i}{\partial t} + \frac{1-\varepsilon}{\varepsilon} \cdot \frac{\partial q_i^*}{\partial t} + u \frac{\partial c_i}{\partial z} = D_{app} \frac{\partial^2 c_i}{\partial z^2}, \quad i = 1, 2, \dots, n \quad (2.17)$$

Initial conditions are as those for IM (eq. (2.15)), while for the column inlet ( $z = 0$ , eq. (2.18)) and outlet ( $z = L$ , eq. (2.19)) most commonly Danckwerts boundary conditions [24] are used:

$$uc_i(z=0, t) = uc_i^{inj}(t) + D_{app} \left( \frac{\partial c_i}{\partial z} \right)_{t,z=0}, \quad \text{for } 0 < t \leq t_{inj} \quad (2.18)$$

$$uc_i(z=L, t) = D_{app} \left( \frac{\partial c_i}{\partial z} \right)_{t,z=L}, \quad \text{for } t > t_{inj}$$

$$\left( \frac{\partial c_i}{\partial z} \right)_{t,z=L} = 0 \quad (2.19)$$

### 2.2.3 Transport dispersive model

Transport-dispersive model (TDM) is used when mass transfer kinetics cannot be neglected, as it is assumed for IM and EDM. The mass balance equation is similar to the one for EDM, with the difference that instead of apparent dispersion coefficient, now the axial dispersion coefficient ( $D_L$ ) is used. This coefficient includes the band broadening effects (axial dispersion) caused by the packing quality:

$$\frac{\partial c_i}{\partial t} + \frac{1-\varepsilon}{\varepsilon} \cdot \frac{\partial q_i}{\partial t} + u \frac{\partial c_i}{\partial z} = D_L \frac{\partial^2 c_i}{\partial z^2}, \quad i = 1, 2, \dots, n \quad (2.20)$$

The initial and boundary conditions are similar to those of the EDM. For TDM there is an additional equation that describes the mass transfer kinetics. Different kinetic models can be used for this purpose. Some of the simplest are [11]: Langmuir kinetics model, linear kinetics model, and the most commonly encountered linear driving force model (LDF) [25], given in eq. (2.21):

$$\frac{\partial q_i}{\partial t} = k_{m,i} (q_i^* - q_i) \quad (2.21)$$

where  $k_m$  is the lumped mass transfer coefficient,  $q$  the concentration in the stationary phase and  $q^*$  is stationary phase concentration at equilibrium.

#### 2.2.4 General rate model

The most accurate chromatographic model, and the most complex one, is the general rate model (GRM). It consists of two mass balance equations for the solute in the bulk mobile phase, which travels through the column (eq. (2.22)), and for the solute in the stagnant fluid phase inside the particle pores (eq. (2.23)):

$$\varepsilon_e \frac{\partial c_i}{\partial t} + u_0 \frac{\partial c_i}{\partial z} + (1 - \varepsilon_e) k_{e,i} a_p \left( c_i - c_{p,i} \Big|_{r=R_p} \right) = \varepsilon_e D_{L,i} \frac{\partial^2 c_i}{\partial z^2}, \quad i = 1, 2, \dots, n \quad (2.22)$$

$$\varepsilon_p \frac{\partial c_{p,i}}{\partial t} + (1 - \varepsilon_p) \frac{\partial q_i}{\partial t} = \frac{1}{r^2} \frac{\partial}{\partial r} \left[ r^2 \left( \varepsilon_p D_{p,i} \frac{\partial c_{p,i}}{\partial r} + (1 - \varepsilon_p) D_{s,i} \frac{\partial q_i^*}{\partial r} \right) \right], \quad i = 1, 2, \dots, n \quad (2.23)$$

In the previous equations, the symbols have the following meaning:  $u_0$  – superficial velocity,  $k_{e,i}$  – mass transfer coefficient from fluid to particle,  $a_p$  – external surface area of the particles,  $c$  – bulk mobile phase concentration,  $c_p$  – stagnant mobile phase concentration,  $r$  – radial coordinate,  $R_p$  – particle radius,  $D_p$  – pore diffusion coefficient,  $D_s$  – surface diffusion coefficient. More details about the model can be found elsewhere (e.g. [10, 11]).

### 2.3 Chromatographic processes in the gas phase

In comparison to the liquid phase, gases behave in the same way, with the difference that we must take into account some of the phenomena, which are normally neglected when investigating liquid systems. Since, unlike liquids, gases are compressible, the velocity, pressure and temperature cannot be considered constant during the processes. That makes the prediction of band profiles in the gas phase much more complex than for the liquid chromatography [26, 27].

In chromatographic processes when a molecule of the solute is adsorbed, it creates a void in the fluid phase. For liquid systems this sorption effect can be considered negligible because the partial molar volumes of the solute in the stationary (solid) and mobile (liquid) phase are similar. However, this is not the case for gas-solid systems, where these differences are significant. In the GC, when a molecule is sorbed, the formed void in the gas phase changes the pressure profile. The partial pressure of the solute is higher within the band than in the rest of the column and for the carrier gas the opposite is valid. Since mass flowrate of the

carrier gas is constant, it implies that the local mobile phase velocity will be greater within the band.

Taking into account the previously stated, when investigating the process in gas phase, the velocity appearing in the mass balances cannot be considered constant as it is assumed for the liquid chromatography. For the gases the velocity is a function of the space and time:  $u = u(z,t)$ . Therefore the term  $u \cdot (\partial c / \partial z)$  in the equations (2.14), (2.17), (2.20) and (2.22), which is commonly used for liquid phase systems becomes  $\partial(c \cdot u) / \partial z$  for the processes in the gaseous phase. One example of a mass balance equation for the GC separation is shown here for the equilibrium dispersive model (for LC it is given by eq. (2.17)):

$$\frac{\partial c_i}{\partial t} + \frac{1-\varepsilon}{\varepsilon} \cdot \frac{\partial q_i^*}{\partial t} + \frac{\partial(c_i u)}{\partial z} = D_{app} \frac{\partial^2 c_i}{\partial z^2}, \quad i = 1, 2, \dots, n \quad (2.24)$$

An adsorption/desorption process includes also heat exchange, which in the gas phase has greater influence than in the liquid systems. Therefore, to take into account the heat generation and its transfer is important for accurate modelling of GC. Temperature variations depend mostly on heat of adsorption, heat transfer characteristics of the packing, as well as on the transport properties of the carrier gas [13].

In the previous sections, the mass balance of a chromatographic process was discussed. By taking into account the compressibility of the gases, for a GC process description mass balances are needed to be set for each component, as well as for the carrier gas. Apart from it, the GC processes in general should take into account the momentum and energy balance. Momentum balance is usually expressed by Ergun [28] or Darcy [29] equation for pressure drop. For some systems the losses in pressure can be neglected, but when the difference between the inlet and outlet pressure is larger, they need to be taken into account.

For GC systems the pressure drop along the column, i.e. the difference between the inlet ( $P_{in}$ ) and outlet ( $P_{out}$ ) pressure, also influences the calculation of some of the parameters that characterize the adsorption bed, such as bed porosity ( $\varepsilon$ ) or the number of theoretical plates ( $NTP$ ). This comes from the fact that the retention volume ( $V_R$ ), which is for LC expressed simply by multiplying the retention time ( $t_R$ ) by the volumetric flowrate ( $Q$ ), in the gaseous phase has to be corrected for the effect of gas compression. This corrected retention volume can be denoted as  $V_R^{GC}$  and is calculated in the following way:

$$V_R^{GC} = j \cdot t_R Q \quad (2.25)$$

where  $t_R$  stands for the measured retention time. The compressibility factor ( $j$ ) is called James-Martin factor and is expressed as [30, 31]:

$$j = \frac{3 \left[ \left( \frac{P_{in}}{P_{out}} \right)^2 - 1 \right]}{2 \left[ \left( \frac{P_{in}}{P_{out}} \right)^3 - 1 \right]} \quad (2.26)$$

The value of the retention time used in calculating the column parameters in the GC processes is therefore the corrected retention time ( $t_R^{GC}$ ):

$$t_R^{GC} = \frac{V_R^{GC}}{Q} = jt_R \quad (2.27)$$

Taking this into account e.g. the expression for calculating the bed porosity (given by equations (2.5) and (2.6) for the liquid phase) in a GC process is:

$$\varepsilon = \frac{t_0^{GC} Q}{V} = j \frac{t_0 Q}{V} \quad (2.28)$$

When the gas system is diluted and when there is no larger pressure change, the simplified model equations, like those used for liquid phase, could still be applied, but their applicability needs to be tested. That is one of the tasks in this thesis. However, for processes like PSA, which include larger pressure changes, more detailed models need to be used. Thus, the more complex model equations for the gas phase will be given together with the description of a PSA process (section 2.5.2.2).

## 2.4 Adsorption isotherms

An expression that gives the relation between the component concentration in the stationary and in the mobile phase in equilibrium for a constant temperature is called adsorption isotherm. It shows the thermodynamic equilibrium of a system and therefore represents an important part of analysis and modelling of adsorption processes.

A wide range of systems can be described using many different relations and, consequently, many adsorption isotherm models have been developed. In general, form of an isotherm model, which shows how the concentration in the stationary phase ( $q$ ) depends on the concentration in the mobile phase ( $c$ ) at constant temperature ( $T$ ), can be written as:

$$q = f(c), \quad T = \text{const.} \quad (2.29)$$

This model is valid when only one component is adsorbed. Adsorption of multicomponent mixtures is characterised by competition between different components for interaction with the stationary phase. Molecules of the substance which is more strongly adsorbed tend to

exclude molecules of other components. In that case, we speak about more complex, competitive, isotherms. The concentration of each component adsorbed at the equilibrium ( $q_i$ ) depends on the concentrations of all other components present in the mixture that can be adsorbed on the stationary phase:

$$q_i = f(c_1, c_2, \dots, c_n), \quad i = 1, 2, \dots, n, \quad T = \text{const.} \quad (2.30)$$

Competitive adsorption isotherms can be determined using experimental methods, which is the most correct way, but can be at the same time very complicated and expensive. Therefore, they are often derived theoretically. One way to perform this, is by extending the equations for the single component isotherms and using their data [11, 12]. This method is very simple and usually correct, but in the higher concentration range the models are not able to describe the adsorption process properly [32]. Another concept used is Ideal adsorbed solution theory [33], based on the work of Myers and Prausnitz [34]. The theory assumes that there is an adsorbed phase that behaves as a Raoult ideal solution. The result is a system of nonlinear algebraic equations, whose solution gives the composition of the adsorbed mixture at equilibrium.

#### 2.4.1 General types of adsorption isotherms

There are different types of adsorption isotherm models that can be found in the literature. Single solute isotherms were classified by Brunauer for adsorption of gases [35] and by Giles (isotherms for liquid-solid systems as well) [36]. Figure 2.4 shows the most typical isotherm shapes for gas adsorption.

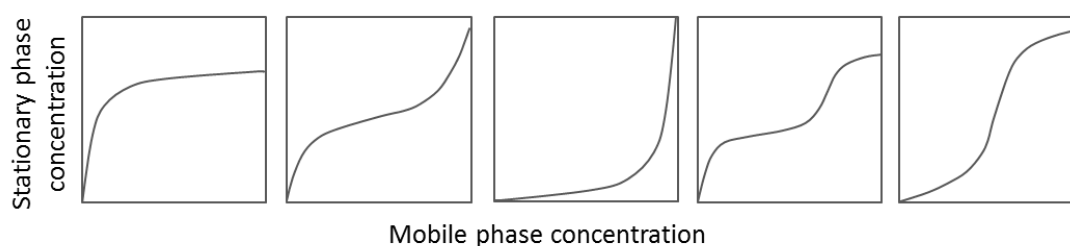


Figure 2.4. Most typical shapes of adsorption isotherms. In the first figure the most often encountered Langmuir-type isotherm is shown.

A number of different adsorption isotherm models has been developed. Some of them are linear, Langmuir, BET, Freundlich isotherm and many others [11]. One of the most often used isotherm models is Langmuir adsorption isotherm [37]. In the case when only one compound is adsorbed, Langmuir isotherm can be written in the following form:

$$q^* = \frac{q_0 bc}{1 + bc} = \frac{Hc}{1 + bc} \quad (2.31)$$

where the adsorption is described using parameters:  $q_0$  – saturation capacity of the stationary phase,  $b$  – the isotherm constant which depends on the adsorption energy,  $H = q_0b$  – Henry constant. This isotherm was derived theoretically assuming that only single layers of adsorbed molecules can be formed, that all adsorption sites are energetically equal and that each adsorption site can adsorb only one molecule. Furthermore, it is considered that there are no interactions between the adsorbed molecules, as well as between the mobile phase and the substance that is adsorbed.

If the surface of the adsorbent is not homogeneous, it is necessary to use more complex isotherm forms. For the simplest model that describes this case, it is assumed that the whole surface is covered with two different kinds of chemical groups (two different homogeneous surfaces). Therefore, the isotherm is called Bi-Langmuir:

$$q^* = \frac{q_{0,I}b_Ic}{1+b_Ic} + \frac{q_{0,II}b_{II}c}{1+b_{II}c} \quad (2.32)$$

In the case when a mixture of many substances is adsorbed, competitive Langmuir and competitive Bi-Langmuir isotherm have been derived. For  $n$ -component mixture ( $i = 1, 2, \dots, n$ ) the expressions are given in eq. (2.33) for Langmuir model and in eq. (2.34) for Bi-Langmuir.

$$q_i^* = \frac{q_{0,i}b_i c_i}{1 + \sum_{i=1}^n b_i c_i} = \frac{H_i c_i}{1 + \sum_{i=1}^n b_i c_i} \quad (2.33)$$

$$q^* = \frac{q_{0,I}b_{I,I}c_i}{1 + \sum_{i=1}^n b_{i,I}c_i} + \frac{q_{0,II}b_{II,II}c_i}{1 + \sum_{i=1}^n b_{i,II}c_i} \quad (2.34)$$

For very low concentrations, when it can be assumed that  $1 + bc \approx 1$  in the expression for Langmuir or Bi-Langmuir isotherm, the isotherm is considered to be linear with only one parameter – Henry constant:

$$q^* = Hc \quad (2.35)$$

Henry constant represents the isotherm slope at infinite dilution and can be calculated from the retention times ( $t_{R,i}$ ) of the peaks resulting from very small injected amounts (from eq. (2.1)):

$$H = \frac{t_R - t_0}{t_0} \cdot \frac{\varepsilon}{1 - \varepsilon} \quad (2.36)$$



Useful is to define the separation factor (selectivity) of a separation system. For two components, the selectivity ( $\alpha_{2,1}$ ) is defined as the ratio of Henry constant of the stronger adsorbed component (component 2) to the less strongly adsorbed one (component 1):

$$\alpha_{2,1} = H_2/H_1 \quad (2.37)$$

## 2.4.2 Methods to experimentally determine adsorption isotherms

Estimation of adsorption isotherms in a correct way is very important. Taking into consideration that theoretical determination of isotherms for fluid-solid equilibria is not possible, adsorption isotherms can be obtained only by using experimental techniques. The key point is to choose the proper method which will provide reliable results. Several different experimental methods for estimation of adsorption isotherms have been developed [10, 11, 38]. They can be classified into two groups: static and dynamic methods. Some of the characteristics of the methods commonly used for liquid systems that are discussed here, are presented in Table 2.2, while further descriptions are provided in sections 2.4.2.1 and 2.4.2.2. For all the experimental methods it is important to remark that the determined isotherms can be considered accurate only within the range of concentration that is used for the experiments. Extrapolation of the isotherm beyond that range should not be done at greater extent.

Table 2.2. Characteristics of the most commonly used methods for determination of adsorption isotherms.

| Method          |  | Possibility to determine competitive isotherms | Sample amount required | High column efficiency required |
|-----------------|--|--|------------------------|---------------------------------|
| Static methods  | Batch method                             | ✓  | Large                  | No column                       |
|                 | Adsorption-desorption method             | ✓  | Large                  | -                               |
|                 | Circulation method                       | ✓  | Small                  | -                               |
| Dynamic methods | Frontal analysis                         | ✓  | Large                  | No                              |
|                 | Perturbation method                      | ✓  | Large                  | No                              |
|                 | Nonlinear frequency response method      | ✓  | Large                  | No                              |
|                 | Elution by characteristic point          | No   | Small                  | Yes                             |
|                 | Frontal analysis by characteristic point | No   | Small                  | Yes                             |
|                 | Peak maxima method                       | No   | Small                  | Yes                             |
|                 | Peak-fitting method                      | ✓  | Small                  | No                              |

#### 2.4.2.1 *Static methods*

Static methods are based on analysis of parameters that correspond to equilibrium states using the overall mass balances. The most often used ones are: batch method, adsorption-desorption method and circulation method.

**Batch method** [11, 39] is based on experiments done in a closed vessel filled at the beginning with solution of a certain volume with the known initial concentration of the component that will be adsorbed. In the next step a known volume or mass of an adsorbent is added, and then the equilibrium concentration in the liquid phase is measured. The equilibrium concentration in the solid phase can be calculated using mass balance. To get the whole adsorption isotherm, several experiments using different initial concentrations or different adsorbent amounts have to be performed. The drawbacks lie in the fact that a lot of experimental work is needed and usually not enough precise parameters can be obtained.

**Adsorption-desorption method** [38] is based on the determination of isotherm in two steps. In the first step an initially unloaded column is equilibrated using feed solution of known concentration. In the second step all the solute is eluted from the column using pure solvent. The solute is collected and analysed in order to determine the equilibrium amount of the component. Knowing the initial concentrations in the liquid phase and equilibrium amount of the component, initial concentration in the solid phase can be calculated. Since, in order to obtain the whole isotherm, it is necessary to repeat the experiments using different initial concentrations, this method includes a lot of experimental work like the batch method, but on the other hand, it is more accurate.

**Circulation method** [10] analyses the concentration of the component in liquid phase when equilibrium state is reached and after that the concentration in the solid phase is calculated. The solution is pumped through a closed cycle in which column of a known volume and total porosity is included. A known amount of the component is injected into the cycle and then equilibrium concentration is measured. This is the way how one point of the isotherm is determined. Another point can be estimated by adding higher amount of the component in the cycle. In this way the solute concentration is successively increased, which can lead to imprecise determinations, especially after many injections because inaccuracies will accumulate. In order to get reliable results, volume of the cycle must be precisely determined.

#### 2.4.2.2 *Dynamic methods*

Dynamic methods analyse the concentration-time curves at the column outlet that correspond to different well defined changes of the column inlet concentrations. These methods are more accurate than static methods and also allow faster determination of isotherm parameters. Many methods have been developed based on different inlet concentration changes.

**Frontal analysis** [38, 40] is one of the most often used methods for determination of isotherm parameters. It includes measurements of the breakthrough curves for different concentration ranges. At the beginning ( $t = 0$ ) a large sample volume with the equilibrium

concentration  $c_i^{eq}$  is injected into the column until a concentration plateau (equilibrium) is reached. After this, often the desorption step starts. The feed concentration is lowered to the initial concentration ( $c_i^{init}$ ), that was in the column before the injection, and the concentration change is recorded. This process can be described by the following integral mass balance equation for component  $i = 1, 2, \dots, n$ :

$$\varepsilon V (c_i^{eq} - c_i^{init}) + (1 - \varepsilon) V (q_i^{eq} - q_i^{init}) = Q \int_0^{\infty} (c_i^{eq} - c_i(t)) dt \quad (2.38)$$

where  $q_i^{eq}$  and  $q_i^{init}$  are equilibrium concentrations in the stationary phase corresponding to  $c_i^{eq}$  and  $c_i^{init}$ , respectively, and  $c_i(t)$  represents the whole adsorption and desorption front recorded. From this mass balance one can calculate the new equilibrium concentration in the stationary phase, when  $c_i(t)$  is recorded. Figure 2.5 gives a typical breakthrough curve used in frontal analysis.

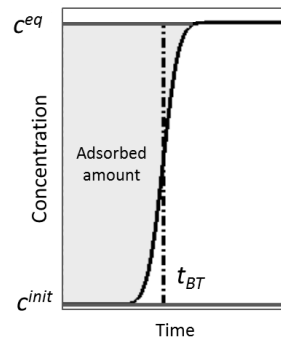


Figure 2.5. Adsorption step in frontal analysis. Adsorbed amount corresponds to the integral in eq. (2.38). The term  $t_{BT}$  represents the breakthrough time.

The figure shows the adsorption step for a single solute adsorption. Using the breakthrough time ( $t_{BT}$ ) one point of the isotherm can be calculated by the following equation derived from eq. (2.38):

$$t_{BT} = t_0 \left( 1 + \frac{1 - \varepsilon}{\varepsilon} \cdot \frac{q_i^{eq} - q_i^{init}}{c_i^{eq} - c_i^{init}} \right) \quad (2.39)$$

In order to determine the isotherm in wider concentration range, different outlet concentration profiles for different feed concentrations have to be taken for calculations. This can be achieved by performing successive step changes of the inlet concentration. Then, column outlet concentration changes are analysed in order to determine intermediate concentrations on each plateau and retention time of shock fronts.

The advantage of frontal analysis is that it is not sensitive to kinetic effects as long as the intermediate plateau concentrations can be identified, therefore an accurate isotherm can be

obtained even if the mass transfer kinetics are relatively slow. The main disadvantage is that it requires large amounts of chemicals.

**Perturbation method** [38, 41] includes very small injections of a component in the previously preloaded column at some other concentration. The injections have to be small enough to leave the column in equilibrium and at the same time large enough to be distinguished from the background noise. In order to determine the whole isotherm, the column has to be equilibrated at different concentrations and then pulse injections should be performed and retention time determined. The illustration of the method for a single component can be seen in Figure 2.6.

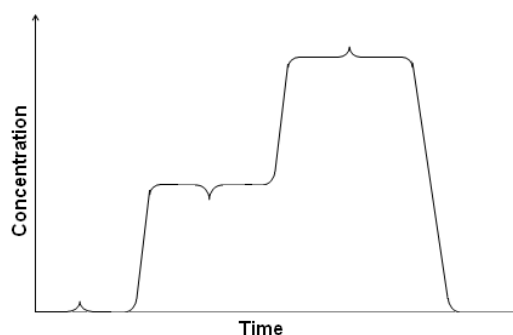


Figure 2.6. Typical curve recorded when applying perturbation method for single component adsorption isotherm determination.

Determined retention times give the local derivatives of the isotherm ( $dq_i/dc_i$ ) calculated from the following expression:

$$t_{R,i} = t_0 \left( 1 + \frac{1-\varepsilon}{\varepsilon} \frac{dq_i}{dc_i} \right) \quad (2.40)$$

By systematic collection of these derivatives, the whole isotherm can be determined by integration. The main drawback of the method is that it consumes a large amount of substances, but on the other hand there are advantages, like no need to calibrate the detection system since the only used data are the retention times.

**Nonlinear frequency response method** is based on analysis of the response of a chromatographic column to sinusoidal change of the inlet concentration (Figure 2.7).

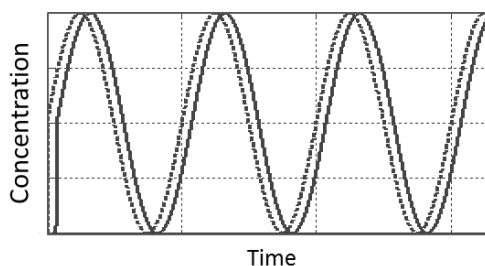


Figure 2.7. Example of column inlet (dashed line) and outlet (solid line) concentration change analysed by nonlinear frequency response method in order to calculate the adsorption isotherm parameters.

The theoretical basis for the method is related to the fact that the adsorption isotherm derivatives can be directly related to the low-frequency asymptotes of the column frequency response functions. The procedure to determine the isotherms includes the following steps:

1. Experiments with the chromatographic column done by modulating the inlet concentration in a sinusoidal way around a steady state value;
2. Harmonic analysis of the inlet and outlet concentrations;
3. Determination of the frequency response functions and calculation of the dimensionless isotherm coefficients;
4. Estimation of the isotherm parameters by fitting the analytical expressions for the sums of the first, second and third order isotherm derivatives to their experimental values.

This method allows determination of the first three derivatives of an isotherm, which provides details about the isotherm shape and is particularly significant for isotherms with inflection points [42-44]. Its application demands large solute amounts and precise detector calibration.

**Elution by characteristic point** and **frontal analysis by characteristic point** evaluate the dispersive front of a chromatogram. The two methods are similar, differing only in the injected amounts. The injection is larger for the second one, providing a wider rectangular profile, while elution by characteristic point considers a pulse injection [11, 45]. The disadvantage of these methods is mainly due to the fact that they can be applied only for very efficient columns, since then the dispersive front is mainly caused by the adsorption isotherm. Both of them, however, are simple and do not require large sample amounts: only one larger injection is sufficient to determine the isotherm for the whole concentration range of interest. More details about elution by characteristic point is given in Chapter 3, section 3.1.

**Peak maxima method** analyses the retention times of the maxima of peaks obtained by pulse injections. By recording the retention time of the maximum, one can calculate the isotherm slope in one point from the equation (for isotherms of Lagmuir-type shape):

$$t_{R,i} = t_{inj} + t_0 \left( 1 + \frac{1-\varepsilon}{\varepsilon} \frac{dq_i}{dc_i} \right) \quad (2.41)$$

The term  $t_{inj}$  stands for the injection time. This equation represents the more general form of eq. (2.1). Eq. (2.41) is also valid when larger amounts of the sample are injected into the system. If the injected amounts are small, then the injection time becomes very close to zero and the derivative  $dq_i/dc_i$  is equal to Henry constant (as it can be seen from eq. (2.35)), which means that we come to the expression given in eq. (2.1). To get the whole isotherm, more pulse injections of different sample concentrations have to be performed, as shown in Figure 2.8. For application of the method more time and chemicals than for elution by characteristic

point and frontal analysis by characteristic point are needed, but it is less sensitive to column efficiency [46].

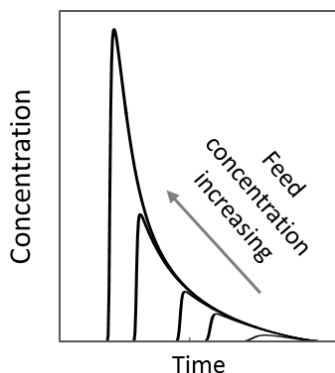


Figure 2.8. Elution profiles for different feed concentrations used for determination of adsorption isotherms with peak maxima method.

**Peak-fitting (or inverse) method** [47] represents a useful tool for calculating the isotherm parameters by minimizing the differences between the simulated values and experimentally obtained chromatogram. The process of determining the right parameters and approaching of the simulated chromatogram to a starting (experimental) peak for a binary mixture is shown in Figure 2.9.

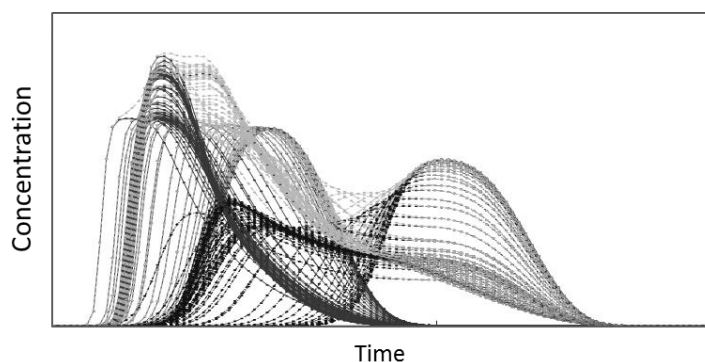


Figure 2.9. Process of isotherm parameter determination using peak-fitting method. The diagram shows the large number of recorded iterations before reaching the shape of the original experimental peak.

Usually many different isotherm models are tested. It is important to describe the injection profiles very accurately in order to obtain the correct data. One of the advantages is that it requires lower amounts of chemicals and time for experimental work, similar to those of elution by characteristic point and frontal analysis by characteristic point. But, in contrary to those methods, here it is not necessary to use highly efficient columns, since the dispersion and mass transfer effects can be accounted for by the model. However, detector calibration is necessary and another disadvantage is that the isotherm model has to be chosen in advance. Additional descriptions of this method and its application to a case when no pure components are available, is presented in Chapter 3, section 3.2.

### 2.4.2.3 Determination of the isotherms in chiral systems

Separation of enantiomers is the focus of this work. Taking this fact into account, it was important to check the availability of the adsorption isotherm determination methods for these substances, especially considering the case when there are no pure components, but only racemic mixture available for experiments. There are numerous examples in the literature; some of them were studied in [48], [49], [16] and [50] by frontal analysis, perturbation method, nonlinear frequency response method and peak-fitting method, respectively.

## 2.5 Continuous multi-column chromatographic processes

Whenever it is possible, preparative chromatographic separations are performed as continuous processes. Batch processes can provide the products of high purity, but it is very often succeeded only by sacrificing the recovery of the substances. To get the highly pure products with high recovery, it is required to do the complete separation, which means that large amounts of solvents have to be utilized and more time has to be invested. Therefore, continuous processes, which can lead to more efficient separation, are favourable. These advanced processes are more complicated than the batch separation and require more parameters to be considered, determined and optimized, in order to provide the best process performance. Here the two commonly applied processes will be briefly discussed: simulated moving bed and pressure swing adsorption.

### 2.5.1 Simulated moving bed (SMB) process

The idea of SMB is to simulate the counter-current flow of the stationary and the mobile phase. The real counter-current behaviour, described in the true moving bed concept, is not feasible in reality. In order to overcome its difficulties, the SMB process was developed [51]. This process is based on columns connected in series, between which there are different ports for inlet (feed and eluent port) and outlet streams (extract and raffinate port). The wanted counter-current movement of the two phases is simulated by discrete changes of the position of the ports in the direction of the mobile phase flow. In practice this shifting moves each column (the stationary phase) by one position backwards in the opposite direction of the mobile phase flow. In Figure 2.10 a typical SMB process with four zones (I-IV) is illustrated. In the example shown each zone contains two columns, but the number can vary. During the operation, the feed is pumped continuously into the system. It enters between the zones II and III and flows in the clockwise direction towards the zone IV. The less strongly adsorbed component (component 1) will move faster through the columns and will reach the raffinate port faster, while the stronger adsorbed compound (component 2) will migrate slower and will approach the extract port. In each zone different part of the process occurs:

- Zone I – Desorption of the remaining components (stationary phase regeneration);

- Zone II – Desorption of the less strongly adsorbed component;
- Zone III – Adsorption of the more strongly adsorbed component;
- Zone IV – Adsorption of the both components (mobile phase regeneration).

In comparison to the batch chromatography, SMB shows many advantages, like saving the eluent since it continuously circulates through the columns, better utilization of the stationary phase and therefore higher productivity, lower requirements of column efficiency etc. In this way the process performance increases, while the cost decreases at the same time [52, 53].

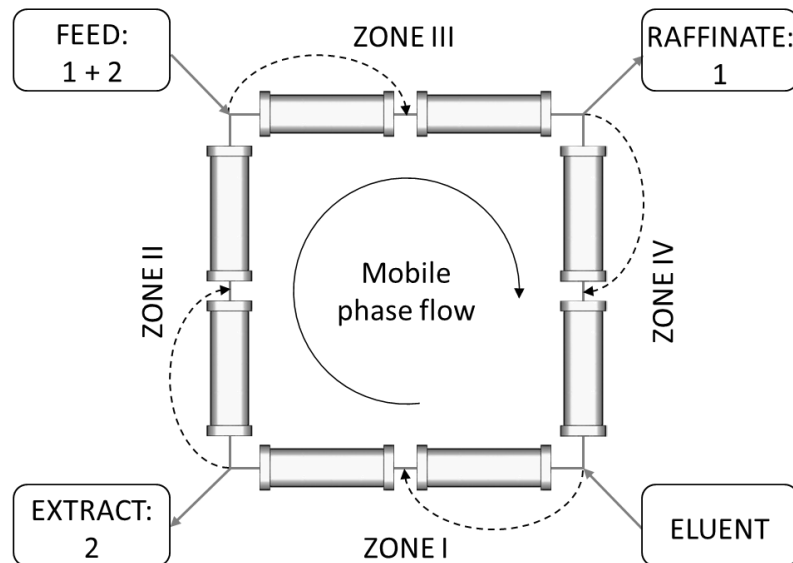


Figure 2.10. Representation of a 4-zone SMB process with two columns in each zone and marked direction of the mobile-phase flow. The dashed arrows show the discrete shifting of the port positions.

The SMB process was developed by Broughton and Gerhold [54] and applied for purification of hydrocarbons. Since then it has been used for research, as well as for industry applications. Besides the classical SMB, several new concepts have also been established in order to adjust the process to a certain separation problem, or to enhance its performance. Furthermore an 8-Zone SMB for separation of ternary and pseudo-ternary mixtures was proposed [55, 56]. Summary of research works involving many different concepts of SMB are given in [57-59].

### 2.5.1.1 Modelling of the SMB process

To model an SMB process one can use a true moving bed concept, but it is more accurate to describe it by a fixed bed approach with periodic movement of the ports [11]. The main model equation is the mass balance. Depending on the process, the corresponding column model (section 2.2) should be used. Since there is no classical steady state, the model equations are solved until the cyclic steady state is established, which is the point where the total outlet mass of a cycle is consistent to the total mass at the inlet introduced during the shifting period. For a successful SMB separation, it is necessary to determine the volumetric



flowrates ( $Q$ ) for each zone and the time between the discrete port shifts. For a 4-zone process, the flowrates are:

$$Q_I = Q_{IV} + Q_{eluent}; \quad Q_{II} = Q_I - Q_{extract}; \quad Q_{III} = Q_{II} + Q_{feed}; \quad Q_{IV} = Q_{III} - Q_{raffinate} \quad (2.42)$$

Here,  $Q_I$  to  $Q_{IV}$  represent the flowrates in the zones I to IV, while  $Q_{eluent}$ ,  $Q_{extract}$ ,  $Q_{feed}$  and  $Q_{raffinate}$  are the flowrates in the corresponding streams (denoted in the subscripts). More convenient is the use of dimensionless flowrate ratios ( $m_z$ ) for each zone ( $z = I, II, III, IV$ ). The  $m_z$  values represent the ratios between the fluid phase flow in the zone ( $Q_z$ ) and the virtual solid phase flow ( $Q_{solid}$ ) [60]:

$$m_z = \frac{Q_z}{Q_{solid}} = \frac{Q_z t_{shift} - V \varepsilon}{V(1 - \varepsilon)} \quad (2.43)$$

The time between port shifts ( $t_{shift}$ ) is defined by the column volume, porosity and  $Q_{solid}$ :

$$t_{shift} = \frac{(1 - \varepsilon)V}{Q_{solid}} \quad (2.44)$$

For the very efficient columns and the systems in the linear adsorption isotherm range, the triangle theory [60, 61] can be applied to choose the  $m_z$  values, based on the Henry constants, by following these relations:

$$m_I \geq H_2; \quad H_1 \leq m_{II} \leq m_{III} \leq H_2; \quad m_{IV} \leq H_1 \quad (2.45)$$

The constraints from eq. (2.45) define a separation region in the  $m_{II}$ - $m_{III}$  plane (Figure 2.11).

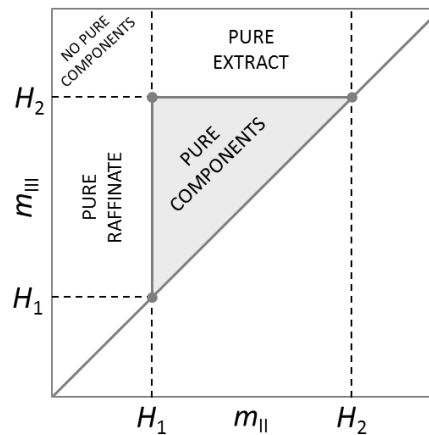


Figure 2.11. SMB triangle diagram with defined separation regions (where pure both components, only pure raffinate, pure extract, or no pure substances can be collected) for linear isotherm range.  $H_1$  and  $H_2$  represent the Henry constants of the first and second eluting component, respectively, while  $m_{II}$  and  $m_{III}$  are dimensionless flowrate ratios in the zones II and III, respectively.

For the non-linear isotherms the triangle theory is more complicated and the  $m_z$  values have been derived in details only for certain special cases.

### 2.5.2 Pressure swing adsorption (PSA) process

In order to provide the continuous separation, adsorption processes can be designed to operate in a cyclic manner. In that case one column can be employed, but very often at least two columns are used, such that one can be regenerated while in the other the adsorption takes place. To obtain this, parameters like pressure, temperature or mobile phase content can be changed during the process. According to which of the parameters vary, there are three basic types of these periodic adsorption processes [12]:

1. Pressure swing adsorption operates by repeating adsorption at higher pressure and desorption on lower pressure or vacuum.
2. Temperature swing adsorption is based on performing adsorption at lower temperature and desorption (bed regeneration) at higher temperature.
3. Concentration swing adsorption assumes the change of the mobile phase or its content after the adsorption step in order to provide better bed regeneration. It is used for liquid mobile phases.

The principle of pressure and temperature swing is schematically shown in Figure 2.12.

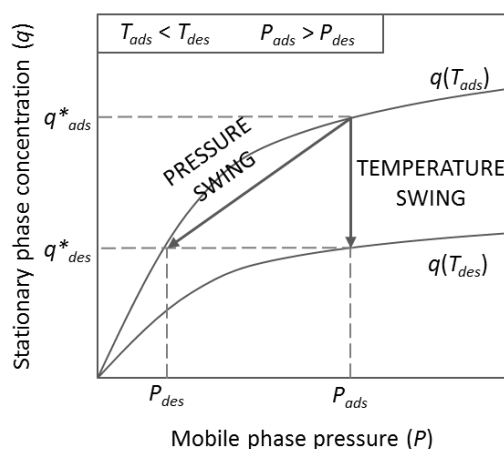


Figure 2.12. Representation of pressure and temperature swing on the adsorption isotherm diagram.  $P$  and  $T$  represent the pressure and the temperature, and the subscripts  $ads$  and  $des$  stand for adsorption and desorption process. The asterisk (\*) shows the value of the stationary phase concentration in equilibrium with the mobile phase pressure.

Here, only pressure swing adsorption (PSA) will be discussed. It represents a very versatile technology used to separate different gas mixtures. It is applied for many processes, such as drying of the gasses, recovery of solvent vapour, production of oxygen and hydrogen, separation of methane and carbon dioxide, carbon dioxide and nitrogen, carbon monoxide and hydrogen and many other problems. Ruthven [13] and Sircar [62] have given detailed summaries of the research done in this field. PSA was introduced by patents of Skarstrom [63], that used low pressure for desorption, and by the one of Guerin de Montgareuil and

Domine [64], who performed the desorption step by vacuum. However, many other works introduced even before the idea and important features of these processes (discussed e.g. in [65, 66]). The firstly developed Skarstrom cycle [63] is considered to be the basic one. It has two beds that undergo four steps: pressurization in the co-current direction (i.e. in the same direction of the mobile phase flow as for adsorption), adsorption, blowdown in the counter-current direction (the opposite to the one during the adsorption step) and purge in the counter-current direction. Many modifications of this configuration have been made in order to improve the performance of the process. Some of them introduced the co-current blowdown, or the addition of the pressure equalization step before the blowdown.

Application of PSA has seen a significant increase in the recent years due to the numerous advantages over the traditional technologies [13]. It operates at ambient temperature and does not require any heating or cooling equipment. In comparison to temperature swing adsorption, the cycle time is much smaller, since the pressure can be changed more rapidly than the temperature. This provides an increase in productivity. Possibility to change the pressure introduces the flexibility in process design, compared for example to absorption, distillation or extraction. The most important operating costs of a PSA process arise from energy needed for compression and vacuum. In the cases when the feed mixture is available at high pressure, PSA process is very favourable. However, PSA has limitations as well, and the major one is that the less strongly adsorbed component can be obtained in very pure form, but the stronger adsorbed one is generally produced as not completely pure stream. Problematic can also be the situation when this component is too strongly adsorbed, since then a very high vacuum is required for bed regeneration and that raises the costs of the process to an uneconomical level. Recovery of the components is usually not very high and therefore PSA separation is most suitable for cheaper components, where loss of the substances is not an important consideration.

Aside from the conventional PSA cycles, there are different specific PSA processes described in the literature [67]. In order to increase the productivity (though sacrificing purity and recovery), rapid PSA processes, with shorter cycle times, have been developed. Other examples are PSA at higher temperatures, multi-bed configurations, use of beds with multi-layered adsorbents [68], new adsorber designs, like radial bed adsorbers, or pressure swing reactor, where a reactor is combined with PSA [69].

### **2.5.2.1 Basic PSA configurations**

The four basic steps of a PSA are represented in Figure 2.13, using just one column as an example. In general, when a process is called PSA, it carries out the adsorption at a high pressure, higher than the ambient (or atmospheric) one, while desorption is performed at near-ambient pressure. When the adsorption step is at near atmospheric value and desorption is done under vacuum, then we speak about vacuum swing adsorption (VSA). When the higher pressure and vacuum are employed in the same process, it is pressure-vacuum swing adsorption (PVSA) [13, 67].

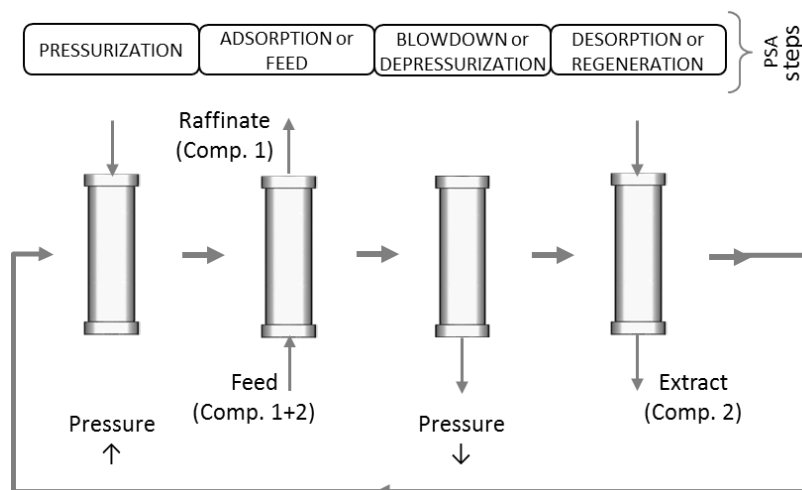


Figure 2.13. Demonstration of four steps (pressurization, adsorption or feed, blowdown or depressurization and desorption or regeneration) for a 1-column PSA. The up- and down-arrows ( $\uparrow$  and  $\downarrow$ ) show that the pressure is increasing or decreasing, respectively. The thin arrows at column inlet and outlet show the flow direction, while the thick ones represent the sequence of the process steps.

The main idea of a PSA process is to provide the adsorption of the components at high pressure. Therefore, prior to the adsorption step, the column has to be pressurized during the pressurization step in order to raise the pressure to the wanted uniform value. During this step one end of the column is kept closed, while the gas is pumped from the other side. Pressurization can be done in co- or counter-current direction using the inert gas (mobile phase eluent), feed mixture, or a mixture of other content, depending on the process requirements. The pressure change during the process is shown in the simple form in Figure 2.14. The pressure increase and decrease are represented by a linear function, but in practice they can follow other pattern.

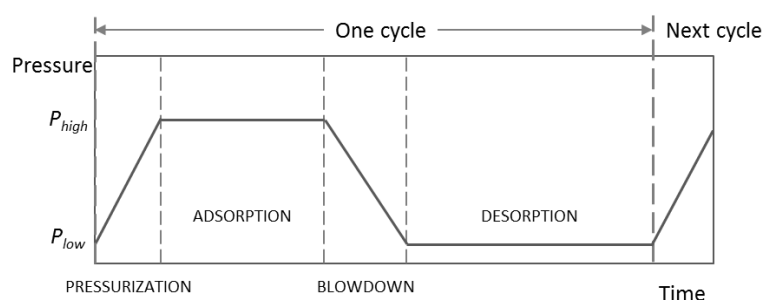


Figure 2.14. Pressure change in a 4-step PSA process. The increase and decrease of the pressure in the pressurization and blowdown step are represented by simplified linear functions.

After reaching the required pressure, the adsorption step takes part. This step is also sometimes indicated as feed step. At the column inlet the feed mixture is introduced (in the co-current direction) in order to produce the stream at the column outlet enriched in the less strongly adsorbed component (the component that first elutes from the column, denoted here

as component 1). This stream is called raffinate. Adsorption step normally ends at the moment when the elution of the more strongly adsorbed components starts.

Another main step of a PSA process is desorption at low pressure. To enable it, between adsorption and desorption step, there is a blowdown (also called depressurization) step. Here again, as during the pressurization step, the column is closed at one end, while the exit stream from the column provides decreasing of the pressure. It basically occurs in the counter-current direction.

Desorption or column regeneration can be done by inserting different mixtures, or an inert into the column at low pressure. During this step the more retained component (component 2) is flushed from the column. The outlet stream, called extract, is therefore enriched in the component 2. The goal of desorption is to enable the re-usability of the adsorbent and to bring the column to the state in which it was before the pressurization started, so the step is terminated when the bed is fully desorbed. After it, the new cycle can take place.

The basic PSA example, Skarstrom cycle, comprises the described four steps, by using two columns. It is schematically represented in Figure 2.15. The columns are connected in the way that desorption of one column is done by the raffinate stream from the other one. In the first step column 2 is pressurized with the feed in the co-current direction, while column 1 is blown down in the counter-current direction. The next step represents adsorption step for the column 2 and desorption in the counter-current direction for the column 1. The raffinate gas stream exiting the column 2 is enriched in component 1. The largest part of it is collected as a product, while one fraction is expanded to low pressure and used to purge column 1 (in its desorption step). The following two steps are the same as the first two, just that the columns are interchanged.

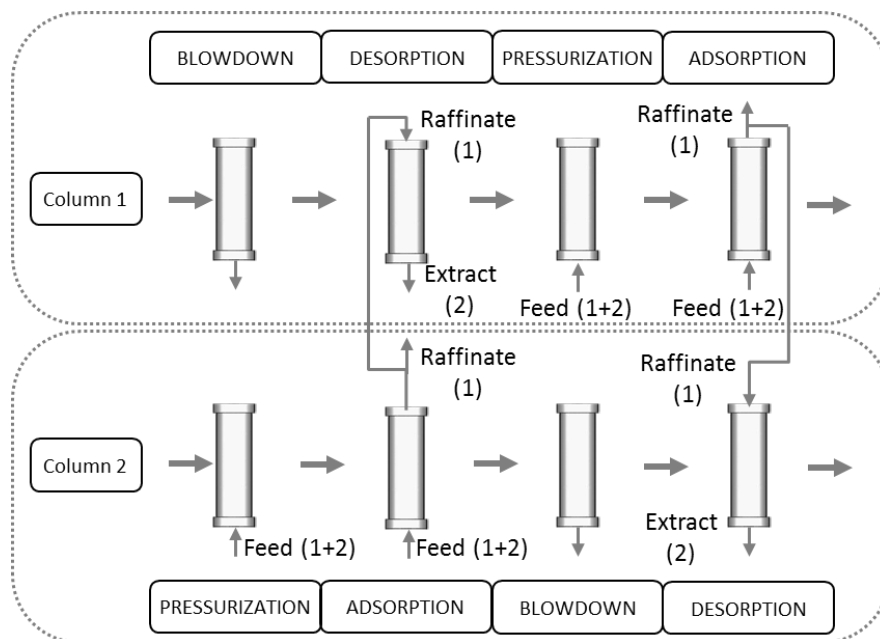


Figure 2.15. Skarstrom cycle representation (1 and 2 in the inlet and outlet streams stand for the first and second eluted component that are contained in the corresponding streams).

For VSA or PVSA processes the steps are similar as for PSA. The main difference is that desorption step is replaced by a vacuum desorption. In this step one end of the column is closed and the vacuum is pulled through the bed in the counter-current direction. If the adsorption step is done at the atmospheric pressure, then the process starts with adsorption step and re-pressurization step comes after vacuum, as shown in Figure 2.16. In the case of PVSA, the pressurization (re-pressurization) is the first step.

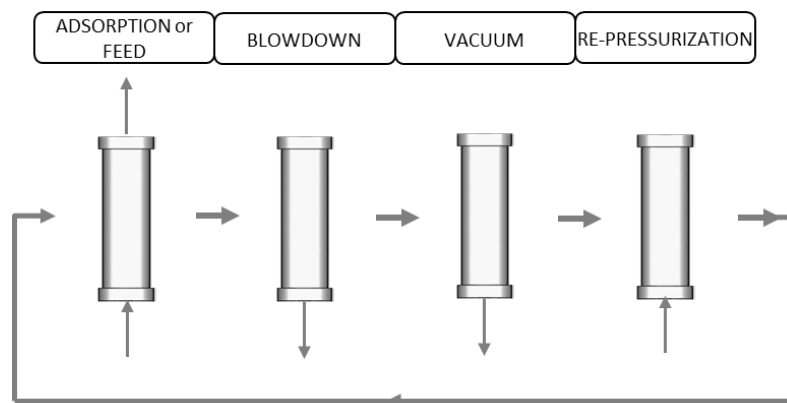


Figure 2.16. Example of a typical four-step VSA cycle for a process with one column.

### 2.5.2.2 Modelling of PSA processes

As stated in the section 2.3, modelling of the processes that occur in the gas phase is more complicated than for those in the liquid phase. To derive a proper model and to simulate a PSA, requires numerical solution of a set of nonlinear partial differential and algebraic equations with different initial and boundary conditions for each cycle and step. This solution procedure is repeated until the cyclic steady state is achieved. At cyclic steady state conditions in the column (or columns) at the end of each cycle are identical to those at the beginning of that cycle.

The equations that play a role in a PSA process depend on the process itself and the possible assumptions that can be taken into account. A complete process model includes [70]: component and overall mass balance, energy balance, momentum balance, mass transfer and isotherm equation, as well as the changes of the pressure with time during pressurization and blowdown step. By combining these equations, the complete PSA process can be properly described.

There are basic assumptions that are accounted in the PSA processes. In the most cases they include the following:

1. Gas phase follows the ideal gas law.
2. Column packing is homogeneous.
3. There is no radial variation of the parameters (temperature, pressure, velocity, concentration...).

4. Physical properties of the packed bed do not depend on temperature.
5. Very often adsorption rate (mass transfer) is calculated by linear driving force model (eq. (2.21)).
6. Pressure drop is calculated from Ergun or Darcy equation.

These assumptions can be used for the bulk separations, where the concentrations of adsorbing components are large. If we work with trace (diluted) systems, with very low concentrations, additional simplifications can be adopted [13]. The most common additional assumptions are negligible temperature change (no energy balance needed), constant velocity, no pressure drop, especially during pressurization and blowdown steps.

At the moment there are only few publications where enantioseparation of fluorinated anaesthetics was investigated not only experimentally, but also theoretically by modelling the process. There are models to be found in [71] for SMB process (mass balance equation is given, though no simulations were performed), [72] for SMB with pressure change and in [54] for SMB and PSA. In all three works only enflurane was studied. The PSA separation described in [54] considers a diluted system and is described mathematically by implementing the previously mentioned assumptions.

Depending on the process, different models can be used for the mass balance, like those described in section 2.2 and additionally in 2.3. For PSA the change in the pressure, velocity and temperature is usually taken into account. Therefore, the concentration of the solutes is most commonly expressed as mole fraction ( $y$ ) using the ideal gas law equation, where  $P_i$  represents partial pressure of a component,  $n_i$  its amount,  $V_g$  gaseous mixture volume,  $T$  temperature,  $R$  universal gas constant ( $R = 8.314 \text{ J/mol/K}$ ) and  $C$  the total concentration of all components (the sum of the single concentrations, i.e. mixture density):

$$P_i V_g = n_i R T \quad (2.46)$$

$$c_i = \frac{y_i P}{R T} = \frac{P_i}{R T} \quad (2.47)$$

$$C = \frac{P}{R T} \quad (2.48)$$

For the case of the transport dispersive model (section 2.2.3), which is considered here, the equation for overall mass balance is analogous to eq. (2.20) with the difference that velocity is not considered constant any more, as explained in section 2.3. Since we speak about the total mass balance, instead of single component concentration in the fluid phase ( $c_i$ ), we use the total concentration ( $C$ ) and the term related to the solid phase concentration is expressed as a sum for all the sorbates adsorbed:

$$-D_L \frac{\partial^2 C}{\partial z^2} + \frac{\partial C}{\partial t} + \frac{\partial(uC)}{\partial z} + \frac{1-\varepsilon}{\varepsilon} \cdot \sum_{i=1}^n \frac{\partial q_i}{\partial t} = 0 \quad (2.49)$$

By replacing eq.(2.48) into this equation, the overall mass balance can be written in the following form:

$$\begin{aligned} -D_L \left[ \frac{2}{T^2} \left( \frac{\partial T}{\partial z} \right)^2 - \frac{1}{T} \frac{\partial^2 T}{\partial z^2} + \frac{1}{P} \frac{\partial^2 P}{\partial z^2} - \frac{2}{TP} \frac{\partial T}{\partial z} \frac{\partial P}{\partial z} \right] + \frac{\partial u}{\partial z} + \frac{u}{P} \frac{\partial P}{\partial z} - \frac{u}{T} \frac{\partial T}{\partial z} - \\ - \frac{1}{T} \frac{\partial T}{\partial t} + \frac{1}{P} \frac{\partial P}{\partial t} + \frac{RT}{P} \frac{1-\varepsilon}{\varepsilon} \sum_{i=1}^n \frac{\partial q_i}{\partial t} = 0 \end{aligned} \quad (2.50)$$

The component mass balance expression according to eq. (2.20) is:

$$-D_L \frac{\partial^2 c_i}{\partial z^2} + \frac{\partial c_i}{\partial t} + \frac{\partial(uc_i)}{\partial z} + \frac{1-\varepsilon}{\varepsilon} \cdot \frac{\partial q_i}{\partial t} = 0 \quad (2.51)$$

Knowing that single component concentration is:

$$c_i = y_i C \quad (2.52)$$

from the overall mass balance we can get the equation for a component  $i$  as follows:

$$-D_L y_i \frac{\partial^2 C}{\partial z^2} + y_i \frac{\partial C}{\partial t} + y_i \frac{\partial(uC)}{\partial z} + \frac{1-\varepsilon}{\varepsilon} y_i \sum_{i=1}^n \frac{\partial q_i}{\partial t} = 0 \quad (2.53)$$

Since equations (2.51) and (2.53) are equal (they correspond to the mass balance of the same component), by combining them and by taking into account the relations given in equations (2.47), (2.48) and (2.52), the more detailed expression for the component mass balance can be obtained:

$$-D_L \left( \frac{\partial^2 y_i}{\partial z^2} - \frac{2}{T} \frac{\partial y_i}{\partial z} \frac{\partial T}{\partial z} + \frac{2}{P} \frac{\partial y_i}{\partial z} \frac{\partial P}{\partial z} \right) + \frac{\partial y_i}{\partial t} + u \frac{\partial y_i}{\partial z} + \frac{RT}{P} \frac{1-\varepsilon}{\varepsilon} \left( \frac{\partial q_i}{\partial t} - y_i \sum_{i=1}^n \frac{\partial q_i}{\partial t} \right) = 0 \quad (2.54)$$

The basic steps of the derivation of the component and the overall mass balance equations can be found in [73], and it is in more details given in the Appendix A.

The term  $\partial q_i / \partial t$  corresponds to the adsorption rate and is expressed by eq. (2.21). There are different expressions used to calculate the coefficient  $k_m$  [13]. Since its determination can represent a complicated procedure, the value is often estimated by fitting the simulated profiles to the experimental results.



To describe the change of the temperature and pressure, we need equations for energy and momentum balance. For a PSA system there are two main effects that influence the change in the temperature [13]: heat release due to the preferential adsorption of the stronger adsorbed component and the gas compression that increases the temperature. Temperature change is affected by the heat of adsorption, heat capacity and heat and mass transfer. These terms are included in the energy balance. The energy balance can be expressed as following:

$$\begin{aligned} (\varepsilon\rho_g C_{pg} + \rho_b C_{ps}) \frac{\partial T}{\partial t} + \rho_g C_{pg} \varepsilon_e u \frac{\partial T}{\partial z} - K_L \frac{\partial^2 T}{\partial z^2} - \rho_b \sum_{i=1}^n \frac{\Delta H_i}{M_i \rho_p} \frac{\partial q_i}{\partial t} + \\ + \frac{2h}{R_b} (T - T_{wall}) = 0 \end{aligned} \quad (2.55)$$

with the used parameters:  $C_{pg}$  – gas heat capacity,  $C_{ps}$  – solid (adsorbent) heat capacity,  $\rho_g$  – bulk gas density,  $\rho_b$  – bed density,  $\varepsilon_e$  – external porosity,  $K_L$  – thermal dispersion coefficient,  $\Delta H$  – isosteric heat of adsorption,  $M$  – molar mass of the solute,  $\rho_p$  – particle density,  $h$  – overall heat transfer coefficient,  $R_b$  – column radius,  $T_{wall}$  – column wall temperature.

To take into account the effect of pressure drop in the column, momentum balance is used. In the PSA models it is commonly done by using expressions like Ergun equation [28]:

$$-\frac{\partial P}{\partial z} = 150 \frac{\mu_g u}{4R_p^2} \frac{(1-\varepsilon_e)^2}{\varepsilon_e^2} + 1.75 \frac{1-\varepsilon_e}{2R_p \varepsilon_e} u |u| \rho_g \quad (2.56)$$

Here,  $\mu_g$  is the gas viscosity. The first term on the right-hand side represents losses due to viscous flow, related to laminar flow and the second term is related to turbulent flow and describes the losses in kinetic energy. In some cases the simpler Darcy equation [29] can be used:

$$-\frac{\partial P}{\partial z} = 180 \frac{\mu_g u}{4R_p^2} \frac{(1-\varepsilon_e)^2}{\varepsilon_e^2} \quad (2.57)$$

Depending on the separation process, different adsorption isotherm models can be employed (section 2.4.1). In this work, competitive Langmuir isotherm (eq. (2.33)) was the one that described the adsorption of the investigated components. If the changes in temperature in the column cannot be neglected, they also influence the adsorption isotherm parameters, which are temperature-sensitive. It can be assumed that the parameters of Langmuir model show normal exponential temperature dependence:

$$b = b_0 e^{-\Delta H/RT} \quad (2.58)$$

where  $b_0$  is a constant value. The values of Henry constant need to be known at different temperatures as well.

The PSA model presented in the previous paragraphs is one of the most complex models, that includes broad range of effects which could influence the separation process. It is nevertheless very common to use simpler models, which could exclude the temperature change, and consequently the energy balance equation (what is justified, for example, in the case of diluted systems), or which describe the mass balance with the ideal or equilibrium dispersive model.

For a PSA process it is needed to describe the change of the pressure with time during the pressurization and blowdown steps. If there is no possibility to measure these variations experimentally, one has to use approximations. The most often encountered ones are the linear and exponential change.

Each of the PSA steps has its own initial and boundary conditions. For the first step (pressurization usually) of the first cycle we have to define the initial values, while for the subsequent steps the condition at the beginning is equal to the condition at the end of the previous step. Boundary conditions depend on the process configuration and the feed mixture. One example is given in Table 2.3. It corresponds to the 4-step PSA process shown in Figure 2.13. Boundary conditions are given for the positions  $z = 0$ , that corresponds to the column inlet looking in the co-current direction (direction during the adsorption step), and  $z = L$ , which is column outlet observed from the same direction (Figure 2.17).

Table 2.3. An example of boundary conditions for the 4-step PSA shown in Figure 2.13. Here pressurization is applied to the feed mixture of the same content as in the adsorption step.

|     | Pressurization                         | Adsorption                             | Blowdown                               | Desorption                             |
|-----|--|--|--|--|
| $y$ | $\partial y_i / \partial z _{z=0} = 0$ | $y_i _{z=0} = y_{feed,i}$              | $\partial y_i / \partial z _{z=0} = 0$ | $\partial y_i / \partial z _{z=0} = 0$ |
|     | $y_i _{z=L} = y_{feed,i}$              | $\partial y_i / \partial z _{z=L} = 0$ | $\partial y_i / \partial z _{z=L} = 0$ | $y_i _{z=L} = y_{des,i}$               |
| $u$ | $u _{z=0} = 0$                         | $u _{z=0} = u_{feed}$                  | $\partial u / \partial z _{z=0} = 0$   | $\partial u / \partial z _{z=0} = 0$   |
|     | $\partial u / \partial z _{z=L} = 0$   | $\partial u / \partial z _{z=L} = 0$   | $u _{z=L} = 0$                         | $u _{z=L} = u_{des}$                   |
| $T$ | $\partial T / \partial z _{z=0} = 0$   | $T _{z=0} = T_{feed}$                  | $\partial T / \partial z _{z=0} = 0$   | $\partial T / \partial z _{z=0} = 0$   |
|     | $T _{z=L} = T_{feed}$                  | $\partial T / \partial z _{z=L} = 0$   | $\partial T / \partial z _{z=L} = 0$   | $T _{z=L} = T_{des}$                   |

The meaning of the parameters from Table 2.3 is as follows:  $y_{feed}$  – mole fraction in the feed,  $u_{feed}$  – feed velocity,  $T_{feed}$  – feed temperature,  $y_{des}$  – mole fraction in the desorption mixture,  $u_{des}$  – desorption velocity,  $T_{des}$  – desorption temperature.

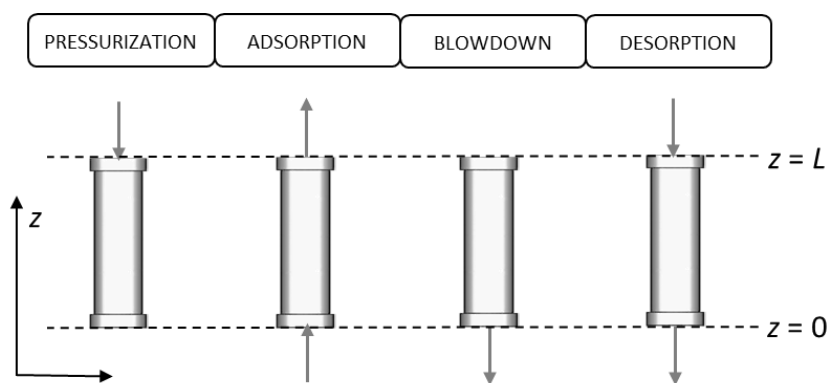


Figure 2.17. PSA process showing the direction of  $z$ -coordinate (with marked  $z = 0$  and  $z = L$  positions).

Optimization plays an important role in the PSA design. A large number of parameters can be manipulated in order to provide the optimal process performance. The selection of a suitable adsorbent is the most important task. After it, the further steps involve determination of the optimal column size and the operation parameters, like pressures, temperature, flowrates for different steps, and step times. In this work only parametric study was performed in order to identify the values that provide the best process performance, without implementing the detailed optimization procedures. The analysis of the PSA process to separate enantiomers of the anaesthetic gases is given in Chapter 8, section 8.4.



### **3 Derivation of specific methods for determining the adsorption isotherms**

There are different methods to determine the adsorption isotherms, as shown in the section 2.4.2. Very often it is challenging to choose the appropriate one since each of them has number of advantages and disadvantages. Difficulties can arise when chiral substances are investigated. The main reasons for this are limited (or none) access to pure components and the fact that physico-chemical properties of these substances are identical. Due to this, most of detectors produce the same signals for the both components, what in many cases makes the calibration procedure more complicated. In other cases, as it will be seen later in this section, that provides a faster way to transfer the signal into concentration values.

The main substances examined in this work are fluorinated anaesthetics, from which we only have racemic mixtures available. Both enantiomers always provide the same intensity of the detector signal and therefore we can only perform the calibration using the column response of the complete mixture. Taking all of this into account, it was necessary to look for methods that do not require pure substances and which at the same time provide fast results without consuming larger solute amounts.

One of the convenient methods that can be used for estimating the adsorption isotherms from racemic mixtures is the nonlinear frequency response method. This method can properly work only with mixtures requiring small amounts of pure substances for the detector calibration purpose. It can be successfully applied for bicalutamide [16] (one of the substances investigated here). When it is used for chiral substances, two types of detectors are needed, from which one should be polarimeter in order to provide difference between the signals of the two enantiomers. Since the use of polarimeters is not suitable for gases and the method requires certain amounts of pure components, it was not possible to apply it for the anaesthetics. Therefore, it will not be explained in this work. More details can be found in [16].

In this thesis two other methods will be developed. The first one is the new extension of the ECP method for a two-component system, whose adsorption can be described with Langmuir isotherms. The method is established in this thesis from the existing analytical expressions for the elution profile. The binary-mixture ECP is fast and simple; however it can be applied only when very efficient columns are used. For that reason another method was applied too. It is the peak-fitting method, which was not developed here, but only examined and adapted for the studied systems. Both methods belong to the group of inverse methods, which determine the process parameters, such as adsorption isotherms by using the existing experimental elution profiles, in contrary to direct conventional way to simulate a chromatogram by utilizing the experimentally obtained parameters (Figure 3.1).

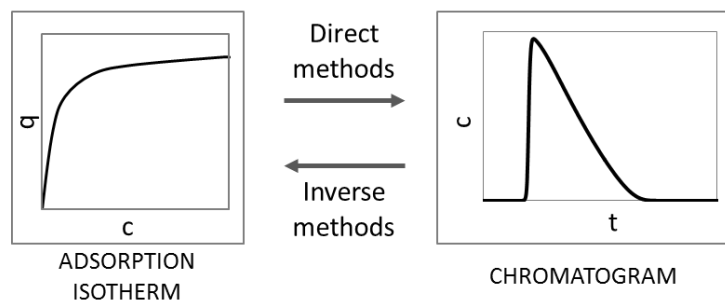


Figure 3.1. Schematic representation of direct methods (simulation of a chromatogram by knowing the adsorption isotherm) and inverse methods (estimation of adsorption isotherm from the recorded chromatogram).

In the following sections the two mentioned methods will be clarified and analysed in terms of their applicability, advantages and drawbacks.

### 3.1 Development of extended elution by characteristic point method (ECP) for estimating competitive Langmuir isotherms

In this section the development of the ECP method for a binary mixture will be described. It is derived from the analytical solution of the ideal model of chromatography (equilibrium theory), like the single-component ECP. In the first part of this section the brief introduction of the known ECP method for one-component systems will be given, followed by the derivation of the equations for the two-component mixture ECP and the description of the new method. The method development will be also presented in the planned future publication [74].

#### 3.1.1 Well-known ECP for single component adsorption isotherms

As introduced in the section 2.4.2, elution by characteristic point (ECP) represents a very fast and convenient method to determine adsorption isotherm parameters. The method was developed by Cremer and Huber [75], originating from the work of Glueckauf [76]. At the beginning, it was only used for Langmuir-type isotherms (convex, without inflection points), but it was adjusted and applied for determination of other isotherm types as well [77]. The ECP method allows calculation of the isotherm parameters from the diffusive part of the elution profile. It is sufficient to work with just one profile, from a single injection, taking into account that the injected sample should be large enough to provide the operation in the nonlinear range (unsymmetrical elution profile). An example of injection of a substance with Langmuir isotherm used in ECP method is presented in Figure 3.2. For this isotherm type the rear part of the overloaded profile, which is in this case the diffusive part, is used. This is the most frequent type of the isotherm and the one that will be considered in the further discussion.

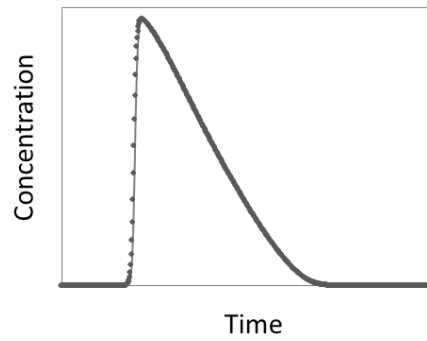


Figure 3.2. An example of elution profile (one component, Langmuir-type isotherm) that can be used for the elution by characteristic point method.

The ECP method is directly derived from the ideal model of chromatography (presented earlier by eq. (2.14)), known also as equilibrium theory. The solution of this theory for the case of intermediate-size pulse injections (injections in the nonlinear isotherm range) can be used for determination of adsorption isotherm parameters (as described in more details in [38]). The following equation provided from equilibrium theory can be formulated:

$$V_R = V_{inj} + V_0 \left( 1 + \frac{V_{ads}}{V_0} \frac{dq}{dc} \right) = V_{inj} + V_0 \left( 1 + \frac{(1-\varepsilon)V}{\varepsilon V} \frac{dq}{dc} \right) \quad (3.1)$$

It is the same equation as the one used for peak maxima method (eq. (2.41)), only multiplied by the volumetric flowrate. Here,  $V_R$  stands for retention volume,  $V_{inj}$  for injected volume,  $V_0$  for column hold-up volume (volume available for the fluid phase), and  $V_{ads}$  for adsorbent volume. This equation is valid for isotherm types that have the shape of Langmuir isotherm. The expression for a system with anti-Langmuir isotherm (concave, without inflection points), for example, does not contain  $V_{inj}$  term, since in that case the diffusive part of the elution profile is its front part.

The eq. (3.1) can be solved [77] by integration:

$$q = \frac{1}{(1-\varepsilon)V} \int_0^c (V_R - V_{inj} - \varepsilon V) dc \quad (3.2)$$

or by expressing the isotherm slope:

$$\frac{dq}{dc} = \frac{V_R - V_{inj} - V_0}{\frac{1-\varepsilon}{\varepsilon} V_0} \quad (3.3)$$

Taking into account that  $t = V/Q$  ( $Q$  – volumetric flowrate), where  $t$  can be  $t_R$ ,  $t_{inj}$  and  $t_0$  and  $V$  stands for  $V_R$ ,  $V_{inj}$  and  $V_0$ , we can also write:

$$\frac{dq}{dc} = \frac{t_R - t_{inj} - t_0}{\frac{1-\varepsilon}{\varepsilon} t_0} \quad (3.4)$$

The term  $dq/dc$  can be easily derived from an adsorption isotherm expression. For the Langmuir isotherm (eq. (2.31)) it is:

$$\left. \frac{dq}{dc} \right|_c = \frac{H}{(1+bc)^2} \quad (3.5)$$

The isotherm parameters are calculated by combining the previous two equations and minimizing the objective function that contains the differences between experimental (eq. (3.4)) and calculated (eq. (3.5)) values of  $dq/dc$  for all the measured points, in the same way as it will be shown later for the binary-mixture ECP method.

### 3.1.2 New extension of the elution by characteristic point method

In this section a new extended ECP method for analysing binary mixture chromatograms will be presented. As shown previously, ECP method is very simple and can be easily applied for isotherm determination if pure substances are available, but there is a problem when we have no access to single components. In that case equilibrium theory (ideal model of chromatography), from which also ECP method is derived, can provide a tool for calculating the parameters. An extensive overview of the ideal model of chromatography (described in chapter 2, section 2.2.1) with its origins and development is given in [78].

Golshan-Shirazi and Guiochon have derived the analytical expressions that describe the whole elution profile when the substances are adsorbed according to Langmuir isotherm. Although it is not completely realistic, since it assumes infinitely efficient column, it is expressed by simple algebraic equations and can serve as a very good first approximation. The exact solution for narrow rectangular injection of one-component can be found in [79]. It was later experimentally validated by comparing real chromatograms with the simulation results obtained by using the developed equations [80]. In the case of a single component there are also analytical solutions for the general isotherm without inflection point (comprising both, Langmuir and anti-Langmuir isotherm) [81], as well as for the Bi-Langmuir model [82].

There are also available analytical solutions for binary mixtures with competitive Langmuir isotherms published by Golshan-Shirazi and Guiochon. For an elution profile with no completely resolved bands, they derived the same equations in two ways, firstly [83] by using the characteristic method of Rhee et. al. [84], and then [85] by  $h$ -transform [86]. All the work done on development of these solutions and their possible applications is reviewed in [11]



and [87]. The solution of an elution profile originating from narrow injection of a binary mixture will be briefly described here.

As already stated, the solution is derived for the ideal equilibrium model (eq. (2.14)). At the beginning the column is filled only with mobile phase, and then starts an injection of a rectangular pulse with the width  $t_{inj}$  and height  $c_{feed} = c_{feed,1} + c_{feed,2}$ . Therefore initial ( $t = 0$ ) and boundary ( $z = 0$ ) conditions are as follows:

$$c_1(z, t = 0) = c_2(z, t = 0) = 0 \quad (3.6)$$

$$\begin{aligned} c_1(z = 0, t) = c_{feed,1}, \quad c_2(z = 0, t) = c_{feed,2}, \quad \text{for } 0 < t \leq t_{inj} \\ c_1(z = 0, t) = c_2(z = 0, t) = 0, \quad \text{for } t > t_{inj} \end{aligned} \quad (3.7)$$

The chromatogram with incomplete band resolution has three zones (I, II and III), as can be observed in Figure 3.3. The first zone contains pure first eluting component (component 1). It is situated between two shocks that appear at the front of each component elution profile. The second zone represents the mixed zone and contains both components. It starts with the shock of the second component (component 2) and ends with complete elution of the first component. The third zone contains only the second component. It starts with a plateau, which is a consequence of the ‘‘tag-along’’ effect [88].

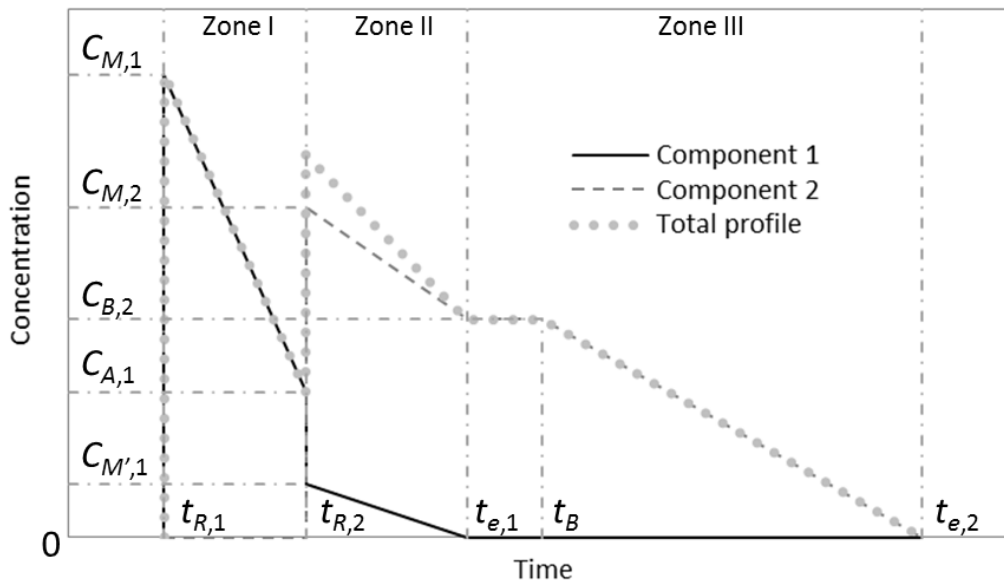


Figure 3.3. Schematic representation of the solution of the ideal model of chromatography for pulse injection of a binary mixture with Langmuir isotherms. Three separation zones (I, II and III) explained in the previous text are marked. The symbols used for defining the specific concentration and time points are given in the upcoming paragraphs.

The analytical solution comprises the equations for each point of the chromatogram, as well as for its continuous parts. There are in total 14 points and expressions (demonstrated in Figure 3.3), classified in three groups:

- 1) Specific retention times
  1. Retention time of the first shock:  $t_{R,1}$
  2. Retention time of the second shock:  $t_{R,2}$
  3. End of the first component band (complete elution of component 1) and start of component 2 concentration plateau:  $t_{e,1}$
  4. End of component 2 concentration plateau:  $t_B$
  5. End of the second component band (complete elution of component 2):  $t_{e,2}$
- 2) Specific concentrations
  6. Maximum concentration of component 1:  $C_{M,1}$
  7. Maximum concentration of the second component:  $C_{M,2}$
  8. Concentration of the first component on the front side of the second shock:  $C_{A,1}$
  9. Concentration of the first component on the rear side of the second shock:  $C_{M',1}$
  10. Concentration at component 2 plateau:  $C_{B,2}$
- 3) Continuous parts of the chromatogram
  11. First arc of component 1 band (in the zone I)
  12. Second arc of component 1 band (in the zone II)
  13. First arc of component 2 band (in the zone II)
  14. Second arc of component 2 band (in the zone III)

For application of the binary-mixture ECP only the equations for the continuous parts of the elution profile are needed. The expressions that describe the profile are taken from the literature [11, 87] and are shown in Appendix B. These equations have been transformed in the frame of this work into expressions that would serve for calculating the parameters of competitive Langmuir isotherm. In the literature the solutions are expressed as a function of concentration from time, except for the first arc of the component 1, where no explicit solution in the form  $c = f(t)$  was possible.

In order to make the equations which define the continuous parts of a chromatogram uniform, for the purpose of the binary-mixture ECP method, they were all expressed as retention time being a function of concentration. The process of deriving the equations for calculating the isotherm parameters is presented in Appendix B. The resulting expressions that describe the elution profiles of both components are given by the following equations:

$$t_{R,1}^I(c_1) = t_{inj} + t_0 + t_0 H_1 F \left( \frac{1}{(1 + b_1 c_1)^2} - \frac{b_2 c_2^{feed} t_{inj} (H_2 - H_1)}{t_0 H_2^2 F \left( \frac{H_2 - H_1}{H_2} + b_1 c_1 \right)^2} \right) \quad (3.8)$$

$$t_{R,1}^{\text{II}}(c_1) = t_{inj} + t_0 + \frac{t_0 H_1 F \left( b_1 r_1 + \frac{H_1 b_2}{H_2} \right)}{(b_1 r_1 + b_2) \left( 1 + b_1 c_1 + \frac{H_1 b_2 c_1}{r_1 H_2} \right)^2} \quad (3.9)$$

$$t_{R,2}^{\text{II}}(c_2) = t_{inj} + t_0 + \frac{t_0 H_2 F \left( \frac{b_1 r_1 H_2}{H_1} + b_2 \right)}{(b_1 r_1 + b_2) \left( 1 + b_2 c_2 + \frac{H_2 b_1 c_2 r_1}{H_1} \right)^2} \quad (3.10)$$

$$t_{R,2}^{\text{III}}(c_2) = t_{inj} + t_0 + \frac{t_0 H_2 F}{(1 + b_2 c_2)^2} \quad (3.11)$$

Here  $t_{R,1}^{\text{I}}(c_1)$  and  $t_{R,1}^{\text{II}}(c_1)$  correspond to the retention time functions for the first component in the zone I and II (for the first and the second arc of component 1), while  $t_{R,2}^{\text{II}}(c_2)$  and  $t_{R,2}^{\text{III}}(c_2)$  are the retention times for the second component in the zones II and III (the first and the second arc of component 2). The variables  $c_1$  and  $c_2$  stand for the concentration points of the part of the elution profile that corresponds to the pure component 1 and 2, respectively. The parameter  $r_1$  is defined in Appendix B.

The idea of the ECP method for a binary mixture is to use just two characteristic segments of the chromatogram where the components are found in the pure form. Those are the segments in the zone I for the component 1 and in the zone III for component 2, as shown in Figure 3.4 with dash-dotted ellipses. Therefore the only equations needed for the adsorption isotherm determination are those for  $t_{R,1}^{\text{I}}(c_1)$  (eq. (3.8)) and  $t_{R,2}^{\text{III}}(c_2)$  (eq. (3.11)). These two expressions can be applied to solve the so-called inverse problem, which means to determine the competitive Langmuir isotherm (eq. (2.33)) parameters  $b_i$  and  $H_i$  ( $i = 1, 2$ ) when we have available the experimental elution profile (time as a function of concentration).

As it can be observed in Figure 3.4, the length of the segments suitable for the method application decreases as the column efficiency is reduced, since the bands are less sharp and not well-defined any more. The data closer to the start and the end of the characteristic sections are more affected by the band broadening than those in the middle and can therefore not predict the isotherms correctly. To get the right results, it is important to choose the proper data range of the used sections. This will be discussed in Chapter 7.

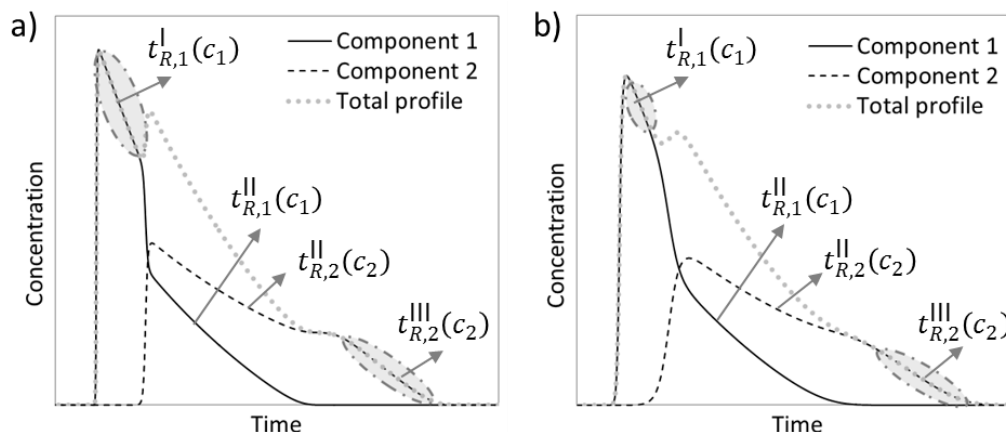


Figure 3.4. Elution profiles with indicated parts for which the analytical expressions – equations (3.8)-(3.11) – are derived (in the form of time as a function of concentration) and marked segments that are used for application of the binary-mixture ECP method (dash-dotted-line ellipses): a) Ideal profile characteristic for the very efficient columns (with more than 10,000 theoretical plates); b) More realistic profile, typical for less efficient columns.

To obtain the values of the isotherm parameters, we need to solve the optimization problem, i.e. to minimize the following objective function, which contains the difference between the experimentally measured retention times ( $t_{R,i}^{exp}$ ) and the ones calculated ( $t_{R,i}^{calc}$ ) by equations (3.8) and (3.11):

$$OF_i = \sum_{j=1}^{n_p} \left( \left( t_{R,i}^{exp} \right)_j - \left( t_{R,i}^{calc} \right)_j \right)^2, \quad i = 1, 2 \quad (3.12)$$

This objective function represents the sum of the squared errors between the real and calculated values for all the experimental points ( $n_p$  – number of points). The optimizer used for solving this problem searches for the parameter values until it obtains the minimal value of  $OF$ .

Calculation of the isotherm parameters in this way is very simple, like for the single-component ECP method. However there are many limitations for its application. The main one is that it can be used only for components that obey Langmuir isotherm model. The second important limitation is that, since it is developed from the ideal model of chromatography, it can be applied just for the systems whose behaviour can be approximated to that model. This means that the good results will be obtained only in the case of efficient columns. Another disadvantage is that, as it is an inverse method, it just gives the adsorption isotherm parameters and no other information about the adsorption (like the isotherm shape, mass transfer parameters or dispersion coefficient).

Even by taking into account all the previously listed limitations, there are numerous cases when the two-component ECP method can be used. Langmuir isotherm is the most frequently encountered adsorption model, which gives lot of possibilities for this method to be applied successfully. The problem with the column efficiency can be solved by using columns with

higher number of theoretical plates. The trend nowadays is the increased use of stationary phases with smaller particles, which can provide near ideal conditions needed for this method. For the columns with low efficiency, the method cannot give correct values, but it can serve to provide initial guesses of the parameters. These approximate values could further be used for methods such as peak fitting (described in the following section) and in that way to reduce the calculation times.

The most important advantage of the method is that it requires very small amount of solutes, since only few or even just one overloaded injection that provides operation in the nonlinear isotherm range, is necessary for the isotherm determination. For the same reason, also the amount of experimental and computational time and effort needed for obtaining the whole isotherm is very low. The method works only with mixtures and does not require pure components. However, there is a need to calibrate the detector. In our case, we work with enantiomers, which give identical detector signal and therefore the mixture can be used for calibration, i.e. no single components are necessary to be provided. For that reason it is advisable to use this method when working with enantiomers or in general for the case when exactly the same signal for both components can be obtained.

The binary-mixture ECP method will be tested and analysed in more details in Chapter 7. It represents a valuable isotherm determination method when only small amounts of the solutes are available for predictions of chromatographic separation performance, as in the case of enantiomers.

### 3.2 Analysis of the peak-fitting method for racemic mixtures

For an efficient column there are more possibilities when it comes to the task of choosing the appropriate method for isotherm determination, but it is more problematic when only small amounts of the mixtures (with no pure components) are available for separation in a column with low number of theoretical plates. In such a situation, which has been considered in this work, the easiest method that could be used for isotherm determination is the peak-fitting (inverse) method (introduced in section 2.4.2). In comparison to the ECP method, peak fitting requires one additional parameter to be calculated and that is the dispersion coefficient, i.e. the (finite) number of theoretical plates.

The peak-fitting method was first time employed by Dose et al. [47] for one component isotherm determination. They investigated adsorption of *N*-benzyl-L-alanine and *N*-benzyl-D-alanine on immobilized bovine serum albumin. Antos et al. [89] worked on separation of dilone acetate and benzophenone, where this method was used to estimate the isotherms from experiments with a mixture. However in that case the binary-mixture elution profile contained two separated peaks. In the study of James et al. [90] the peak-fitting method was applied for determination of competitive isotherms of ketoprofen enantiomers on a Chiracel OJ column. Single bands were determined by collecting fractions of the eluent and analysing

their content. Felinger et al. [50] determined isotherms of 1-indanol enantiomers in a mixture without knowing the single bands and by estimating the parameters of single component isotherms using pure substances. Forssen et al. [91] presented a set of improvements to be implemented in the computational part and for processing the experimental data.

When applying the peak-fitting method, one estimates the isotherm parameters numerically by solving several times the set of partial differential equations forming the column model [11] and by minimizing the errors between the simulated and real (experimental) profiles. The method requires initial estimates of the parameters. These estimates could be assumed, or, in order to reduce the computational time, calculated using some of the simple and fast methods like already described ECP. Experiments consist of one or few injections with the sample amount large enough to provide nonlinear conditions. When working with mixtures, the sample size has to be chosen properly to provide the needed competitive data (Figure 3.5). On one hand, if the sample size is too small, the two peaks resulting from two substances will be completely separated and, since in that case there is almost no interference between the components, no proper data about competitive behaviour could be obtained. Another problem in that case is that the concentrations of the solutes are lower and the isotherms can be estimated only for a small concentration range. On the other hand, when the injected amount is too large, it will provide larger concentration range for isotherm estimation, but can at the same time lead to a very low degree of separation (or even no separation), so that there is no information about the rear part of the elution profile of the first-eluting component. Therefore, usually more than one profile of different injection volumes or concentrations are used for the estimation procedure.

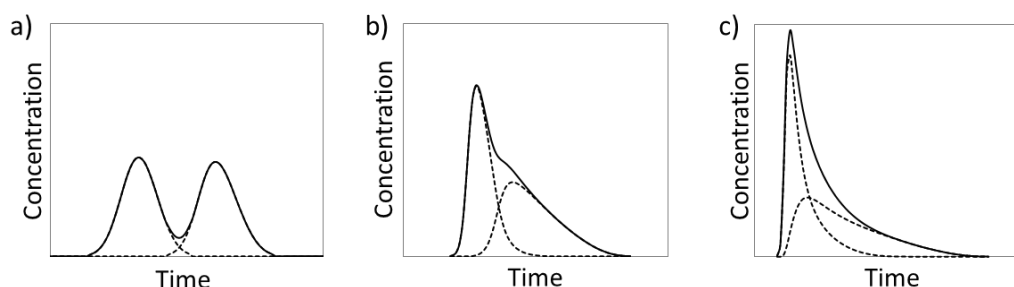


Figure 3.5. Three examples of binary-mixture elution profiles resulting from different injected volumes: a) Very small injection amount, which provides almost complete separation of the components and gives the profile that could only be used for providing the single component information; b) Proper injection amount for determining the competitive isotherms of both components with peak-fitting method; c) Too large injection amount that cannot provide correct data for the first eluting component.

The key requirement in the determination process is to select the isotherm and the column model (such as those given in section 2.2) before starting the calculation procedure. Then, having provided the initial values of isotherm parameters (assumed or pre-calculated), we simulate the corresponding elution profile or profiles. A computer optimization routine is applied to compare the calculated ( $c^{calc}$ ) and experimental ( $c^{exp}$ ) chromatograms and to minimize the differences between them. The objective function used in this procedure is:

$$OF = \sum_{j'}^{n_{elut}} \sum_j^{n_p} (c_{j,j'}^{exp} - c_{j,j'}^{calc})^2 \quad (3.13)$$

The number  $n_p$  represents the number of experimental points  $j$  and  $n_{elut}$  number of the elution profiles  $j'$  involved in the calculation process. After the minimization procedure, one obtains the best set of isotherm parameters.

Like in the case of binary-mixture ECP method, the application of the peak-fitting method encounters the difficulties with detector calibration. Except for enantiomers, when the mixture can be used for this purpose without complications, the easiest way to determine the profile concentration is to collect fractions of the column outlet stream and to later determine their concentrations. Another possibility would be to use single components to compute the calibration curves for each substance. For an UV detector, the signal can be recorded at two different wavelengths at which the components have different absorbance and then to combine these measurements for calculation of the exact concentration of each component.

Apart from the already discussed drawbacks that this method experiences, another disadvantage is the same as for the ECP: it just provides the best fit of the isotherm parameters to the experimental elution profile, without giving any insight into the isotherm shape. Still, it is very often used, since it was shown that its results can provide good predictions of the real processes. It allows rapid estimation of the parameters without requiring large solute amounts, so it is especially favourable for rare or expensive substances, as well as in the cases when no complete separation of components is possible. In comparison to the binary-mixture ECP method, the peak-fitting requires larger amounts of substances and more computational effort, but on the other hand it can be applied for any isotherm shape. By choosing the proper column model, it can take into account the column low efficiency and can estimate not just the isotherms, but also other parameters, such as mass transfer coefficient, or the number of theoretical plates.

As already mentioned, it is considered that for more precise results the objective function  $OF$  should contain the sums for different elution profiles. Moreover, it should include profiles of pure substances and for different ratios of the components in the mixture. If that is not possible, at least the exact shape of the profiles for each substance should be previously determined. There are, though, examples, like in [92], which show that the method could also be applied to racemic mixtures, when there is no possibility to change the ratio between the components and to provide pure enantiomers. In this work that case is checked further, since it is the one that corresponds to the investigated substances, the fluorinated anaesthetic gases. The possibility to successfully apply the peak-fitting method when we have only available restricted amounts of a 1:1 mixture is investigated. The method application for two types of chiral systems in liquid and gaseous phase is given in Chapter 7.





## **4 Simplified concept for performance analysis, scale-up and product capture**

In this chapter the simplified way to analyse the gas-phase separation of enantiomers is presented. For gaseous systems, when the adsorbed species is present in the large excess of the carrier gas, the change of the gas velocity due to adsorption and desorption (described in the section 2.3 of Chapter 2) is very small and can be neglected. Moreover, if the pressure drop through the bed is not significant, then the pressure can be assumed to be constant, as well as the gas velocity [13]. This simplifies the chromatographic model and reduces importantly the computing time. The separation of the anaesthetic gases in a GC single-column system represents a diluted system with small pressure-drop, as it will be shown in the experimental part (section 6.1.2). Therefore for investigating purposes, relations that require less parameters and much shorter experimental and computational times were chosen. In order to validate the assumptions, the results from this simplified concept were compared to the experimental data (this part is shown in Chapter 8).

This chapter is divided into three parts. The first part consists of the study of process performance (purity, recovery and productivity). The goal is to determine the input parameters, which would provide the highest possible productivity of the pure enantiomers. In the second part the possibilities of performing the separation in larger columns are discussed by applying a simple scale-up procedure. The predictions and assumptions are later experimentally validated. The third part of this chapter briefly introduces the process that would follow the separation procedure. It comprises capture and storage of pure substances in order to isolate them from the carrier gas and to prepare them for the subsequent use.

### **4.1 Process performance analysis**

Estimation of the process performance characteristics [10, 93, 94] is an important task for evaluation of the separation and for the comparison with other developed processes. In order to obtain the best performance of a chromatographic separation, one usually needs to use a trade-off approach. It is known that in order to get the higher productivity, it is necessary to sacrifice purity or recovery. The same applies for the other two parameters. Depending on the requirements of our process, we need to find the optimal relation between purity, recovery and productivity (Figure 4.1). If the substances are not needed at very high purity, or if there is purification process available that is inexpensive, in comparison to the chromatography, then the productivity should be maximized. In another scenario, when product is needed in pure form, which has much higher value than the mixture, recovery is sacrificed.

For the target system discussed in this work, the fluorinated anaesthetics, the available racemic mixtures are considered much less valuable than the pure enantiomers and the goal was to focus on obtaining the highest possible purity and productivity.



Figure 4.1. Trade-off between productivity, purity and recovery to provide the optimal process performance.

Purity ( $PU_i$ ) of the certain component ( $i, i = 1, 2, \dots, n$ ) represents the fraction of amount of that component in the whole collected substance(s). Therefore, we can express it as the collected amount of the examined substance over the complete collected amount. The most common way to evaluate the collected amount is by using the mass of the component or components ( $m_{coll}$ ). Accordingly, the purity can be determined as follows:

$$PU_i = \frac{m_{coll,i}}{\sum_{j=1}^n m_{coll,j}} \quad (4.1)$$

Related to purity, in chiral systems a parameter that is commonly calculated is enantiomeric excess ( $ee$ ). For the component present in larger amount in the collected sample (e.g. R-enantiomer) enantiomeric excess is expressed as:

$$ee_R = \frac{m_{coll,R} - m_{coll,S}}{m_{coll,R} + m_{coll,S}} \quad (4.2)$$

Recovery or yield ( $RE_i$ ) of a component ( $i$ ) is the ratio of the amount of the component collected in the purified fraction ( $m_{coll,i}$ ) and the total amount of this component injected with the feed mixture ( $m_{feed,i}$ ):

$$RE_i = \frac{m_{coll,i}}{m_{feed,i}} \quad (4.3)$$

Productivity or production rate can be defined in different ways. It represents the amount of the isolated substance ( $m_{coll,i}$ ) at certain purity produced per unit of time. For the chromatographic process the time for which the production is evaluated is the cycle time

( $t_{cycle}$ ). In the batch process we take that the cycle time is the interval needed for one injection. Then the production rate for a given column (denoted as  $PR_i^*$ ) is:

$$PR_i^* = \frac{m_{coll,i}}{t_{cycle}} \quad (4.4)$$

Productivity can also be expressed as a more universal, normalized, value ( $PR_i$ ) by dividing the collected substance amount by the cycle time and the adsorbent volume ( $V_{ads}$ ) or mass ( $m_{ads}$ ). Taking the definition of the adsorbent volume as:

$$V_{ads} = (1 - \varepsilon)V = (1 - \varepsilon)d^2\pi L/4 \quad (4.5)$$

(with  $V$  as a column volume,  $d$  its inner diameter and  $L$  the length), the productivity is expressed in the following way:

$$PR_i = \frac{m_{coll,i}}{t_{cycle}V_{ads}} \quad (4.6)$$

This representation of the production rate is more suitable for comparison of the performance of a certain process to other processes' performances or even for the same separation, but just when columns of different sizes are used. In this work the productivity given per adsorbent volume is applied.

For expressing and calculating the process performance characteristics, the important terms are the cut times. Those are the times that define the intervals at which the components in pure form can be collected. For each substance  $i$  there is the starting ( $t_{s,i}$ ) and ending ( $t_{e,i}$ ) cut time, as shown in Figure 4.2. The time  $t_{s,1}$  represents the starting point for collecting component 1 and it is the time when this component starts to elute. This time is therefore the start of the chromatogram. For a two component system, considered in this work, the last cut time ( $t_{e,2}$ ) is the time when collection of component 2, as well as the whole chromatogram, is completed.

Theoretically the cut time  $t_{s,1}$  represents the moment when the concentration changes from zero to a positive, greater than zero, value, while  $t_{e,2}$  is the moment when it reaches zero again. In praxis, since there is always present noise and fluctuations of the concentration value, the starting and ending cut times are defined as times when the concentration increases above or decreases below a certain threshold value, which represents the detector sensitivity. During experiments only concentrations that exceed the threshold value can be detected. In the simulation typical concentration threshold value is 1 % of the maximal concentration achieved.

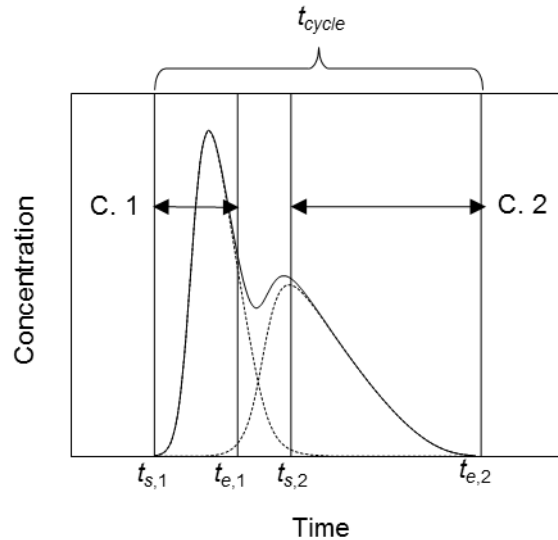


Figure 4.2. Representation of a binary-mixture elution profile with defined cycle time and the cut times ( $t_s$  – starting cut time, and  $t_e$  – ending cut time), between which the pure substances (C. 1 – first and C. 2 – second eluted component) can be collected.

The ending cut time for the first component ( $t_{e,1}$ ) is the time when collection of component 1 stops, because component 2 starts eluting. The starting cut time for the second component ( $t_{s,2}$ ) represents the time when component 2 begins to be collected. That is the moment when component 1 is completely eluted. These two cut times ( $t_{e,1}$  and  $t_{s,2}$ ) are determined in a way to provide that some of the parameters, such as purities of the collected fractions, are higher than certain required values. The difference between the first ( $t_{s,1}$ ) and the last ( $t_{e,2}$ ) cut time is the cycle time ( $t_{cycle}$ ), as demonstrated in Figure 4.2. It is the duration of the elution resulting from one injection into the column.

The amount  $m_{coll,i}$  is the mass of the substance  $i$  that is collected between starting and ending cut time, so it is expressed as:

$$m_{coll,i} = \int_{t_{s,i}}^{t_{e,i}} Q_m dt = \int_{t_{s,i}}^{t_{e,i}} Q c_i(t) dt = \varepsilon \frac{d^2 \pi}{4} \int_{t_{s,i}}^{t_{e,i}} u c_i(t) dt \quad (4.7)$$

where  $Q_m$  is the mass flowrate,  $Q$  is the volumetric flowrate,  $d$  column diameter and  $u$  interstitial velocity of the mobile phase.

In a PSA process the same equations are valid, but instead of cut times the starting and finishing time of a step are used. For the PSA configuration explained in the sections 2.5.2.1 (Figure 2.13) and 2.5.2.2 the pure component 1 is being collected during the adsorption step, while the pure second component is obtained from the desorption step. The both components are fed in column in the adsorption step. Then, by considering the expression for the concentration in the gas phase (eq. (2.48) and (2.52)) and if we take that each step starts at  $t = 0$  and ends at  $t = t_{step}$ , where  $t_{step}$  is a certain step duration (for the adsorption it is  $t_{ads}$ , for

desorption  $t_{des}$ , for pressurization  $t_{press}$  and for blowdown  $t_{blow}$ ), we can calculate purity, recovery and productivity of the components 1 and 2 as follows:

$$PU_1 = \frac{\int_0^{t_{ads}} (uPy_1/RT)_{z=L} dt}{\int_0^{t_{ads}} (uPy_1/RT)_{z=L} dt + \int_0^{t_{ads}} (uPy_2/RT)_{z=L} dt} \quad (4.8)$$

$$PU_2 = \frac{\int_0^{t_{des}} (uPy_2/RT)_{z=0} dt}{\int_0^{t_{des}} (uPy_1/RT)_{z=0} dt + \int_0^{t_{des}} (uPy_2/RT)_{z=0} dt} \quad (4.9)$$

$$RE_1 = \frac{\int_0^{t_{ads}} (uPy_1/RT)_{z=L} dt}{\int_0^{t_{ads}} (uPy_1/RT)_{z=0} dt} \quad (4.10)$$

$$RE_2 = \frac{\int_0^{t_{des}} (uPy_2/RT)_{z=0} dt}{\int_0^{t_{ads}} (uPy_2/RT)_{z=0} dt} \quad (4.11)$$

$$PR_1 = \frac{\int_0^{t_{ads}} \left( \varepsilon \frac{d^2 \pi}{4} uPy_1 / RT \right)_{z=L} dt}{t_{cycle} V_{ads}} \quad (4.12)$$

$$PR_2 = \frac{\int_0^{t_{des}} \left( \varepsilon \frac{d^2 \pi}{4} uPy_2 / RT \right)_{z=0} dt}{t_{cycle} V_{ads}} \quad (4.13)$$

In this case  $t_{cycle}$  is the sum of all four steps:

$$t_{cycle} = t_{press} + t_{ads} + t_{blow} + t_{des} \quad (4.14)$$

The most common goal of a separation process is to obtain the maximal possible production rate. In order to achieve it, different design and operating factors can be manipulated, such as stationary phase particle size, column dimensions, temperature, or the mobile phase flowrate. Higher flowrate provides shorter cycle times, but inhibits the column efficiency. Additional

problem is that it is often limited by the pump performance. Another important parameter that is easy to vary, is the amount of the injected substances (this will be discussed in Chapter 8). For a PSA process the possibilities to optimize the production rate are greater, since the separation depends on more parameters. Besides the mentioned ones, the most commonly used parameters in the optimization are the step times (especially for adsorption and desorption step), flowrates in single steps, and the values of the high and low pressure.

## 4.2 Chromatographic column scale-up

The ability to predict behaviour of a system on a different-scale level is very convenient in practice. In chromatography, scaling up is typically done in such a way that the same pattern of the chromatograms in the smaller and the larger column is maintained. To accomplish this, the two columns have to be equivalent, which means that the same stationary and mobile phase have to be used, as well as equal column lengths and linear mobile phase velocities [95]. Then the most common way to increase the column volume is to keep the same length and only to increase its diameter, as it is shown in Figure 4.3.

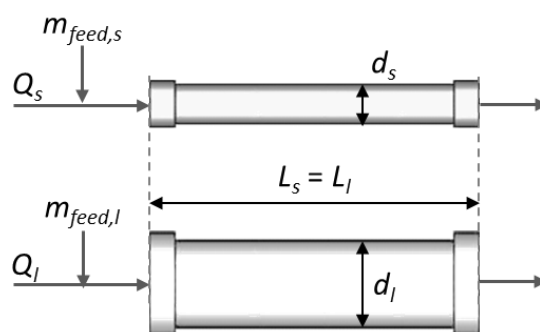


Figure 4.3. Representation of the scale-up procedure when the same column length ( $L$ ) is kept and the diameter ( $d$ ) is increased. Accordingly, the volumetric flowrate through the column ( $Q$ ) and the injected amount ( $m_{feed}$ ) have to be increased as well.

To keep the same patterns of the chromatograms in two different columns, one should provide the same number of theoretical plates for both. This means the following relation between the feed sample ( $V_{feed}$ ) and the column volume ( $V$ ) [95]:

$$\frac{V_{feed,l}}{V_{feed,s}} = \frac{V_l}{V_s} \quad (4.15)$$

The subscript  $l$  stands for the larger column and  $s$  for the smaller one. If the ratio between the larger and the smaller column volumes is denoted as scaling factor ( $SF$ ), then, by expressing the column volume in terms of its length and the diameter, we can get the following basic scale up equation:

$$SF = \frac{V_{feed,l}}{V_{feed,s}} = \frac{m_{feed,l}}{m_{feed,s}} = \frac{V_l}{V_s} = \frac{L_l d_l^2}{L_s d_s^2} \quad (4.16)$$

If we use the already mentioned well-established scale-up concept in preparative liquid chromatography to keep the same column lengths and to increase just the column diameters, this equation can be easily used to determine the sample size that has to be introduced into the larger column in order to provide the same separation performance. Since the mobile phase velocity needs to be the same in both columns, the volumetric flowrate ( $Q$ ) has to be increased due to the increase of the column diameter. Therefore, we come to the simple scale-up rule presented by the following equation [96, 97]:

$$SF = \frac{m_{feed,l}}{m_{feed,s}} = \frac{Q_l}{Q_s} = \left( \frac{d_l}{d_s} \right)^2 \quad (4.17)$$

In the case when the length of the column changes, to preserve the same efficiency in two columns, we need to change the velocity of the mobile phase accordingly. Dependency of the column plate height from the velocity is given by van Deemter equation (eq. (2.12)). When the velocity in the system is high, as it is common in preparative chromatography, the first two terms of the van Deemter equations (depending on parameters  $A$  and  $B$ ) can be neglected, which further gives the following relation (using equations (2.11) and (2.12)):

$$\frac{L}{u} = C \cdot NTP \quad (4.18)$$

Therefore, in order to have constant value of  $C \cdot NTP$ , the ratio  $L/u$  has to be kept equal in the two columns and the velocity needed in the larger column is calculated as:

$$u_l = \frac{L_l}{L_s} u_s \quad (4.19)$$

The previous equations are valid when we are able to use the same particle sizes in the both columns. If the particle size ( $d_p$ ) changes, it also influences the length of the column required for the scale-up. In realistic separations the common case is that the band spreading is dominated by pore diffusion, which gives the subsequent relation for the number of theoretical plates [12, 95]:

$$NTP \sim \frac{L}{u d_p^2} \quad (4.20)$$

as well as the equation which can be used for the scale-up process:

$$\frac{L_l}{u_l d_{p,l}^2} = \frac{L_s}{u_s d_{p,s}^2} \quad (4.21)$$

If the velocity in two columns is taken to be the same, the length of the larger bed is calculated as:

$$L_l = d_{p,l}^2 \frac{L_s}{d_{p,s}^2} \quad (4.22)$$

The presented equations can be correctly used only when the efficiency of the larger bed and its porosity are the same as for the smaller bed. In that case the elution profiles of the two columns should be identical. In practice this perfect match is a rare case, especially for the larger scale-up factors. This is mainly due to differences in packing of two columns and different influences of higher flowrate on peak broadening. For that reason, in order to obtain more correct results, the porosity for the larger column should be determined experimentally and that value used in simulation instead of the porosity of the small bed. Therefore, one should be aware that the simple rule given in eq. (4.17), and in other equations presented in this section, can be taken as a useful, but in some cases only a rough estimate to quantify the performance increase when using larger columns. In this work the increase of the column diameter was considered and the change of other parameters was estimated from eq. (4.17).

### 4.3 External capture of products after the separation

After the successful separation of a mixture, an important task is to find the optimal way to isolate the pure target substances from the mobile phase and to store them. The main process studied in this work concerns the separation of fluorinated anaesthetics. Since these substances are very volatile and obtained in a highly diluted form after the separation, one convenient way for their isolation and storage is the three-step procedure described in this section. This procedure is developed in collaboration with the parallel SPP1570 Subproject II (introduced in section 1.3).

In the previous studies on the separation of enantiomers of anaesthetic gases [71, 98-103] the condensation of the anaesthetics in cooling traps was performed directly after the separation (explained in more details later, in section 5.2.2). In that case, since the concentration of the anaesthetics in the outlet stream is very low, their partial pressure in the carrier gas is low as well. Thus, extreme cooling of the mixture must take place after the separation. To provide such conditions, liquid nitrogen was used for cooling, which introduces more complexity in the process design and increases the hazard potential. Because of the high dilution, the efficiency of the cooling traps operated in that way is not 100 %, since certain amounts of the products are lost in the process (as it is reported in [71]).



To overcome the mentioned disadvantages that existed in the previous works, in this project capture columns are introduced after the production process. In that way, the concentrated stream is obtained at the column outlet before the final product isolation in the cooling traps occurs. After desorbing the capture columns only small amounts of the carrier gas will be present in the outlet stream and therefore only moderate cooling (around 0 °C) is enough to provide the condensation of the anaesthetics [104]. In this manner, the condensation of the anaesthetic gases is provided in great extent by their high partial pressure, what makes the cooling process much more efficient.

In the first step the substances are adsorbed in the so-called capture columns until the columns are completely saturated. The capture columns serve for storing the substances and require only cheap unselective adsorbents. Here, they are denoted as non-selective columns. After the capture stage, in a second step, regeneration of the capture columns takes place, where streams with concentrated target substances are produced. The third step involves freezing out the enantiomers in cooling traps to finally separate them from the carrier gas.

The capture process in non-selective columns will be described in the next paragraphs. After the separation the resulting chromatogram contains three fractions, two with pure substances and the mixture fraction between them, as shown previously in Figure 4.2. The idea of the capture process is to use three columns (I, II and III) for storing each of these fractions. In the first column (capture column I) the first eluting fraction containing the pure first component will be stored. Then the outlet stream from the separation column will be sent to the second capture column (II) where the mixed fraction of the both components will be collected. At the end, the least fraction with the pure second component will be passed through the third capture column (III). The whole process can be presented by a scheme given in Figure 4.4.

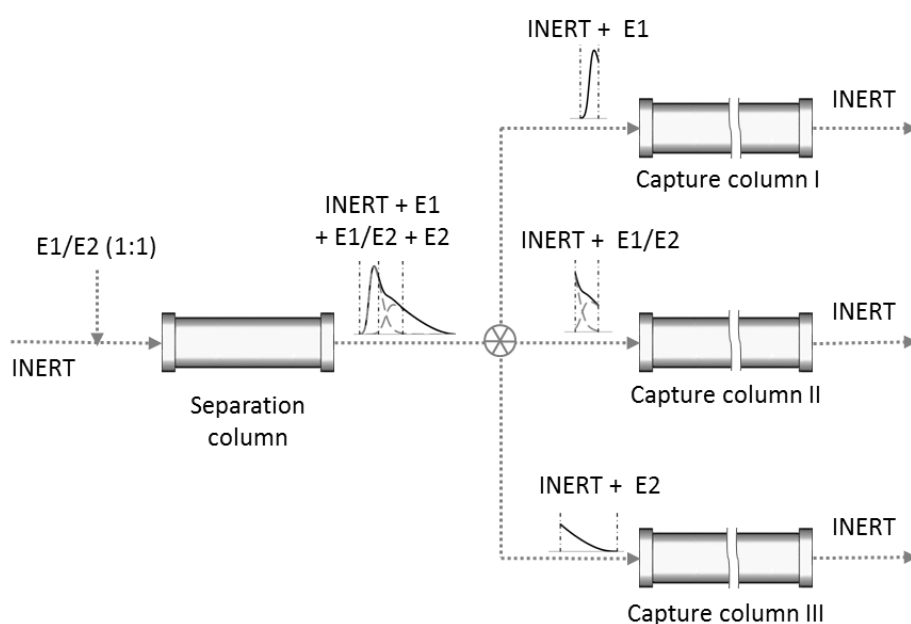


Figure 4.4. Schematically presented complete coupled production unit. It consists of one separation column and three capture columns for storing the three fractions resulting from the separation process. Here the inlet mixture is a racemate containing the E1 and E2 enantiomers.

The capacity of the capture columns should be large enough to provide storage for the substances during a certain desired period of time or for a wanted amount of pure components. To characterize these columns, one needs to specify their dimensions and the adsorbent used. In this case, there is no separation occurring, therefore we do not need costly selective adsorbents. In the literature there are various examples of different types of adsorbing materials that could be used for isolating racemic mixtures of fluorinated anaesthetics (e.g. [104-108]). A main requirement for the adsorbent is a high sorption capacity. If the diameter of all three capture columns is the same as the one of the separation column, then the only parameter that has to be determined is the length required for storing product from a wanted number of cycles.

The capturing procedure is illustrated in Figure 4.5. At the outlet of the separation column there is continuous flow and the chromatogram is composed of successive elution profiles. After the first cut time (starting cut time for the component 1) the outlet stream is directed to the capture column I. When the ending cut time of the first component is reached, the inlet flow in the capture column I is stopped and the stream from the separation column is directed into the capture column II. The stream flows into this column between the ending cut time of the first component and the starting cut time of the second component. Afterwards, between the starting and ending cut times of the component 2, the separation-column outlet flow is passed through the capture column III, where pure component 2 is stored. With this, one separation cycle ends, followed by the next cycle. The fractions are captured in the same way for all cycles.

At the inlet of a capture column one fraction comes after another in certain time intervals. For simplicity and due to the self-sharpening effect, these fractions can be approximated by rectangular profiles. In the columns they are “parked” one next to another until the column saturation has been reached.

After filling the capture columns completely, i.e. after storing the wanted amounts of the separated components, the column regeneration procedure starts. Regeneration is carried out by desorption at a higher temperature. The streams from the capture-column outlets are directed to the cooling traps where the temperature is lowered to the point which provides the freezing of the substances of interest (in our case the pure anaesthetics). Since the carrier gas (e.g. helium) has much lower condensation and freezing point, it remains in the gaseous phase. In that way the investigated substances are finally separated from the carrier gas and isolated in the pure form. They are then ready to be distributed to the medical laboratories for further testing. More details about column regeneration and freezing procedure could be found in the future publication [109] and the doctoral thesis of Thomas Munkelt [14].

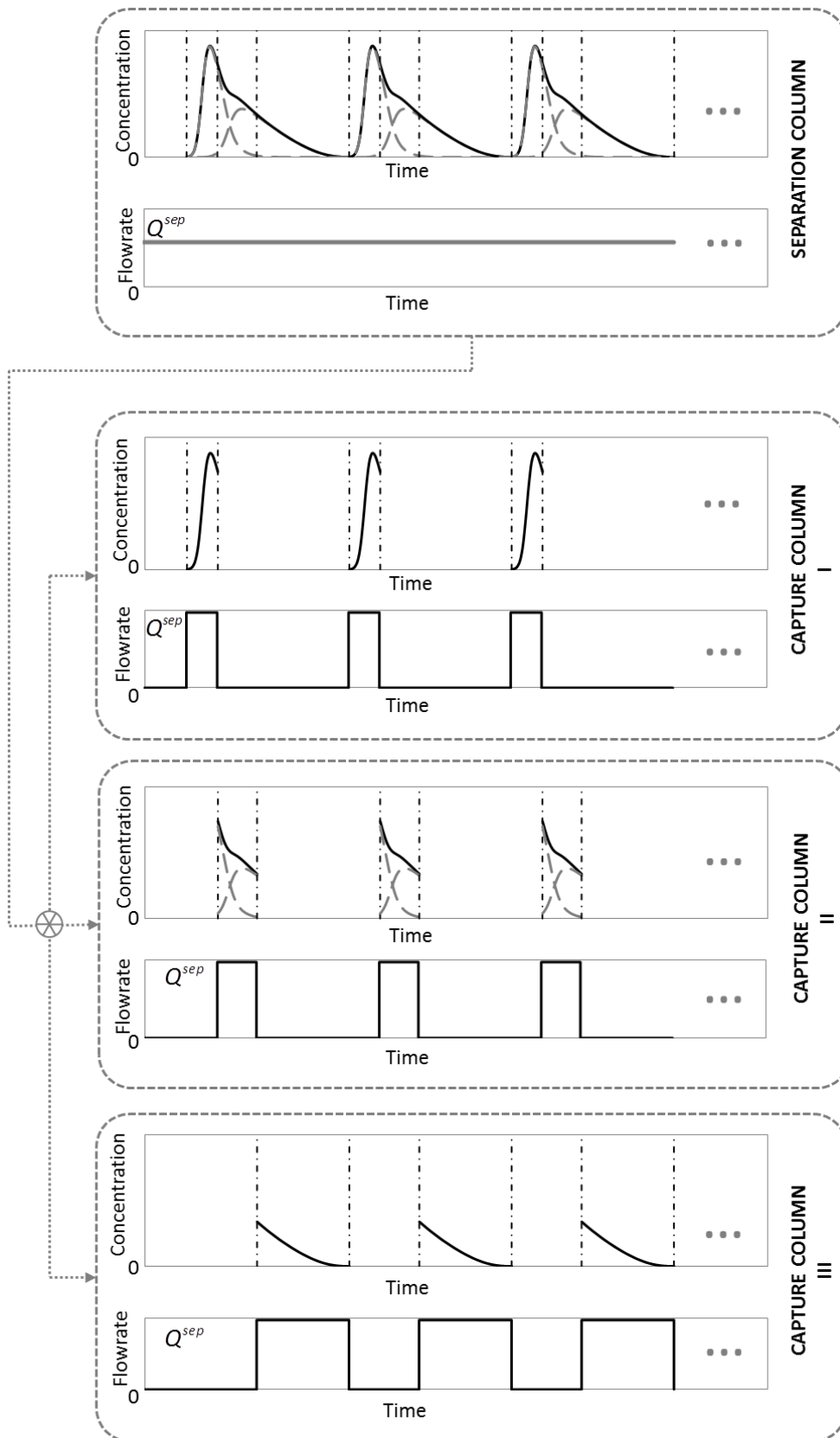


Figure 4.5. Procedure of capturing the three fractions (pure component 1, mixed fraction and pure component 2) which are resulting from the separation. For the separation column the outlet stream is presented, while for the capture columns I, II and III the inlet streams are depicted. The dash-dotted lines represent the cut times that separate the collected fractions at the outlet of the separation column. This example shows the first three consecutive injections that enter the capture columns.

### 4.3.1 Sizing of the capture columns

In order to determine the length of a capture column ( $L^{cap}$ ), one has to calculate first the length needed for one injection ( $\Delta x^{cap}$ ). Then, by multiplying this value by the specified desired number of injections that have to be stored in the column ( $n_{inj}$ ), the total column length can be obtained.

First we will discuss the “parking” process of the peaks (i.e. injections coming from the separation column) into the capture columns for the ideal case (parameters denoted by the subscript *id*), driven only by convection, without taking into accounts additional band-broadening effects such as molecular diffusivity (shown schematically in Figure 4.6).

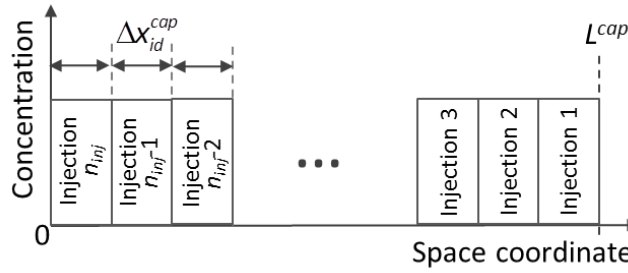


Figure 4.6. "Parking" of the fractions into a capture column for an ideal case without including the effect of the molecular diffusion. The rectangular shape of the fractions is assumed due to the self-sharpening effect.  $L^{cap}$  and  $\Delta x_{id}^{cap}$  are the length of the capture column and the length  $L$  needed for one injection (one fraction), respectively.

The required column length can be roughly calculated using the equation for the breakthrough time ( $t_{BT}$ ), which results from the ideal model of chromatography presented by eq. (2.14) (and also discussed in section 2.4.2.2: eq. (2.39) for a component  $i$  when the initial values  $c^{init}$  and  $q^{init}$  are zero):

$$t_{BT} = t_0 \left( 1 + F \frac{q^{eq}}{c^{eq}} \right) \quad (4.23)$$

By definition, breakthrough time represents the time when a solute starts eluting from the column (in the ideal case). What we here want to determine, is the column length needed to store one injection. That means that we need to know which is length, that the column should have, in order to provide that the elution starts as soon as the injection is finished. In other words, the time  $t_{BT}$  is equal to the injection time for the capture column ( $\Delta t^{cap}$ ).

As it was previously described, the inlet profile for capture columns is approximated to rectangular function. The height of the rectangle is equal to the maximal concentration of the

peak that is detected at the outlet of the separation column ( $c_{max}^{sep}$ ) and its length represents the capture time ( $\Delta t^{cap}$ ). This time is calculated from the mass conservation law, i.e. by knowing that the peak area of the outlet profile from the separation column is equal to the area of the rectangular injection that enters the capture column.

In eq. (4.23) concentration  $c^{eq}$  represents the maximum mobile phase concentration  $c_{max}^{sep}$ , while  $q^{eq}$  is the corresponding stationary phase concentration calculated according to the adsorption isotherm of the capture-column adsorbent ( $q_{max}^{cap}$ ). The hold-up time  $t_0$  (eq. (2.2)) can be denoted as  $\Delta t_0^{cap}$ , since it corresponds to the section of the capture column required to store one injection ( $\Delta V_{id}^{cap}$ ), and is expressed as:

$$\Delta t_0^{cap} = \frac{\varepsilon^{cap} \cdot \Delta V_{id}^{cap}}{Q^{cap}} \quad (4.24)$$

The parameters  $Q^{cap}$  and  $\varepsilon^{cap}$  are volumetric flowrate and total porosity of the capture column. Also the phase ratio  $F$  will get the superscript  $cap$  ( $F^{cap}$ ). With the introduced capture-column notation, the equation for the breakthrough time of one injection, introduced in a capture column, becomes:

$$t_{BT}^{cap} = \Delta t^{cap} = \Delta t_0^{cap} \left( 1 + F^{cap} \frac{q_{max}^{cap}}{c_{max}^{sep}} \right) \quad (4.25)$$

By expressing the volume of the column segment required to store one injection ( $\Delta V_{id}^{cap}$ ) from eq. (4.24) and the hold-up time  $\Delta t_0^{cap}$  from eq. (4.25), we come to the equation for  $\Delta V_{id}^{cap}$ :

$$\Delta V_{id}^{cap} = \frac{Q^{cap} \Delta t^{cap}}{\varepsilon^{cap} \left( 1 + F^{cap} \frac{q_{max}^{cap}}{c_{max}^{sep}} \right)} \quad (4.26)$$

The bed length needed to store one injection in the ideal case ( $\Delta x_{id}^{cap}$ ) is obtained by dividing the volume  $\Delta V_{id}^{cap}$  by the column cross-sectional area available for the fluid flow ( $\varepsilon^{cap} \cdot (d^{cap})^2 \pi / 4$ ):

$$\Delta x_{id}^{cap} = \frac{4 \cdot Q^{cap} \Delta t^{cap}}{(d^{cap})^2 \pi \cdot \varepsilon^{cap} \left( 1 + F^{cap} \frac{q_{max}^{cap}}{c_{max}^{sep}} \right)} \quad (4.27)$$

However, in practice more factors influence the shape of the bands and the assumption of perfect rectangular pulses is not always realistic. The broadening of the bands in the capture columns with time due to diffusion should be considered. Therefore the more reliable estimation of the needed column length contains two steps that take into account:

1. Ideal peak width due to mass transport by convection ( $\Delta x_{id}^{cap}$ ), as described in the previous paragraphs;
2. Peak width increase due to mass transport by axial diffusion ( $\Delta x_{diff}^{cap}$ ) during the “parking” time, that will be discussed further now.

When the first injection enters the capture column, at the time  $t = 0$ , it has initially the shape that can be considered as rectangular (ideal shape) with the width  $\Delta x_{id}^{cap}$ . After some time interval ( $\Delta t$ , e.g. by “parking”), simply due to unavoidable mass transfer driven by diffusion, the peak will get broader. The width of the peak ( $\Delta x_{real}^{cap}$ ) includes the width of the ideal rectangular injection and the width of the mass transfer zone ( $\Delta x_{MTZ}^{cap}$ ). In case of assumed symmetrical peaks the total real peak width would be:

$$\Delta x_{real}^{cap} = \Delta x_{id}^{cap} + \Delta x_{MTZ}^{cap} = \Delta x_{id}^{cap} + 2\Delta x_{diff}^{cap} \quad (4.28)$$

The term  $\Delta x_{diff}^{cap}$  represents the width due to diffusion on each side of the peak. The peak broadening process is shown in Figure 4.7 for two time intervals,  $\Delta t_1$  and  $\Delta t_2$  ( $\Delta t_2 > \Delta t_1$ ). The widths  $\Delta x_{id}^{cap}$ ,  $\Delta x_{diff,1}^{cap}$  and  $\Delta x_{diff,2}^{cap}$  are defined in the figure as well.

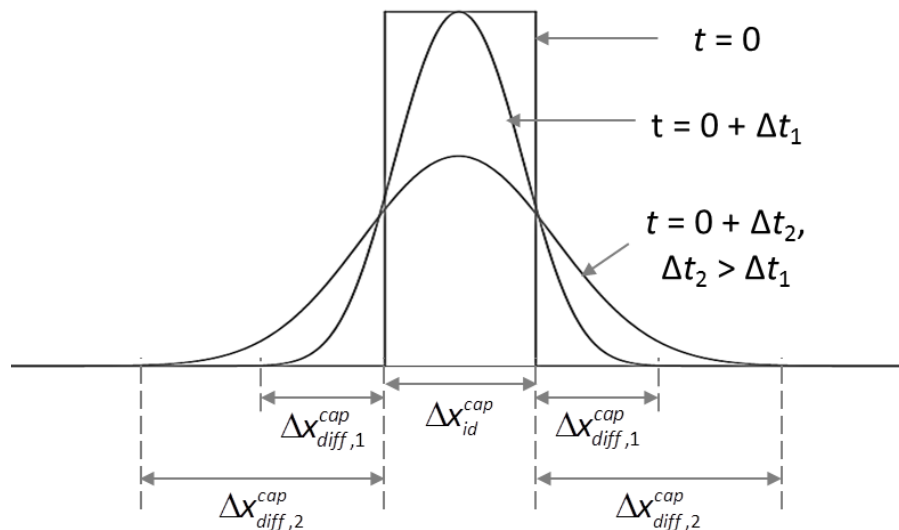


Figure 4.7. Process of the peak broadening with time due to molecular diffusion. At the beginning ( $t = 0$ ) the peak has ideal rectangular shape, while after time intervals  $\Delta t_1$  and  $\Delta t_2$ , the dispersed shapes can be observed. The meaning of the  $\Delta x$  parameters is explained in the text.

The width due to diffusion can be estimated from an equation equivalent to Fick's first law [110], but containing an effective diffusion coefficient ( $D_{eff}$ ) instead of the molecular diffusivity ( $D_{mol}$ ):

$$J = -D_{eff} \frac{dc}{dx} \quad (4.29)$$

Here  $J$  represents the diffusion flux of a substance. The effective diffusivity for the porous media represents the molecular diffusivity corrected by porosity ( $\varepsilon$ ) and tortuosity factor ( $\tau$ ) [12]:

$$D_{eff} = \frac{\varepsilon}{\tau} D_{mol} \quad (4.30)$$

Taking into account that the diffusion flux is the amount divided by the time ( $t_{diff}$ ) and the cross-sectional area ( $S$ ), and concentration is the ratio of the amount and volume (which is equal to  $S \cdot \Delta x_{diff}^{cap}$ ), the following expression can be derived for  $\Delta x_{diff}^{cap}$ :

$$\Delta x_{diff}^{cap} = \sqrt{D_{eff} t_{diff}} \quad (4.31)$$

The time  $t_{diff}$  is the duration of the diffusion process ("parking" time and the collection time).

The "parking" of the peaks into a capture column is presented in Figure 4.8. As it can be seen, after the time of one injection ( $\Delta t^{cap}$ ) the peak has the ideal rectangular shape (Figure 4.8 a)). With time, before the next injection starts, the peak gets broader due to diffusion effect. In Figure 4.8 b) the shape of the peak after the first cycle time interval ( $t_{cycle}$ ) is shown. After that moment the next injection starts entering the column and occupies the previous position of the first injection (injection 1), while the injection 1 "travels" further along the column. The moment, when the injection 2 is completely into the column (after the time interval  $t_{cycle} + \Delta t^{cap}$ ), is depicted in the part c) of Figure 4.8. The part d) of Figure 4.8 shows the situation with two peaks that are "parked" in the capture column after two cycle times, when the broadening of the injection 2 and further broadening of the injection 1 takes place. In Figure 4.8 e) the same situation is shown for the case when five peaks are captured. Injections that are longer in the column are more affected by the mass transfer (broadening) effect.

In Figure 4.9 the part e) of Figure 4.8 is shown in more details. The column length required for storage of the injections consists of the part that comes from the convection process (i.e.  $\Delta x_{id}^{cap}$ ) and the broadening due to diffusion ( $\Delta x_{diff}^{cap}$ ). After the peak that spent the longest time in the column (injection 1) there is a mass transfer zone that is wider than those between the peaks, denoted as  $\Delta x_{diff,end}^{cap}$ .

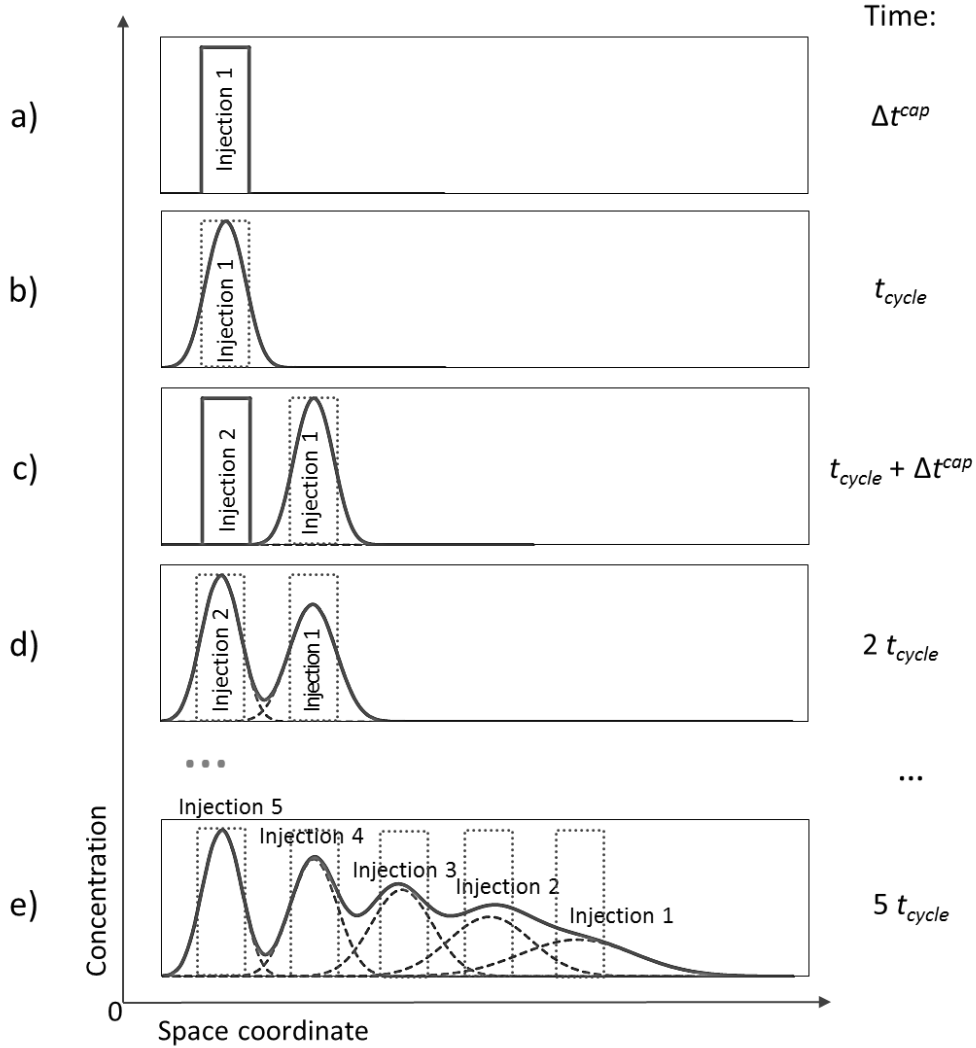


Figure 4.8. Schematic representation of the process of "parking" several peaks (5 peaks in the part e)) into the capture column, including the convection and diffusion effects (the solid line shows the overall concentration profile, dashed lines – the single profiles for each injection and the dotted lines – the rectangular shape of the injections that corresponds to the ideal case without diffusion effects): a) The first injection (injection 1) after the one-injection interval ( $\Delta t^{cap}$ ); b) The injection 1 after the cycle time interval ( $t_{cycle}$ ); c) Two injections at the time  $t_{cycle} + \Delta t^{cap}$ ; d) Injections 1 and 2 after the time interval  $2t_{cycle}$ ; e) The situation after the time interval  $5t_{cycle}$  (the larger influence of the peak broadening on the injections that are longer time in the capture column can be observed).

As it can be seen from Figure 4.9 the total required length of the capture column for storing the desired number of injection  $n_{inj}$  is:

$$L^{cap} = n_{inj} (\Delta x_{id}^{cap} + \Delta x_{diff}^{cap}) + \Delta x_{diff,end}^{cap} \quad (4.32)$$

The value  $\Delta x_{id}^{cap}$  is calculated from eq. (4.27) and both  $\Delta x_{diff}^{cap}$  and  $\Delta x_{diff,end}^{cap}$  can be expressed from eq. (4.31), by taking different values for the diffusion time. The width  $\Delta x_{diff}^{cap}$  results



from the time equal to the duration of one injection, while  $\Delta x_{diff,end}^{cap}$  is the width of the mass transfer zone formed during the whole capture process (i.e. for the time needed for  $n_{inj}$  cycles):

$$\Delta x_{diff}^{cap} = \sqrt{D_{eff} \Delta t^{cap}} \quad (4.33)$$

$$\Delta x_{diff,end}^{cap} = \sqrt{D_{eff} n_{inj} t_{cycle}} \quad (4.34)$$

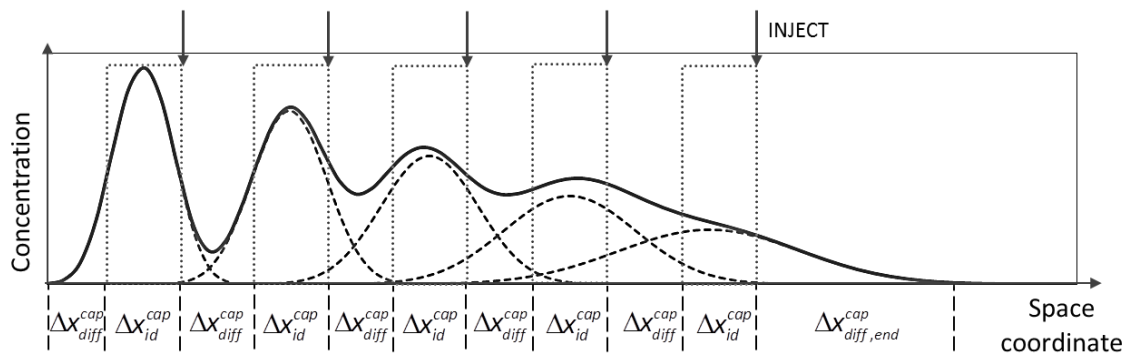


Figure 4.9. The broadening effect due to molecular diffusion of the "parked" injections in the capture column represented for the example of five injections. The lengths required for storing the peaks due to convection ( $\Delta x_{id}^{cap}$ ) and diffusion ( $\Delta x_{diff}^{cap}$  and  $\Delta x_{diff,end}^{cap}$ ) are marked. The superscript *cap* denotes the capture column, solid line shows the overall concentration profile, dashed lines – the single profiles for each injection and the dotted lines – the ideal rectangular shape of the injections that correspond to the ideal case without diffusion effects included. The arrows show the positions where each injection has started.

The exact value of the effective diffusion is not easy to determine. Therefore in this work it was estimated from the experiments, as it will be later explained in Chapter 8. The calculations of the required column lengths and volumes based on the specific adsorption isotherms of the capture columns can be found in the same chapter as well.



## 5 Investigated substances

Two types of chiral substances were investigated in this thesis. In the liquid phase the separation of bicalutamide enantiomers is studied in order to introduce and validate the methods developed within the scope of this work. The second type of the substances are fluorinated volatile anaesthetics, isoflurane and desflurane, whose enantioseparation is examined in the vapour phase. The developed methodology was applied to these systems with the aim to produce larger amounts of pure enantiomers.

This chapter provides an overview of the substances used. It first includes their medical application and different effect of single enantiomers, and then the possible ways of obtaining pure enantiomers and the literature review of work already done in that area.

### 5.1 Bicalutamide

Bicalutamide, marketed under the trade name Casodex<sup>®</sup>, is a non-steroidal anti-androgen administrated for prostate cancer treatment [111-113]. As a medicine, it provides delaying of the disease progression in patients with locally advanced cancer. Bicalutamide is widely used since it is well tolerated by the patients and shows very few side effects. As already mentioned, bicalutamide is a chiral substance, containing S(+)- and R(-)-enantiomer, which are represented in Figure 5.1.

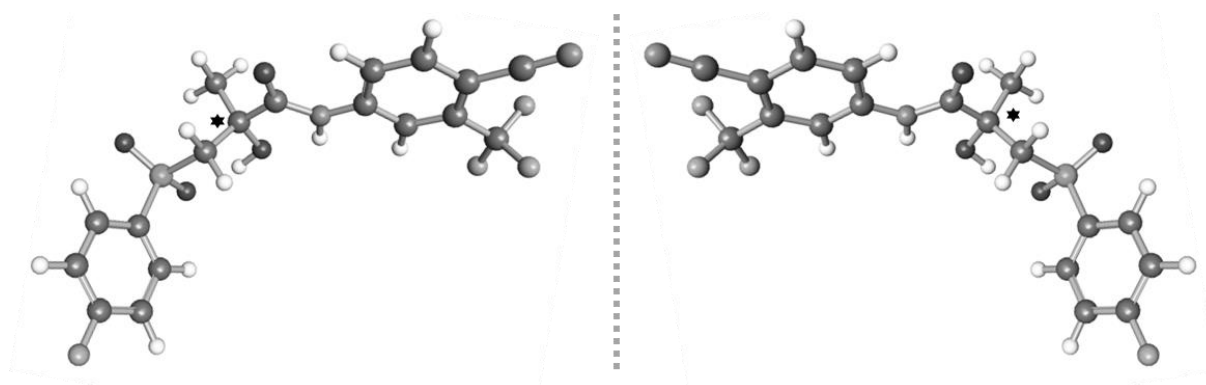


Figure 5.1. Molecules of bicalutamide enantiomers. The chiral carbon atom is marked by an asterisk (\*).

The chemical name of the compound is (R,S)-N-[4-cyano-3-(trifluoromethyl)phenyl]-3-[(4-fluorophenyl)sulfonyl]-2-hydroxy-2-methyl-propanamide. When produced, bicalutamide is in the form of fine white to off-white powder. Additional chemical and physical data are given in Table 5.1 [114, 115].

Table 5.1. Some of the chemical and physical properties of bicalutamide.

|                  |                     |   |
|------------------|---------------------|---|
| Chemical formula |                     | $C_{18}H_{14}N_2O_4F_4S$                            |
| Molecular weight |                     | 430.37 g/mol  |
| Melting point    |                     | 191-193 °C  |
| Vapour pressure  |                     | $1.005 \cdot 10^{-15}$ kPa at 25 °C                 |
| Solubility       | In water            | Practically insoluble (5 g/m <sup>3</sup> at 37 °C) |
|                  | In chloroform       | Slightly  |
|                  | In absolute ethanol | Slightly  |
|                  | In methanol         | Sparingly   |
|                  | In acetone          | Soluble   |
|                  | In tetrahydrofuran  | Soluble   |

Tests of the pharmacokinetics of individual enantiomers in healthy people [116], as well as in patients with impaired liver function [117] showed that bicalutamide, as expected by being a chiral substance, exhibits differences in the effect of single enantiomers. It was found that the bicalutamide medical action is almost completely due to the R-enantiomer [118, 119], while S-component has very little or even no activity. The application of bicalutamide and the differences between the single enantiomers is reviewed in [120].

The R-enantiomer exhibits more favourable pharmacokinetic and toxicological properties. It has a much higher binding affinity to the androgen receptor (which is how it functions as a medicine) than the S-component [121]. For the S-enantiomer it was shown that it does not exhibit any harmful effect, but is metabolized and eliminated faster from the body [116], which exerts more strain on the liver and is therefore advisable to apply only the R-component. The usage of the single active R-enantiomer would make the dosages of the medicine twice as lower as what is dosed currently and would lower the demands on the liver to work on metabolising it.

### 5.1.1 Previous provisions of pure bicalutamide enantiomers

Even though only R-bicalutamide serves as an active component, bicalutamide is still marketed as racemic mixture. There are published data about the synthesis route to obtain single enantiomers (e.g. [122]), but since the synthesis of pure components is not economically justified [15], the separation of racemic mixture still represents the more attractive way to provide pure R-bicalutamide.

The studies on chromatographic separation of enantiomers of bicalutamide started already by the time when it was discovered as a medicine, as shown in [118]. It was managed to separate the enantiomers by forming diastereoisomers in a Spherisorb-NH<sub>2</sub> column. Analytical separation of bicalutamide and its analogues on different chiral stationary phases was reported in [123] along with the retention factors, selectivity and resolution data. It was shown that bicalutamide separation was most successful on Chirobiotic T and TAG columns. Another two stationary phases, Chiracel OD-H and Chiralpak AD-H, were tested in a new rapid HPLC process again on analytical level [124]. Separation parameters, such as selectivity and resolution, were presented for different temperatures and mobile phase compositions. It was shown that Chiralpak AD-H column can provide a very good resolution of two bicalutamide enantiomers. The analytical, as well as semi-preparative separation of bicalutamide, was presented in [125] using a Chiralpak IA column with immobilized amylose-based stationary phase. Retention factors, selectivity and resolution were determined for bicalutamide and its analogues using different mobile phase compositions.

The resolution of bicalutamide enantiomers was also achieved using a two-step crystallization process [126], as well as crystallization coupled with simulated moving bed [15]. In the latter example the SMB with Chiralpak AD columns was used for pre-enrichment of the mixture with R-enantiomer, after which the resulting extract was purified in the crystallization step.

## 5.2 Fluorinated volatile anaesthetics

The purpose of general anaesthetics is to produce in patients a sleep-like or stupor condition under which the painless surgery can take place. The role of the anaesthetics is to depress the consciousness, pain sensitivity and reflexes, but at the same time the vital centres – especially those for controlling respiration and circulation, should remain relatively unaffected [127]. Depending on the way that general anaesthetics are administered to a patient, they can be classified in three large groups: inhalation, intravenous and combination anaesthetics. Fluorinated volatile anaesthetics belong to the group of inhalation agents. To induce and maintain the anaesthesia, they are inhaled in a mixture with air or oxygen. The main advantages of inhalation anaesthetics are their great stability and the fact that they are taken up quickly in the lungs and eliminated from the body rapidly and mostly unchanged [127].

The anaesthetics studied in this work, isoflurane and desflurane, are halogenated methyl ethyl ethers. The chemical name of isoflurane is 2-chloro-2-(difluoromethoxy)-1,1,1-trifluoroethane, and of desflurane 2-(difluoromethoxy)-1,1,1,2-tetrafluoroethane. The molecules of both substances are shown in Figure 5.2. As it can be noticed, the only difference between their molecules is in one atom connected to the chiral carbon. In the case of isoflurane, it is chlorine, while desflurane has a fluorine atom connected to the chiral centre. It was shown that the enantiomers of both compounds have the same absolute

configurations [128, 129], namely (+)-S-isoflurane, (-)-R-isoflurane and (+)-S-desflurane, (-)-R-desflurane.

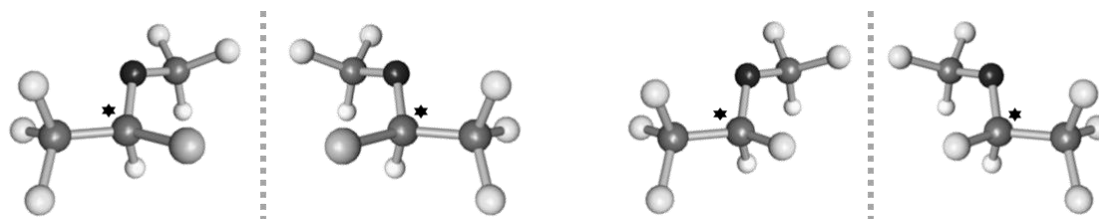


Figure 5.2. Molecules of isoflurane (left) and desflurane (right) enantiomers. The chiral carbon atom is marked by an asterisk (\*).

Isoflurane (trade name Forane<sup>®</sup>) and desflurane (trade name Suprane<sup>®</sup>) are produced in the form of colourless liquids. Some of the chemical and physical properties of these two substances is presented in Table 5.2 [127, 130, 131].

Table 5.2. Some of the chemical and physical properties of isoflurane and desflurane.

| Anaesthetic         | Isoflurane   | Desflurane  |
|---------------------|--|---|
| Chemical formula    | C <sub>3</sub> H <sub>2</sub> ClF <sub>5</sub> O (CF <sub>3</sub> -CHCl-O-CHF <sub>2</sub> ) | C <sub>3</sub> H <sub>2</sub> F <sub>6</sub> O (CF <sub>3</sub> -CHF-O-CHF <sub>2</sub> ) |
| Molecular weight    | 184.49 g/mol   | 168.04 g/mol  |
| Colour              | None   | None  |
| Odour               | Slight   | Slight, non-pungent   |
| Boiling point       | 48.5 °C  | 23.5 °C   |
| Vapour pressure     | 32 kPa at 20 °C  | 89 kPa at 20°C  |
| Density             | 1.5 g/cm <sup>3</sup> (at room temperature)  | 1.5 g/cm <sup>3</sup> (at room temperature)   |
| Flammability        | Noninflammable   | Noninflammable  |
| Solubility in water | 4470 g/m <sup>3</sup> at 37 °C   | 5950 g/m <sup>3</sup> at 25 °C  |

Nowadays isoflurane, desflurane and the third chiral fluorinated anaesthetic ether – enflurane are synthesized and applied in racemic form, although the mechanism of action of single enantiomers is not completely known. There is a possibility to improve the effects of anaesthesia by using only the enantiomer with more favourable pharmacological and toxicological properties. These anaesthetics have low therapeutic index (the ratio between the toxic and therapeutic amount) and thus even a small increase in potency that can be achieved by using only the more potent enantiomer can lead to lower doses applied in patients and therefore to provide large clinical benefits [132]. Another reason to obtain pure enantiomers

is to use them in investigations of the mechanism of general anaesthesia [132]. Therefore, it is of great interest to produce single enantiomers of high purity in larger amounts, for the medical tests and for the potential use during surgeries.

### 5.2.1 Different effects of isoflurane and desflurane enantiomers

Differences in action of single enantiomers of the fluorinated anaesthetics in humans and animals were examined in numerous studies. Isoflurane represents the most investigated substance from all halogenated ethers. Only a few studies refer to the effects of desflurane enantiomers.

The first study of the effect of isoflurane enantiomers was reported in [133]. The investigations were done on isolated snail neurons (*in vitro*). It was concluded that S-enantiomer is more effective as anaesthetic. The first *in vivo* studies of the effect of isoflurane enantiomers were reported in [134]. By applying isoflurane to mice, it was shown that S-isoflurane has higher potency than R-enantiomer. It was found that the sleeping time is not the same when equal amounts of two single enantiomers were separately applied and that S-isoflurane is able to provide longer sleep. Another example of a study done on animals *in vivo* is the intravenous administration of single isoflurane enantiomers to rats [135]. The S-enantiomer proved to be more potent than R-component producing a loss of righting reflex and by providing longer sleeping time, so the result obtained in [134] was confirmed. The action of racemic isoflurane, as well as of the single enantiomers, on the GABA<sub>A</sub> receptor was tested by [136] *in vitro* by using cerebellar Purkinje neurones of rats. It was again found that S-enantiomer is more effective. The same results as in the previously mentioned works were published in reviews [137] and [138]. Both of them give summaries of different effects caused by using just one of the enantiomers.

Regarding desflurane, preliminary tests in mice showed that S-desflurane is slightly more potent than R-enantiomer or the racemate, while other experiments done in rats indicated that the use of R-enantiomer provided shorter recovery time than when S-enantiomer or the racemic mixture were applied, as reported in [139].

When analysing the effect of single enantiomers in humans, Haeberle et al. [140] determined the concentrations of isoflurane enantiomers in breath and blood samples taken daily from the patients after surgery. Higher concentration of S-isoflurane was detected in the first days, after what the percentage of R-enantiomer increased, which shows that S-component is faster eliminated from the body and therefore advantageous over R-enantiomer. Similar tests of the blood samples were performed and described in [141] and [142]. The enrichment of S-isoflurane in blood was observed after anaesthesia. It was again concluded that S-isoflurane exhibits better properties.

### 5.2.2 Previous separations of isoflurane and desflurane enantiomers

Even though the syntheses of single isoflurane and desflurane enantiomers were reported [139, 143, 144], still the most promising and easiest way to obtain them in pure form is by performing the separation of racemic mixtures, as it is the case for the most of chiral compounds. A detailed report on enantioseparation of fluorinated anaesthetics was provided by V. Schurig [98]. This review summarizes the work done on the analytical and preparative separation of enantiomers of enflurane, isoflurane, desflurane and halothane, starting from the preliminary work of Schurig et. al [99, 145] until the application of more advanced SMB processes [102, 103]. The key task was to develop a suitable chiral selector that provides effective separation. Among other results, the absolute configurations of the single enantiomers of the studied substances were given, as well as the results of *in vivo* studies of the enantiomer's effect on humans after anaesthesia.

The physical and chemical properties of the fluorinated anaesthetics, such as low boiling point and high volatility have made gas chromatography (GC) the most suitable technique for separating their enantiomers. Due to its advantages like simplicity, accuracy and reproducibility, GC is often applied in the case of racemic mixtures that can be vaporized without decomposition. In comparison to liquid chromatography, GC gives the possibility to use an inert gas as the mobile phase, avoiding in that way the complications caused by solvent effects. The enantioseparation of fluorinated anaesthetics was first used on capillary GC columns and was further studied on packed single beds, multicolumn SMB processes, and theoretically by using PSA separation. Table 5.3 gives a summary of previous research on this topic including the type of the studies carried out and the applied processes.

Establishment of gas chromatographic processes for separating enflurane, isoflurane and desflurane racemates started and gained more importance with the introduction of stationary phases based on  $\alpha$ -,  $\beta$ - and  $\gamma$ -cyclodextrins (CDs) for separation of enantiomers in general [146], and furthermore by producing different derivatives of these compounds, which were proven to be good selectors for resolving racemic mixtures of fluorinated anaesthetics [145, 147, 148]. Cyclodextrins are homologues series of cyclic oligosaccharides. They contain six or more ( $\alpha$ )-D-glucopyranose units that are linked together by  $\alpha$ -1,4-glycoside bonds, forming in that way truncated-cone structures. Cyclodextrins provide adsorption thanks to their ability to form inclusion complexes with different molecules or ions, which can completely or partially fit into the cavity of the CDs. What made CDs attractive for chiral separations is the fact that they are themselves chiral compounds and have therefore ability to selectively interact with enantiomers [146, 147]. The three CDs that are commercially available contain six, seven and eight units of ( $\alpha$ )-D-glucopyranose and are denoted as  $\alpha$ -,  $\beta$ - and  $\gamma$ -cyclodextrin, respectively (Figure 5.3).

Some of the physical data and dimensions of the molecules of  $\alpha$ -,  $\beta$ - and  $\gamma$ -cyclodextrin are presented in Table 5.4 [147]. Different CD derivatives used as selectors for enantioseparation of fluorinated anaesthetics are listed in Table 5.5, where the stationary and mobile phases are indicated for the studies shown in Table 5.3.



Table 5.3. Overview of the previous publications on enantioseparation of the fluorinated anaesthetics: The used separation processes are listed followed by indications if experiments, modelling and simulations were performed (the sign “✓” stands for the performed actions and “-” for the non-performed ones).

|     | Reference | Year | Substance*                | Process   | Experiments done | Simulations done | Model of the process given |
|-----|-----------|------|---------------------------|-----------|------------------|------------------|----------------------------|
| 1.  | [149]     | 1991 | H, E, I                   | GC        | ✓                | -                | -                          |
| 2.  | [148]     | 1993 | E, I, D                   | GC        | ✓                | -                | -                          |
| 3.  | [145]     | 1993 | E                         | GC        | ✓                | -                | -                          |
| 4.  | [99]      | 1994 | E, I, (H)                 | GC        | ✓                | -                | -                          |
| 5.  | [150]     | 1994 | I                         | GC        | ✓                | -                | -                          |
| 6.  | [151]     | 1994 | E                         | GC        | ✓                | -                | -                          |
| 7.  | [152]     | 1996 | E, I, other substances    | GC        | ✓                | -                | -                          |
| 8.  | [153]     | 1997 | E, I, D, other substances | GC        | ✓                | -                | -                          |
| 9.  | [100]     | 1997 | E, I, D                   | GC        | ✓                | -                | -                          |
| 10. | [101]     | 1998 | E                         | GC-SMB    | ✓                | -                | ✓                          |
| 11. | [102]     | 2000 | E                         | GC-SMB    | ✓                | -                | -                          |
| 12. | [103]     | 2002 | I                         | GC-SMB    | ✓                | -                | -                          |
| 13. | [71]      | 2002 | E                         | GC-SMB    | ✓                | -                | ✓                          |
| 14. | [72]      | 2008 | E                         | SMB / PSA | -                | ✓                | ✓                          |
| 15. | [54]      | 2011 | E                         | SMB, PSA  | -                | ✓                | ✓                          |
| 16. | [154]     | 2013 | D                         | GC        | ✓                | -                | -                          |

\* Substances are denoted as: E – Enflurane, I – Isoflurane, D – Desflurane; H - Halothane

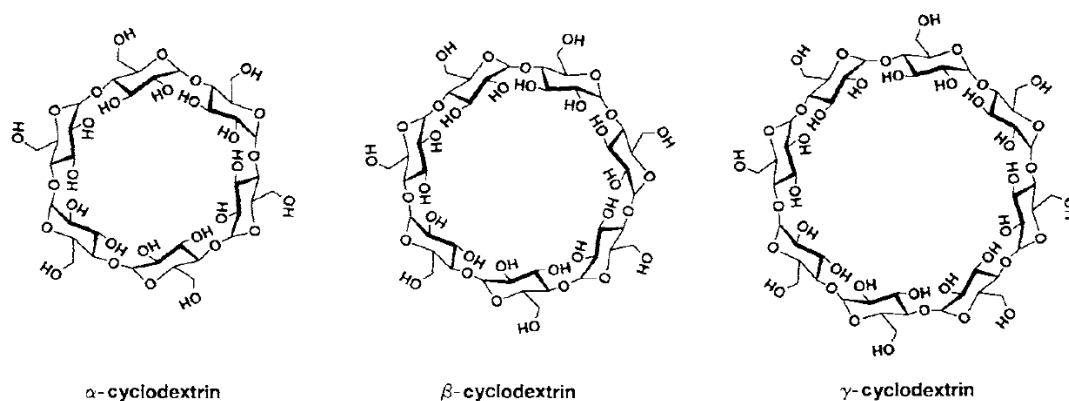


Figure 5.3. Molecules of  $\alpha$ -,  $\beta$ - and  $\gamma$ -cyclodextrin suggested in [147] (The figure is adapted from [147]).

Table 5.4. Selected characteristics of  $\alpha$ -,  $\beta$ - and  $\gamma$ -cyclodextrins.

| Cyclodextrin                                 | $\alpha$  | $\beta$   | $\gamma$  |
|--|-----------|-----------|-----------|
| Number of ( $\alpha$ )-D-glucopyranose units | 6         | 7         | 8         |
| Molecular weight [g/mol]                     | 972.86    | 1135.01   | 1297.15   |
| External diameter [pm]                       | 1370-1460 | 1530-1540 | 1690-1750 |
| Internal diameter [pm]                       | 470-520   | 600-650   | 750-850   |
| Melting and decomposition point [°C]         | 278       | 299       | 267       |
| Solubility in water [g/l at 25 °C]           | 14.50     | 1.85      | 23.20     |
| Number of chiral centers                     | 30        | 35        | 40        |

A number of stationary phases, including cyclodextrins, used in chiral GC were described in [155]. This review of Prof. Schurig gives characteristics of different adsorbents, together with their mechanisms of selection, applications and limitations. Resolution of racemic mixtures of enflurane, isoflurane and desflurane are just some of the presented examples.

The first enantioseparation of enflurane and isoflurane (and the anaesthetic halothane, which is not investigated in this thesis) was performed by Meinwald et al. in 1991 [149] by gas chromatography on a microscale level (analytical), using derivatives of  $\alpha$ - and  $\gamma$ -CD. The capillary columns were coated with cyclodextrin compounds. Separation was completed successfully; however no data such as injected amounts or process performance details were reported. The separation of enflurane, isoflurane and also desflurane was studied experimentally on many commercially available capillary columns on the analytical scale by Shitangkoon et al. [148]. The capillary columns were coated with films of different  $\alpha$ -,  $\beta$ - and  $\gamma$ -cyclodextrins. Thermodynamic parameters such as enthalpy and entropy were determined and further used for calculations of capacity and selectivity factors with varying temperatures. It was shown that  $\gamma$ -trifluoro-acetyl-CD can be successfully used for the separation of all three investigated substances.

The synthesis of a new  $\gamma$ -CD derivative – Octakis(3-O-butryryl-2,6-di-O-pentyl)- $\gamma$ -cyclodextrin (trade name Lipodex<sup>®</sup> E) was reported in 1989 by König et al. [156]. Its molecule is shown in Figure 5.4. It was demonstrated that this compound can successfully be used in capillary columns for enantioseparation of different substances, such as protein and non-protein amino acids, alcohols, ketones, lactones, cyclopropane derivatives, amines, cyclic acetals, alkyl halides, hydroxy acids and di- and poly-hydroxy compounds. For the separation of the enantiomers of the fluorinated anaesthetics this  $\gamma$ -CD derivative was later widely applied since it provided the best separation performance.

Table 5.5. Overview of the previous publications on enantioseparation of the fluorinated anaesthetics: Applied stationary and mobile phases are shown.

|  | Reference               | Stationary phase  | Mobile phase |
|--|-------------------------|---|--------------|
| 1.   | [149]                   | Hexakis-(2,3,6-tri-O-pentyl)- $\alpha$ -CD (Lipodex <sup>®</sup> A); Octakis(6-O-methyl-2,3-di-O-pentyl)- $\gamma$ -CD  | Not reported |
| 2.   | [148]                   | $\alpha$ -, $\beta$ - and $\gamma$ -dipentyl-CD; $\alpha$ -, $\beta$ - and $\gamma$ -permethyl-(S)-2-hydroxy-propyl-CD; $\alpha$ -, $\beta$ - and $\gamma$ -trifluoro-acetyl-CD | Hydrogen     |
| 3.   | [145]                   | Selector developed in [156]* dissolved in polysiloxane SE-54 and coated on Chromosorb particles   | Helium       |
| 4.   | [99]                    | Selector developed in [156]* dissolved in polysiloxane SE-54 and coated on Chromosorb P AW DMCS and W AW DMCS particles   | Helium       |
| 5.   | [150]                   | Trifluoroacetyl 2,6-O-dipentyl- $\gamma$ -CD coated on Chromosorb W AW and W HP   | Helium       |
| 6.   | [151]                   | Trifluoroacetyl- $\gamma$ -CD coated on Chromosorb A  | Hydrogen     |
| 7.   | [152]                   | Selector developed in [156]*; 2,5-di-O-pentyl-3-O-butanoyl- $\gamma$ -CD; 2,3,5-tri-O-pentyl- $\beta$ -CD; 2,3,5-tri-O-pentyl- $\alpha$ -CD                                     | Helium       |
| 8.   | [153]                   | Chirasil- $\gamma$ -Dex (Selector developed in [156]* + polysiloxane)   | Hydrogen     |
| 9-11.  | [100], [101], [102]     | Selector developed in [156]* dissolved in polysiloxane SE-54 and coated on Chromosorb P AW DMCS   | Nitrogen     |
| 12-15.   | [103], [71], [72], [54] | Selector developed in [156]* dissolved in polysiloxane SE-54 and coated on Chromosorb A NAW   | Nitrogen     |
| 16.  | [154]                   | Heptakis(3-O-butyryl-2,6-di-O-pentyl)mono(6-azido-6-deoxy-3-O-butyryl-2-O-n-pentyl)- $\gamma$ -CD covalently bound to porous glass  | Helium       |
| * Selector: octakis(3-O-butanoyl-2,6-di-O-n-pentyl)- $\gamma$ -CD (Lipodex <sup>®</sup> E) |                         |   |              |

Among fluorinated anaesthetics this selector was for the first time used for separating enflurane enantiomers in 1993 by Schurig et al. employing analytical and preparative GC [145]. The preparative column was packed with Chromosorb particles coated with the selector dissolved in polysiloxane SE-54. The separation of the 47 mg of racemate was achieved in 45 min with purity over 99 % (of both enantiomers) and recovery 50-60 %. The same result for enflurane was reported in [99], where the separation was performed with the same columns and stationary phase. In that work a semi-preparative enantioseparation of isoflurane was also completed (6 mg were separated in 28 min at >99 % purity and 60 % recovery). The selectivity values for both enantiomers were determined as well. The single enantiomers were recovered (isolated from the carrier gas – helium) via condensation in cooling traps using liquid nitrogen as a cooling medium. After the collection, the traps were warmed up to -40 °C, so that the samples become liquid. The pure substances were then collected with syringes and sealed in ampoules.

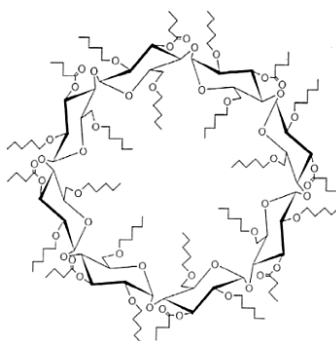


Figure 5.4. The molecule of Octakis(3-O-butyl-2,6-di-O-pentyl)- $\gamma$ -Cyclodextrin, used as a chiral selector.

Preparative separation of isoflurane [150] and enflurane [151] was performed by Staerk et al. using another CD-derivative based on trifluoroacetyl- $\gamma$ -CD as a selector and coated onto Chromosorb particles. The investigation was done only on experimental level with no separation parameters calculated. Process performance characteristics were investigated and the changes of production rate with purity and other parameters were reported.

In [152] four stationary phases based on  $\alpha$ -,  $\beta$ - and  $\gamma$ -CD were tested in capillary GC for separation of enflurane, isoflurane and 18 of their analogues by determining the separation factors. It was concluded that  $\gamma$ -CD derivatives could provide better separation. The selector developed by König et al. [156] was in more details studied by Grosenick and Schurig [153] and Juza et al. [100]. In the research reported in [153] the selector was linked to polysiloxane forming the stationary phase called Chirasil- $\gamma$ -Dex. Using many different substances (including enflurane, isoflurane and desflurane) the influence of the selector percentage in the stationary phase was checked and the separation factors were determined. The effect of selector percentage in the stationary phase was studied in [100] as well. The Chromosorb particles were coated with  $\gamma$ -CD dissolved in polysiloxane. The GC separation process was described, followed by the collection of the pure enantiomers in cooling traps immersed in liquid nitrogen. Enflurane and isoflurane enantiomers were produced at high purity (over 99 %) in the amounts 250 mg/day and 300 mg/day, respectively, by repetitive injections. In the case of desflurane, the separation was more difficult and the obtained amounts were of lower purity; it was collected 500 mg/day of the less retained enantiomer (with  $ee = 91$  %) and 450 mg/day of the more retained component (with  $ee = 68$  %).

Based on the previous batch GC processes, the continuous GC-SMB process was first employed by Juza et al. for preparative enantioseparation of enflurane and then further elaborated [71, 101, 102]. They used the established stationary phase constructed of Chromosorb particles (two types of them) coated with  $\gamma$ -CD derivative developed in [156] and dissolved in polysiloxane SE-54. For isoflurane the SMB enantioseparation was only studied in the research performed by Biressi et al. [103]. In all these papers only the experimental investigation was reported followed by parametric study in order to provide the optimal process performance. The purities of the collected raffinate and extract streams were given for a large number of different operating conditions resulting from varying temperature, flowrates, feed concentration, and shift time. For enflurane enantiomers very

high purity (>99 %) for each of them and the production of about 0.01 g/day/g<sub>(adsorbent)</sub> was achieved. For isoflurane such high purities of the two enantiomers in the same experiment could not be obtained. It was possible to provide the extract purity of 95.3 %, while for the raffinate it was 99.5 %. No productivity values per collection time were provided. After the SMB separation, the collection of the enantiomers was done by the cooling traps using liquid nitrogen, as it was described in the previous publications. In order to design the SMB process, Henry constants and selectivity were calculated at different temperatures [71, 101-103]. In [101] the isotherms of enflurane enantiomers in the nonlinear range were also reported. They contain two terms: the first one is linear, and the second one added to it is expressed by the Langmuir model.

Using the experimental results from the previous SMB studies for enflurane, a new hybrid SMB/PSA process was developed and investigated only on the simulation level [72]. It represents the SMB process with changing the pressure in order to reduce the desorbent consumption. Purity and recovery of the separated enantiomers were calculated for different operating conditions and different SMB configurations. The conventional 4-step one-column PSA process for enflurane enantioseparation was described by Bentley et al. [54], by simulations only and compared to a 4-zone 8-columns SMB separation. As for SMB/PSA process, the experimental data from the previously reported SMB studies were used. The performed multi-objective optimization of the both processes showed that by SMB purity and recovery >99 % can be obtained, while PSA achieved less than 50 % raffinate recovery. However, PSA process could be advantageous since it reduces the desorbent consumption.

While in all previously mentioned studies the selector was coated or bound to the capillary column or by employing Chromosorb particles, Munkelt et al. [154] introduced new particle type for enantioseparation. In this preliminary study, using the racemic mixture of desflurane, few samples differing in particle and pore size were examined. The selector used in this case was a derivative of  $\gamma$ -CD (see Table 5.5), which was covalently bound to a support made of porous glass beads. Even though low degree of separation was provided and further adsorbent optimization was recommended, the results showed good potential of the porous glass beads for enantioseparation of the anaesthetic gases.

Based on the pioneer's works of Schurig et al. and Juza et al. [99, 100, 145] the separation of enantiomers of isoflurane and desflurane was studied in this thesis using  $\gamma$ -CD derivative established in [156] dissolved in polysiloxane SE-54 and coated onto the newly developed porous glass beads (similar to those described in [154]). The separations were performed experimentally (in collaboration with SPP1570 Subproject II) and by simulations using GC repetitive injections and in less details by simulating a PSA process. The emphasis is set on developing the process that will provide the highest productivity of the pure enantiomers. For the later comparison, the previous separations of enflurane, isoflurane and desflurane are presented in order to check the process performance characteristics. The data are presented in Table 5.6.

Table 5.6. Overview of the previous publications on enantioseparation of the fluorinated anaesthetics: Indicated if thermodynamic parameters and process performance characteristics were determined and calculated (the sign “✓” stands for the determined parameters and “-” for the non-determined ones).

|     | Reference and Process | Substance* | Determined $\alpha^*$ , $H^*$ , or the whole isotherm | Determined process performance (when not specified, provided for both enantiomers of all substances and all processes) |                |  |
|-----|-----------------------|------------|---|--|----------------|--|
|     |                       |            |   | $PU^*$   | $RE^*$         | $PR^*$   |
| 1.  | [149] GC              | E, I       | -   | -  | -              | -  |
| 2.  | [148] GC              | E, I, D    | $\alpha$  | -  | -              | -  |
| 3.  | [145] GC              | E          | $\alpha$ (for analytical column)                      | ✓  | -              | ✓ (as mass per time and per adsorbent mass)                |
| 4.  | [99] GC               | E, I       | $\alpha$  | ✓  | ✓              | ✓ (as mass per time; no adsorbent amount)                  |
| 5.  | [150] GC              | I          | -   | (Only diagrams reported) <sup>1</sup>  |                |  |
| 6.  | [151] GC              | E          | -   | ✓ <sup>2</sup>   | ✓              | ✓ (as mass per time; no adsorbent amount) <sup>2</sup>     |
| 7.  | [152] GC              | E, I       | $\alpha$  | -  | -              | -  |
| 8.  | [153] GC              | E, I, D    | $\alpha$  | -  | -              | -  |
| 9.  | [100] GC              | E, I, D    | $\alpha$  | ✓  | -              | ✓ (as mass per time; no adsorbent amount)                  |
| 10. | [101] GC-SMB          | E          | $H$ , $\alpha$ , isotherm Linear+Langmuir             | ✓  | -              | ✓ (as mass per time and per adsorbent mass)                |
| 11. | [102] GC-SMB          | E          | $H$ , $\alpha$  | ✓ <sup>3</sup>   | -              | (Only diagrams reported) <sup>3</sup>                      |
| 12. | [103] GC-SMB          | I          | $H$ , $\alpha$  | ✓  | -              | - (only as mass per adsorbent volume – no time interval)   |
| 13. | [71] GC-SMB           | E          | $H$ , $\alpha$  | ✓ <sup>4</sup>   | -              | ✓ (as mass per time and per adsorbent mass)                |
| 14. | [72] SMB/PSA          | E          | - (only simulations done)                             | ✓  | ✓              | ✓ <sup>5</sup> (as mass per time and per adsorbent volume) |
| 15. | [54] SMB, PSA         | E          | - (only simulations done)                             | ✓ <sup>6</sup>   | ✓ <sup>6</sup> | ✓ (as feed mass per time and per adsorbent volume)         |
| 16. | [154] GC              | D          | Bi-Langmuir isotherm <sup>7</sup>                     | -  | -              | -  |

\* Substances are denoted as: E – enflurane, I – isoflurane, D – desflurane;  $\alpha$  – selectivity,  $H$  – Henry constant;  $PU$  – purity,  $RE$  – recovery,  $PR$  – productivity.

<sup>1</sup> Presented curves purity - production (as product mass, no adsorbent amount) and purity - recovery.

<sup>2</sup> Additionally presented diagrams: purity - productivity, productivity - injected amount - purity, purity - injected amount - daily production, purity of the component 1 - purity of the component 2 - daily production.

<sup>3</sup> Presented dependencies of purity on the  $m$  values and of productivity on the velocity in the SMB zone I.

<sup>4</sup> Additionally presented dependency of purity on the  $m_2$  value and on the feed concentration.

<sup>5</sup> Not specified for which enantiomer.

<sup>6</sup> Only for the component 1 (R-enantiomer).

<sup>7</sup> Isotherm of the racemic mixture.

## 6 Experiments, models and simulations of the separation processes

In this work two systems (bicalutamide and anaesthetic gases) were studied experimentally as well as theoretically by computer simulations. The experimental part consists of the starting and validation tests. In the case of anaesthetics, the experiments were performed with the goal to test the feasibility of the enantioseparation using a new stationary phase (developed within SPP1570 Subproject II – explained in Chapter 1, section 1.3). The starting experiments served in this thesis for obtaining the necessary data for simulations and later for comparison of the predicted data with the real ones. The experiments with bicalutamide were carried out as a part of this project.

Modelling and simulations represent another part of the investigation. The purpose of the theoretical studies was to examine different parameters that influence the separation process and to identify the values that should be implemented in order to achieve the optimal operation in terms of maximal production of the pure enantiomers. In this chapter only the introduction into the modelling and simulations will be given, while the further results are presented in Chapter 8.

### 6.1 Experimental part

In this section the equipment and the materials used in experiments will be listed and afterwards the system characterization and calculation of the parameters needed for the process analysis will be presented first for the liquid phase experiments with bicalutamide and then for the separation of the anaesthetics in the vapour phase.

#### 6.1.1 Separation of the enantiomers of bicalutamide

Since the separation of bicalutamide enantiomers was studied just as a reference system, the goal was to provide the similar experimental outcomes as those seen in the experiments with the anaesthetic gases (section 6.1.2). In that way the results from the liquid and gas phases could be properly compared. The complete experimental investigation of bicalutamide was done in the framework of this thesis project.

##### 6.1.1.1 *Materials, equipment and chromatographic method*

The racemic mixture of bicalutamide was obtained from AstraZeneca PLC, London, UK. The mobile and stationary phases were chosen based on previous experiments with bicalutamide [15, 16]. Accordingly, as mobile phase in all experiments pure methanol (“HPLC-gradient

grade”) was used. It was purchased from VWR Chemicals, BDH Prolabo, Fontenay-sous-Bois, France and used in the form obtained from the supplier. The column used for separation was a commercial Chiralpak AD column (Daicel Chemical Industries Ltd.) with dimensions of 5 x 0.46 cm. This column is packed with the selector – amylase tris-(3,5-dimethylphenylcarbamate) coated on 20  $\mu\text{m}$  particles of silica-gel. As a non-adsorbing (unretained) compound 1,3,5-tri-tert-butylbenzene (TTBB, produced by TCI Deutschland GmbH, Eschborn, Germany) was taken.

The chromatographic experiments were done in a standard HPLC system Agilent Technologies 1200 Series (Agilent, Palo Alto, CA, USA) shown in Figure 6.1, with the software Agilent 1200 ChemStation for LC 3D Systems. The HPLC unit is equipped with a high pressure four-channel pump, a sample injector, a thermostatted column compartment, an auto-sampler and a diode array detector.



Figure 6.1. HPLC unit used for separation of bicalutamide enantiomers.

#### **6.1.1.2 Procedures and calculation of the required parameters**

Using the aforementioned stationary phase for separating the bicalutamide enantiomers, the first eluting component (component 1) is found to be the S-enantiomer and therefore the second one (component 2) is the R-enantiomer. The eluting order was determined by injecting the pure S-enantiomer and measuring the peak retention time. The obtained results are in accordance with the data published in the literature [15, 16].

The main bicalutamide experiments consist of injecting various amounts of racemic mixture in order to produce different resolution of the peaks. All the experiments were performed at 25  $^{\circ}\text{C}$  using the maximal possible feed concentration that is allowed by the solubility range of bicalutamide in methanol (about 20 g/l). With the injector incorporated into the HPLC unit, it was possible to inject amounts from 0.1  $\mu\text{l}$  to 100  $\mu\text{l}$ . Different volumetric flowrates were tested in order to fulfil the requirement to provide complete or nearly complete separation



with the small injections and almost no separation when injecting larger amounts. The flowrate of 2.5 ml/min was chosen. Larger flowrates were not advisable in the column specifications because of the large pressure drop caused in these cases. The data discussed here are summarized in Table 6.1 together with the parameters calculated later. For the column characterization lower flowrate (1 ml/min) was used.

In order to characterize the column in terms of determining the extra-column dead volumes and the void volume inside the column, injections of small pulses (1 and 5 microliter) of the unretained substance TTBB (concentration in methanol 20 g/l) were performed. Extra-column volume includes the volume of all the capillary tubes within the HPLC unit between the injector and the detector, and also the volumes of the injector, detector and other additional parts of the instrument. To estimate the extra-column volume, the column is removed from the system and replaced by the unit of negligible volume. The column void volume ( $V_f$ ) is measured in the same way, but with the column installed in the system. Knowing the flowrate, the volume can be calculated from the measured retention time of the TTBB peak. Based on this value, the total bed porosity ( $\epsilon$ ) is calculated according to eq. (2.5). The values of these parameters are reported in Table 6.1.

The column efficiency and Henry constants were calculated from the elution profiles resulting from small injections, where there is no interference (or only slight) between two peaks. Henry constants, which represent the initial slope of the adsorption isotherms, were obtained using eq. (2.36) from the injection of 5  $\mu$ l of racemic mixture with the concentration of 9.7 g/l at 1 ml/min flow (Figure 6.2). From their values the selectivity was determined (eq. (2.37)). The values of all three parameters are given in Table 6.1. By analysing them it can be seen that the separation of the enantiomers in the applied column is very good.

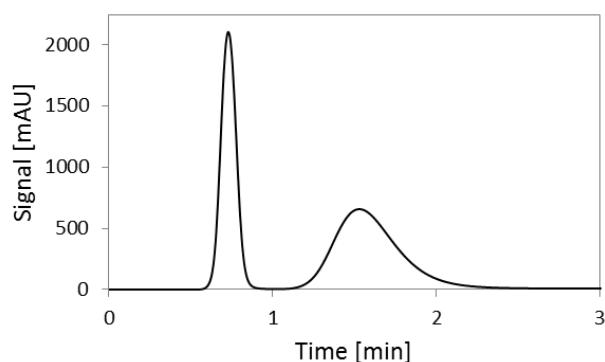


Figure 6.2. Elution profile with no interference between peaks used to calculate Henry constants of bicalutamide enantiomers and *NTP* (injected volume 5  $\mu$ l, injected mass of racemic mixture 0.192 mg and concentration 9.7 g/l, flowrate 1 ml/min, signal recorded at wavelength of 230 nm).

The number of theoretical plates (*NTP*), which demonstrates the column efficiency, was determined for the both enantiomers (using eq. (2.11)) for different flowrates of the mobile phase in the range from 0.5 to 5 ml/min. The injected amounts (5  $\mu$ l), as well as the feed concentration (9.7 g/l), were the same as those in the experiments for determining Henry

constants. After calculating the height of the plates (*HETP* values), Van Deemter curves (section 2.1) could be constructed, as presented in Figure 6.3.

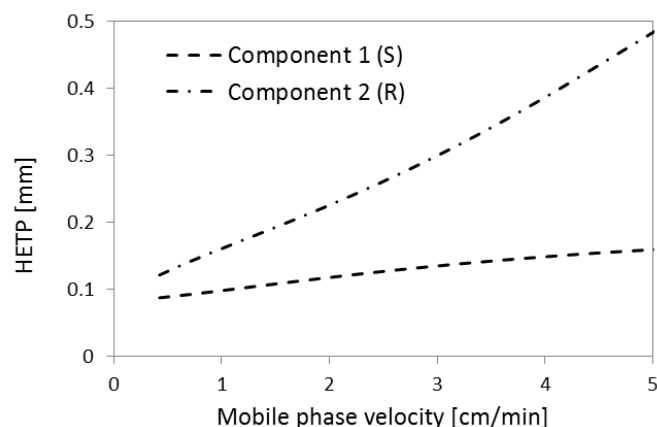


Figure 6.3. Van Deemter curves for bicalutamide enantiomers.

Commonly these curves contain a minimum that represents the optimal value for obtaining the highest separation efficiency. However, the efficiency optimum is not always the optimal operation point since for higher productivities it is very often more advantageous to work with higher flowrates. As it can be seen in this case, the minimum of both curves can be reached for the velocity values below the investigated range, i.e. for very low flowrates. Therefore, the chosen volumetric flowrate (2.5 ml/min) was not based on these calculations. The *NTP* values for the flowrate used in further experiments are shown together with the other experimental data in Table 6.1.

Table 6.1. Experimental data for bicalutamide injections (S-enantiomer – component 1, R-enantiomer – component 2).

|  |                                   |          |
|--|-----------------------------------|----------|
| Column length                                | 5 cm                              |          |
| Column inner diameter                        | 0.46 cm                           |          |
| Feed concentration (racemic mixture)         | 19.2 g/l                          |          |
| Mobile phase flowrate                        | 2.5 ml/min                        |          |
| Injected volumes                             | 1, 10, 30, 70, 90 and 100 $\mu$ l |          |
| Temperature                                  | 25 $^{\circ}$ C                   |          |
| Extra-column dead volume                     | 0.064 ml                          |          |
| Column hold-up volume                        | 0.59 ml                           |          |
| Total bed porosity (eq. (2.5) and (2.6))     | 0.713                             |          |
| Number of theoretical plates<br>(eq. (2.11)) | Component 1 (S)                   | 62       |
|  | Component 2 (R)                   | 20       |
| Henry constant<br>(eq. (2.36))               | Component 1 (S)                   | 0.31 l/l |
|  | Component 2 (R)                   | 3.73 l/l |
| Selectivity (eq. (2.37))                     | 12.0                              |          |

For calculating the adsorption isotherms and for process performance estimation, the elution profiles resulting from injections of different sizes were recorded by a UV detector. The peaks were recorded using two wavelengths, 300 nm for the injections in the range 0.1-5  $\mu\text{l}$  and 320 nm for 10-100  $\mu\text{l}$ . The detector calibration, i.e conversion from signal to the concentration, was done using the pulse injections and by plotting the area of the elution peak versus the known injected amount. Since two enantiomers produce the same value of the UV detector signal, the calibration was done only by using the racemic mixture. The plots are shown in Figure 6.4. The calculated values of the calibration factors ( $CF$ ) expressed from the following equation

$$c = CF \cdot \text{Signal} \quad (6.1)$$

were  $CF = 1.0235 \cdot 10^{-4}$  g/l/mAU for the wavelength of 300 nm and  $CF = 0.0718$  g/l/mAU for 320 nm.

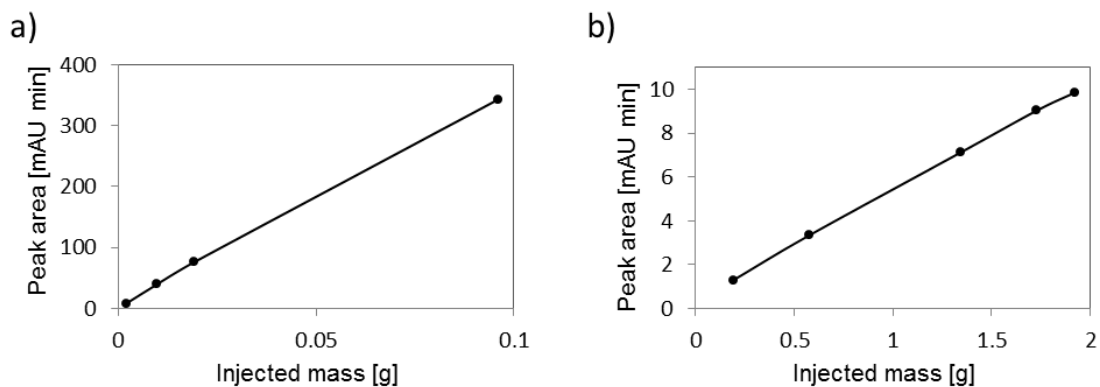


Figure 6.4. Dependency of peak area from the injected mass, used for detector calibration for bicalutamide experiments, done with racemic mixture: a) Wavelength 300 nm, injected amounts 0.1-5  $\mu\text{l}$ ; b) Wavelength 320 nm, injected amounts 10-100  $\mu\text{l}$ .

As it can be seen from Figure 6.4, the dependencies of peak area from the injected mass are linear and therefore this calibration strategy can be applied. However, in order to prove the linearity in the higher concentration range, the system response from the staircase change of the inlet concentration was analysed in addition. The concentration was changed in steps from zero to 17.86 g/l. In the first five steps it was increased by 5 % of the maximal value and afterwards by 10 %. The obtained outlet curve at 320 nm is presented in Figure 6.5.

It can be noticed that the signal changes linearly when concentration is increased by equal steps, what proves that the signal is recorded in the linear detection range. The calibration factor was calculated using this method for the signals from 0 to 45 mAU (the range observed in the pulse experiments), and the obtained value was 0.0798 g/l/mAU, which is very close to the value calculated using the pulse injections method.

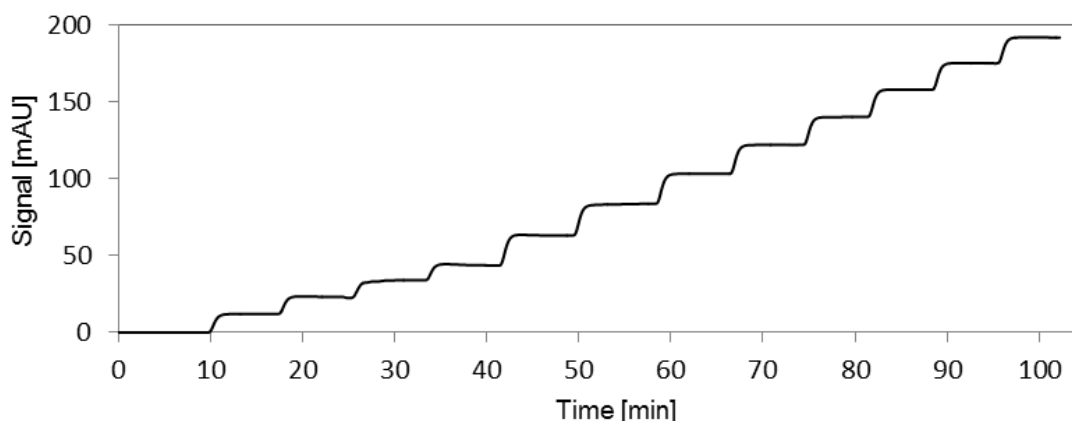


Figure 6.5. Staircase function recorded at the wavelength of 320 nm used for detector calibration for bicalutamide experiments done with racemic mixture. The maximal concentration (in the last step) was 17.86 g/l and the flowrate 0.5ml/min.

### 6.1.1.3 Experiments for measuring the adsorption isotherms and process analysis

In order to estimate the adsorption isotherm parameters with both methods described in Chapter 3, a series of pulse injections using different amounts of racemic mixture should be performed. The elution profiles resulting from the injections of 1 to 100  $\mu\text{l}$  are given in Figure 6.6. These injections represent the main experiments with bicalutamide that served first for isotherm determination (Chapter 7), and then for the estimation of productivity and other process performance criteria (Chapter 8).

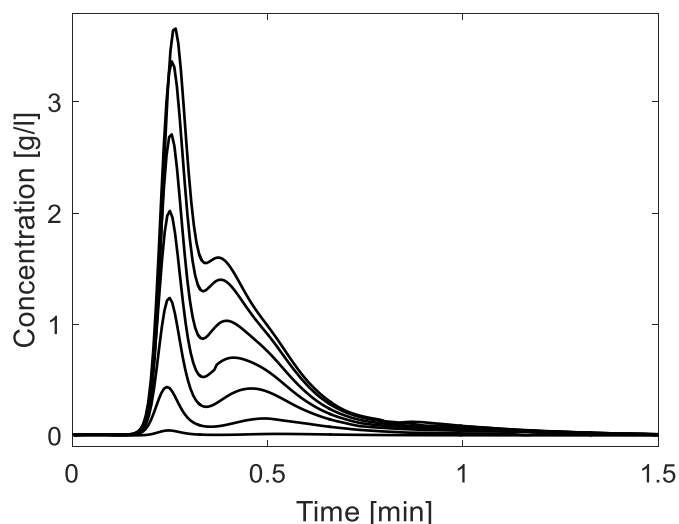


Figure 6.6. Elution profiles of bicalutamide for different injection volumes (in the brackets the feed mass of one enantiomer is given): 1  $\mu\text{l}$  (0.019 mg), 10  $\mu\text{l}$  (0.192 mg), 30  $\mu\text{l}$  (0.576 mg), 70  $\mu\text{l}$  (1.34 mg), 90  $\mu\text{l}$  (1.73 mg), 100  $\mu\text{l}$  (1.92 mg). The lowest-concentration profile corresponds to the smallest injected amount and higher-concentration profiles to larger amounts injected. Feed concentration is 19.2 g/l (of racemic mixture), and mobile phase flowrate 2.5 ml/min.

### 6.1.2 Separation of the enantiomers of anaesthetic gases

The experimental work related to the separation of enantiomers of anaesthetics isoflurane and desflurane was done as part of the parallel Subproject II. Part of the parameter calculations was also performed in the frame of that subproject. Therefore, in this section, only the calculations not completed in Subproject II will be described, while the rest of the data, which were needed for the simulation part, will be just mentioned and listed.

#### 6.1.2.1 Materials, equipment and methods

The racemic mixtures of isoflurane and desflurane (originally produced by Baxter International Inc., USA) were provided by a local hospital. The carrier gas (mobile phase) employed in these separations was helium of 99.99 % purity purchased from Linde AG, Germany.

The columns used were in-house packed with the stationary phase (adsorbent) developed and produced in the frame of SPP1570 Subproject II. The adsorbent consists of the selector based on  $\gamma$ -cyclodextrin and the support made of newly developed porous glass beads [157]. The raw glass beads were prepared by the research group of Professor Enke, Leipzig University and then their surface was modified and coated with selector at Otto von Guericke University Magdeburg by Thomas Munkelt. The chosen selector was Octakis(3-O-butyl-2,6-di-O-pentyl)- $\gamma$ -cyclodextrin, developed by König et al. [156], which was already well-established for the enantioseparation of the fluorinated anaesthetics. Glass beads were prepared first by treating their active surface sites with hexamethyldisilazane and afterwards by coating them with the selector dissolved in polysiloxane SE-54 [158] with a weight ratio of 1:1 and a surface concentration of 4.5 mg/m<sup>2</sup>. In this way prepared enantioselective glass beads have the following characteristics: particle diameter distribution of 52-100  $\mu\text{m}$ , mean pore diameter  $d_{\text{pore}} = 53$  nm, specific pore volume  $V_{\text{pore}} = 1.208$  cm<sup>3</sup>/g and porosity  $\epsilon_p = 0.727$ . The particles were mechanically packed into the stainless steel columns.

Columns of three different sizes were used. For the starting experiments, the smaller-diameter columns were employed. Four equal columns with the inner diameter 0.6 cm and total length 40 cm (10 cm each) were connected in a line and treated in analysis as one single column. They are presented in Figure 6.7. Two larger columns with dimensions 1.0 x 40 cm and 1.66 x 40 cm were used for the scale-up tests and the validation experiments.

The GC measurements were performed with a gas chromatographic unit 7890 A from Agilent Technologies, USA, equipped with column thermostat and flame ionization detector. The flowrate through the column was controlled by a mass flow controller.

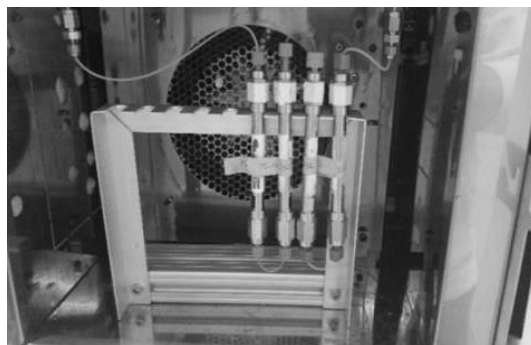


Figure 6.7. Four columns placed in the gas chromatograph used for the first tests and successful separation of isoflurane and desflurane enantiomers (The image is provided together with the data from SPP1570 Subproject II).

More details about the experimental part and especially the adsorbent characteristics and production information could be found in the future thesis of Thomas Munkelt [14], where Subproject II will be presented.

#### **6.1.2.2 Procedures and calculation of the required parameters**

The experimental data provided by the parallel Subproject II are listed in Table 6.2. The samples containing pure racemate of the corresponding anaesthetic were injected in the liquid phase in the GC unit, where instantaneous evaporation occurs. The detector calibration was done by injecting the known amounts of the racemic mixture and calculating the peak area in the same way as in the case of bicalutamide experiments.

The total porosity was determined from eq. (2.28), taking into account the gas compressibility effects (James-Martin factor). The column hold up time ( $t_0$ ) needed for porosity calculation was estimated by injecting methane in the same columns that were used for separation of desflurane and isoflurane racemates. Methane, as a non-retained substance on the applied stationary phase, was chosen based on the previous studies [71, 101-103, 152].

As it can be observed from Table 6.2 the pressure drop ( $P_{drop}$ ), calculated as the difference between the inlet ( $P_{in}$ ) and the outlet pressure ( $P_{out}$ ) is not very high, especially in the desflurane experiments. For isoflurane higher flowrate was used and, consequently, the pressure drop was larger. The low pressure drop values justify the use of the simplified models, as mentioned at the beginning of Chapter 3.

The investigation of different flowrates, as well as detector calibration for both of the substances was performed as part of the Subproject II.

It is important at the beginning to clarify which of the enantiomers is the first and which the second eluting substance. When using octakis(3-O-butanoyl-2,6-di-O-n-pentyl)- $\gamma$ -CD as selector, for both of the anaesthetics, isoflurane and desflurane, the elution order of the enantiomers is the same, as stated in [98]: first eluting component (component 1) represents the S-enantiomer and the second one (component 2) is the R-enantiomer.

Table 6.2. Experimental data for isoflurane and desflurane injections provided from SPP1570 Subproject II [14].

|  |                     |  |
|--|---------------------|--|
| Column length  |                     | 40 cm  |
| Column inner diameter  | Small column        | 0.6 cm   |
|  | Intermediate column | 1.0 cm   |
|  | Large column        | 1.66 cm  |
| Total bed porosity   |                     | 0.81   |
| Temperature  |                     | 28 °C  |
| Substance  |                     | Isoflurane                      Desflurane                       |
| Mobile phase flowrate*   |                     | 71 ml/min                      21 ml/min                         |
| Inlet pressure*  |                     | 176.7 kPa                      116.3 kPa                         |
| Outlet pressure*   |                     | 101.3 kPa                      101.3 kPa                         |
| Injected volumes (liquid phase)*   |                     | 0.04, 0.4, 1, 2, 3, 4 and 5 $\mu$ l      0.04, 0.4 and 1 $\mu$ l |
| * For the small column (the calculations for the larger columns will be given in section 8.2.2). |                     |  |

The previously listed experimental data obtained from SPP1570 Subproject II were used for the further calculations. The column efficiency (expressed as *NTP*) and Henry constants were determined for isoflurane and desflurane in the same way as for bicalutamide using the elution profile when the least amount of racemic mixture was injected (0.04  $\mu$ l). These profiles are given in Figure 6.8.

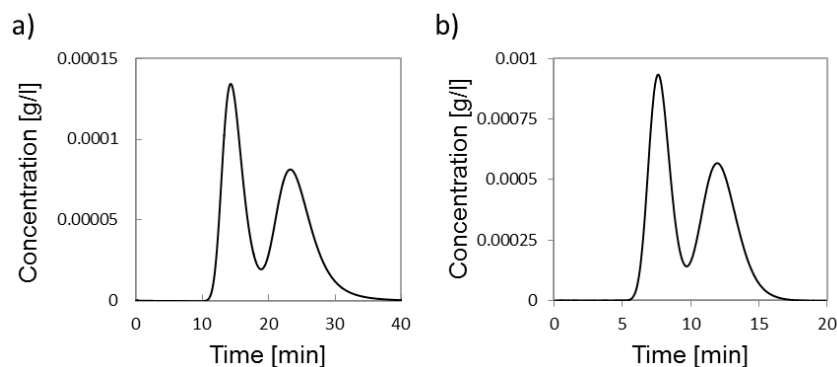


Figure 6.8. Elution profiles used to calculate Henry constants and *NTP* of: a) Isoflurane (Injected volume 0.04  $\mu$ l of racemate, injected mass 0.060 mg of racemate, flowrate 71 ml/min); b) Desflurane (Injected volume 0.04  $\mu$ l of racemate, injected mass 0.076 mg of racemate, flowrate 21 ml/min).

The calculated values of the parameters are listed in Table 6.3 for both anaesthetics. As observed from Figure 6.8, the resolution of the peaks is not complete and therefore the calculated values include a certain error. Since the degree of peak overlapping is not very high, these errors should be considered small enough and not to have bigger influence on the further calculations. The values of Henry constants will be checked by applying peak-fitting method in Chapter 7. From Henry constants the selectivity was estimated to be around 1.6 for both substances, which are the typical values for this type of systems and show a reasonable potential for separation.

Table 6.3. Calculated parameters for isoflurane and desflurane (S-enantiomer – component 1 and R-enantiomer – component 2) using the small injection amounts, based on mean retention times.

| Substance                                    |                 | Isoflurane | Desflurane |
|--|-----------------|------------|------------|
| Number of theoretical plates<br>(eq. (2.11)) | Component 1 (S) | 89         | 98         |
|  | Component 2 (R) | 80         | 85         |
| Henry constant<br>(eq. (2.36))               | Component 1 (S) | 467.7 l/l  | 70.03 l/l  |
|  | Component 2 (R) | 765.5 l/l  | 112.4 l/l  |
| Selectivity (eq. (2.37))                     |                 | 1.64       | 1.61       |

### 6.1.2.3 Experiments for measuring the adsorption isotherms and process analysis

As for bicalutamide analyses, in the case of anaesthetic gases the same type of pulse injections were completed and used for estimation of the isotherms and for validation of the results from the simulation studies. The recorded elution profiles for isoflurane and desflurane are presented in Figure 6.9 and Figure 6.10, respectively. For injecting the racemic mixtures into the GC unit two syringes of different sizes were used, the smaller one for the injections 0.04 – 1  $\mu\text{l}$  and another one for the larger amounts. Due to technical constraints (like syringe not being completely gas tight), the larger syringe could not be used for desflurane since the substance was evaporating owing to its low boiling point (23.5  $^{\circ}\text{C}$ , Table 5.2). That problem was not encountered in the case of isoflurane (boiling point 48.5  $^{\circ}\text{C}$ ). Therefore for desflurane no larger injections than 1  $\mu\text{l}$  were possible.

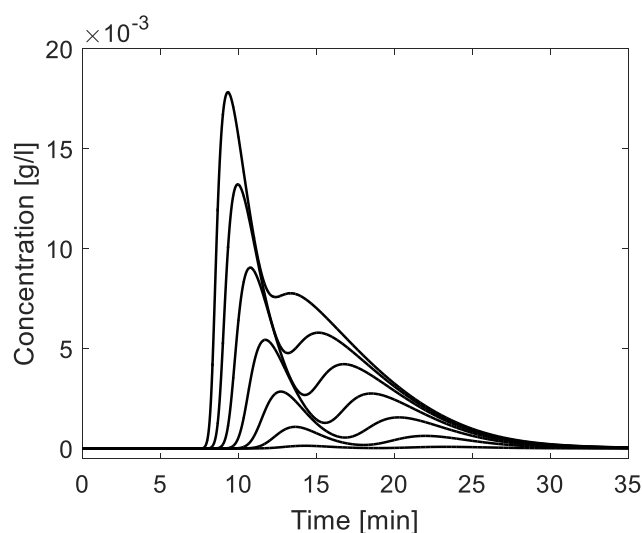


Figure 6.9. Elution profiles of isoflurane for different injection volumes of pure isoflurane racemate (in the brackets the feed mass of one enantiomer is given): 0.04  $\mu\text{l}$  (0.030 mg), 0.4  $\mu\text{l}$  (0.30 mg), 1  $\mu\text{l}$  (0.75 mg), 2  $\mu\text{l}$  (1.50 mg), 3  $\mu\text{l}$  (2.15 mg), 4  $\mu\text{l}$  (2.98 mg), 5  $\mu\text{l}$  (3.84 mg); Volumes are given for the samples in the liquid phase. The lowest-concentration profile corresponds to the smallest injected amount and higher-concentration profiles to larger amounts injected. Flowrate is 71 ml/min.



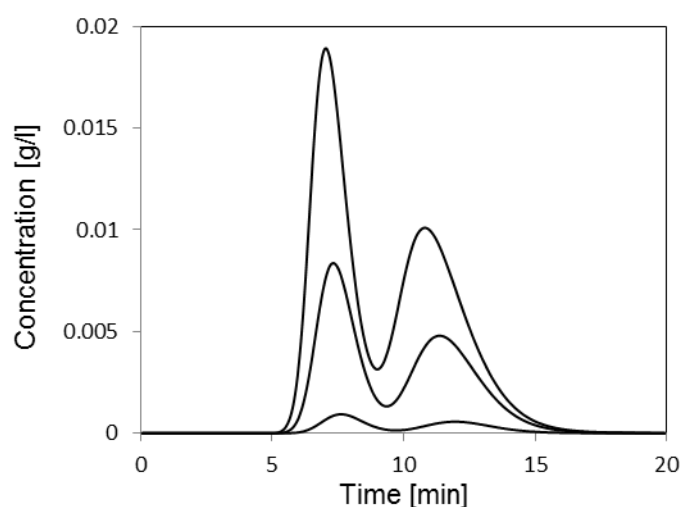


Figure 6.10. Elution profiles of desflurane for different injection volumes of pure desflurane racemate (in the brackets the feed mass of one enantiomer is given): 0.04  $\mu\text{l}$  (0.038 mg), 0.4  $\mu\text{l}$  (0.382 mg), and 1  $\mu\text{l}$  (0.70 mg); Volumes are given for the samples in the liquid phase. The lowest-concentration profile corresponds to the smallest injected amount and higher-concentration profiles to larger amounts injected. Flowrate is 21 ml/min.

In order to test the new adsorbent studied in this work, repetitive injections in close succession were performed. As illustration, one segment of five consecutive injections of isoflurane is presented in Figure 6.11. In this way stability of the stationary phase and of the entire system is verified, as well as the reproducibility of the separation process.

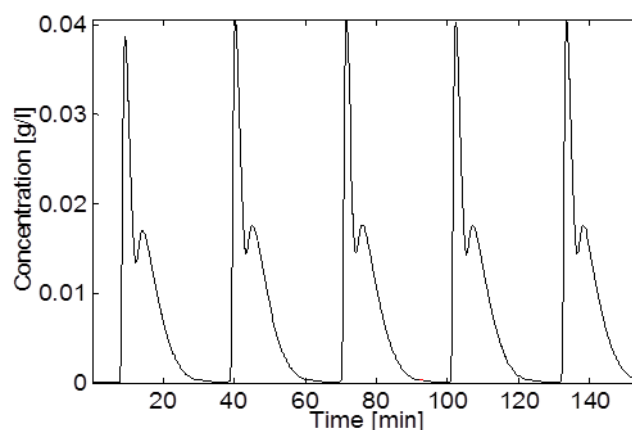


Figure 6.11. Repetitive injections of isoflurane (Injected volume 4  $\mu\text{l}$ , flowrate 71 ml/min).

The production process is planned to be carried out by consecutive injections (more about it can be found in Chapter 8) in order to minimize the carrier gas consumption and to maximize the production rate by avoiding waste of time between two injections. This is due to the fact that repetitive injections are timed in such way that the second and each of the following elution profiles start exactly at the time when the previous peak ends.

## 6.2 Modelling and simulation studies

The simulation of the separation processes was performed after obtaining the adsorption isotherms and acquiring all other required parameters. For enantioseparation of fluorinated anaesthetics two types of processes were studied: the one-column GC separation, characterized and examined in more details, and a continuous PSA process, while bicalutamide separation was investigated only by using the batch (1-column) HPLC system.

### 6.2.1 Models and parameters used for description of the processes

The chromatography models were described in Chapter 2, sections 2.2, 2.3, and in the section 2.5.2 for a PSA process. To investigate the GC separation, a simple model was chosen. It consists of mass balance equation described by the equilibrium dispersive model (EDM, eq. (2.17)) and the adsorption isotherm equation. The model assumes no changes in velocity or temperature due to adsorption/desorption effects, as well as no pressure drop along the column. As explained at the beginning of Chapter 4, these assumptions can be justified when working with diluted systems, since in that case the pressure drop, as well as the changes of the gas velocity can be considered negligible. The same model was taken for the bicalutamide simulation.

For the simulation of the PSA separation of isoflurane and desflurane, the more complex model was used, which is typical for the gas phase. Due to the higher pressure during the adsorption step, the changes in velocity and pressure could not be neglected. Therefore mass balance was expressed using the EDM with non-constant velocity typical for the gas phase (eq. (2.24)) and the pressure drop was calculated by Ergun equation (eq. (2.56)). Since the investigated systems were diluted, the temperature was assumed to be constant during the process, so there was no need to introduce the energy balance. The same assumptions were adopted by Bentley et al. for PSA separation of enflurane enantiomers [54]. The pressure change with time during the pressurization and blowdown steps were described by linear functions.

In order to provide faster calculations, the dispersion coefficient of two enantiomers was assumed to have the same value in the models, i.e. it was assumed that there was the same number of theoretical plates for each of two components. Since from the experimental tests it was clear that these values are not exactly equal, the average value was always taken for the calculation.

In all the cases investigated in this work, the adsorption of the substances was described by competitive Langmuir isotherms (Chapter 2, section 2.4, eq. (2.33)). They were assumed in advance and it was shown that this model can successfully be applied for all the studied systems.

In order to simulate a gas chromatographic system, first it is necessary to calculate the injection parameters for the gas phase. In practice, the sample is injected into a GC system in the liquid form. Inside the system, due to high temperature, it instantaneously evaporates, becoming gaseous and travels as a gas sample to the separation column. The feed concentration, as well as the volume that is taken as injected volume in the gas phase can be determined by knowing temperature and pressure at column inlet and by applying the ideal gas law and the conservation of the mass during the evaporation [159].

### 6.2.2 Solutions of the system of equations

A separation process in an adsorption bed is described by algebraic and partial differential equations, distributed in time and space. For models that include the mass transfer expression, even if they are the simplified ones, it is not possible to provide an analytical solution. Therefore, we need different numerical methods. In order to solve the equations numerically, one can use complete discretization, where both spatial and time domains are simultaneously discretized. This results in a large number of nonlinear algebraic equations that has to be solved. More often the method of lines [160] is applied. According to it, partial differential equations are first discretized in space domain and then the set of obtained differential equations (distributed only in time) and algebraic equations is integrated using standard time integration routines. There are also available software packages, like gPROMS (used in this work for PSA analysis) that can solve the set of coupled partial differential and algebraic equations without any previous discretization.

To discretize the system in space, and consequently to reduce partial differential equations into ordinary differential equations, finite volume methods are used most often, but there are also applications of orthogonal collocation, finite difference methods, finite element methods, or method of characteristics [13].

### 6.2.3 Simulation software

In this work process simulations solving chromatographic column model were mainly done in Matlab R2013b (8.2.0.701), MathWorks Inc, Natick, Massachusetts, USA. Differential equations were solved by finite difference method using Rouchon algorithm [161]. The axial dispersion term is neglected and replaced by numerical dispersion [11]. Number of calculation points (space and time increments) is determined according to the number of theoretical plates. For a few fast tests the pulse injections were simulated using ChromSim 1.2 software under Eurochrom 2000 for Windows. This software also uses integrated Rouchon algorithm. Pressure Swing Adsorption simulations were performed in gPROMS Model Builder 4.2.0 (x64), product of Process Systems Enterprise Ltd, London, United Kingdom. In gPROMS different schemes for solving the partial differential equation are available. For the system investigated in this work (enantioseparation of isoflurane and desflurane) centered finite difference method of the second order was chosen. Besides

gPROMS, which is very often applied for PSA simulations, e.g. in [54, 73, 162], there are other packages that could be used, such as ADSIM (Product of Aspen Technology) [72], Matlab [163], Fortran [164], combination of more packages or different non-commercial in-house built programmes [165, 166].

In the procedure of adsorption isotherm estimation using both, extended ECP and peak-fitting method, the important task was the minimization of the objective functions. The minimization process was completed by solving the least-squares problem using Matlab and applying the Levenberg-Marquardt algorithm (Matlab function *lsqnonlin*) or the Nelder-Mead simplex method (Matlab function *fminsearch*).

## **7 Determination of adsorption isotherm parameters (only racemic mixtures available)**

In order to analyse and optimize a chromatographic process, the knowledge of adsorption isotherms is one of the essential requirements. Since their determination is often complicated, it is of considerable importance to develop particular methods that are suitable for different systems. In Chapter 3 two methods were described for estimating the isotherms of enantiomers for the case when only racemic mixtures are available for the experimentations. This chapter reveals the results obtained from testing the statements made there and shows the application of the presented methods. First the newly developed extension of the elution by characteristic point (ECP method) for binary mixtures will be presented using an example with pseudo-experimental data generated by simulations. Afterwards the tests of its applicability for the substances investigated in this work will be shown. The peak-fitting method was also applied for determining the isotherms from racemic mixture and the resulting values were given for all the three examined substances, bicalutamide, isoflurane and desflurane. The method validation is done using the bicalutamide enantioseparation.

### **7.1 Binary-mixture ECP method**

The new ECP method for estimating the Langmuir adsorption isotherms of a binary mixture (explained in Chapter 3, section 3.1) will be evaluated here. Before its use for determining the isotherms of the investigated systems, first a test-system with data generated by simulations was taken to analyse the method in more details. This non-real experimental system was applied since it gives more flexibility in changing the parameters and investigating their influence on the calculated numbers. The obtained isotherms can then be compared to their exact values (that were used for the starting simulation). If a real system had been examined, it would be possible only to do the comparison with the parameters determined by some other methods that do not have to be necessarily correct.

#### **7.1.1 Preliminary systematic simulation study for evaluating the binary-mixture ECP method**

For the description and testing of the ECP binary-mixture method, a so-called simulation example with hypothetical (not existing) substances was used. The application of the method requires one elution profile with incomplete resolution of the two peaks. This profile was acquired by the simulation with Langmuir isotherm (eq. (2.33)) and equilibrium dispersion model of chromatography (eq. (2.17)). The apparent dispersion coefficient for this model was calculated from the number of theoretical plates, according to eq. (2.13). Since the used

information does not come from an existing experimental system, here it is indicated as pseudo-experimental data. Table 7.1 lists the simulation data. The isotherm parameters were chosen in order to provide the desired shape of the elution profile, while for the number of theoretical plates ( $NTP$ ) an intermediate value of 1500, which can already provide high efficiency, was taken.

Table 7.1. Data used for the simulation study to evaluate the binary-mixture ECP method. These data do not originate from any experimental system and therefore the substances are denoted as hypothetical.

|  |                 |                           |                            |
|--|-----------------|---------------------------|----------------------------|
| Column length                            |                 | 100 cm                    |                            |
| Column inner diameter                    |                 | 0.21 cm                   |                            |
| Bed porosity                             |                 | 0.8                       |                            |
| Number of theoretical plates             |                 | 1500                      |                            |
| Volumetric flowrate                      |                 | 40 ml/min                 |                            |
| Feed concentration (racemic mixture)     |                 | 0.68 g/l                  |                            |
| Injection volume                         |                 | 0.41 ml                   |                            |
| Competitive Langmuir isotherm parameters | $H_i (i = 1,2)$ | $H_1 = 971.8 \text{ l/l}$ | $H_2 = 1089.2 \text{ l/l}$ |
|  | $b_i (i = 1,2)$ | $b_1 = 20.2 \text{ l/g}$  | $b_2 = 55.0 \text{ l/g}$   |

When an overloaded elution profile is available (from experiments or in this case simulations), the first step in applying the extended ECP method is to choose the segments of the elution profile that will be used for the calculations. These segments should represent the parts of the chromatogram where the components are found in the pure form. However, when having experimentally obtained elution profile, these parts are not easy to define. In Figure 7.1 we can see one chromatogram simulated with the data from Table 7.1 and another one which can be considered as theoretical one (simulated with the same data, except for the  $NTP$  which is 10000). It can be seen that the two profiles follow the similar shape, yet there are deviations especially in the region of the chromatogram that represents the pure first component.

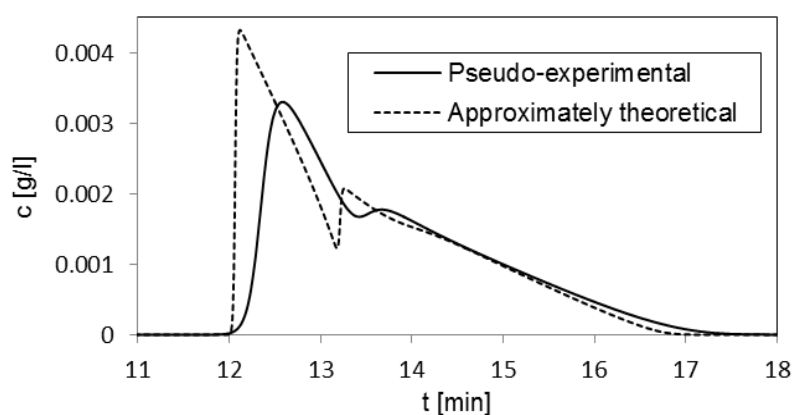


Figure 7.1. Comparison of an approximately theoretical elution profile of the binary mixture of the hypothetical substances ( $NTP = 10000$ ) to the one representing pseudo-experimental data ( $NTP = 1500$ ).

In order to investigate which data range would give the most correct isotherm parameters, diverse sequences shown in Figure 7.2 were tested. Four sections of different length were chosen from the part of the profile used for determination of component 1 isotherm and four lengths from the part used for component 2. The sections are named as follows:

- W1 – the so-called whole range of data that could be used for determining the isotherm of the component 1, starting from the peak maximum and ending to the first local minimum;
- W2 – the whole range used for the component 2, starting from the inflection point of the chromatogram after the second, local, maximum and ending at the end of the profile (when it reaches zero);
- L1 – the large data range used for the first component, starting from the maximum, but ending before the minimum, since the part close to the minimum is representing the mixture of the two components and not the pure component 1;
- L2 – the large data range for the second component that starts at the inflection point like W2, but ends before zero at the point where dispersion (which is not present in the theoretical case, Figure 7.1) starts to be noticeable;
- M1 and M2 – the medium ranges that do not include the end points of the ranges L1 and L2, since larger deviations from the theoretical case are expected there;
- S1 and S2 – the small ranges that only contain the near linear parts of the chromatogram.

The isotherm parameters were calculated for all 16 combinations of the defined sections. The sections W1 and W2 are chosen just in order to check the method, since the data ranges include the profile parts where the components are not in the pure form; thus the wrong results are expected to be produced. The large ranges L1 and L2 are considered as potentially correct, as they contain the larger amount of data, but at the same time exclude the parts of W1 and W2 that are certainly wrong.

The determination procedure starts from giving the first guesses for the isotherm parameters and calculating the theoretical values of the retention times for each concentration point using equations (3.8) and (3.11). The final values (the best ones) of the parameters are determined using a minimization procedure, as explained in the section 3.1.2. The objective function used contains the difference between the original and calculated retention times and is given by eq. (3.12). All four parameters of the two competitive Langmuir isotherms were simultaneously determined. An example of the result of this procedure is presented in Figure 7.3. It shows how the calculated retention times are matching the original values (from pseudo-experimental data).

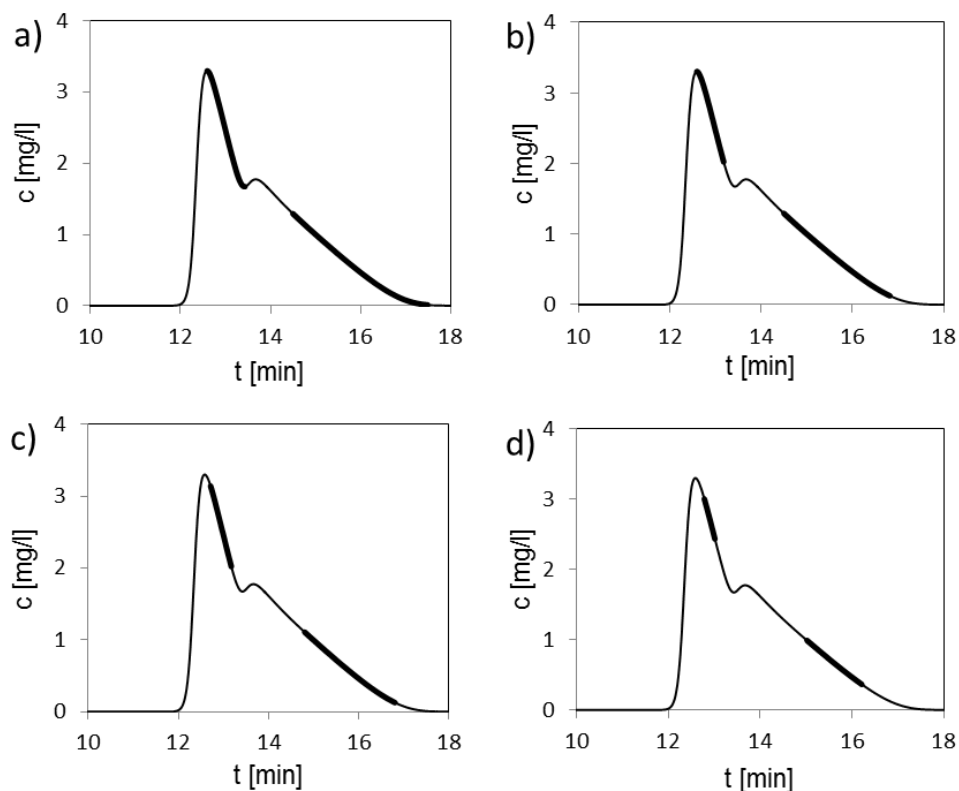


Figure 7.2. Different data ranges used for estimating the adsorption isotherms of the hypothetical substances by binary-mixture ECP method. Thicker parts of the lines represent the data sequences used for component 1 (those are the sequences in the higher concentration range) and component 2 (sequences in the lower concentration range). The sequences, which are defined in the previous text, are presented as follows: a) W1 and W2; b) L1 and L2; c) M1 and M2; d) S1 and S2.

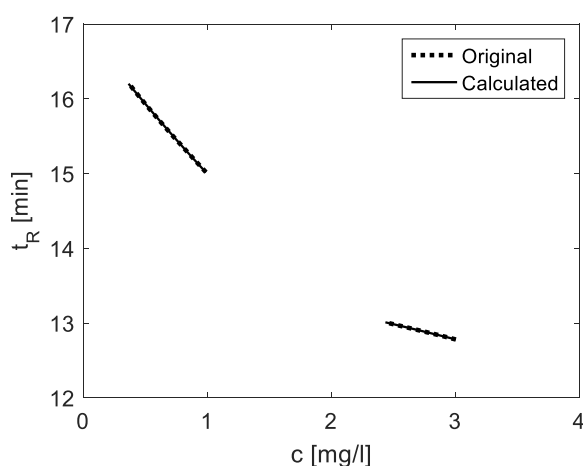


Figure 7.3. An example of the function of the retention times from the concentration presented for the component 1 (the data in the higher concentration range) and component 2 (the data in the lower concentration range) of the hypothetical mixture: The original values (pseudo-experimental data) are compared to those calculated using isotherm parameters obtained by binary-mixture ECP method. The sequences of the pseudo-experimental data used for the component 1 and 2 are S1 and S2 regions (defined in Figure 7.2), respectively.



After calculating the values of the adsorption isotherm parameters using different combinations of the chromatogram sequences, it was concluded that their accuracy was corresponding to the expectations made when the sequences were chosen. The combination of the sections W1 with W2 gave the poorest results, while the most accurate ones were obtained when S1 and S2 were used. The smaller the data range for determination of the component 2 isotherm was used, the better were the parameters obtained not only for the second component, but also for the first one. This is due to the fact that the isotherm parameters of the second component are included in the expression for the retention time of the first component (eq. (3.8)). Similarly, when smaller range for component 1 was taken, the isotherm parameters of the first component were more correct. In Table 7.2 two most accurate values and the least accurate one are shown together with the original parameters used for the starting simulation.

The presented sequences were chosen imagining that we have only experimental elution profiles available, without knowing the shape of the theoretical case. However from Figure 7.1 we can see that the part near the inflection point after the second maximum of the pseudo-experimental profile is the closest to the theoretical case, while the linear sequence S2 deviates from it to a certain extent. Therefore, for determining the isotherm of the component 2, that range, named IP2 was additionally considered. The sequence IP2 starts after the inflection point, like section W2, and ends at the point where the linear part starts, so it contains the points present in W2, but excluded in S2. The calculations of the parameters when the previously defined sections were combined with IP2 revealed that the most accurate values can be obtained when the sections S1 and IP2 are combined. The results are summarized in Table 7.2.

Table 7.2. Competitive Langmuir adsorption isotherm parameters of the hypothetical substances (simulation study,  $NTP = 1500$ ): Comparison of the original data used for the simulation and those determined by the binary-mixture ECP method using three different combinations of the larger data sequences, defined in the previous text.

| Component 1 and 2 isotherm parameters | Original values | Calculated values obtained by using the combination of the following chromatogram sections (relative error given in the brackets after the parameter value): |                |                |                |
|---------------------------------------|-----------------|--|----------------|----------------|----------------|
|                                       |                 | S1 and S2  | M1 and S2      | W1 and W2      | S1 and IP2     |
| $H_1$ [l/l]                           | 971.8           | 1005.6 (3.5 %)   | 1007.9 (3.7 %) | 1026.6 (5.6 %) | 1004.6 (3.4 %) |
| $b_1$ [l/g]                           | 20.2            | 23.8 (18 %)  | 24.4 (21 %)    | 27.9 (38 %)    | 23.8 (18 %)    |
| $H_2$ [l/l]                           | 1089.2          | 1110.4 (1.9 %)   | 1110.4 (1.9 %) | 1124.8 (3.3 %) | 1108.0 (1.7 %) |
| $b_2$ [l/g]                           | 55.0            | 63.9 (16 %)  | 63.9 (16 %)    | 72.0 (31 %)    | 62.7 (14 %)    |

For further analyses, the nearly-linear sections S1 and S2 were divided each into three smaller sub-sections. The isotherm parameters were estimated by combining these new small sequences. For the second component the best values were obtained when the third of the S2 section closest to the inflection point, denoted as S2-1, was used, while the worst were for the

part closest to zero (S2-3). For component 1 the most accurate values were achieved when the middle part of the section S1 (S1-2) was taken. The least accurate ones were for the third of S1 sequence closest to the maximum (S1-1). The results of the best combination (S1-2 and S2-1) and the worst one (S1-1 and S2-3) are given in Table 7.3.

After these examination the best data range for the component 1 (middle part of the linear section: S1-2) was combined with the section for component 2 that is close to the inflection point (the closest to the theoretical profile: IP2). These two sequences gave the most accurate isotherm parameters for the components 1 and 2 and it was expected that their combination would produce better results than the previous case. The results are presented in Table 7.3 and as it can be seen, the values calculated in this way are the closest to the original numbers.

Table 7.3. Competitive Langmuir adsorption isotherm parameters of the hypothetic substances (simulation study,  $NTP = 1500$ ): Comparison of the original data used for the simulation and those determined with the binary-mixture ECP method using three different combinations of the smaller data sequences, defined in the previous text.

| Component 1 and 2 isotherm parameters | Original values | Calculated values obtained by using the combination of the following chromatogram sections (relative error given in the brackets after the parameter value): |                |                |
|---------------------------------------|-----------------|--|----------------|----------------|
|                                       |                 | S1-2 and S2-1  | S1-1 and S2-3  | S1-1 and IP2   |
| $H_1$ [l/l]                           | 971.8           | 1004.4 (3.4 %)   | 1008.8 (3.8 %) | 1003.9 (3.3 %) |
| $b_1$ [l/g]                           | 20.2            | 23.6 (17 %)  | 24.3 (20 %)    | 23.6 (17 %)    |
| $H_2$ [l/l]                           | 1089.2          | 1109.4 (1.9 %)   | 1112.5 (2.1 %) | 1108.0 (1.7 %) |
| $b_2$ [l/g]                           | 55.0            | 63.3 (15 %)  | 66.0 (20 %)    | 62.7 (14 %)    |

The results of testing the sub-sequences of the linear ranges S1 and S2 and the IP2 section show that even when less data points are used, the better values for the adsorption isotherm parameters are obtained, as long as the proper sections of the profile are chosen. The most correct values are achieved when the middle part of the linear profile section for the first component (S1-2) and the part directly after the inflection point for the second component (IP2) are taken for the calculations.

However, it can be noticed that when using the data ranges IP2, S1, S2, or only the parts of S1 and S2, all the values calculated are relatively close to each other and can all be considered correct. To check this statement the competitive adsorption isotherms calculated with determined parameters were plotted in Figure 7.4 and Figure 7.5, for the first and the second component, respectively. In the both figures the original isotherm (with the starting parameters used for the simulation) was presented together with three selected cases, denoted as Case A, B and C, in the following way:

- Case A: obtained from combination of the sequences S1 and S2;
- Case B: obtained from combination of the sequences S1-2 and IP2, when the most correct values were achieved;

- Case C: obtained by combining the sections W1 and W2, when the least accurate values were obtained.

Isotherms were constructed for the concentration range for which the parameters of the corresponding components were determined. As it can be concluded, when observing the whole isotherm curves, there is almost no discrepancy between the original isotherm and the cases A and B. Compared to the case C, there is very small difference, that can also be considered negligible. The figures contain two insets, which show two different parts of the isotherms zoomed in order to see which of the cases is closest to the original one. As it can be seen at the different parts different cases show better results, since the curvatures are different and the isotherms intersect each other.

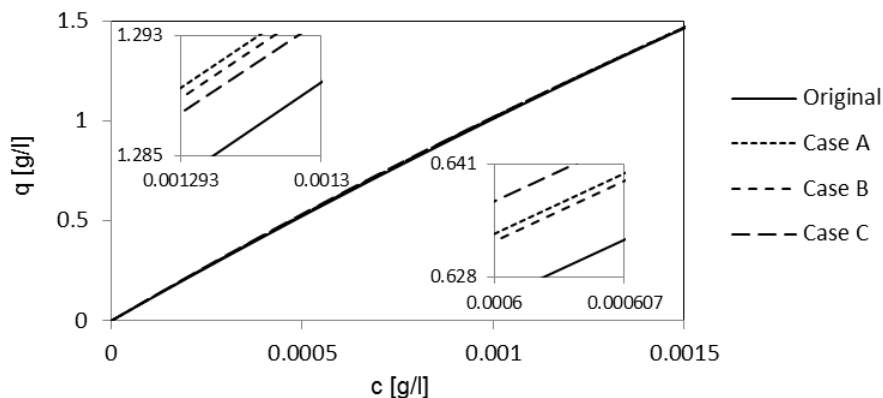


Figure 7.4. Isotherm of the first eluting component of the hypothetical system (simulation study) determined with the binary-mixture ECP method. It is calculated using the parameters from different cases, defined in the previous text. The two insets show the zoomed parts of the isotherm.

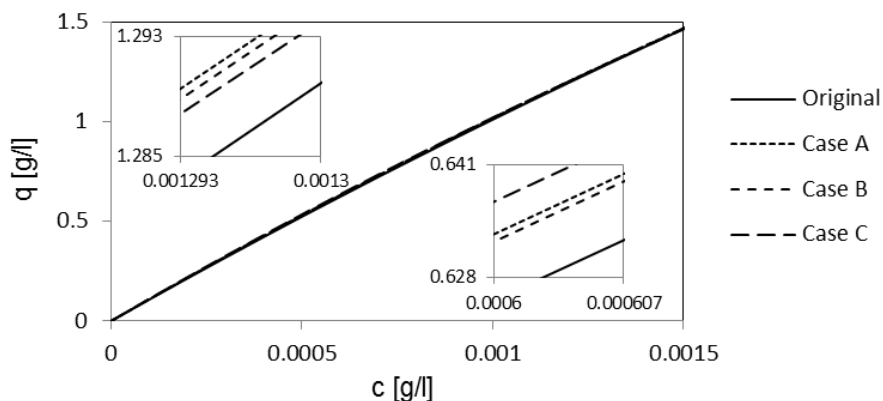


Figure 7.5. Isotherm of the second eluting component of the hypothetical system (simulation study) determined with the binary-mixture ECP method. It is calculated using the parameters from different cases, defined in the previous text. The two insets show the zoomed parts of the isotherm.

When the elution profiles simulated with the calculated parameters are compared, the differences are more noticeable. Figure 7.6 shows the profile simulated with the original parameters compared with two other profiles simulated with the parameters that correspond to the cases B and C (the most and least correct ones). Case B and C produced similar

profiles, but still different from the original one, although all the isotherm plots are very close to each other. The chromatograms show that the Case C is the closest to the original one and that the parameters obtained by using the profile sections S1-2 and IP2 provide the best prediction of the chromatogram.

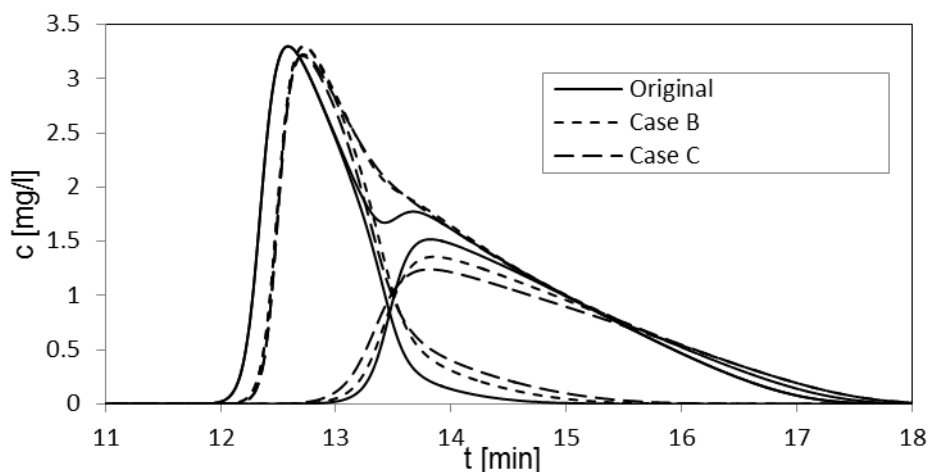


Figure 7.6. Elution profiles of the hypothetical system (simulation study): Comparison of the profile simulated with the original isotherm parameters and two profiles where the isotherms were determined with the binary-mixture ECP method. The cases B and C are defined in the previous text.

For the binary-mixture ECP method, it is important to know the number of theoretical plates for which the method could be applied and give correct results. For that purpose, four chromatograms simulated with the original data given in Table 7.1 and different  $NTP$  were used for isotherm determination. The taken  $NTP$  values were: 750, 1500, 2500 and 10000. The sections of the elution profile taken for the isotherm determination procedure correspond to those that gave the best results in the previous analysis (S1-1 for the component 1 and IP2 for the component 2). The calculated Langmuir isotherm parameters from the simulation study are listed in Table 7.4 and compared to the original ones.

Table 7.4. Competitive Langmuir adsorption isotherm parameters of the hypothetical substances (simulation study): Comparison of the original data used for the simulation and those determined with the binary-mixture ECP method using elution profiles generated by simulations with different number of theoretical plates ( $NTP$ ).

| Component 1 and 2 isotherm parameters | Original values | Calculated values from chromatograms simulated using different $NTP$ (relative error given in the brackets after the parameter value): |                |                |                |
|---------------------------------------|-----------------|--|----------------|----------------|----------------|
|                                       |                 | $NTP = 750$  | $NTP = 1500$   | $NTP = 2500$   | $NTP = 10000$  |
| $H_1$ [l/l]                           | 971.8           | 1056.6 (8.7 %)   | 1003.9 (3.3 %) | 993.4 (2.2 %)  | 979.6 (0.80 %) |
| $b_1$ [l/g]                           | 20.2            | 35.3 (1.6 %)   | 23.6 (0.35 %)  | 22.3 (0.22 %)  | 20.9 (0.07 %)  |
| $H_2$ [l/l]                           | 1089.2          | 1122.8 (3.5 %)   | 1108 (1.9 %)   | 1104.3 (1.6 %) | 1094.7 (0.6 %) |
| $b_2$ [l/g]                           | 55.0            | 66.4 (1.2 %)   | 62.7 (0.79 %)  | 62.0 (0.72 %)  | 58.0 (0.31 %)  |

The calculated results met the expected values. The more efficient the column is, the more correct parameter values can be achieved. For the most efficient column with 10000

theoretical plates, the parameters are almost equal to the original ones. When the  $NTP$  was 1500, the results were satisfactory, as previously stated and could be considered as correct, while for the column with  $NTP = 2500$  very good parameter values can be obtained.

The isotherm parameters calculated for different  $NTP$  were further used to simulate elution profiles. Figure 7.7 shows the simulated peaks for each case compared to the original ones. When observing the plots and the matching between simulated and original profiles, the same conclusion as in the previous paragraph can be derived.

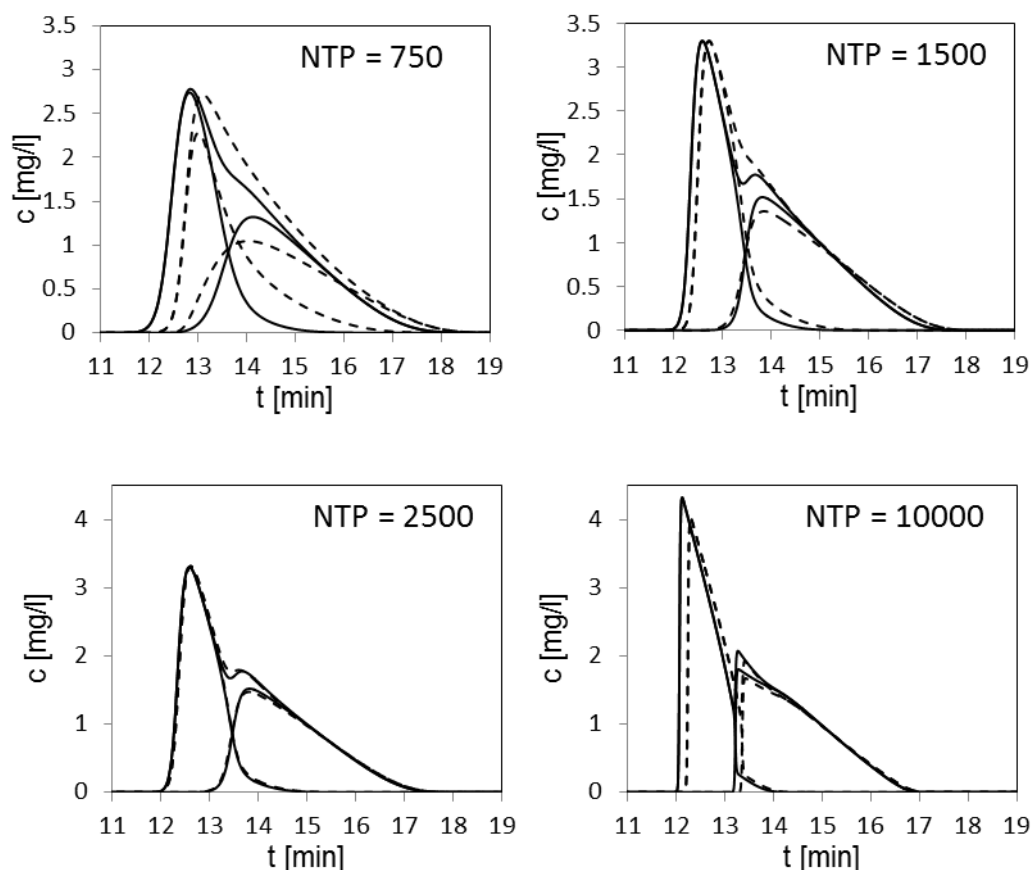


Figure 7.7. Elution profiles of the hypothetical system (simulation study): Comparison of the profiles simulated with the original isotherm parameters, by applying different number of theoretical plates (as defined in the sub-figures), to those where the isotherms were determined from the corresponding original chromatograms using the binary-mixture ECP method. Solid lines represent original profiles and dashed lines – simulated profiles with the estimated parameters.

To summarize, when using a column with  $NTP = 1500$ , we can get satisfactory results, and already with the one that has 2500 theoretical plates the obtained results are very good. When less efficient column is used, the results are not completely correct and could be used for the estimations of the peak positions, but not for the exact shape (as shown in the example when  $NTP$  was 750).

Therefore, for the successful application of the binary-mixture ECP method, the efficient columns with  $NTP$  that is at least 2000 are advisable to be taken for the experiments. The

method can still be used with small error for the systems where the columns have the *NTP* values between 1500 and 2000.

### 7.1.2 Estimation of the adsorption isotherms of the investigated substances with the binary-mixture ECP method

The binary-mixture ECP method, described and analysed in the previous section using a simulation study, was also applied for the systems investigated in this thesis, namely for the enantioseparation of bicalutamide, isoflurane and desflurane. For these examples the experimental elution profiles were available for the calculation procedure. It was not expected to acquire very precise values for the estimated isotherm parameters since for all the three systems the number of theoretical plates is lower than 100 (as reported in Table 6.1 and Table 6.3), and as it was concluded, ECP method requires at least 2000 theoretical plates.

The experimental data for the three systems are presented in Chapter 6 (Table 6.1 for bicalutamide and Table 6.2 for isoflurane and desflurane). From different injection amounts, for isoflurane and desflurane the largest injections were chosen for the isotherm estimation, since they cover larger concentration range and give the shape of the elution profile that is suitable for the ECP method. That is 5  $\mu\text{l}$  of liquid isoflurane racemate and 1  $\mu\text{l}$  for desflurane. In the case of the bicalutamide the injection of 90  $\mu\text{l}$  was taken because it provided the best shape of the elution profile for the method application.

For determining the isotherm parameters, the procedure explained in the previous section was applied. The chosen data range for the first eluting component was the middle fraction of the linear part between the peak maximum and the local minimum. For the second component estimation of the proper data range was not so easy, because due to low column efficiency, the inflection point could not be located with certainty. Therefore the section approximately situated near the estimated inflection point was taken for the calculations.

The results are presented in Table 7.5. As can be seen, the values obtained for desflurane seem realistic, while those of bicalutamide and isoflurane are not expected to be accurate since the Henry constants (*H*) for both components have approximately the same values.

Table 7.5. Adsorption isotherm parameters of bicalutamide, isoflurane and desflurane enantiomers determined using the binary-mixture ECP method.

| Component: 1, 2 | Bicalutamide | Isoflurane | Desflurane |
|-----------------|--------------|------------|------------|
| $H_1$ [V]       | 5.78         | 866.38     | 90.92      |
| $b_1$ [l/g]     | 4.30         | 34.05      | 7.13       |
| $H_2$ [V]       | 5.75         | 866.53     | 133.93     |
| $b_2$ [l/g]     | 0.61         | 45.53      | 12.76      |

The calculated isotherms were used to simulate the elution profiles. Comparisons of the experimental and simulated profiles are presented in Figure 7.8. When observing the peaks, the same can be concluded as when the values of the isotherm parameters were analysed. For desflurane the matching between the experimental and simulation peak is very good and the method can be considered as successful. One of the reasons is that for desflurane the elution profile resulting from the smaller injection was used, where the effect of the dispersion is not so large. For isoflurane and bicalutamide even when the profiles resulting from the small injection amounts were used, the obtained values were not correct.

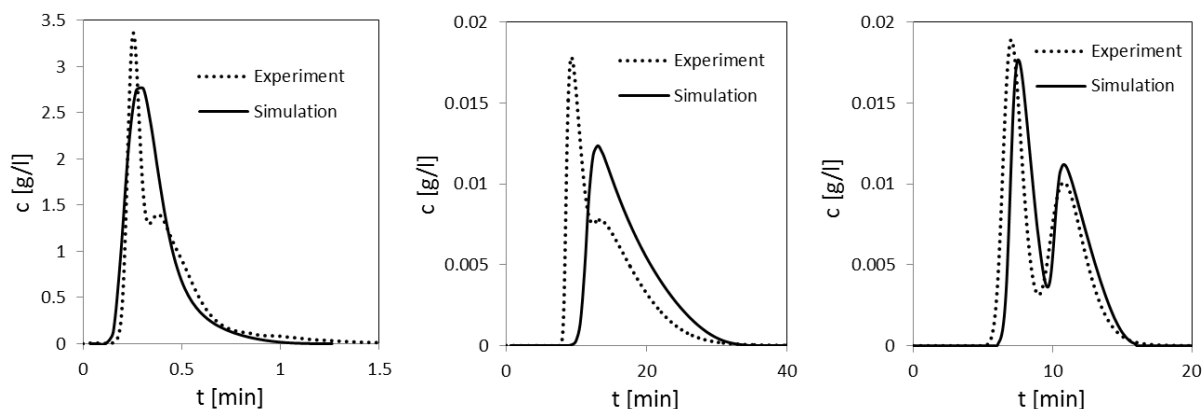


Figure 7.8. Comparison of the experimental elution profiles to those simulated with the adsorption isotherm parameters (Table 7.5) determined using the binary-mixture ECP method for: Left – Bicalutamide ( $V_{inj} = 90 \mu\text{l}$ ,  $Q = 2.5 \text{ ml/min}$ ); Middle – Isoflurane ( $V_{inj} = 5 \mu\text{l}$ ,  $Q = 71 \text{ ml/min}$ ); Right – Desflurane ( $V_{inj} = 1 \mu\text{l}$ ,  $Q = 21 \text{ ml/min}$ ).

It can be concluded that, except for desflurane, the matching between the experiment and the simulation with the parameters determined by the binary-mixture ECP method is not good when low efficient columns ( $NTP < 100$ ) are employed for the separation. Yet, the positions of the peaks on the time scale are relatively correct, so the obtained data could be used as first estimates and for rough predictions. Since for the systems investigated in this work the columns are not efficient enough, here the binary-mixture ECP method is used to obtain the first guess for the adsorption isotherm parameters, while the peak-fitting method (elaborated in the next section, 7.2) is applied for their more accurate determination.

When the isotherm parameters of bicalutamide and isoflurane determined with the ECP method in this section are compared to the values that are considered correct and are calculated using the peak-fitting method in the next section (see Table 7.6 and Table 7.7), we can see that the values of the adsorption isotherm parameters for the first eluting component deviate strongly from the correct ones, while those for the second component are much closer. This shows that the binary-mixture ECP method can be applied to certain extent, when only parameters of the second eluting component are desired to be determined, even if the columns exhibit very low efficiencies. One possibility to improve the results would be, instead of using the optimization routine to determine all four isotherm parameters at the time, to provide Henry constants independently from non-overloaded chromatograms and then to apply the ECP method only for determination of the two parameters ( $b_1$  and  $b_2$ ).

## 7.2 Peak-fitting method

Application of the ECP method did not provide satisfactory results for the case of bicalutamide and anaesthetic gases. The main reason for that was the low number of theoretical plates of the columns (41 for bicalutamide, 84 for isoflurane and 91 for desflurane). Therefore, the adsorption isotherm parameters were also determined by peak-fitting method. It is a well-known method in chromatography for adsorption isotherm estimation.

In Chapter 3, section 3.2 the concept of the method was described with introducing the idea to apply it for estimation of the enantiomer isotherms from experiments with racemic mixtures. Before employing this method, one needs first to propose a model that would describe the process properly, and then to provide the values of all model parameters except the adsorption isotherms. Here the method applicability will be tested and validated using the example of bicalutamide and afterwards it will be applied for the anaesthetic gases. Since the use of the peak-fitting method requires adopting a column model in advance, its application also served here as evidence that the equilibrium dispersive model with assumed constant mobile phase velocity can be used for describing the gas-chromatographic process with diluted systems.

### 7.2.1 Peak-fitting method representation and validation using bicalutamide

The application of the peak-fitting method for chiral systems was first tested for bicalutamide. In general, possible difficulties when using racemic mixtures include inaccessibility of pure components, as well as detection issues. The latter is due to the fact that for most of the detectors intensity of signal of both enantiomers is equal. While this is a problem when applying other isotherm determination methods, for the peak-fitting it represents an advantage, because here the complete elution profile that contains both enantiomers is analysed. The fact that the signal from racemic mixture is equal to the signal of single enantiomers, makes the calibration easier and does not require pure components.

By simulating the elution profile with adopted column model and competitive Langmuir isotherm (eq. (2.33)) for different injection volumes and by applying the optimization routine for minimizing the objective function given by eq. (3.13) the isotherm parameters that provided the best fit were estimated. The first guesses used in the fitting procedure were the values obtained in the previous section from the binary-mixture ECP method.

The obtained values of the isotherm parameters  $H$  and  $b$  are given in Table 7.6 for both bicalutamide enantiomers.



Table 7.6. Competitive Langmuir adsorption isotherm (eq. (2.33)) parameters of bicalutamide enantiomers at 25 °C determined with the peak-fitting method.

| Isotherm parameters | S-Enantiomer (Component 1) | R-Enantiomer (Component 2) |
|---------------------|----------------------------|----------------------------|
| $H$ [l/l]           | 0.29                       | 4.98                       |
| $b$ [l/g]           | 0.43                       | 0.53                       |

The competitive adsorption isotherms are shown graphically in Figure 7.9. From the figure the same can be concluded as by analysing the parameter values. The used column provides efficient separation of bicalutamide enantiomers with high selectivity.

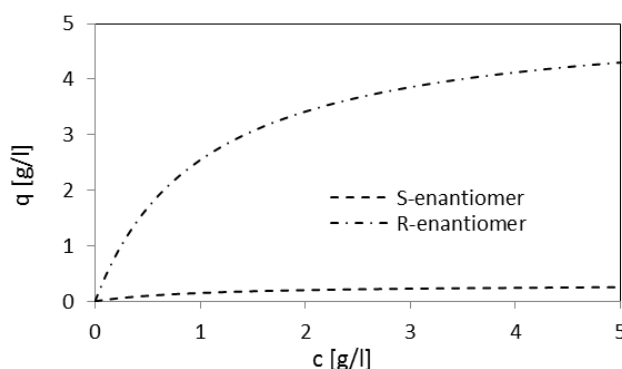


Figure 7.9. Adsorption isotherms of bicalutamide enantiomers (S and R) at 25 °C determined for a Chiralpak AD stationary phase. The isotherms are described by the competitive Langmuir model (eq. (2.33)) with the parameters given in Table 7.6.

Separation process for different injection amounts was simulated using the calculated parameters and compared to the experimental results. Four examples are given in Figure 7.10. By observing the elution profiles, it can be stated that the matching between the experiments and simulation is very good, what means that the determined adsorption isotherms can be used for further predictions. The comparison of the experimental and theoretical profiles reveals that better matching is obtained for greater injected volumes. Larger deviations are observed in the peak shape, while the positions were correct, with only small difference for the 50  $\mu$ l injection.

Even though the determined isotherm parameters provided good predictions by simulating elution profiles, they were estimated only from experiments with 1:1 mixture and therefore additional validation would be advantageous. As it was introduced in section 1.3, one of the reasons why bicalutamide was chosen as a reference substance, was that its single enantiomers were available for experiments. Therefore, to confirm the validity of the calculated isotherm parameters, they were used for simulating a chromatographic process with single enantiomers. Like for the tests with the mixture, the simulations were compared with experiments. While on one hand R-enantiomer was found not to be completely pure and it could only be concluded that the peak position was correct, on the other hand S-enantiomer was successfully employed for the method validation. Elution profiles resulting from pulse injections of S-enantiomer (first eluting component) are shown in Figure 7.11. It can be seen

that the difference between the simulation and experimental profiles is very small and almost negligible.

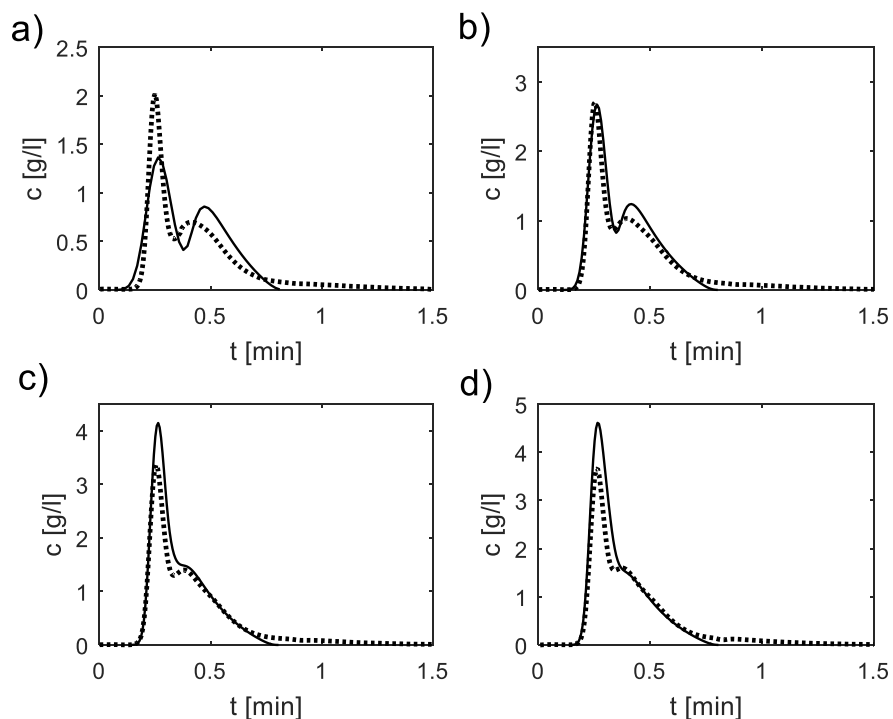


Figure 7.10. Comparison of experimental (dotted line) and simulated (solid line) elution profiles of bicalutamide racemate for different injection volumes: a) 50  $\mu$ l, b) 70  $\mu$ l, c) 90  $\mu$ l, d) 100  $\mu$ l. Feed concentration was 19.2 g/l of racemic mixture and flowrate 2.5 ml/min.

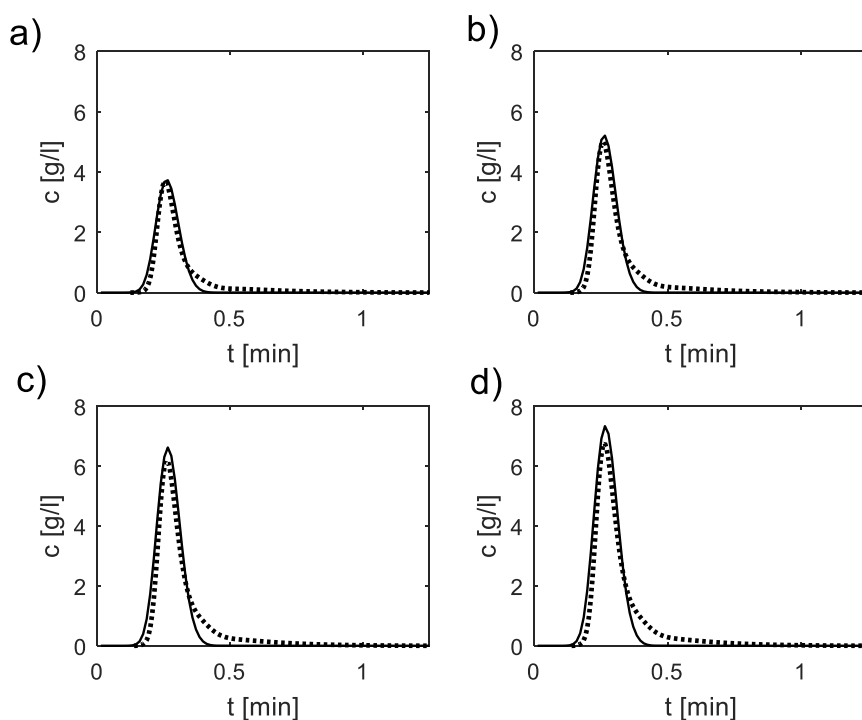


Figure 7.11. Comparison of experimental (dotted line) and simulated (solid line) elution profiles of S-bicalutamide for different injection volumes: a) 50  $\mu$ l, b) 70  $\mu$ l, c) 90  $\mu$ l, d) 100  $\mu$ l. Feed concentration was 20 g/l and flowrate 2.5 ml/min.

With these tests it could be concluded that the determined isotherm parameters can be considered as reliable, thus the described method can be applied to other racemic mixtures, even when no pure enantiomers are available for experiments.

### 7.2.2 Peak-fitting method application for isoflurane and desflurane

As for the demonstrational case of bicalutamide, in the case of isoflurane and desflurane the starting experiments included pulse injections of different amounts (shown previously in Figure 6.9 and Figure 6.10). These profiles were used for isotherm calculation. Taking the already calculated values of Henry constants (Table 6.3) and the first estimates from the ECP method (Table 7.5), the procedure for estimating the complete isotherm was performed. The values of the determined isotherm parameters are presented in Table 7.7.

Table 7.7. Competitive Langmuir adsorption isotherm parameters of isoflurane and desflurane enantiomers at 28 °C determined by the peak-fitting method.

| Isotherm parameters | Isoflurane                 |                            | Desflurane                 |                            |
|---------------------|----------------------------|----------------------------|----------------------------|----------------------------|
|                     | S-Enantiomer (Component 1) | R-Enantiomer (Component 2) | S-Enantiomer (Component 1) | R-Enantiomer (Component 2) |
| $H$ [l/l]           | 467.7                      | 765.5                      | 70.03                      | 112.4                      |
| $b$ [l/g]           | 17.6                       | 39.3                       | 1.91                       | 5.03                       |

The competitive Langmuir isotherms of S- (Component 1) and R-enantiomer (Component 2) of isoflurane and desflurane are shown in Figure 7.12. The isotherms are presented for the mobile-phase concentration range (0 - 0.03 g/l) that corresponds to the values in the elution profiles of both substances.

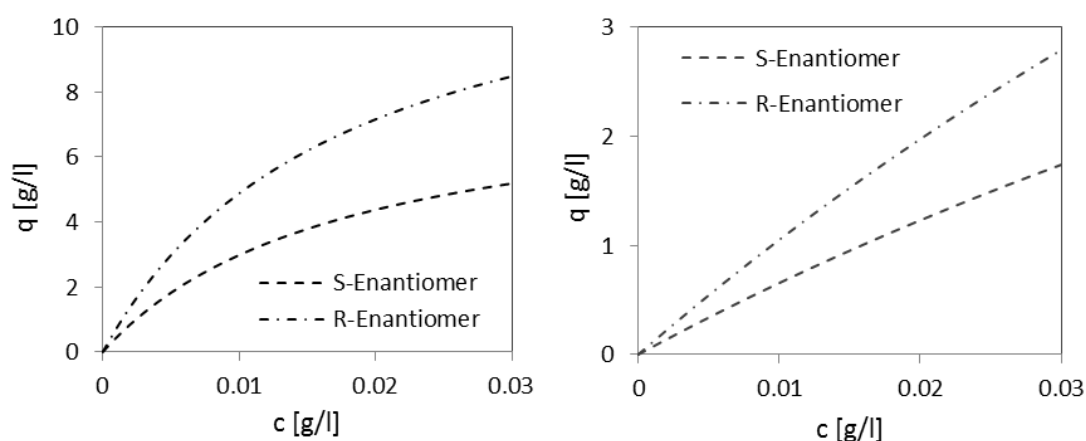


Figure 7.12. Adsorption isotherms of isoflurane (left) and desflurane (right) enantiomers (S – component 1 and R – component 2 for both substances) at 28 °C on stationary phase based on modified  $\gamma$ -cyclodextrin (defined in section 6.1.2.1). The isotherms are described by the competitive Langmuir model (eq. (2.33)) with the parameters given in Table 7.7.

As pointed out before, by comparing these isotherm parameters, determined by peak-fitting method, with those estimated by binary-mixture ECP method (Table 7.5), we can see that they follow the same pattern and that the corresponding values are in the similar ranges. In order to check if the values calculated now give better agreement with the experimental peaks, the simulated elution profiles are compared to the experimental ones, as it was done for bicalutamide. In Figure 7.13, it can be seen that for isoflurane there is a very good agreement between the experimental and simulated profiles for different injection amounts.

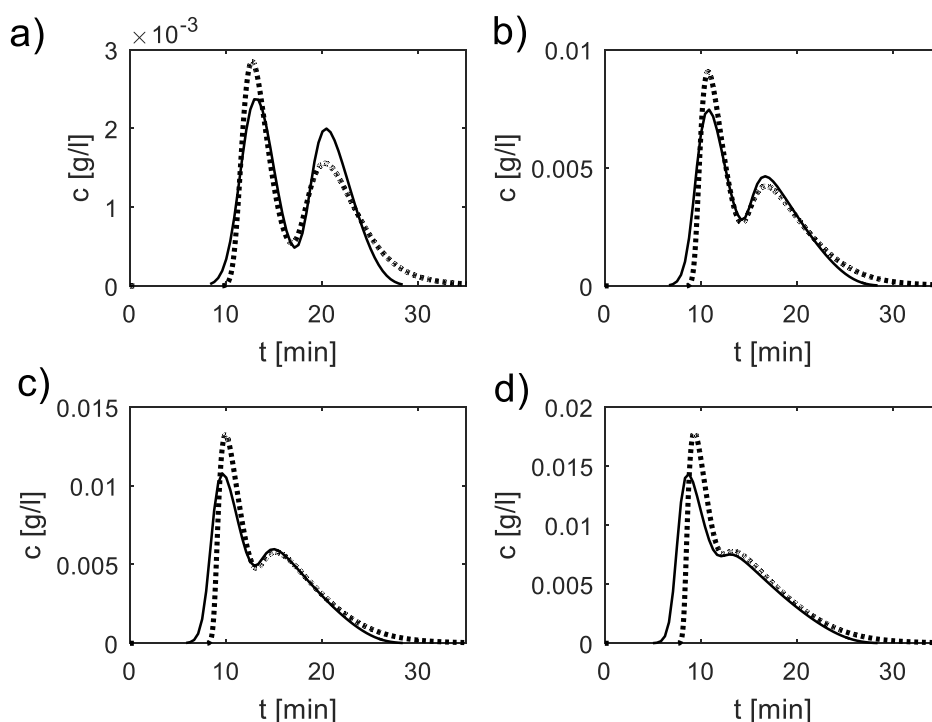


Figure 7.13. Comparison of experimental (dotted line) and simulated (solid line) elution profiles of isoflurane for different injection volumes: a) 1  $\mu\text{l}$ , b) 3  $\mu\text{l}$ , c) 4  $\mu\text{l}$ , d) 5  $\mu\text{l}$ . Injected pure racemic mixture in liquid phase. Flowrate was 71 ml/min.

The same comparison for desflurane is shown in Figure 7.14. For desflurane the largest injection available from the experiments was the one of 1  $\mu\text{l}$  and since the elution profiles resulting from even lower injection amounts are not relevant for the further process analysis, only this one was presented.

When analysing the simulated and experimental profiles in Figure 7.13 and Figure 7.14 it can be seen that they correspond well to each other. There are small discrepancies and it can be noticed that for all the cases they have the same form. This is mainly due to the fact that in the model used for simulations the same dispersion coefficient (and accordingly also *NTP*) was taken for both enantiomers. On the other hand, as reported in Table 6.3, it is known that these values are close to each other, but still larger for the *S*-enantiomer (first component). Therefore, simulations predict slightly higher degree of dispersion for the first component and lower for the second component as it is in the reality.

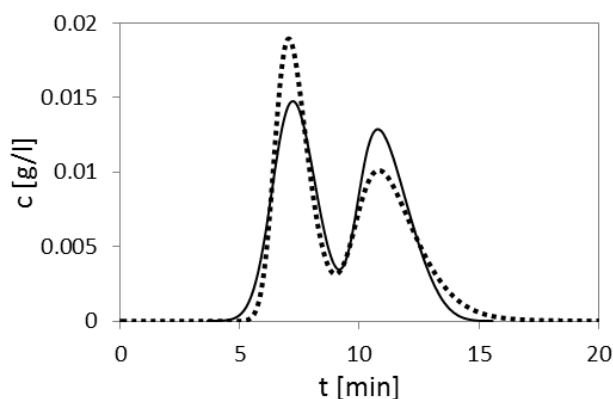


Figure 7.14. Comparison of experimental (dotted line) and simulated (solid line) elution profiles of desflurane for injection volume of 1  $\mu\text{l}$ . Injected pure racemic mixture in liquid phase. Flowrate was 21 ml/min.

Since the differences between simulation and experiments are not significant, it can be concluded and that the matching is very good and that the calculated isotherms could be used for the correct prediction of the separation of the enantiomers of fluorinated anaesthetics.

### 7.3 Summary and discussion

Two inverse methods for estimation of adsorption isotherms from experiments with racemic mixtures were presented and evaluated in this chapter. The developed extension of the ECP method for competitive Langmuir isotherms was tested and was demonstrated that this new method is very convenient for fast and simple determination of the two-component system parameters. The tests showed that it can be successfully applied for the systems that include efficient columns, having over 2000 theoretical plates. Since the columns used for enantioseparation of bicalutamide and fluorinated anaesthetics have very low efficiency (less than 100 theoretical plates), this method could only be used to provide good estimates of the isotherm parameters, or for the first guesses for another method, such as peak-fitting. For desflurane, even though the enantioseparation was not very efficient, the ECP method provided very good prediction of its isotherms.

In contrary to the ECP method, which assumes ideal case of column with infinite efficiency, peak-fitting method takes into account the real number of theoretical plates. It was applied successfully for determining the isotherms of bicalutamide, isoflurane and desflurane. As introduced in the section 1.3, the separation of bicalutamide enantiomers in a HPLC system was investigated in order to test the methods developed in this thesis. The peak-fitting method was validated by taking the parameters determined from the racemic mixture and using them to simulate the one-component elution profile. It was revealed that the simulation matches the experiments very well for the one-component system, as well as for the racemic mixtures. The peak-fitting method is shown to be reliable even when no pure components are accessible and when the column plate number is very low.

The matching of the simulation profiles to the experimental data for isoflurane and desflurane demonstrated not only that the peak-fitting method can be used for determination of the isotherms of enantiomers, but also that the assumed relatively simple equilibrium-dispersive model of chromatography and the constant values of velocity, pressure and temperature were justified for our systems. For the separations in the gaseous phase, these assumptions are not always reliable and have to be checked, but since in this work the systems were diluted to large extent, the usage of the simple model that reduces the calculation effort is shown to be reasonable.

It should be mentioned that only Langmuir adsorption isotherm models (eq. (2.33)) were used for enantiomers. In practice, it is often encountered that the adsorption for chiral systems is described by Bi-Langmuir isotherms (eq. (2.34)). However, there are several examples which show that the simple Langmuir model can also adequately predict the adsorption behaviour of enantiomeric systems (e.g. [167], [168]). The same was shown in this chapter, where it can be seen that the simulation results are matching the experiments reasonably. The existing small differences are mainly due to the fact that the same column efficiency for both components was assumed.

In this work the adsorption isotherms were estimated based only on experiments with racemic mixtures. For that reason, the experimental data do not include the information that is commonly considered to be needed for the calculation of competitive adsorption isotherms, such as column outlet concentrations recorded for other ratios between components except for 1:1, or the single component data. Thus, the method accuracy can be limited and the results have to be validated. The required validation can be performed in different ways. The first way was performed and described on the example of bicalutamide. Another way to do the validation is the indirect one, by using the estimated data for subsequent calculations and then comparing those to the experiments. This indirect way is presented in the next chapter (Chapter 8).

The results of this chapter represent the basis for the further work done on developing and analysing the chromatographic separation. Determination of isotherm parameters is one of the most important tasks for investigation of adsorption processes. This chapter demonstrates the estimation of isotherms of three chiral substances for the most complicated case when only racemic-mixture data are available for experiments. The isotherm parameters provided here are essential for understanding the processes and for the future optimization of the separation and its practical implementation.

## 8 Design and evaluation of the enantiomer production process

This chapter presents the results of the simulation studies on analysing the enantiomer production process by the way introduced in Chapter 4. Moreover, the validation tests are given for the predictions that were made.

In the first part the process performance of the batch GC enantioseparation of bicalutamide and fluorinated anaesthetics was analysed and discussed. The separation is performed by implementing consecutive injections, as it was explained at the end of the section 6.1.2 and illustrated in Figure 6.11. Process performance was predicted by calculating productivity and recovery for different injected amounts of the racemic mixture and by defining the conditions that provide the highest production of pure enantiomers. The required purity of isolated single components was defined and set to  $\geq 99\%$ .

The second part shows the tests for the column scale-ups. For each of the three substances (bicalutamide, isoflurane and desflurane) two additional columns, with larger diameter than the initially experimentally studied one, were investigated in terms of production rate. The goal was to provide one gram of pure enantiomers of the fluorinated anaesthetics in less than one day (24 hours).

In the third part of this chapter the coupled separation and capture process is described for the collection of pure enantiomers of desflurane. The work presented includes the determination of the dimensions of the columns needed to capture at least one gram of both pure enantiomers.

Finally, in the last part the next level of enantioseparation of isoflurane and desflurane using the PSA process is described. The basic PSA configuration is examined, with four steps and including one column. Presented are the parametric studies in order to check the influence of different parameters on component purity, recovery and productivity.

Important task of this chapter was to provide the validation tests of the predictions previously made. Validation was done firstly by estimating the productivity and recovery of the enantiomers of bicalutamide and the fluorinated anaesthetics from the experimental elution profiles and by comparing them to the curves generated from the simulation studies. The other validation was performed as part of the scale-up tests, where the elution profiles from the small column were compared to those resulting from the larger ones.

## 8.1 Process performance of repetitive-injection separation

Performance of the separation process was studied in terms of productivity, purity and recovery of the single enantiomers (as described in Chapter 4, section 4.1). This section gives results for a single-column batch process, where the separation is done by performing repetitive injections of racemic mixture in close succession, one directly after another.

The goal was to identify the operating parameters that will provide optimal separation. The main systems studied in this work are the anaesthetic gases, so the criteria to evaluate the separation performance were chosen in the way that the goals important for their production are achieved. Since larger amounts of the anaesthetics in racemic form can be obtained from hospitals and, on the other hand, there is no access to pure enantiomers, the parameter that is maximized in this work is the productivity of pure components. Purity of the single enantiomers was kept all the time above 99 %, while for recovery lower values than that were allowed. The volume overloading simulation tests were performed in order to examine the effects of different injection amounts on the productivity, recovery and cut times. The volumetric flowrate, established due to the limitations and requirements of the experimental set-up, was kept constant. For the anaesthetics few additional tests on the simulation level with different purities and flowrates are also shown.

### 8.1.1 Process performance of bicalutamide enantioseparation

Bicalutamide served as a reference (test) substance, to illustrate the procedures that would be later applied for the anaesthetics and for validation of the predictions. Using the isotherms from Chapter 7, section 7.2.1 (parameters showed in Table 7.6) it was preceded with the simulations of the separation process. Tests with different injected amounts were performed. By keeping the same feed concentration the injected (feed) mass was increased by increasing the injection volume of the racemic mixture. The feed mass of each enantiomer was varied from 0.00019 mg (which corresponds to the lowest possible injected volume of 0.01  $\mu$ l) to 96 mg and for each test the cut times were estimated, as well as productivity and recovery of both enantiomers. The concentration threshold value, which resembles the detection limit in the experiments, was chosen so that it was 100-1000 times lower than the maximum recorded concentration in the elution profile.

Cut times (defined previously in Figure 4.2) show the points between which the fractions containing pure components are collected. The variation of the starting ( $t_s$ ) and ending ( $t_e$ ) cut times with increasing feed mass is presented in Figure 8.1. The figure shows also the variation of the cycle time.



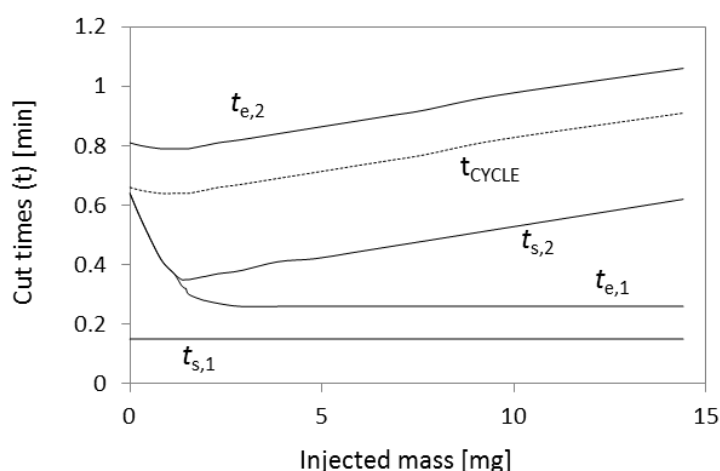


Figure 8.1. Dependency of the values of the cut times and the cycle time (defined in Figure 4.2) for the bicalutamide enantioseparation on the injection amount of one enantiomer. Volumetric flowrate is 2.5 ml/min.

As it can be observed the starting cut time of component 1 ( $t_{s,1}$ ) is constant, while its end time ( $t_{e,1}$ ) starts decreasing by increasing the injection amount and then becomes constant. The same can be concluded by looking at the elution profiles of the single components that result from different injections (Figure 8.2). The time  $t_{s,1}$  corresponds to the start of component 1 elution and  $t_{e,1}$  to the elution start of component 2. For the second enantiomer, for very low amounts, the values of both cut times decrease and afterwards they start increasing in the same manner. As it can be seen from Figure 8.2, the behaviour of the peaks corresponds to the linear isotherm range, where the peaks are symmetric, and from there the trends in cut time variations originate.

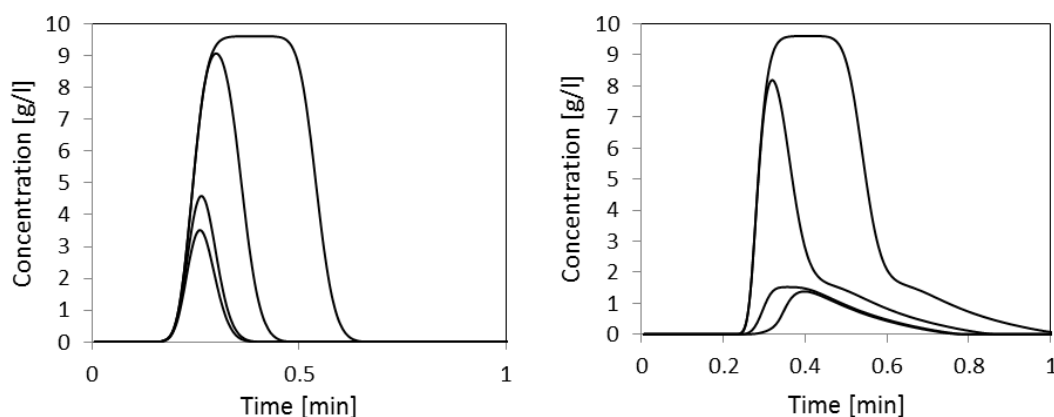


Figure 8.2. Elution profiles of the first (S-enantiomer, left diagram) and the second (R-enantiomer, right diagram) eluting components of bicalutamide for increasing injection amounts: 1.4 mg, 1.9 mg, 5.7mg and 14.5 mg. Volumetric flowrate is 2.5 ml/min

The changes of productivity (eq. (4.6)) and recovery (eq. (4.3)) of both bicalutamide enantiomers with the injected amount is shown in Figure 8.3 and Figure 8.4, respectively. The values estimated from the experiments are given along with the simulation results. The

experimental elution profiles used for this estimation are those presented in Chapter 6, Figure 6.6. Since in the experiments the exact shapes of the single component peaks were not known, they were assumed according to the overall profile shape. By comparing the experimental and simulated values, it can be seen that they match each other very well. This represents one way of validating the predictions that were made. It was shown that the isotherms determined in section 7.2 can be considered correct, as well as the model used for the process simulation (mentioned in chapter 6, section 6.2.1). Because of experimental constraints (explained in section 6.1.1.2), larger amounts of racemic mixture could not be injected in the column, so the matching was proved only in the range from 0 to the point where maximum productivity is achieved for R-enantiomer, while for S-enantiomer it goes slightly beyond the maximum. However, since the interest here was the injection amount that provides optimal (maximal) productivity, it can be considered that the validation was successful. The behaviour after reaching the maximum is not of practical importance.

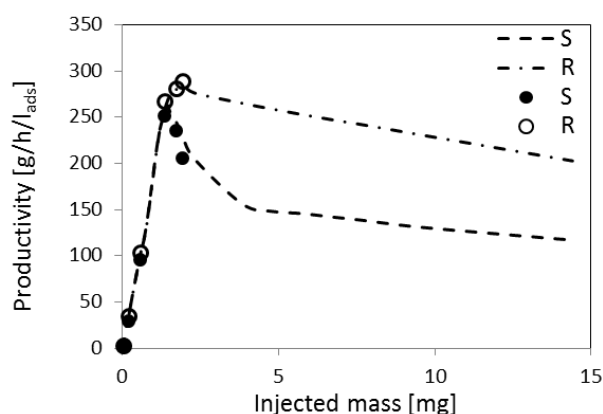


Figure 8.3. Dependency of productivity of bicalutamide enantiomers on the injection amount of one enantiomer. Volumetric flowrate is 2.5 ml/min. Lines represent the results from the simulation study and symbols the values estimated from the experiments.

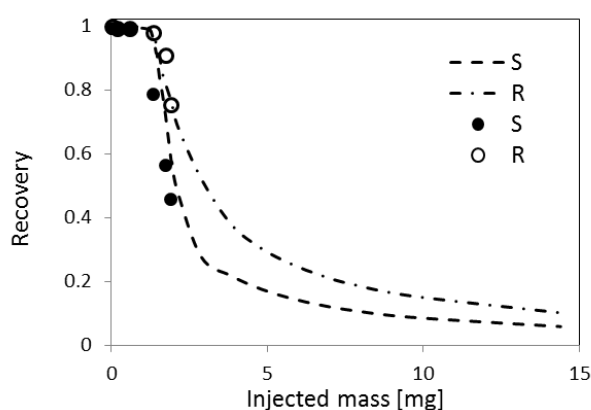


Figure 8.4. Dependency of recovery of bicalutamide enantiomers on the injection amount of one enantiomer. Volumetric flowrate is 2.5 ml/min. Lines represent the results from the simulation study and symbols the values estimated from the experiments.

The productivity of the both enantiomers starts increasing by increasing the injected mass, simple because the peak resolution is still good and the process includes larger injected

amounts. At certain point the productivity reaches its maximum and after that starts decreasing, since the separation degree of the peaks is lower. The decrease of the productivity becomes constant with time, as it was the case with the difference between ending and starting cut time for the both components. For component 2 higher productivity can be obtained. Figure 8.5 shows the elution profiles for the cases when the highest productivity of the first (S) and second (R) enantiomer is achieved.

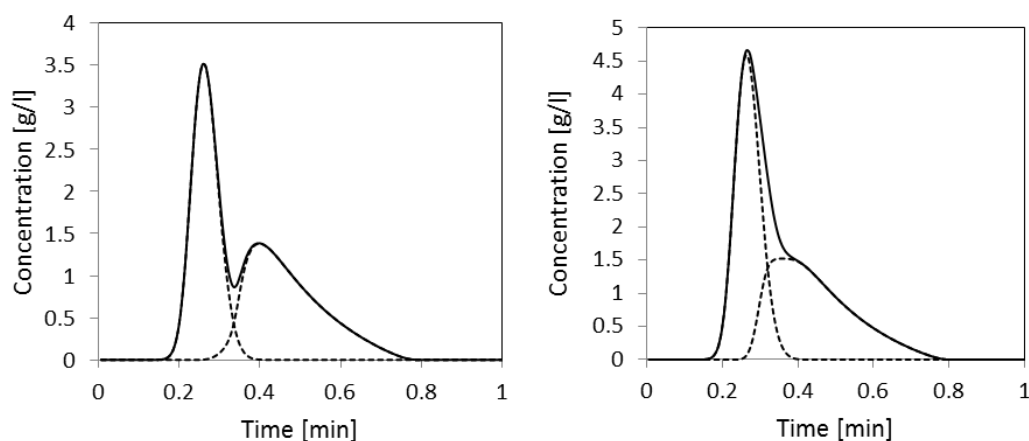


Figure 8.5. Elution profiles of bicalutamide given for the cases when maximum productivity of the first component – S-enantiomer (left, injected volume 76  $\mu$ l, injected mass 1.46 mg of each enantiomer) and second component – R-enantiomer (right, injected volume 101  $\mu$ l, injected mass 1.94 mg of each enantiomer) is achieved (flowrate 2.5 ml/min). Dashed lines show single component profiles and solid lines the total concentration.

Recovery of the both enantiomers decreases by increasing the injection volume. For low amounts it is close to 100 %, since the single peaks are well separated, but after the mixed fraction between the pure components starts to dominate, the recovery is slowly lowered towards the value of zero.

The values of the process productivity, recovery and purity of both bicalutamide enantiomers are summarized in Table 8.1 for three representative cases: touching bands of the two components (when still almost complete recovery is achieved), the point when the productivity of S-enantiomer is maximal and the point when the productivity of R-enantiomer is maximal.

The touching-bands situation provides excellent purity and recovery of the desired single enantiomers, but they are obtained at very low production level in comparison to the two other given cases. Purity is always higher than 99 %, since it was set as a starting requirement and therefore it will not be discussed. For the two situations when maximal productivity of the components is achieved, productivity rates are similar, while recovery of both enantiomers is much lower when maximal production of R-enantiomer is obtained. In general, when aiming to provide the optimal overall process performance, the case with maximal S-enantiomer production should be chosen. Only if we are aiming to produce just R-component (since it is the one with medical effect) and losses of the racemic mixture are not

of considerable importance, the case with maximal production of R-enantiomer would be taken as the optimal one.

Table 8.1. Process performance characteristics (productivity - *PR*, recovery - *RE* and purity - *PU*) of bicalutamide enantiomers (S-enantiomer – component 1 and R-enantiomer – component 2) for three typical cases: touching bands (recovery of both components is close to 100 % i.e. 1), when the maximal productivity of S- enantiomer is achieved and when the maximal productivity of R-enantiomer is achieved.

| Case                              | Touching bands |       | Achieved maximal productivity of S-enantiomer |       | Achieved maximal productivity of R-enantiomer |       |
|-----------------------------------|----------------|-------|---|-------|---|-------|
|                                   | S              | R     | S   | R     | S   | R     |
| Enantiomer                        |                |       |   |       |   |       |
| $V_{inj}$ [ $\mu$ l]              | 10.0           |       | 76.0  |       | 101   |       |
| $m_{feed,1} = m_{feed,2}$ [mg]    | 0.192          |       | 1.46  |       | 1.94  |       |
| <i>PR</i> [g/h/l <sub>ads</sub> ] | 33.1           | 33.0  | 262.4   | 268.9 | 214.8   | 283.9 |
| <i>RE</i>                         | 1              | 1     | 0.915   | 0.937 | 0.575   | 0.760 |
| <i>PU</i>                         | 0.991          | 0.992 | 0.990   | 0.992 | 0.993   | 0.990 |

### 8.1.2 Process performance of isoflurane and desflurane enantioseparation

The procedure of analysing the process performance for the fluorinated anaesthetics isoflurane and desflurane was the same as for bicalutamide. The separation process was simulated using the isotherms calculated in Chapter 7, section 7.2.2. Different injected amounts were studied with the goal to determine when the production optimum is achieved by keeping the purity of both enantiomers over 0.99. The feed concentration was kept constant, while the injection volumes were gradually increased. The feed mass of one enantiomer was varied in the range from 0.038 mg to 23 mg for both anaesthetics. The threshold concentration was chosen in the same way as for bicalutamide.

First the change of the cycle time and cut-time values was analysed by changing the injected amounts. The same trends were observed for isoflurane and desflurane. The curves are presented in Figure 8.6.

The cut times change in the different way as it was in the case of bicalutamide, because here the separation is performed in the nonlinear isotherm range. By increasing the injected amount, the values of the starting and ending cut times for the first component (S-enantiomer for both anaesthetics) decrease, since both fronts (of the first and second component) move forwards (Figure 6.9 and Figure 6.10). The starting cut time for the second component (R-enantiomer) slightly decreases while the concentrations are still in the linear isotherm range, and afterwards becomes constant. The cut times of the component 2 are the times when the first and second component are completely eluted, which means that they correspond to the

retention times of the components at infinite dilution and these values do not depend on the injected amount (in the nonlinear range).

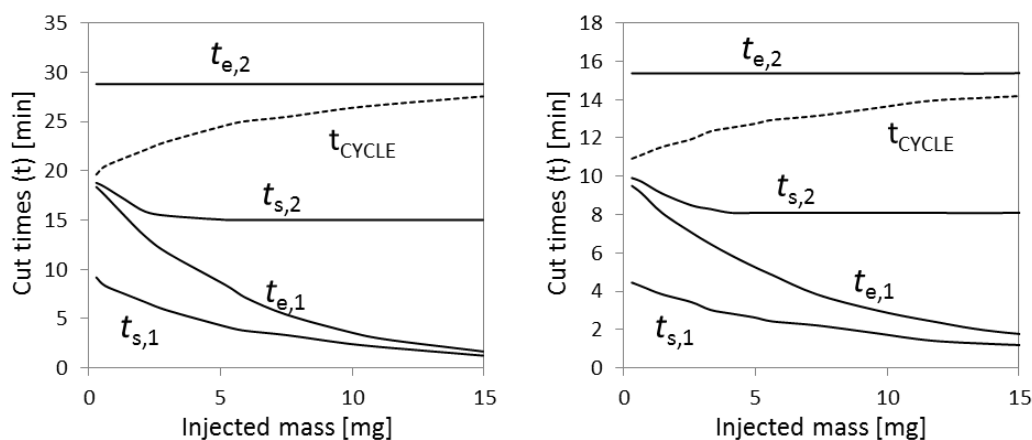


Figure 8.6. Dependency of the values of cut times and the cycle time (defined in Figure 4.2) for the isoflurane (left) and desflurane (right) enantioseparation on the amount of one enantiomer injected at the column inlet. Volumetric flowrate is 71 ml/min for isoflurane and 21 ml/min for desflurane.

The variations of productivity and recovery of isoflurane and desflurane enantiomers with the injected mass were recorded and presented in Figure 8.7 and Figure 8.8. As for bicalutamide, here the parameter values were also estimated from the experimental peaks (shown in Figure 6.9 and Figure 6.10) and compared to the simulation results. It can be seen that the simulated values correspond very well to the experimental ones, which is one of the confirmations that the use of the equilibrium dispersive model was justified even though the separation was conducted in the gaseous phase.

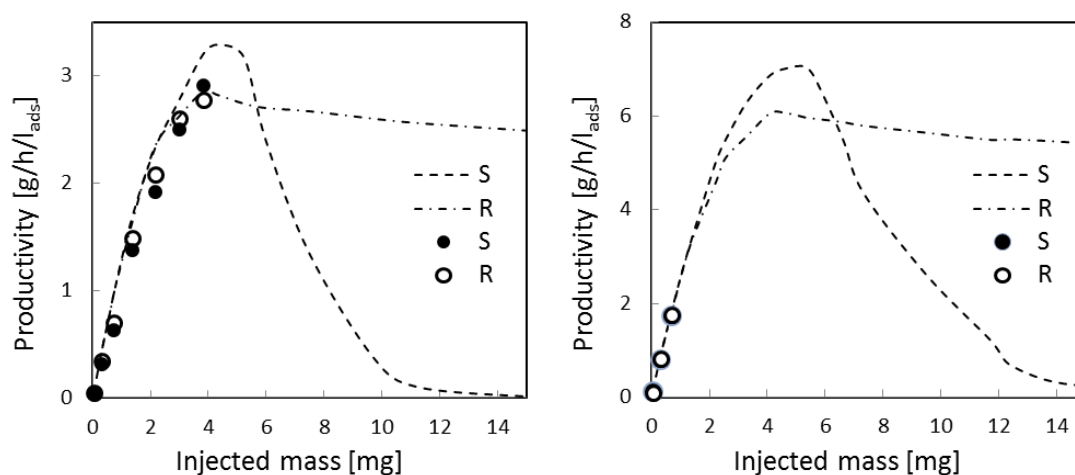


Figure 8.7. Dependency of productivity of isoflurane (left) and desflurane (right) enantiomers on the amount of one enantiomer injected at the column inlet. Volumetric flowrate is 71 ml/min for isoflurane and 21 ml/min for desflurane. Lines represent the results from the simulation study and symbols the values estimated from the experiments.

For isoflurane matching between experimental and simulation was confirmed only for the range from zero to the productivity maxima. Here the tests done with bicalutamide were useful, because there the same trends as in the case of anaesthetics were in general observed.

Since for bicalutamide the matching was correct in larger data range and for the anaesthetics the same laws and assumptions were used, it can be considered that the predictions are accurate in this case as well. For desflurane was possible to calculate only experimental values in the low-amounts range, since from the SPP Subproject II only three small injections (up to 1  $\mu\text{l}$ ) were available. However, the behaviour is the same as for isoflurane and, owing to shorter cycle time (than for isoflurane), maximal calculated productivities are in the expected range compared to the isoflurane values.

For both anaesthetics, by increasing the injected amount, productivity starts increasing due to the increase of the mass, until a point after which enantiomers cannot be separated as good as before. After reaching the maximal value, productivity of both enantiomers begins to decrease. For the first eluted component it approaches zero, while in the case of component 2 it decreases slowly, but indefinitely. The reason for this is that the fronts of both peaks move forward as the injected amount is increased, but their tails (that correspond to the state of infinite dilution) remain constant. The same conclusion has already been derived when the changes of the cut times  $t_{s,2}$  and  $t_{e,2}$  were analysed. The similar shapes of productivity curves were observed in the literature for different systems (e.g. in [169]).

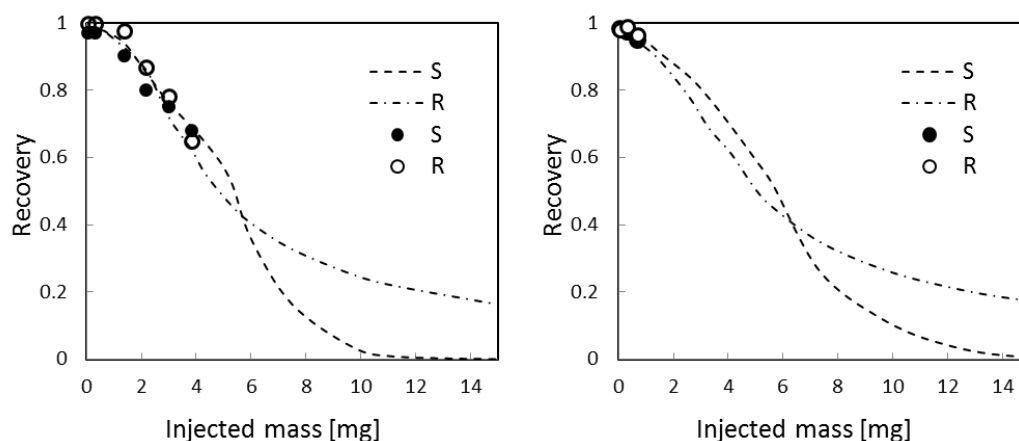


Figure 8.8. Dependency of recovery of isoflurane (left) and desflurane (right) enantiomers on the amount of one enantiomer injected at the column inlet. Volumetric flowrate is 71 ml/min for isoflurane and 21 ml/min for desflurane. Lines represent the results from the simulation study and symbols the values estimated from the experiments.

As it is expected, recovery decreases by increasing the injected mass, since for this type of systems it is the case that when larger feed amounts are applied, the peak resolution of the two components becomes worse. Like for the productivity, recovery of the first eluting enantiomer (S) reaches zero, while for the second one (R) it starts dropping faster, but with larger injected mass it decreases much slower.

The maximum productivity that can be reached for the S-enantiomer (component 1) of both anaesthetics is higher than the one for R-enantiomer and is achieved for slightly larger feed mass. As an illustration, in Figure 8.9 for isoflurane and Figure 8.10 for desflurane the elution profiles for the cases with maximum productivities, are shown.

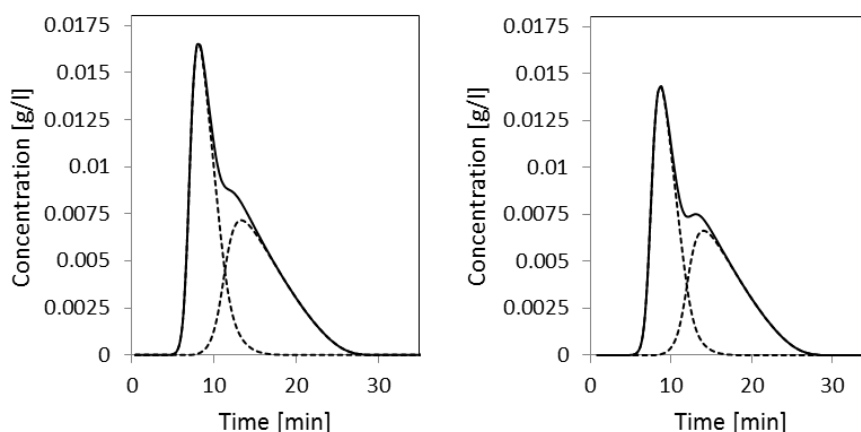


Figure 8.9. Elution profiles of isoflurane given for the cases when maximum productivity of the first component – S-enantiomer (left, injected volume 5.8  $\mu\text{l}$ , injected mass 4.34 mg of each enantiomer) and of the second component – R-enantiomer (right, injected volume 5.1  $\mu\text{l}$ , injected mass 3.81 mg of each enantiomer) is achieved (flowrate 71 ml/min). Dashed lines show single component profiles and solid lines the total concentration.

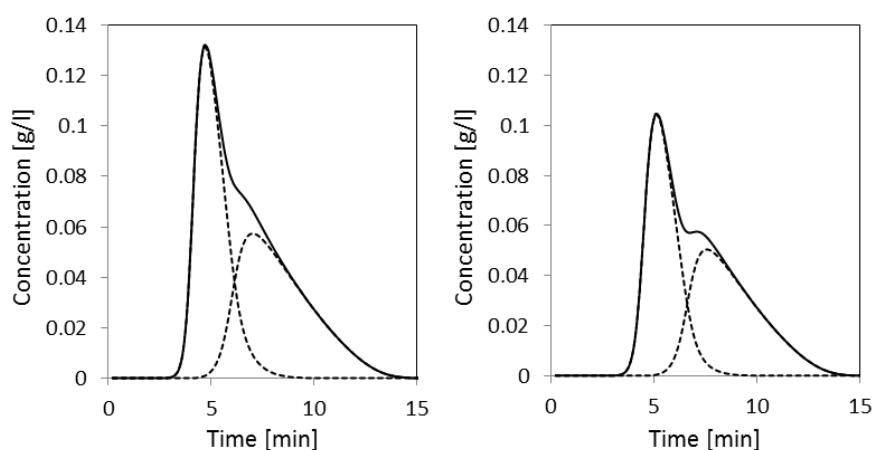


Figure 8.10. Elution profiles of desflurane given for the cases when maximum productivity of the first component – S-enantiomer (left, injected volume 6.8  $\mu\text{l}$ , injected mass 4.98 mg of each enantiomer) and of the second component – R-enantiomer (right, injected volume 5.6  $\mu\text{l}$ , injected mass 4.10 mg of each enantiomer) is achieved (flowrate 21 ml/min). Dashed lines show single component profiles and solid lines the total concentration.

The values of productivity, recovery and purity of the two enantiomers together with the injected volumes and amounts are presented in Table 8.2 and Table 8.3 for isoflurane and desflurane, respectively. The parameters are given for the cases when two-enantiomer bands are touching and when the production maxima are obtained. By analysing the production values, it can be seen that, while the productivity of the R-component (second component) is only slightly higher for the case when R-enantiomer maximum is achieved, than when achieving it for S, for the S-enantiomer this difference is greater. Since the values of recovery are not very different, as the optimal case for isoflurane and desflurane separation, the point with the highest production of S-enantiomer (component 1) is selected. For the touching-

bands case the recoveries are very high, but it cannot provide the productivity values comparable to the other two presented cases.

Table 8.2. Process performance characteristics (productivity - *PR*, recovery - *RE* and purity - *PU*) of isoflurane enantiomers (S-enantiomer – component 1 and R-enantiomer – component 2) for three typical cases: touching bands (recovery of both components is close to 100 % i.e. 1), when the maximal productivity of S- enantiomer is achieved and when the maximal productivity of R-enantiomer is achieved.

| Case   | Touching bands |        | Achieved maximal productivity of S-enantiomer |       | Achieved maximal productivity of R-enantiomer |       |
|--|----------------|--------|---|-------|---|-------|
|  | S              | R      | S   | R     | S   | R     |
| <i>V<sub>inj</sub></i> [ $\mu$ l]                          | 0.0508         |        | 5.8   |       | 5.1   |       |
| <i>m<sub>feed,1</sub></i> = <i>m<sub>feed,2</sub></i> [mg] | 0.0380         |        | 4.34  |       | 3.81  |       |
| <i>PR</i> [g/h/l <sub>ads</sub> ]                          | 0.0465         | 0.0465 | 3.29  | 2.82  | 3.2   | 2.85  |
| <i>RE</i>  | 0.989          | 0.988  | 0.644   | 0.551 | 0.704   | 0.625 |
| <i>PU</i>  | 0.993          | 0.992  | 0.991   | 0.991 | 0.991   | 0.991 |

To summarize, for the further tests the optimal chosen case was for isoflurane the one when injected mass of one enantiomer was 4.34 mg (injected total volume 5.8  $\mu$ l), providing the productivity of 3.29 g/h/l<sub>ads</sub> for S-enantiomer and 2.82 g/h/l<sub>ads</sub> for R-enantiomer. For desflurane in the optimal case the 4.98 mg of one enantiomer injected (total injected volume 6.8  $\mu$ l) gives the productivity values 7.06 g/h/l<sub>ads</sub> and 6.02 g/h/l<sub>ads</sub> for the S- and R-enantiomer, respectively.

Table 8.3. Process performance characteristics (productivity - *PR*, recovery - *RE* and purity - *PU*) of desflurane enantiomers (S-enantiomer – component 1 and R-enantiomer – component 2) for three typical cases: touching bands (recovery of both components is close to 100 % i.e. 1), when the maximal productivity of S- enantiomer is achieved and when the maximal productivity of R-enantiomer is achieved.

| Case   | Touching bands |       | Achieved maximal productivity of S-enantiomer |       | Achieved maximal productivity of R-enantiomer |       |
|--|----------------|-------|---|-------|---|-------|
|  | S              | R     | S   | R     | S   | R     |
| <i>V<sub>inj</sub></i> [ $\mu$ l]                          | 0.0522         |       | 6.80  |       | 5.60  |       |
| <i>m<sub>feed,1</sub></i> = <i>m<sub>feed,2</sub></i> [mg] | 0.0383         |       | 4.98  |       | 4.1   |       |
| <i>PR</i> [g/h/l <sub>ads</sub> ]                          | 0.126          | 0.127 | 7.06  | 6.02  | 6.87  | 6.06  |
| <i>RE</i>  | 0.982          | 0.976 | 0.595   | 0.507 | 0.693   | 0.612 |
| <i>PU</i>  | 0.992          | 0.990 | 0.992   | 0.991 | 0.992   | 0.990 |

In the further text some of the possibilities to additionally increase the productivity will be theoretically discussed. One way is to produce enantiomers of lower purity, and the other to use higher flowrates. If demand for high purity of the enantiomers is reduced, the increases in productivity and especially in recovery of the collected single enantiomers can be significant.



There are examples in the literature presenting the separation of enantiomers of fluorinated anaesthetics, where the achieved purity was not as high as in this work (e.g. in [103] for isoflurane and [100] for desflurane).

The plots showing the dependency of productivity and recovery from the desired enantiomer purity are given for isoflurane and desflurane in Figure 8.11 and Figure 8.12, respectively. In both figures the represented cases were simulated with the injection amount that corresponds to the maximal S-enantiomer production. The purity range is 90-100 %, because for even lower purity than 90 %, the substances cannot be considered pure any more. The analysis shows that, for example, when the wanted purity is just 90 %, the productivity of both isoflurane enantiomers would reach the value of 4.97 g/h/l<sub>ads</sub>, while the recovery will increase more drastically, from 50-60 % (when the purity is 99.1 %) to 92 %. For desflurane the similar trend is observed. Productivity of both enantiomers would increase to 10.9 g/h/l<sub>ads</sub>, and recovery to 91 % when the purity demand is set to 90 %.

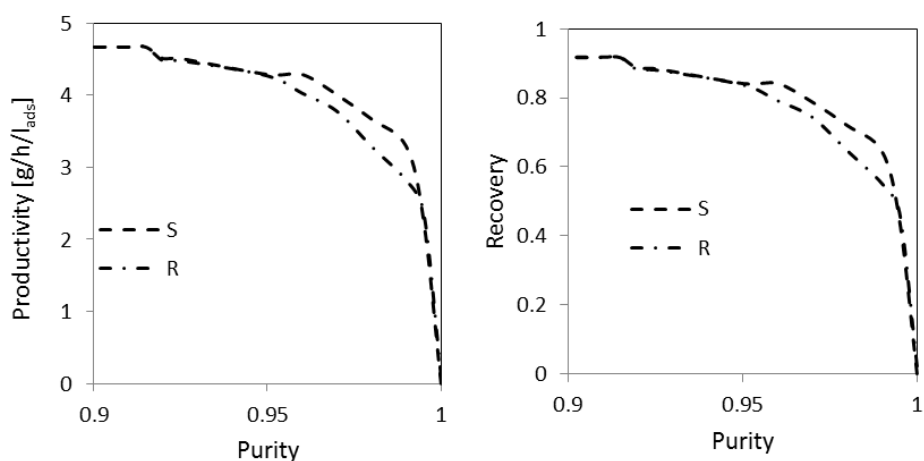


Figure 8.11. Dependency of productivity (left) and recovery (right) on required purity of isoflurane enantiomers (flowrate 71 ml/min, injected volume 5.8  $\mu$ l, injected mass 4.34 mg of each of the enantiomers).

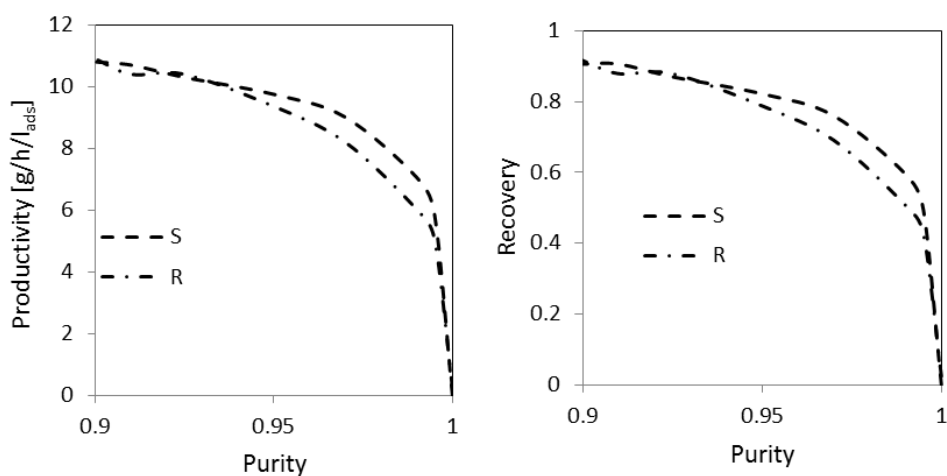


Figure 8.12. Dependency of productivity (left) and recovery (right) on required purity of desflurane enantiomers (flowrate 21 ml/min, injected volume 6.8  $\mu$ l, injected mass 4.98 mg of each of the enantiomers).

The demanded purity of the enantiomers is defined by the medical doctors that will use them in their research, but in general it should be as high as possible. Therefore, even though the lowered purity provides much better results in terms of production and recovery, in this work the  $\geq 99\%$  standard was applied for the further calculations.

As already introduced, another way to increase the productivity of the pure enantiomers can be done by increasing the flowrate of the carrier gas. One problem when working with high flowrates is that the column efficiency can become very low, which would lead to poorer component separation. As a part of SPP1570 Subproject II different flowrates were tested for separation of isoflurane and desflurane and *NTP* and *HETP* values were calculated. The change of the *HEPT* with volumetric flowrate (and accordingly also with the mobile phase velocity) is presented in Figure 8.13.

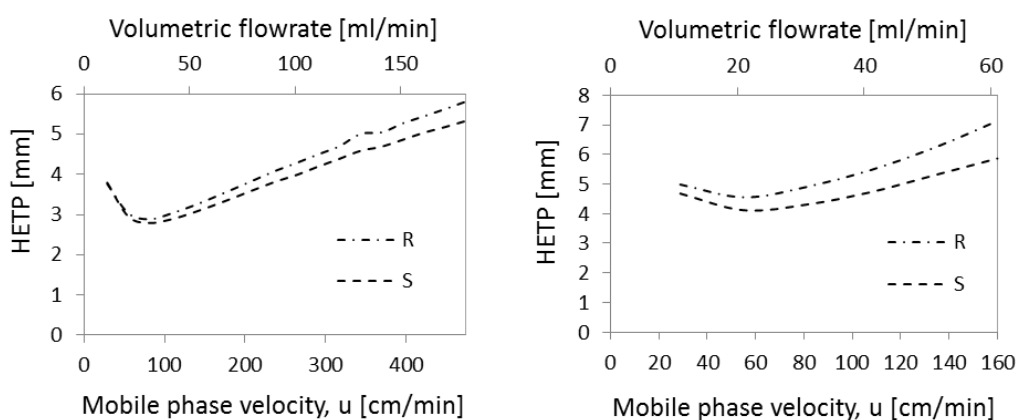


Figure 8.13. Dependency of HETP (column efficiency) on the mobile phase flowrate (upper horizontal axis) and at the same time on velocity (lower horizontal axis) – Van Deemter curves, for isoflurane (left) and desflurane (right) enantiomers. Diagrams are constructed from the data provided from the parallel SPP1570 Subproject II.

To analyse the influence of the flowrate (and therefore the column efficiency) on the process performance, productivity was calculated as a function of injected mass by using different flowrates ranging from 11 ml/min to 181 ml/min. An illustration of the results for the case of isoflurane is shown in Figure 8.14 (the behaviour of desflurane follows the same tendencies).

The productivity-mass curves have the same shape for all the tested flowrates. With increasing the flowrate we can observe that the productivity of both enantiomers increases, first very fast and then by a smaller extent. For the flowrate of 181 ml/min the production of 6.25 g/h/l<sub>ads</sub> of S- and 6.01 g/h/l<sub>ads</sub> of R-isoflurane could be achieved, which is about two times higher than for the flow of 71 ml/min. Recovery values for this case would be slightly lower than when the flow is 71 ml/min (0.552 and 0.543 for S- and R-isoflurane). It can be concluded that even for lower column efficiency caused by higher flowrate, the productivity would increase, because the higher flowrate and accordingly the shorter cycle time have more influence on the production than the decreased peak resolution due to lower column efficiency.

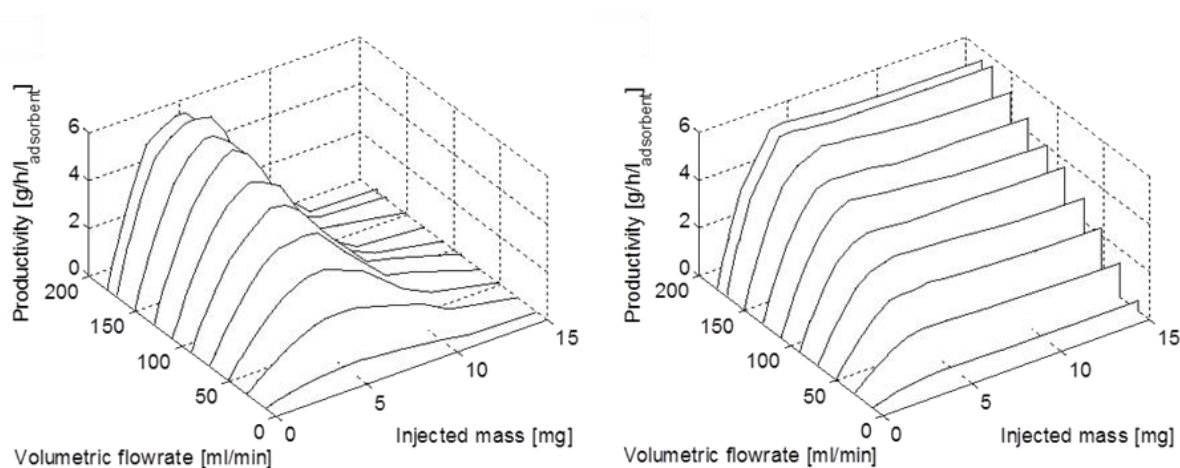


Figure 8.14. Dependency of productivity of S- (left) and R-enantiomer (right) of isoflurane from injected mass of one enantiomer and volumetric flowrate.

However, because of the equipment constraints, there was no possibility to perform experiments with higher flowrates and therefore it was not possible to provide higher production of single enantiomers in practice.

#### 8.1.2.1 Process performance evaluation by comparison with the previous works

In order to evaluate the developed batch GC process for enantioseparation of the fluorinated anaesthetics, it is necessary to compare its performance with the results of the previous separations available in the literature, as it was mentioned at the end of section 5.2.2. In Table 5.6 the published process performance parameters of the previous research are listed. Here only publications with the same chiral selector [156] as in this work and those which provided productivity values of isoflurane [99, 100, 103] and desflurane [100] were selected for comparison.

To properly compare the productivities of diverse processes, the normalized productivity expressed as collected amount over the time and the amount of the adsorbent (eq. (4.6)) should be used. The problem was that in the available published data usually only the collected amounts per time could be found, without providing the values for adsorbent volume or bed porosity (e.g. for the batch GC processes presented in [99] and [100]) or just the collected mass without time interval (for the GC-SMB separation [103]). Therefore, here the calculations were done by assuming two different values of porosity, 0.5 and 0.81 (the value for the columns used in this work), while for the SMB process four estimated operation times were considered. The checked process durations were 1 day (24 h), 2 days, 5 days and one week (7 days). The rough comparison of the process performance achieved in this work and the literature findings, without going into details regarding different operation procedures, is represented in Table 8.4 for isoflurane and Table 8.5 for desflurane. As can be seen, except for the batch process described in [100], the purity reported in this work is comparable or higher than in the other processes. Recovery achieved in the previous research works is higher only for the SMB process (where the purity is lower for both isoflurane enantiomers). When comparing productivity, it can be concluded that in this work larger

amount of pure enantiomers of both isoflurane and desflurane can be obtained at the same time interval for all the assumed porosity and operation time values. The presented comparison shows that the separation described in this work provides higher production of isoflurane and desflurane enantiomers than what was previously achieved. It represents a promising process for successful production of pure enantiomers of the anaesthetic gases.

Table 8.4. Comparison of process performance parameters of S- (component 1) and R-enantiomer (component 2) of isoflurane achieved in this work (batch GC when maximal production of S-enantiomer was obtained) and the examples from the literature where the same chiral selector was used (three batch GC processes and one GC-SMB). The values for the case done in this thesis are extracted from Table 8.2.

| Parameter              |                      | Productivity<br>[g/h/l <sub>ads</sub> ] |        | Recovery     |              | Purity |       |
|------------------------|----------------------|---|--------|--------------|--------------|--------|-------|
|                        |                      | S                                       | R      | S            | R            | S      | R     |
| This thesis (Batch GC) |                      | 3.29                                    | 2.82   | 0.644        | 0.551        | 0.991  | 0.991 |
| [99]:<br>Batch GC      | $\epsilon^* = 0.5$   | 0.0836                                  | 0.0836 | About<br>0.6 | About<br>0.6 | 0.994  | 0.994 |
|                        | $\epsilon^* = 0.81$  | 0.220                                   | 0.220  |              |              |        |       |
| [100]:<br>Batch GC     | $\epsilon^* = 0.5$   | 0.0553                                  | 0.0553 | Not reported |              | 0.999  | 0.999 |
|                        | $\epsilon^* = 0.81$  | 0.146                                   | 0.146  |              |              |        |       |
| [103]:<br>GC-SMB       | $t^* = 24$ h         | 1.926                                   | 1.775  | > 0.95       |              | 0.981  | 0.967 |
|                        | $t^* = 2 \cdot 24$ h | 0.958                                   | 0.885  |              |              |        |       |
|                        | $t^* = 5 \cdot 24$ h | 0.383                                   | 0.354  |              |              |        |       |
|                        | $t^* = 7 \cdot 24$ h | 0.274                                   | 0.253  |              |              |        |       |

\* In the publications where the values of bed porosity ( $\epsilon$ ) and the time for collecting the separated components ( $t$ ) were not reported, a couple of supposed values were used to estimate the productivity (eq. (4.6)). These values are required to express the production in grams of the substance per time and adsorbent volume, which is the form that could be used for comparison between different processes.

Table 8.5. Comparison of process performance parameters of S- (component 1) and R-enantiomer (component 2) of desflurane achieved in this work (batch GC when maximal production of S-enantiomer was obtained) and the example available in the literature (batch GC process). The values for the case done in this thesis are extracted from Table 8.3.

| Parameter              |                     | Productivity<br>[g/h/l <sub>ads</sub> ] |       | Recovery     |       | Purity        |               |
|------------------------|---------------------|---|-------|--------------|-------|---------------|---------------|
|                        |                     | S                                       | R     | S            | R     | S             | R             |
| This thesis (Batch GC) |                     | 7.06                                    | 6.02  | 0.595        | 0.507 | 0.992         | 0.991         |
| [100]:<br>Batch GC     | $\epsilon^* = 0.5$  | 0.737                                   | 0.663 | Not reported |       | About<br>0.91 | About<br>0.68 |
|                        | $\epsilon^* = 0.81$ | 1.94                                    | 1.75  |              |       |               |               |

\* The values of bed porosity ( $\epsilon$ ) was not reported and therefore two supposed values were used to estimate the productivity (eq. (4.6)), as explained in Table 8.4.

## 8.2 Scale-up of the batch HPLC and GC processes

In order to increase the production rate per time unit, one can develop a process on a larger scale. As introduced in Chapter 4, section 4.2, scale-up of the chromatographic columns can easily be done by keeping the same bed length and just increasing its diameter. For both of the systems studied here, bicalutamide and the anaesthetic gases, the enantioseparation in two columns with larger diameter was studied. The introduced columns were named “intermediate” (the one with the smaller diameter, but still larger than the one tested at the beginning) and “large” (the one with larger diameter). For all three columns the process performance characteristics were compared. Moreover, additional tests with hypothetical columns of even larger scale were performed and presented.

This section contains also the validation experiments for the fluorinated anaesthetics (originating from the parallel SPP1570 Subproject II), that demonstrate that the predictions made using the simple relations, are justified and can be implemented for obtaining the reliable results with less time and computational effort invested.

### 8.2.1 Scale-up for bicalutamide enantioseparation

By applying the scale-up rule given in the form of eq. (4.17), the parameters for columns with larger or smaller diameter can be determined. Here we tested only the possibility to perform the separation in larger-scale beds since the goal was to maximize the production. For starting experiments with bicalutamide (section 6.1.1) a commercial column Chiralpak AD was used. Therefore diameters of the two examined larger columns were selected based on the sizes of the columns with the same stationary phase that are commercially available. The chosen diameters were 1.0 cm for the intermediate and 2.0 cm for the large column.

Previously in this chapter, in section 8.1.1 the case with maximal production of S-enantiomer was defined as the optimal one. Here that case was further explored for separation in the intermediate and large column. First the operating parameters such as volumetric flowrate and injected volume and mass were calculated. Then, by simulating the process, performance characteristics were determined. Table 8.6 lists the obtained values for the cycle time, as well as for productivity and recovery of both enantiomers. By applying the introduced scale-up rule, purity, recovery and normalized productivity (given per amount of adsorbent) remain the same as they were for the smaller column. What increases is the overall production. In Table 8.6 this production is expressed as collected mass from the specific column per hour ( $m_{coll}$ ). As an illustration, two more parameters are presented in the table: time needed to collect one gram of pure enantiomer and the number of cycles (i.e. number of injections) that have to be operated in order to achieve it. For both enantiomers production rates are in the similar range. To collect one gram of both of them, one needs about 8.5 hours.

Table 8.6. Scale-up results for bicalutamide enantiomers obtained from eq. (4.17) and by performing simulations with the data for the larger-scale columns. The operation and performance parameters are presented for the three examined column sizes (referred as small, intermediate and large).

| Column   | Small |       | Intermediate |       | Large   |       |
|--|-------|-------|--------------|-------|---------|-------|
| $d$ [cm]                                       | 0.46  |       | 1.0          |       | 2.0     |       |
| Scale-up factor ( $SF$ )                       | 1     |       | 4.73         |       | 18.90   |       |
| $Q$ [ml/min]                                   | 2.5   |       | 11.81        |       | 47.26   |       |
| $m_{feed}$ (one component) [mg]                | 1.94  |       | 9.17         |       | 36.67   |       |
| $V_{inj}$ [ $\mu$ l]                           | 101   |       | 477.32       |       | 1909.26 |       |
| Enantiomer: S (component 1) or R (component 2) | S     | R     | S            | R     | S       | R     |
| $RE$   | 0.915 | 0.937 | 0.915        | 0.937 | 0.915   | 0.937 |
| $PR$ [g/h/ $\lambda_{ads}$ ]                   | 262.4 | 268.9 | 262.4        | 268.9 | 262.4   | 268.9 |
| $t_{cycle}$ [min]                              | 0.65  | 0.65  | 0.65         | 0.65  | 0.65    | 0.65  |
| $m_{coll}$ [mg/h]                              | 6.24  | 6.40  | 29.51        | 30.24 | 118.04  | 121.0 |
| $t$ ( $m_{coll} = 1$ g) [h]                    | 160.1 | 156.3 | 33.89        | 33.07 | 8.47    | 8.27  |
| $n_{inj}$ ( $m_{coll} = 1$ g)                  | 14783 | 14426 | 3129         | 3053  | 783     | 764   |

At the moment there are no commercially available Chiralpak AD columns with the length of 5 cm and diameter larger than 2 cm. However, since the introduction of the bicalutamide scale-up tests was mainly done in order to illustrate the presented methodology, further simulations with hypothetical columns of even larger diameters were performed. The idea was to analyse how the collected mass and the time needed for producing one gram of pure enantiomers change with the diameter. This dependency is shown in Figure 8.15 for the diameters in the range 0.46 cm to 5.0 cm.

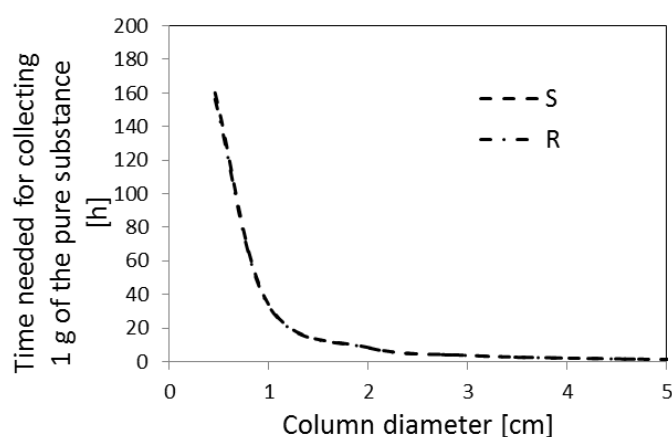


Figure 8.15. Decrease of the time needed to collect 1 g of pure bicalutamide enantiomers by increasing the column diameter. Column length is kept constant (5 cm). Volumetric flowrate and the injected amount are changed with the column diameter according to eq. (4.17).

The time needed for one gram of pure components is approximately the same for both enantiomers. It starts decreasing very fast between 0.46 cm and 1 cm diameter and then for

the values larger than 3 cm it is reduced at much lower degree. For the columns with diameter of 3 cm, the needed time for collecting 1 g is about 3.7 h, while for 5 cm it is about 1.3 h for both enantiomers.

### 8.2.2 Scale-up for isoflurane and desflurane enantioseparation

For the fluorinated anaesthetics the scale-up procedure was applied in order to increase the production of the pure enantiomers needed for later medical tests. Here, like in the case of bicalutamide, the calculations were performed for two larger-scale columns. The chosen diameters were 1 cm and 1.66 cm. Those columns were available in our laboratories and could be used for validation tests and final production.

For the both anaesthetics the same calculations were performed. The operating parameters (carrier-gas flowrate and injected amount) were first determined from eq. (4.17) and used for process simulations, from which the performance characteristics were further estimated. The collected amounts per time increase in the large column by the factor of 7.63. This means that for collecting one gram of pure isoflurane enantiomers in the column with diameter of 1.66 cm one needs 18.7 h for S- and 21.6 for R-enantiomer. For desflurane the cycle time is shorter and productivity higher. Therefore to get one gram from the large column, 8.7 h are needed for S-enantiomer and 10.1 h for R. The other values can be seen in Table 8.7 for isoflurane and in Table 8.8 for desflurane.

Table 8.7. Scale-up results for isoflurane enantiomers obtained from eq. (4.17) and by performing simulations with the data for the larger-scale columns. The operation and performance parameters are presented for the three examined column sizes (referred as small, intermediate and large).

| Column                          | Small |       | Intermediate |       | Large |       |
|---------------------------------|-------|-------|--------------|-------|-------|-------|
| $d$ [cm]                        | 0.6   |       | 1.0          |       | 1.66  |       |
| Scale-up factor ( $SF$ )        | 1     |       | 2.78         |       | 7.63  |       |
| $Q$ [ml/min]                    | 71    |       | 197.2        |       | 541.5 |       |
| $m_{feed}$ (one component) [mg] | 4.34  |       | 12.1         |       | 33.1  |       |
| $V_{inj}$ [ $\mu$ l]            | 5.8   |       | 16.1         |       | 44.3  |       |
| Enantiomer                      | S     | R     | S            | R     | S     | R     |
| $RE$                            | 0.64  | 0.55  | 0.64         | 0.55  | 0.64  | 0.55  |
| $PR$ [g/h/ $l_{ads}$ ]          | 3.29  | 2.82  | 3.26         | 2.82  | 3.26  | 2.82  |
| $t_{cycle}$ [min]               | 23.79 | 23.79 | 23.79        | 23.79 | 23.79 | 23.79 |
| $m_{coll}$ [mg/h]               | 7.07  | 6.05  | 19.45        | 16.82 | 53.4  | 46.2  |
| $t$ ( $m_{coll} = 1$ g) [h]     | 141.5 | 165.1 | 51.42        | 59.43 | 18.7  | 21.6  |
| $n_{inj}$ ( $m_{coll} = 1$ g)   | 356.9 | 416.4 | 130.1        | 149.9 | 47.2  | 54.6  |

Table 8.8. Scale-up results for desflurane enantiomers obtained from eq. (4.17) and by performing simulations with the data for the larger-scale columns. The operation and performance parameters are presented for the three examined column sizes (referred as small, intermediate and large).

| Column                          | Small |       | Intermediate |       | Large |       |
|---------------------------------|-------|-------|--------------|-------|-------|-------|
| $d$ [cm]                        | 0.6   |       | 1.0          |       | 1.66  |       |
| Scale-up factor ( $SF$ )        | 1     |       | 2.78         |       | 7.63  |       |
| $Q$ [ml/min]                    | 21    |       | 58.3         |       | 160.7 |       |
| $m_{feed}$ (one component) [mg] | 4.98  |       | 13.8         |       | 38.1  |       |
| $V_{inj}$ [ $\mu$ l]            | 6.80  |       | 18.89        |       | 52.05 |       |
| Enantiomer                      | S     | R     | S            | R     | S     | R     |
| $RE$                            | 0.595 | 0.507 | 0.593        | 0.508 | 0.592 | 0.509 |
| $PR$ [g/h/l <sub>ads</sub> ]    | 7.02  | 6.02  | 7.00         | 6.02  | 7.00  | 6.02  |
| $t_{cycle}$ [min]               | 11.73 | 11.73 | 11.73        | 11.73 | 11.73 | 11.73 |
| $m_{coll}$ [mg/h]               | 15.2  | 12.9  | 41.9         | 35.9  | 115.1 | 99.0  |
| $t$ ( $m_{coll} = 1$ g) [h]     | 65.9  | 77.3  | 23.9         | 27.8  | 8.7   | 10.1  |
| $n_{inj}$ ( $m_{coll} = 1$ g)   | 337.3 | 395.6 | 122.1        | 142.4 | 44.5  | 51.7  |

These results show that increase of the column diameter from 0.6 cm to 1.66 cm gives the possibility to collect within a reasonable time period (less than one day for 1 gram) sufficient amounts of pure enantiomers, which can be then used for further analyses and investigations.

By being able to produce one gram of enantiomers in less than one day, the goals set in SPP1570 project were fulfilled. Still, when even larger columns would be applied, the production could be more efficient. To analyse the outcomes of possible experiments with larger columns, different diameters were taken and the time for collecting 1 g was determined. Figure 8.7 shows the results for enantiomers of both anaesthetics. The tested diameter range varied from 0.1 cm to 5 cm.

As for the previously tested columns, the needed collection times for two enantiomers are close to each other, but always slightly lower for the first enantiomer (S). By analysing the results, it can be concluded that by using a column with 3.5 cm diameter 1 g of both enantiomers of isoflurane could be collected in less than 5 hours and with the diameter of 5 cm it is possible to obtain 1g of S- and R-enantiomer in 2.0 and 2.3 hours, respectively. For desflurane already by having a column with diameter of 2.4 cm it is possible to prepare 1g of enantiomers in less than 5 hours and with 5 cm diameter in about one hour. Therefore, the use of larger columns would be advisable for the future preparative enantioseparations.



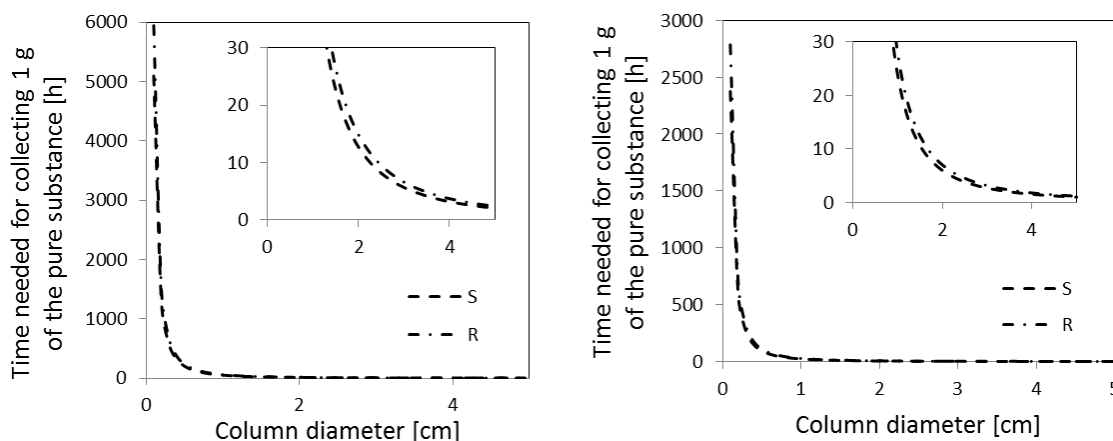


Figure 8.16. Decrease of the time needed to collect 1 g of pure enantiomers of isoflurane (left) and desflurane (right) by increasing the column diameter. Column length is kept constant (40 cm). Volumetric flowrate and the injected amount are varied with the column diameter according to eq. (4.17).

In order to check if the stated predictions were reasonable, since they were based on the simple scale-up relations typical for liquid phase separations, in the frame of Subproject II validation experiments were conducted. By applying the scaling rule given by eq. (4.17), the resulting chromatograms from different columns with the same length should be identical. In the performed simulation this was confirmed and validation tests were planned so that this statement can also be tested in practice. Due to equipment constraints it was not possible to provide exactly the same conditions as the scale-up rule predicted.

In Table 8.9 the values of volumetric flowrates and injected volumes that are required theoretically are given along with those that were possible for the experiments. As it can be seen from the table, the differences in the parameters are not very large and they can be considered correct. In all the experiments it was a problem to adjust the correct flow of the carrier gas. For isoflurane the injected volumes are different than required due to the syringe limitations. The used syringe allows only the injections of 10, 20, 30, 40 etc. microliters. For isoflurane it was possible to perform experiments with different injection amounts. They all led to the same conclusions, so here only the results for the cases that correspond to the largest injection in the small column (5 microliter) are presented. For desflurane the selection of the injected volume was even more constrained. As it was explained in the experimental section of this thesis (section 6.1.2), desflurane could only be injected by using a syringe with possibility to inject 0.04, 0.2, 0.4, 0.6, 0.8 or 1 microliter. Therefore, the elution profile from the small column resulting from the injection of 0.4  $\mu\text{l}$  was compared to the one of intermediate column with  $V_{inj} = 1 \mu\text{l}$ . For the validation of the large column the profiles resulting from injections of 0.04  $\mu\text{l}$  and 0.4  $\mu\text{l}$  of the small and large column, respectively, were compared.

Table 8.9. Data of the scale-up validation procedure for isoflurane and desflurane (shown in Figure 8.17 and Figure 8.18). Presented are the volumetric flowrates ( $Q$ ) and injected volumes ( $V_{inj}$ ) for the small column, while for the intermediate and large column the values, which are required according to the scale-up rule (eq. (4.17)), are compared to those applied in the experiments carried out in Subproject II.

| Column     |                      | Small<br>( $d = 0.6$ cm) | Intermediate ( $d = 1$ cm) |          | Large ( $d = 1.66$ cm) |          |
|------------|----------------------|--------------------------|----------------------------|----------|------------------------|----------|
|            |                      |                          | Required                   | Executed | Required               | Executed |
| Isoflurane | $Q$ [ml/min]         | 71                       | 197.2                      | 191      | 541.5                  | 492      |
|            | $V_{inj}$ [ $\mu$ l] | 5                        | 13.9                       | 20       | 38.1                   | 40       |
| Desflurane | $Q$ [ml/min]         | 21                       | 58.3                       | 54       | 160.7                  | 152      |
|            | $V_{inj}$ [ $\mu$ l] | 0.04                     | -                          | -        | 0.31                   | 0.4      |
|            |                      | 0.4                      | 1.11                       | 1        | -                      | -        |

The elution profiles of isoflurane for three different column scales are represented in Figure 8.17, while for desflurane the separate comparisons of small to intermediate and small to large column are shown in Figure 8.18. For the sake of simplicity only the experimental profiles are shown here. The simulations for all three columns produce identical elution profiles and the comparison of the simulations and experiments was already presented in Figure 7.13 for isoflurane and Figure 7.14 for desflurane.

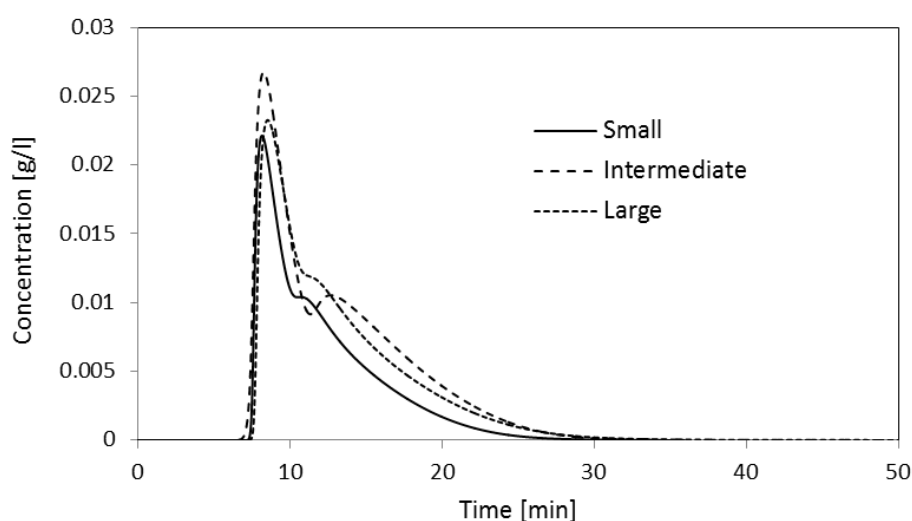


Figure 8.17. Experimental validation of the scale-up procedure for isoflurane illustrated by comparison of the experimental elution profiles for the small (diameter 0.6 cm, flowrate 71 ml/min, injected volume 5  $\mu$ l), intermediate (diameter 1 cm, flowrate 191 ml/min, injected volume 20  $\mu$ l) and the large column (diameter 1.66 cm, flowrate 492 ml/min, injected volume 40  $\mu$ l). The elution profiles originate from the experiments carried out in SPP1570 Subproject II.

The agreement between the peaks can be characterized as very good, especially for isoflurane. For both of the substances the results are better in case of the large column than for the intermediate one. The main deviation can be observed for the peak position, which

can originate from the lower flowrates used in the larger-scale columns, as well as from differences in the packing quality of two columns with different cross-sectional areas.

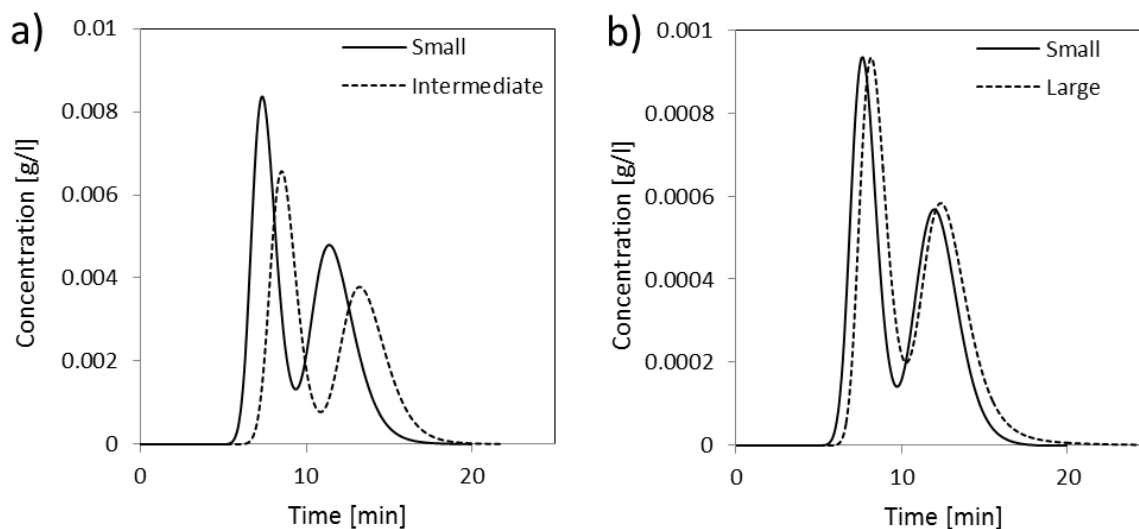


Figure 8.18. Experimental validation of the scale-up procedure for desflurane illustrated by comparison of the experimental elution profiles for: a) Small column (diameter 0.6 cm, flowrate 21 ml/min, injected volume 0.4  $\mu$ l) and intermediate column (diameter 1 cm, flowrate 54 ml/min, injected volume 1  $\mu$ l); b) Small column (diameter 0.6 cm, flowrate 21 ml/min, injected volume 0.04  $\mu$ l) and large column (diameter 1.66 cm, flowrate 152 ml/min, injected volume 0.4  $\mu$ l). The elution profiles resulted from the experiments done in SPP1570 Subproject II.

The differences in the peak shape are almost negligible (with exception of the isoflurane separation in the intermediate column). Other reasons for deviations could originate from the fact that the injection amounts were not proper (as seen in Table 8.9), as well as from different experimental conditions. Furthermore, since there was a time difference between performing experiments with small and larger-scale columns, the particles and selector used were prepared separately, although the same procedure was applied (more details about it could be found in the outcomes of Subproject II).

The presented results of the experiments with the intermediate and large column show that the simulation could provide correct predictions, which means that the assumptions made, when the model was chosen, were justified. At the same time, these experiments represent the first step for the successful production of pure enantiomers of the anaesthetic gases. The successive step in the complete process is the development of a unit for storing the pure substances that will be discussed in the following section.

### 8.3 Design of the product capture process for desflurane

As explained in Chapter 4, section 4.3, an important part of the complete separation process for the fluorinated anaesthetics isoflurane and desflurane, is to develop the procedure for their isolation from the carrier gas by introducing the capture columns. The capture columns were designed for the GC separation with the so-called large columns with the diameter of 1.66 cm (characterized in the previous section). The first step in designing the product capture process is to find the suitable adsorbent with high capacity to store the injections coming from the separation column. The experimental investigation of different adsorbing materials was done in the frame of SPP1570 Subproject II and therefore here only the final result will be given. At the time when this thesis was written, only the results for desflurane were available from the research carried out in the Subproject II. The work on testing the isoflurane adsorption was in process. Therefore, the capture procedure will be described only for the case of desflurane. The calculations for isoflurane follow the same pattern.

There are more materials available for non-selective adsorption of the anaesthetic gases. One adsorbent that was found to have high capacity and was therefore analysed here, is controlled porous glass in the form of beads (pore size 4.1 nm, surface area 961 m<sup>2</sup>/g). The raw material was produced in the laboratories of Leipzig University (by the research group of Professor Enke) and it was then transformed into its final form at the University of Hamburg (by the research group of Professor Fröba). Using frontal analysis, the single-component adsorption isotherms of the racemic mixture were determined and could be fitted to the Langmuir model (given in eq. (2.31)). The parameter values at the temperature of 10 °C are presented in Table 8.10. The adsorbent was also completely characterized. The determined bed porosity was 0.797. Additional details about the capture materials could be found in the future doctoral thesis of Thomas Munkelt [14] and the planned publication [109].

Table 8.10. Parameters of the Langmuir adsorption isotherms of desflurane racemic mixture at 10 °C on the non-selective controlled porous glass beads (prepared by the research groups of Prof. Enke, Leipzig University and Prof. Fröba, University of Hamburg) used as adsorbent in the capture columns (data obtained from the parallel SPP1570 Subproject II).

| Isotherm parameters             | Value |
|---------------------------------|-------|
| $H$ (R- and S-enantiomer)       | 18302 |
| $b$ [l/g] (R- and S-enantiomer) | 23.6  |

Using the experimental data provided from the project Subproject II and the other needed parameters, the further calculation of the required length for the three capture columns was performed as part of this thesis. The important expressions are given in the section 4.3.1, by eq. (4.32) for the total required column length and eq. (4.27), (4.33) and (4.34) for the single sections.

A key task is to determine the number of injections ( $n_{inj}$ ) that have to be stored in the capture columns. Since each peak from the outlet of the separation column is divided into three

fractions (I, II and III) that are sent to the three capture columns (with the same notation, I, II and III, as described in the section 4.3), each capture column has to store the same number of injections. The decision made here was to store at least 1 gram of each pure enantiomer in the corresponding columns I and III. As it can be seen from Table 8.8, larger number of injections (51.7) is needed to collect the R-enantiomer (component 2). Therefore the first larger integer for the R-enantiomer will be taken as the number of injections for the capture columns, i.e.  $n_{inj} = 52$ .

The value of the effective diffusion coefficient ( $D_{eff}$ ) was estimated from the experimental tests (part of Subproject II). The procedure was to “park” desflurane injections into a test column. The number of injections that could be “parked” is denoted as  $n_{inj(test)}$ , and the length of the used column as  $L_{(test)}$ . By combining equations (4.32), (4.33) and (4.34), we get the expression for the column length  $L_{(test)}$  depending on  $n_{inj(test)}$ ,  $\Delta x_{id}^{cap}$ ,  $t^{cap}$ ,  $t_{cycle}$  and  $D_{eff}$ . The term  $\Delta x_{id}^{cap}$  is expressed by equation (4.27). Since the only unknown parameter is  $D_{eff}$ , it can be calculated from this expression. The estimated value was  $D_{eff} = 8.5 \cdot 10^{-8}$  m<sup>2</sup>/s and is used with the purpose to illustrate the capture process. However, for the planned production further experiments are advisable, in order to calculate this number with higher accuracy.

The values of the parameters involved in the sizing of the capture columns, as well as their final required length and volume, and the adsorbent volume are presented in Table 8.11. The time intervals  $\Delta t^{cap}$  were calculated from the area of the peaks that are detected at the outlet of the separation column, as it was explained in Chapter 4, section 4.3.1.

Table 8.11. Parameters of the capture columns required for storing at least one gram of desflurane enantiomers: Calculated column length ( $L^{cap}$ ), its volume ( $V^{cap}$ ) and adsorbent amount ( $V_{ads}^{cap}$ ) together with the needed additional parameters (notation given in the text) for the three capture columns (I, II and III) used to collect desflurane fractions after the separation process. The volumetric flowrate (160.7 ml/min) and the diameter (1.66 cm) of all the three columns is equal to those of the large separation column. The number of the cycles to be stored in each of the columns is 52. The cycle time is 11.7 min.

| Capture columns for desflurane   | I<br>(Component 1,<br>S-enantiomer) | III<br>(Mixed fraction) | II<br>(Component 2,<br>R-enantiomer) |
|----------------------------------|-------------------------------------|-------------------------|--------------------------------------|
| $\Delta t^{cap}$ [min]           | 1.17                                | 5                       | 2.28                                 |
| $\Delta x_{id}^{cap}$ [cm]       | 0.0954                              | 0.134                   | 0.101                                |
| $\Delta x_{diff}^{cap}$ [cm]     | 0.244                               | 0.307                   | 0.341                                |
| $\Delta x_{diff,end}^{cap}$ [cm] | 5.58                                | 5.58                    | 5.58                                 |
| $L^{cap}$ [cm]                   | 23.2                                | 28.5                    | 28.6                                 |
| $V^{cap}$ [ml]                   | 50.2                                | 61.6                    | 61.8                                 |
| $V_{ads}^{cap}$ [ml]             | 10.2                                | 12.5                    | 12.6                                 |

The values obtained for the capture column dimensions are not completely accurate, since more rigorous calculations have to be done. Still, they can be considered as very good estimates and helpful for planning the further experimental work. According to these preliminary calculations, to capture one gram of each of desflurane enantiomer in the pure form (purity over 99 %), three columns of 1.66 cm diameter and minimal lengths 23.2 cm, 28.5 cm and 28.6 cm are required with the total adsorbent volume of 35.3 ml. The determined column dimensions have reasonable values and it is feasible to implement them into the planned production unit. More detailed calculations and supporting experiments done as part of Subproject II are at the moment in progress and could be found in the future report [109].

#### 8.4 Continuous enantioseparation using a PSA process

In order to illustrate the potential of performing separation of enantiomers in a continuous mode, simulation of a PSA process was done. Having more degrees of freedom in comparison to the batch GC, this process offers larger range of possibilities to improve the separation by manipulating different parameters. Here is just given a brief representation of the PSA application for the gaseous systems, isoflurane and desflurane. More work can be included in the future projects.

The idea was to compare the PSA process with the batch GC for the enantioseparation of the anaesthetic gases. Since in the batch-GC experiments the largest injected amount for desflurane was 1 microliter, that example was taken for comparison. Accordingly, also for isoflurane the 1 microliter injection was taken as a reference system. In the PSA models mole fractions were used instead of the concentration expressed in g/l. They were calculated from the ideal gas law (equations listed in Chapter 2, section 2.5.2.2, e.g. eq. (2.47)). The model used for the PSA simulation and other simulation details are given in Chapter 6, section 6.2.

The investigated PSA includes a one-column process with the four basic steps: pressurization, adsorption, blowdown and desorption. The steps were performed in the way as it is shown in Figure 2.13. Pressurization is done with the inert gas (helium) in the counter-current direction, as well as the desorption step. Blowdown was performed counter-currently, too. In the adsorption step (co-current direction) the feed contained the diluted racemic mixture with the concentration corresponding to that of the 1  $\mu$ l injection batch GC experiment.

The parameters (such as column dimensions, porosity, temperature) used for the simulations are equal to those from the batch experiments (Table 6.2 and Table 6.3) performed with the large column (diameter 1.66 cm, mobile phase flowrate 541.5 ml/min for isoflurane and 160.7 ml/min for desflurane). Low pressure was chosen to be the atmospheric pressure (101.325 kPa), while the high pressure in the adsorption step was first taken to be 500 kPa. Later different lower and higher values were tested. The duration of the pressurization and blowdown steps was equal, 0.5 minutes. Adsorption and desorption times were selected in

such a way that the optimal process performance could be achieved. The way of their determination is described in the following paragraphs.

The important times for the adsorption step of a PSA process are the times when the first and the second component start eluting, i.e. are detected at the column outlet. The times are denoted as  $t_{ads-s,1}$  and  $t_{ads-s,2}$  (following the analogy with the starting cut times,  $t_s$ ), representing the intervals between the start of the adsorption step and the start of the elution.

For the desorption step, the key times are those when the first and the second component exit the column. Since they represent the “end” times for components 1 and 2, they are denoted as  $t_{des-e,1}$  and  $t_{des-e,2}$ , respectively, thus representing the intervals between the beginning of the desorption step and the moment when complete elution occurs. The values of these times are given in Table 8.12.

Table 8.12. The times when elution of the components starts during the adsorption step of the PSA process ( $t_{ads-s,1}$  and  $t_{ads-s,2}$ ) and when the components exit the column during the desorption step ( $t_{des-e,1}$  and  $t_{des-e,2}$ ). The values are given as time intervals from the start of the corresponding step until elution (as explained in the text above). Flowrate is 541.5 ml/min for isoflurane and 160.7 ml/min for desflurane, temperature 28 °C, high pressure 500 kPa.

|                     | Isoflurane | Desflurane |
|---------------------|------------|------------|
| $t_{ads-s,1}$ [min] | 14.7       | 8.2        |
| $t_{ads-s,2}$ [min] | 25.0       | 13.0       |
| $t_{des-e,1}$ [min] | 20.5       | 11.0       |
| $t_{des-e,2}$ [min] | 28.0       | 15.2       |

The goal was to obtain the highest productivity for the first eluting enantiomer (S-enantiomer for both isoflurane and desflurane) by keeping its purity over 99 %. The first component is collected in the adsorption step, therefore the duration of this step was adjusted in such a way that the step ends as soon as the second enantiomer (R) starts eluting, which is at  $t_{ads-s,2}$ . The elution of both enantiomers of desflurane at the end of the adsorption step is depicted in Figure 8.19.

The separation is, due to low concentration, done in the nearly linear range of the adsorption isotherms. This can be also seen from the shape of the breakthrough curve, which does not exhibit typical competitive behaviour. The profile for isoflurane has the same shape.

The purpose of the desorption step is to provide the complete bed regeneration, so it was chosen to last until no more solutes remained in the column. The time when the column regeneration is achieved, is the time when the second component (R-enantiomer) left the column ( $t_{des-e,2}$ ).

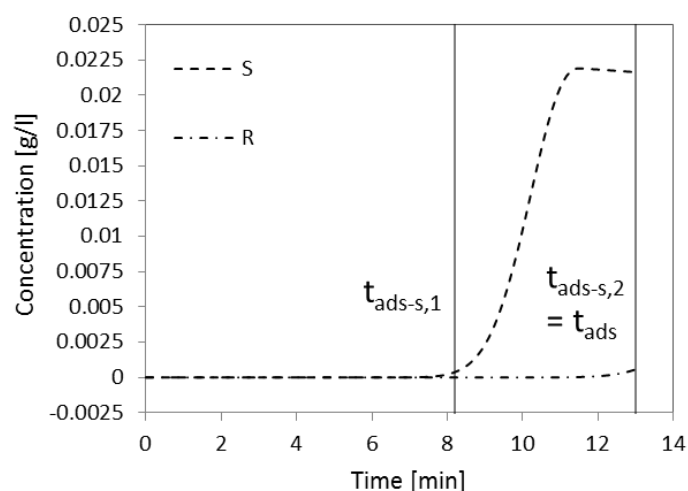


Figure 8.19. Breakthrough curves of desflurane enantiomers at the end of the adsorption step (when elution of the second component begins). The elution of the S-enantiomer starts at  $t_{ads-s,1} = 8.2$  min and for R-enantiomer it is at  $t_{ads-s,2} = 13.0$  min – this time represents also the end of the adsorption step. Flowrate is 160.7 ml/min, temperature 28 °C, high pressure 500 kPa.

The used values are summarized in Table 8.13. The simulation process was repeated for a number of cycles ( $n_{cycles}$ ) until a cyclic steady state (CSS) was reached. These numbers for the isoflurane and desflurane simulations are given in Table 8.13, too.

Table 8.13. Parameters selected for the PSA simulations of the isoflurane and desflurane enantioseparation. The other data are the same as for the batch GC systems (Table 6.2 and Table 6.3).

|   | Isoflurane | Desflurane |
|---|------------|------------|
| Volumetric flowrate [ml/min]              | 71         | 21         |
| Pressurization time ( $t_{press}$ ) [min] | 0.5        | 0.5        |
| Adsorption time ( $t_{ads}$ ) [min]       | 25.0       | 13.0       |
| Blowdown time ( $t_{blow}$ ) [min]        | 0.5        | 0.5        |
| Desorption time ( $t_{des}$ ) [min]       | 28.0       | 15.2       |
| High pressure ( $P_{ads}$ ) [kPa]         | 500        | 500        |
| Low pressure ( $P_{des}$ ) [kPa]          | 101.325    | 101.325    |
| Number of cycles for achieving CSS        | 6          | 3          |

In order to analyse the PSA processes, a parametric study was performed, by changing the values of the adsorption and desorption step times, as well as the value of the high pressure used during adsorption. Other parameters could also be varied and investigated, but here the idea was to keep them same as for the batch process.

Since the behaviour of isoflurane and desflurane is the same and variations of the parameters have the same effect, only the diagrams for desflurane will be presented. The isoflurane enantiomers follow the same trends.



The influence of the adsorption time on productivity of desflurane enantiomers is presented in Figure 8.20, while Figure 8.21 shows the changes of the purity and recovery. Until the time  $t_{ads-s,1}$ , when S-enantiomer (component 1) starts eluting, it is still not detected at the column outlet, so it cannot be collected and accordingly the productivity of the S-component is zero. The recovery of this enantiomer is also zero, while the purity is not defined. R-enantiomer (second component) is collected in the desorption step, during which the column is “cleaned” from all the components adsorbed in the adsorption step. Productivity of R-component is increasing while the adsorption time increases from 0 to  $t_{ads-s,1}$ , because with longer adsorption step, more feed (and therefore more R-enantiomer) is adsorbed in the column and more can be desorbed later as well. Its recovery is around 100 %, since all the introduced substance is collected later in the desorption step. However the collected fraction contains also S-enantiomer and therefore the purity is about 50 %, which means there is no separation occurring in this time interval.

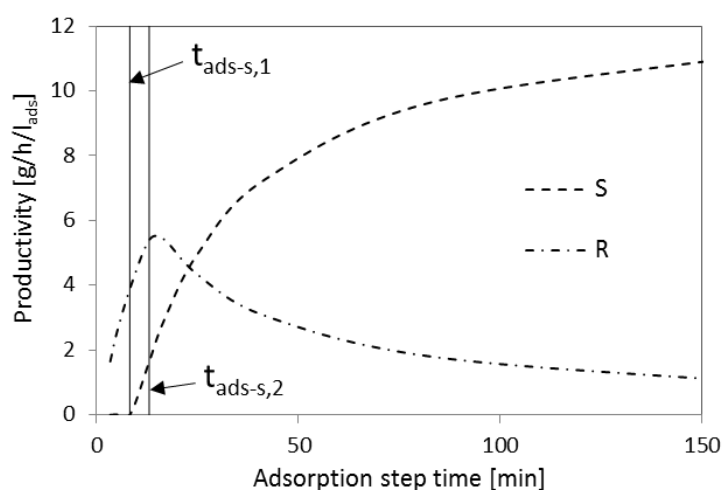


Figure 8.20. Influence of the adsorption step time variation on the productivity of desflurane enantiomers in the 4-step PSA process.

Between the times  $t_{ads-s,1}$  and  $t_{ads-s,2}$  the elution of the S-enantiomer occurs, while R-enantiomer still does not leave the column. The collection of the S-enantiomer begins and due to the increase of the duration of the feed (adsorption) step, more components are introduced in the column and the productivity of the S-enantiomer increases. By increasing the adsorption time, more of the S-component is collected in the adsorption step and less left to undergo the desorption step and therefore its recovery increases as well. Purity is constant and in the range 99-100 %. For the R-enantiomer, productivity still increases for the same reason as in the previous time interval (by increasing the adsorption time, more feed is introduced into the system and larger amount of R-enantiomer is collected in the desorption step). Recovery does not change in comparison to the previous time interval and the purity slightly increases, because the first component (S) starts to be collected and does not contaminate in such large extent the stream that contains R-enantiomer.

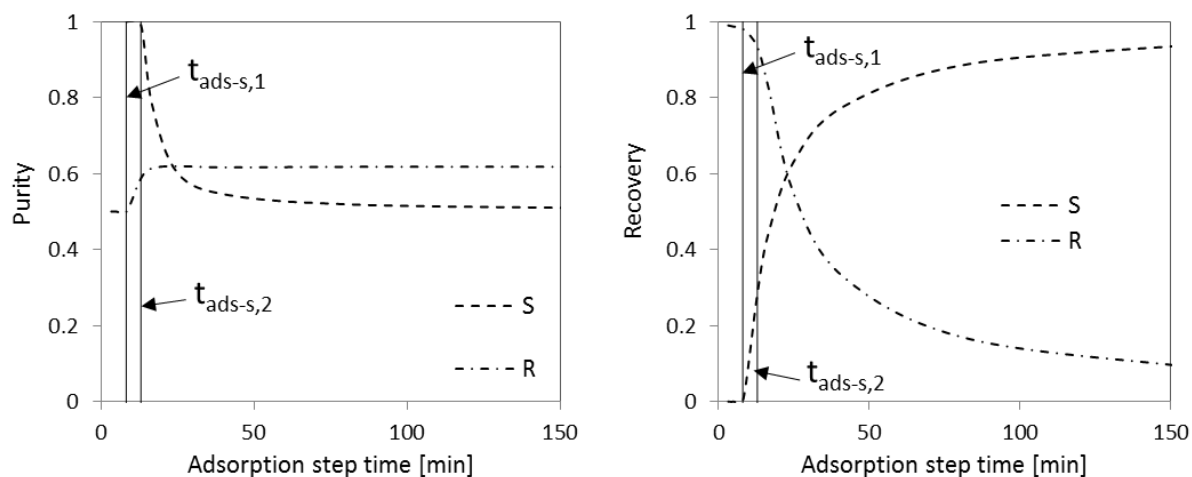


Figure 8.21. Influence of the adsorption step time variation on the purity (left) and recovery (right) of desflurane enantiomers in the 4-step PSA process.

When the adsorption time is larger than  $t_{ads-s,2}$ , the productivity and recovery of the S-enantiomer increase, due to the longer collecting time, when more product is gained, but since the R-enantiomer started to elute, the stream is not pure any more (S-enantiomer purity is decreasing). For R-enantiomer productivity and recovery decrease because it is collected with S-component during the adsorption step (and not completely recovered during the desorption, as it was in the previous time intervals), while purity becomes constant.

The effect of the variations of the desorption time on the productivity of desflurane enantiomers can be seen in Figure 8.22 and the influence on the purity and recovery is presented in Figure 8.23. The desorption time influences the process performance in the following way: on one hand, if it is too short, the column is not regenerated and the substances are present there at the beginning of the subsequent step; on the other hand, when the desorption lasts longer than it is needed to regenerate the column, its further increase unnecessary increases the total cycle time and therefore reduces the productivity.

Since S-enantiomer is collected in the adsorption step, the increase of the desorption time makes its productivity to decrease due to the longer cycle time. At the beginning, for very short desorption times the stream collected during the adsorption step contains both enantiomers from the previous step and therefore the purity of the S-enantiomer is very low (about 50 %). By increasing the desorption time, column becomes better regenerated at the start of the new cycle and purity of S-enantiomer increases. For the desorption time larger than  $t_{des-e,2}$  (complete elution of R-component), column is completely regenerated and therefore the purity of S-enantiomer reaches 100 % and remains at that value. This is valid when the adsorption step time is well adjusted, as it was done in our case. Recovery of the S-enantiomer is higher for the smaller values of the desorption time, since during the adsorption step, apart from the feed, also material (though not pure) from the previous cycle is collected. By increasing the desorption time, the recovery decreases (S-enantiomer is in larger amount collected during the longer desorption step and less remains for the subsequent adsorption

step). This trend lasts until the time  $t_{des-e,2}$  is reached and then recovery remains constant (it depends only on  $t_{ads}$ ).

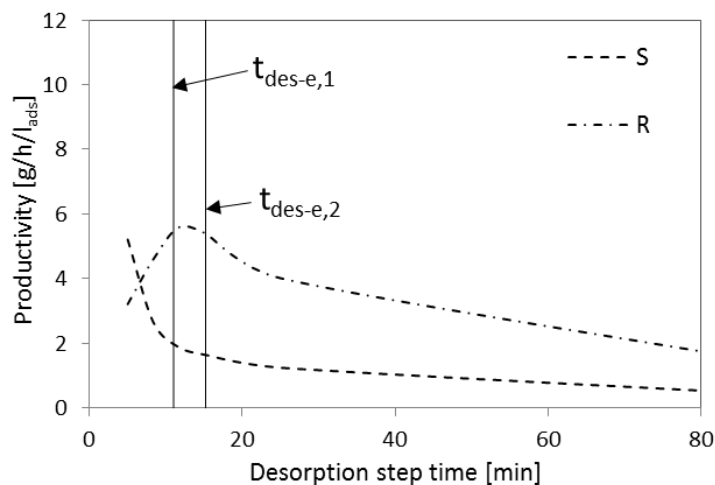


Figure 8.22. Influence of the desorption step time variation on the productivity of desflurane enantiomers in the 4-step PSA process.

For the second component (R-enantiomer) the productivity starts to grow with the desorption time until the value of  $t_{des-e,2}$  is reached (because with longer time more of the component R is collected during the desorption step). For desorption time larger than  $t_{des-e,2}$  the column becomes completely regenerated, so the productivity of R-component starts decreasing, since there is no more substance left in the column, but the cycle time is still increasing. For small  $t_{des}$  recovery follows the same pattern as productivity. For short desorption step, recovery is low, since large fractions of R-enantiomer are transferred to the following cycle and not collected. By increasing the desorption time, the amount of collected R-enantiomer increases and so does the recovery. At  $t_{des} = t_{des-e,2}$  the whole amount of R is eluted, so since there is no more substance left in the column, by further increasing  $t_{des}$ , the recovery remains constant and close to 100 %. For low desorption times, until  $t_{des-e,1}$  is reached (complete elution of S-component), during the desorption step racemic mixture is collected. Therefore, purity of R-enantiomer is 50 %. For  $t_{des} \geq t_{des-e,1}$  it starts growing until the complete elution of R-enantiomer ( $t_{des-e,2}$ ). After this point, there are no more eluents left in the column, so the further increase of the desorption time does not affect the substance purity (i.e. it remains constant).

As it could be observed from the previously showed diagrams, the first eluting component (S-enantiomer) could be collected with purity over 99 %, while for the R-enantiomer high purity could not be achieved. The reason for this is the way in which PSA processes are designed. During the desorption step the mixed fraction of both components is collected together with the pure second component. If the mixed fraction would be collected at the beginning of the desorption step until component S is completely eluted (until  $t_{des-e,1}$ ) and then collected the fraction with only R-enantiomer, the purity of about 100 % of R would be achieved. In that way highly pure R-enantiomer could be produced, but its recovery and productivity would be lowered.

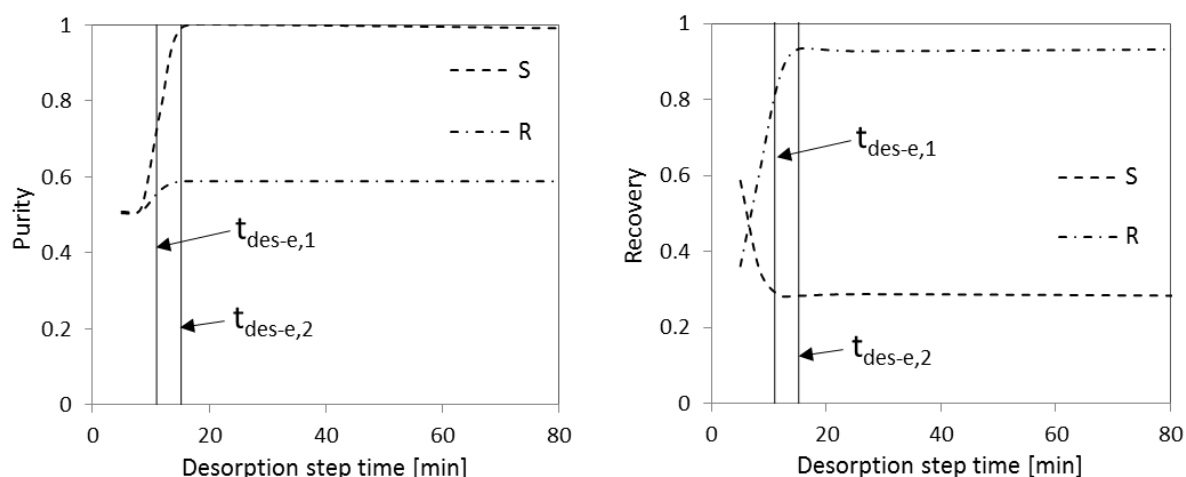


Figure 8.23. Influence of the desorption step time variation on the purity (left) and recovery (right) of desflurane enantiomers in the 4-step PSA process.

Apart from the step times, also the effect of different high-level pressure for the adsorption step was investigated. The lowest value was the atmospheric pressure (equal to the low pressure applied in the desorption step) and the highest tested pressure was 1000 kPa. The changes of the pressure do not influence the purity and recovery of the collected components when the adsorption and desorption times are fixed. The characteristic that changes is the productivity. It increases by increasing the feed pressure for the both of the components. This result was expected, since the idea of introducing PSA processes is to improve the production by using higher pressures. The variation of the productivity for desflurane enantiomers is presented in Figure 8.24. The production rate changes linearly with the applied pressure. It was calculated that, when compared to the production rates achieved for batch GC process, PSA can provide higher productivity of S-enantiomer when the adsorption pressure is higher than 605 kPa for isoflurane enantioseparation and higher than 560 kPa for desflurane.

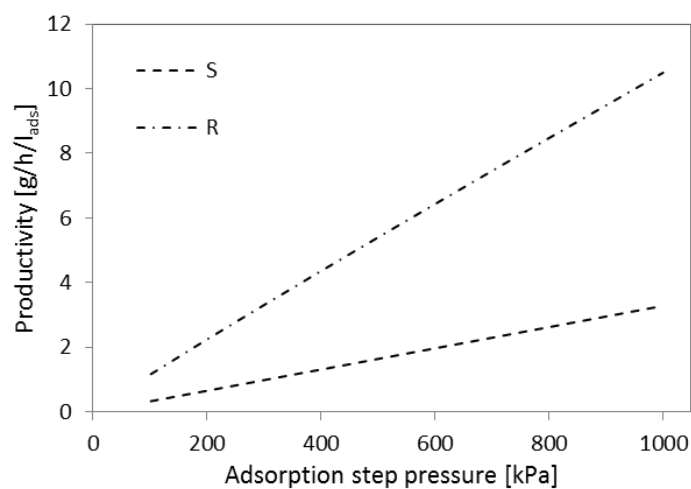


Figure 8.24. Influence of the high pressure variation during the adsorption step on the productivity of desflurane enantiomers in the 4-step PSA process.

The resulting values of the process performance parameters for the case that was selected as the optimum, i.e. when the highest productivity of S-enantiomer is achieved with the purity over 99 %, is presented in Table 8.14 for isoflurane and desflurane enantiomers. The values of the adsorption and desorption time that provide this situation are those given in Table 8.13. Calculated values are shown for two different high pressures, 500 kPa and 1000 kPa. In order to compare the PSA separation to the batch GC process discussed in the previous sections, the values of the process performance parameters are given in Table 8.14 for the case when 1 microliter of racemic mixture was injected in the GC column. Since in the PSA process the R-enantiomer was collected together with the mixed fraction, it will not be discussed now.

Table 8.14. Process performance characteristics for the 4-step PSA separation of isoflurane and desflurane enantiomers at two different adsorption pressures. The other operating parameters are given in Table 8.13. The comparison of the PSA to the batch GC process with 1 microliter injection of racemic mixture is also presented.

| Parameter   | Productivity<br>[g/h/l <sub>ads</sub> ] |       | Recovery |       | Purity |       |
|---|---|-------|----------|-------|--------|-------|
|   | S                                       | R     | S        | R     | S      | R     |
| Isoflurane  |   |       |          |       |        |       |
| PSA: $P_{ads} = 500$ kPa  | 0.770                                   | 2.54  | 0.299    | 0.988 | 0.995  | 0.589 |
| PSA: $P_{ads} = 1000$ kPa   | 1.54                                    | 5.06  | 0.299    | 0.984 | 0.995  | 0.589 |
| Batch: $V_{inj} = 1$ $\mu$ l*   | 0.992                                   | 0.990 | 0.972    | 0.970 | 0.992  | 0.990 |
| Desflurane  |   |       |          |       |        |       |
| PSA: $P_{ads} = 500$ kPa  | 1.64                                    | 5.40  | 0.283    | 0.933 | 0.991  | 0.588 |
| PSA: $P_{ads} = 1000$ kPa   | 3.28                                    | 10.5  | 0.283    | 0.907 | 0.991  | 0.590 |
| Batch: $V_{inj} = 1$ $\mu$ l*   | 1.86                                    | 1.82  | 0.968    | 0.946 | 0.991  | 0.991 |
| * As explained before in this section the feed concentrations used for simulating the PSA process were comparable to those used for 1microliter injections in the GC regime (which is the largest injection volume possible to be tested for desflurane experimentally in our laboratories) |   |       |          |       |        |       |

The purity of S-enantiomer achieved in the batch and PSA process is comparable for isoflurane, as well as for desflurane, but the recovery is much higher for the batch GC system (97 %) than for PSA (only around 29 %). As it can be seen from Figure 8.24, the productivity in the PSA process increases linearly by increasing the adsorption pressure. When the applied pressure was 500 kPa the productivity of the S-enantiomer was in the similar range as for the batch process, but if the pressure was increased to 1000 kPa, PSA could provide better production of the pure S-enantiomer. The results were same for both anaesthetics. Therefore, whenever the operating conditions allow it, for the PSA process it is advantageous to use higher pressures during the adsorption step. However, there are always limitation, such as pressure drop and the possible condensation of the volatile substances at even higher pressures.

The calculations done in this section clearly show the potential of performing the advantageous production of S-enantiomer (component 1) of both anaesthetics by using higher pressures. This process could be successfully applied when no R-enantiomer is wanted and no high recovery is required. The possibility to collect the pure R-enantiomer would include the separate collection of the mixed fraction that leaves the column at the beginning of the desorption step and then the collection of the remaining pure enantiomer. The investigation of such a concept could be a part of the future work on this topic.

In order to improve the recovery of the products, process with two or more beds could be employed. In that way, while one column is in adsorption step, the others would be in different stages of desorption, pressurization or blowdown. This concept also provides great conservation of energy and separation work.

By comparing the overall performance of the here examined four-step PSA with the GC separation operated by repetitive injections and by taking into account that the PSA process is more complicated, the batch GC is selected as a more suitable process for enantioseparation of the anaesthetic gases.

## **8.5 Summary and discussion**

This chapter described a procedure to analyse the separation of enantiomers and adjust operating conditions in order to get the highest possible production of the pure substances. To make the examinations more efficient in terms of invested time, substances and equipment, all the tests were done theoretically using the concepts described in this thesis. The chapter presented different ways to increase the production by manipulating the feed amounts and column diameters, as well as by estimating theoretically the potential of a continuous four-step PSA process, as an alternative to single-column batch chromatography. Also, in order to complete the production of the pure enantiomers, an efficient way to finally isolate (capture) them from the carrier gas after the separation was presented.

As introduced before, the target substances are the anaesthetic gases isoflurane and desflurane. Nevertheless, selected evaluations of process performance and scale-up were done for bicalutamide as well. The idea was to provide a reference system for the enantioseparation of the anaesthetics. The trends observed for bicalutamide were found to be the same as for isoflurane and desflurane, which gives an indication that the assumptions made for the gas phase system are transferable from the liquid phase.

In this chapter the results of four aspects in developing and analysing the production of single enantiomers were presented:

### **1. Process performance of a batch single-column process.**

Separation in the batch mode is done by performing repetitive injections, where the end of one peak coincides with the start of the peak from the subsequent injection. The first step in the analysis was to perform volume-overloading tests in order to determine the conditions that would provide highest production of pure enantiomers. It is shown that the process is able to provide high purity (over 99 %) and high productivity of the single components. The recovery for the anaesthetics was in the range 50-70 %, while for bicalutamide the achieved values were over 90 %. The productivity and recovery could be further increased by allowing lower purity and higher flowrates.

### **2. Scale-up procedure for the batch separation.**

To achieve the goal set in this thesis for the anaesthetics, which was to produce at least 1 g of both pure enantiomers in less than 24 h, larger separation columns were introduced. When the bed length was kept constant, and the diameter was increased from 0.6 cm to 1.66 cm, the time needed for collecting 1 g was reduced from 166 h to 22 h for isoflurane and from 78 h to 11 h for desflurane. These findings served for planning further experiments of the SPP1570 Subproject II.

### **3. Product capture after the separation.**

The production of pure substances cannot be considered complete without providing the way to separate them from the carrier gas (or the solvent for HPLC) and to store them properly. This thesis shows a new capture procedure for anaesthetics (done in collaboration with Subproject II) that directly follows the separation step. Dimensions of three capture columns (characterized by independently measured adsorption isotherms), required for collecting at least 1 g of each pure enantiomer and the mixed fraction, were roughly calculated for the case of desflurane. The obtained values can be used as good estimates for designing future experiments. The capture was described for the batch GC, but the same procedure can be applied for PSA separations.

### **4. Alternative separation using a PSA process.**

In order to evaluate the potential of a continuous separation process of anaesthetic gases, simulation of a four-step one-column PSA was done. After parametric studies, the achieved optimal process performance was compared to the batch separation. It was concluded that this simple PSA configuration can provide higher production of S-enantiomer of both anaesthetics, when the adsorption-step pressure was higher than 605 kPa for isoflurane and 560 kPa for desflurane. However, the recovery values were much lower than in the batch mode. Therefore and due to its simplicity, the batch separation including consecutive injections was selected as more suitable process to separate enantiomers of isoflurane and desflurane.

When performing simulation studies, an important task is to provide experimental validation of the made predictions. By using the experimentally determined elution profiles of the anaesthetics from Subproject II, validation was done first by comparing the values of productivity and recovery resulting from the simulations to those estimated from the

experimental peaks. The matching was found to be very good. Another validation step was done after implementing the scale-up procedure. According to the applied scale-up rule (eq. (4.17)) the elution profiles from columns with the same length should be exactly the same. The experimental peaks originating from three used columns (with the same length and different diameters) were compared and it was concluded that they were indeed very close to each other. These validation tests show not only that the assumptions taken for the scale-up calculations were correct, but also that the usage of the simple model for describing the gas-phase process was justified.

The calculations and experimental validation show that production of pure enantiomers of isoflurane and desflurane is feasible by using the investigated system and that it is possible to collect in just one week, using a laboratory unit, sufficient amounts of the enantiomers that medical doctors need for the first tests of the pharmacological effect of single components. The further results of the investigation will be presented in the upcoming publications [109, 170].



## 9 Conclusions

The human body is a chiral system and thus exhibits enantioselectivity in interaction with the chiral substances. For medical compounds using a single enantiomer – the one with higher or complete activity – instead of the racemic mixture might lead to the reduction of adverse effects, as well as to better pharmacological effects. This means that provision of enantiopure substances is very important for production of safer medications.

The main focus of this thesis was to investigate the separation of enantiomers of two fluorinated volatile anaesthetics, namely isoflurane and desflurane, by applying gas chromatography. Before this work took place and until the present time, there have not been reported another complete study of these fluorinated anaesthetics that would comprise experimental work and simulation tests at the same time. By using the chiral selector based on  $\gamma$ -cyclodextrin [156] studied in the preliminary systematic research of Schurig et al. and Juza et al. [99, 100, 145], in this thesis the complete process for separating and storing the enantiomers of anaesthetics was developed (in collaboration with an experimentally oriented parallel project).

In order to describe the enantioseparation theoretically and to determine the optimal conditions for maximal production, it was necessary to provide the understanding of the fundamentals of the occurring processes. Therefore, to test the applicability of the developed methods and to validate them, another chiral substance, bicalutamide, was studied in the liquid phase, both experimentally and by simulations.

For successful analysis and optimization of separation processes, it is crucial to provide good stationary phases and to perform the correct characterization of the used columns. For studying a chromatographic process, adsorption isotherms represent the most important relations. There are only a few methods available for experimental determination of competitive adsorption isotherms when only mixtures are available, as it is often the case for chiral substances. To overcome this problem, here an extension of the elution by characteristic point (ECP) was derived from the analytical solution of the ideal model of chromatography. The ECP method, whose application was limited so far exclusively to one-component systems, was here extended to determination of the binary-mixture adsorption isotherms which can be expressed with the most frequently encountered Langmuir model. Like a standard ECP method, this new extension represents a very fast and simple way to obtain the needed isotherms, with the minimal amount of the solutes used in experiments. The method was tested on a theoretical example and it was found that it predicts the isotherm parameters very well when columns with at least 2000 theoretical plates are used. For inefficient separations, such as those studied in this work (the columns with less than 100 theoretical plates), it is possible to use the method for obtaining good first estimates. In this

thesis, to finally calculate improved isotherm parameters, the established peak-fitting method was applied.

Starting from the knowledge of the adsorption isotherms, in this work the complete chromatographic separation process for chiral anaesthetics isoflurane and desflurane could be simulated using a simplified model (equilibrium dispersive model). This was justified by knowing that the studied gaseous systems were diluted. The effect of the gas compressibility was just introduced by applying simple corrections of the bed porosity and dispersion coefficients with the James-Martin factor. The main process that was analysed, was classical discontinuous batch gas chromatography operated by performing repetitive injections.

The central part of the simulation study represents the process performance evaluation. It was implemented by studying different injected amounts in order to provide the maximal productivity and high purity (over 99 %) of the single enantiomers. It was predicted to be possible to produce about 3 g/h/l<sub>ads</sub> of pure isoflurane enantiomers and for desflurane about 6.5 g/h/l<sub>ads</sub>. The other way to improve the process performance is to do the separation in larger columns. This potential was analysed by simple scale-up tests. It was found that by using a column of 1.66 cm diameter and 40 cm length, one gram of pure enantiomers can be produced in about 22 hours for isoflurane and for desflurane in about 10 hours. This result shows that the production is feasible and can be done in a short time interval. After the establishment of the most productive enantioseparation process, a step that follows the separation was analysed. It involved the development of the procedure for capturing and isolation of the pure components by introducing columns packed with non-selective and non-costly adsorbents. This provides the products to be harvested from more concentrated streams and makes the isolation process safer and more energy-efficient.

Finally, a potential of providing better performance by a more advanced continuous PSA process was investigated for enantioseparation of the fluorinated anaesthetics. After employing a parametric study and defining the enantiomer purity, recovery and productivity, the achieved results were compared to the batch system. Even though the productivity of providing the first eluting component was higher, the used one-column four-step PSA could not provide high recovery of the enantiomers. The simpler batch operation with repetitive injections was therefore selected as more suitable technique for this particular separation.

The study performed in this thesis was also supported by validation experiments carried out in a parallel project, which demonstrated that the made predictions and the use of simple model are justified for the diluted systems like those investigated in the frame of this thesis. In cases when no extreme precision is required, it is possible to use such models that significantly reduce the computational time and experimental efforts.

It should be mentioned that further work on investigation of the gaseous systems needs still to be performed. Additional validation could be carried out by implementing more rigorous models that include velocity variations and then comparing the resulting chromatograms with those previously obtained, as well as with the experiments. More detailed research of the

---

possibilities of PSA enantioseparation of isoflurane and desflurane could be a topic of a future study, too. Different configurations could be tested, including additional columns and process steps.

In summary, the most important outcome of this thesis is the established production of the pure enantiomers of isoflurane and desflurane. The complete separation and capture process was described and quantified theoretically. It was shown that it should be possible to collect in 10 days more than 10 g of each enantiomer in the pure form for both of the anaesthetics. These amounts are enough for future experiments on testing the drug effects in the area of medicine.



## References

- [1] V. Prelog, G. Helmchen, Basic Principles of the CIP-System and Proposals for a Revision, *Angewandte Chemie International Edition in English*, 21 (1982) 567-583.
- [2] E. Fischer, Ueber die Configuration des Traubenzuckers und seiner Isomeren. II, *Berichte der deutschen chemischen Gesellschaft*, 24 (1891) 2683-2687.
- [3] F.W. Lichtenthaler, Emil Fischer's Proof of the Configuration of Sugars: A Centennial Tribute, *Angewandte Chemie International Edition in English*, 31 (1992) 1541-1556.
- [4] R.S. Cahn, C.K. Ingold, V. Prelog, The specification of asymmetric configuration in organic chemistry, *Experientia*, 12 (1956) 81-94.
- [5] L. Pasteur, Recherches sur les relation qui peuvent exister entre la forme cristalline e al composition chimique, et le sens de la polarisation rotatoire, *Ann. Chim. Phys.*, DOI (1848) 442-459.
- [6] E. Francotte, *Chirality in drug research*, 1. Aufl. ed., WILEY-VCH, Weinheim, Bergstr., 2006.
- [7] W.H. De Camp, The FDA perspective on the development of stereoisomers, *Chirality*, 1 (1989) 2-6.
- [8] FDA's policy statement for the development of new stereoisomeric drugs, *Chirality*, 4 (1992) 338-340.
- [9] H. Lorenz, A. Seidel-Morgenstern, Processes to separate enantiomers, *Angewandte Chemie - International Edition*, 53 (2014) 1218-1250.
- [10] H. Schmidt-Traub, M. Schulte, A. Seidel-Morgenstern, *Preparative chromatography*, Wiley-VCH, Weinheim, 2013.
- [11] G. Guiochon, A. Felinger, D.G. Shirazi, A.M. Katty, *Fundamentals of Preparative and Nonlinear Chromatography*, 2nd ed., Academic Press, Boston, 2006.
- [12] D.M. Ruthven, *Principles of adsorption and adsorption processes*, Wiley, New York, 1984.
- [13] D.M. Ruthven, S. Farooq, K.S. Knaebel, *Pressure swing adsorption*, VCH Publishers 1994.
- [14] T. Munkelt, Doctoral thesis, In preparation, 2018.
- [15] H. Kaemmerer, Z. Horvath, J.W. Lee, M. Kaspereit, R. Arnell, M. Hedberg, B. Herschend, M.J. Jones, K. Larson, H. Lorenz, A. Seidel-Morgenstern, Separation of Racemic Bicalutamide by an Optimized Combination of Continuous Chromatography and Selective Crystallization, *Organic Process Research & Development*, 16 (2012) 331-342.
- [16] I. Mutavdžin, A. Seidel-Morgenstern, M. Petkovska, Estimation of competitive adsorption isotherms based on nonlinear frequency response experiments using equimolar mixtures-numerical analysis for racemic mixtures, *Chemical Engineering Science*, 89 (2013) 21-30.
- [17] H. Kaemmerer, Doctoral thesis: New concepts for enantioselective crystallisation, Shaker, Aachen, 2012.
- [18] I. Mutavdžin, Master thesis: Estimation of competitive adsorption isotherms of enantiomers based on nonlinear frequency response analysis, University of Belgrade, Belgrade, 2011.
- [19] M. Tsweet, Adsorptionsanalyse und chromatographische Methode. Anwendung auf die Chemie des Chlorophylls, *Ber. Dtsch. Botan. Ges.*, 24 (1906) 384.
- [20] R.-M. Nicoud, *Chromatographic processes: modeling, simulation, and design*, Cambridge University Press, Cambridge, 2015.
- [21] J.J. van Deemter, F.J. Zuiderweg, A. Klinkenberg, Longitudinal diffusion and resistance to mass transfer as causes of nonideality in chromatography, *Chemical Engineering Science*, 50 (1995) 3869-3882.

- [22] H.-K. Rhee, R. Aris, N.R. Amundson, First-order partial differential equations. I Theory and application of single equations, Prentice-Hall, Englewood Cliffs, N.J., 1986.
- [23] H.-K. Rhee, R. Aris, N.R. Amundson, First-order partial differential equations. II Theory and application of hyperbolic systems of quasilinear equations, Prentice-Hall, Englewood Cliffs, N.J., 1989.
- [24] P.V. Danckwerts, Continuous flow systems, *Chemical Engineering Science*, 2 (1953) 1-13.
- [25] E. Glueckauf, J.I. Coates, 241. Theory of chromatography. Part IV. The influence of incomplete equilibrium on the front boundary of chromatograms and on the effectiveness of separation, *Journal of the Chemical Society (Resumed)*, DOI 10.1039/JR9470001315(1947) 1315-1321.
- [26] L. Jacob, G. Guiochon, A model for preparative scale gas chromatography, *J. Chromatogr. A*, 65 (1972) 19-27.
- [27] J. Roles, G. Guiochon, Prediction of the elution profiles of high-concentration bands in gas chromatography, *Journal of Chromatography*, 589 (1992) 223-230.
- [28] S. Ergun, Fluid Flow through Packed Columns, *Chem. Eng. Prog.*, 48 (1952) 89.
- [29] S. Whitaker, Flow in porous media I: A theoretical derivation of Darcy's law, *Transport in Porous Media*, 1 (1986) 3-25.
- [30] A.T. James, A.J. Martin, Gas-liquid partition chromatography; the separation and micro-estimation of volatile fatty acids from formic acid to dodecanoic acid, *The Biochemical journal*, 50 (1952) 679-690.
- [31] R. Kaiser, *Gas Phase Chromatography, Volume I* (translated by P.H. Scott), Butterworths, London, 1963.
- [32] F. Gritti, G. Guiochon, Band splitting in overloaded isocratic elution chromatography: II. New competitive adsorption isotherms, *J. Chromatogr. A*, 1008 (2003) 23-41.
- [33] C.J. Radke, J.M. Prausnitz, Thermodynamics of multi-solute adsorption from dilute liquid solutions, *AIChE Journal*, 18 (1972) 761-768.
- [34] A.L. Myers, J.M. Prausnitz, Thermodynamics of mixed-gas adsorption, *AIChE Journal*, 11 (1965) 121-127.
- [35] S. Brunauer, L.S. Deming, W.E. Deming, E. Teller, On a Theory of the van der Waals Adsorption of Gases, *Journal of the American Chemical Society*, 62 (1940) 1723-1732.
- [36] C.H. Giles, T.H. MacEwan, S.N. Nakhwa, D. Smith, 786. Studies in adsorption. Part XI. A system of classification of solution adsorption isotherms, and its use in diagnosis of adsorption mechanisms and in measurement of specific surface areas of solids, *Journal of the Chemical Society (Resumed)*, DOI 10.1039/JR9600003973(1960) 3973-3993.
- [37] I. Langmuir, The adsorption of gases on plane surfaces of glass, mica and platinum, *The Journal of the American Chemical Society*, 40 (1918) 1361-1403.
- [38] A. Seidel-Morgenstern, Experimental determination of single solute and competitive adsorption isotherms, *J. Chromatogr. A*, 1037 (2004) 255-272.
- [39] A.W.J. De Jong, J.C. Kraak, H. Poppe, F. Nooitgedacht, Isotherm linearity and sample capacity in liquid chromatography, *J. Chromatogr. A*, 193 (1980) 181-195.
- [40] O. Lisec, P. Hugo, A. Seidel-Morgenstern, Frontal analysis method to determine competitive adsorption isotherms, *J. Chromatogr. A*, 908 (2001) 19-34.
- [41] C. Blümel, P. Hugo, A. Seidel-Morgenstern, Quantification of single solute and competitive adsorption isotherms using a closed-loop perturbation method, *J. Chromatogr. A*, 865 (1999) 51-71.
- [42] M. Petkovska, A. Seidel-Morgenstern, Nonlinear frequency response of a chromatographic column. Part I: Application to estimation of adsorption isotherms with inflection points, *Chemical Engineering Communications*, 192 (2005) 1300-1333.
- [43] M. Ilić, M. Petkovska, A. Seidel-Morgenstern, Determination of competitive adsorption isotherms applying the nonlinear frequency response method. Part I. Theoretical analysis, *J. Chromatogr. A*, 1216 (2009) 6098-6107.

- [44] M. Ilić, M. Petkovska, A. Seidel-Morgenstern, Determination of competitive adsorption isotherms applying the nonlinear frequency response method. Part II. Experimental demonstration, *J. Chromatogr. A*, 1216 (2009) 6108-6118.
- [45] H. Guan, B.J. Stanley, G. Guiochon, Theoretical study of the accuracy and precision of the measurement of single-component isotherms by the elution by characteristic point method, *J. Chromatogr. A*, 659 (1994) 27-41.
- [46] J.Å. Jönsson, P. Lökvist, Determination of adsorption isotherms from chromatographic measurements, using the peak maxima method, *J. Chromatogr. A*, 408 (1987) 1-7.
- [47] E.V. Dose, S. Jacobson, G. Guiochon, Determination of Isotherms from Chromatographic Peak Shapes, *Analytical chemistry*, 63 (1991) 833-839.
- [48] A. Cavazzini, A. Felinger, K. Kaczmarski, P. Szabelski, G. Guiochon, Study of the adsorption equilibria of the enantiomers of 1-phenyl-1-propanol on cellulose tribenzoate using a microbore column, *J. Chromatogr. A*, 953 (2002) 55-66.
- [49] P. Forssén, J. Lindholm, T. Fornstedt, Theoretical and experimental study of binary perturbation peaks with focus on peculiar retention behaviour and vanishing peaks in chiral liquid chromatography, *J. Chromatogr. A*, 991 (2003) 31-45.
- [50] A. Felinger, D. Zhou, G. Guiochon, Determination of the single component and competitive adsorption isotherms of the 1-indanol enantiomers by the inverse method, *J. Chromatogr. A*, 1005 (2003) 35-49.
- [51] D.B. Broughton, C.G. Gerhold, Continuous sorption process employing fixed bed of sorbent and moving inlets and outlets, Google Patents, 1961.
- [52] M. Juza, Development of an high-performance liquid chromatographic simulated moving bed separation from an industrial perspective, *J. Chromatogr. A*, 865 (1999) 35-49.
- [53] D.W. Guest, Evaluation of simulated moving bed chromatography for pharmaceutical process development, *J. Chromatogr. A*, 760 (1997) 159-162.
- [54] J. Bentley, Q. Huang, Y. Kawajiri, M. Eic, A. Seidel-Morgenstern, Optimizing the separation of gaseous enantiomers by simulated moving bed and pressure swing adsorption, *Adsorption*, 17 (2011) 159-170.
- [55] A. Nicolaos, L. Muhr, P. Gotteland, R.-M. Nicoud, M. Bailly, Application of equilibrium theory to ternary moving bed configurations (four+four, five+four, eight and nine zones): I. Linear case, *J. Chromatogr. A*, 908 (2001) 71-86.
- [56] J. Nowak, D. Antos, A. Seidel-Morgenstern, Theoretical study of using simulated moving bed chromatography to separate intermediately eluting target compounds, *J. Chromatogr. A*, 1253 (2012) 58-70.
- [57] A. Seidel-Morgenstern, L.C. Keßler, M. Kaspereit, New developments in simulated moving bed chromatography, *Chemical Engineering and Technology*, 31 (2008) 826-837.
- [58] J. Blehaut, R.M. Nicoud, Recent aspects in simulated moving bed, *Analisis*, 26 (1998) M60-M70.
- [59] P. Sá Gomes, M. Minceva, A.E. Rodrigues, Simulated moving bed technology: Old and new, *Adsorption*, 12 (2006) 375-392.
- [60] G. Storti, M. Mazzotti, M. Morbidelli, S. Carrà, Robust design of binary countercurrent adsorption separation processes, *AIChE Journal*, 39 (1993) 471-492.
- [61] M. Mazzotti, G. Storti, M. Morbidelli, Optimal operation of simulated moving bed units for nonlinear chromatographic separations, *J. Chromatogr. A*, 769 (1997) 3-24.
- [62] S. Sircar, Publications on adsorption science and technology, *Adsorption*, 6 (2000) 359-365.
- [63] C.W. Skarstrom, Method and apparatus for fractionating gaseous mixtures by adsorption, 1960.
- [64] P. Guerin de Montgareuil, D. Domine, French Patent 1,223,261 (U.S. 3,155,468 - 1964), to Air Liquide, 1957.
- [65] H. Kahle, Die „reversible“ Adsorption als Mittel zur Vorreinigung und Zerlegung von Gasgemischen, *Chemie Ingenieur Technik*, 25 (1953) 144-148.

- [66] H. Kahle, Luftreinigung durch Adsorption nach dem Sorbogen I-Verfahren, *Chemie Ingenieur Technik*, 26 (1954) 75-81.
- [67] S. Sircar, Pressure swing adsorption, *Industrial and Engineering Chemistry Research*, 41 (2002) 1389-1392.
- [68] Q. Huang, M. Eić, Simulation of hydrogen purification by pressure-swing adsorption for application in fuel cells, *Environanotechnology2010*, pp. 221-244.
- [69] G.G. Vaporciyan, R.H. Kadlec, Equilibrium-limited periodic separating reactors, *AIChE Journal*, 33 (1987) 1334-1343.
- [70] L.T. Biegler, L. Jiang, V.G. Fox, Recent advances in simulation and optimal design of pressure swing adsorption systems, *Separation and Purification Reviews*, 33 (2004) 1-39.
- [71] G. Biressi, M. Mazzotti, M. Morbidelli, Experimental investigation of the behavior of gas phase simulated moving beds, *J. Chromatogr. A*, 957 (2002) 211-225.
- [72] K.P. Kostroski, P.C. Wankat, Separation of dilute binary gases by simulated-moving bed with pressure-swing assist: SMB/PSA processes, *Industrial and Engineering Chemistry Research*, 47 (2008) 3138-3149.
- [73] D. Ko, R. Siriwardane, L.T. Biegler, Optimization of pressure swing adsorption and fractionated vacuum pressure swing adsorption processes for CO<sub>2</sub> capture, *Industrial and Engineering Chemistry Research*, 44 (2005) 8084-8094.
- [74] I. Mutavdžin, A. Seidel-Morgenstern, Extended elution by characteristic point method for determination of binary-mixture competitive Langmuir isotherms, In preparation, 2018.
- [75] E. Cremer, H. Huber, Messung von Adsorptionsisothermen an Katalysatoren bei hohen Temperaturen mit Hilfe der Gas-Festkörper-Eluierungschromatographie, *Angewandte Chemie*, 73 (1961) 461-465.
- [76] E. Glueckauf, Theory of chromatography. Part 10.-Formulae for diffusion into spheres and their application to chromatography, *Transactions of the Faraday Society*, 51 (1955) 1540-1551.
- [77] J. Samuelsson, T. Undin, T. Fornstedt, Expanding the elution by characteristic point method for determination of various types of adsorption isotherms, *J. Chromatogr. A*, 1218 (2011) 3737-3742.
- [78] G. Guiochon, S. Golshan-Shirazi, A retrospective on the solution of the ideal model of chromatography, *J. Chromatogr. A*, 658 (1994) 173-177.
- [79] S. Golshan-Shirazi, G. Guiochon, Analytical solution for the ideal model of chromatography in the case of a langmuir isotherm, *Analytical chemistry*, 60 (1988) 2364-2374.
- [80] S. Golshan-Shirazi, G. Guiochon, Experimental characterization of the elution profiles of high concentration chromatographic bands using the analytical solution of the ideal model, *Analytical chemistry*, 61 (1989) 462-467.
- [81] S. Golshan-Shirazi, G. Guiochon, General solution of the ideal model of chromatography for a single-compound band, *Journal of Physical Chemistry*, 94 (1990) 495-500.
- [82] F. Gritti, G. Guiochon, Analytical solution of the ideal model of chromatography for a bi-Langmuir adsorption isotherm, *Analytical chemistry*, 85 (2013) 8552-8558.
- [83] S. Golshan-Shirazi, G. Guiochon, Analytical solution for the ideal model of chromatography in the case of a pulse of a binary mixture with competitive langmuir isotherm, *Journal of Physical Chemistry*, 93 (1989) 4143-4157.
- [84] H.K. Rhee, R. Aris, N.R. Amundson, On the theory of multicomponent chromatography, *Phil Trans Roy Soc London Ser A. Math Phys Sci*, 267 (1970) 419-455.
- [85] S. Golshan-Shirazi, G. Guiochon, Analytical solution of the ideal model of elution chromatography in the case of a binary mixture with competitive Langmuir isotherms: II. Solution using the h-transform, *Journal of Chromatography*, 484 (1989) 125-151.
- [86] F. Helfferich, G. Klein, *Multicomponent chromatography: theory of interference*, Dekker, New York, NY, 1970.



- [87] S. Golshan-Shirazi, G. Guiochon, Modeling of preparative liquid chromatography, *J. Chromatogr. A*, 658 (1994) 149-171.
- [88] S. Golshan-Shirazi, G. Guiochon, Theoretical explanation of the displacement and tag-along effects, *Chromatographia*, 30 (1990) 613-617.
- [89] D. Antos, W. Piątkowski, K. Kaczmarski, Mathematical modelling of preparative liquid chromatography with a binary mobile phase, *Acta Chromatographica*, DOI (1999) XI-XII.
- [90] F. James, M. Sepúlveda, F. Charton, I. Quinones, G. Guiochon, Determination of binary competitive equilibrium isotherms from the individual chromatographic band profiles, *Chemical Engineering Science*, 54 (1999) 1677-1696.
- [91] P. Forssén, R. Arnell, T. Fornstedt, An improved algorithm for solving inverse problems in liquid chromatography, *Computers and Chemical Engineering*, 30 (2006) 1381-1391.
- [92] A. Felinger, A. Cavazzini, G. Guiochon, Numerical determination of the competitive isotherm of enantiomers, *J. Chromatogr. A*, 986 (2003) 207-225.
- [93] S. Golshan-Shirazi, G. Guiochon, Theory of optimization of the experimental conditions of preparative elution using the ideal model of liquid chromatography, *Analytical chemistry*, 61 (1989) 1276-1287.
- [94] S.C. Jacobson, G. Guiochon, Experimental study of the production rate of pure enantiomers from racemic mixtures, *Journal of Chromatography*, 590 (1992) 119-126.
- [95] A. Rathore, A. Velayudhan, *Scale-Up and Optimization in Preparative Chromatography: Principles and Biopharmaceutical Applications*, CRC Press 2002.
- [96] C. Heuer, P. Hugo, G. Mann, A. Seidel-Morgenstern, Scale up in preparative chromatography, *J. Chromatogr. A*, 752 (1996) 19-29.
- [97] K. Unger, *Handbuch der HPLC, Teil 2: Präparative Säulenflüssig-Chromatographie*, GIT Verlag, Darmstadt, 1994.
- [98] V. Schurig, Salient features of enantioselective gas chromatography: the enantiomeric differentiation of chiral inhalation anesthetics as a representative methodological case in point, in: V. Schurig (Ed.) *Differentiation of Enantiomers I*, Springer, Heidelberg, 2013, pp. 153-207.
- [99] V. Schurig, H. Grosenick, Preparative enantiomer separation of enflurane and isoflurane by inclusion gas chromatography, *J. Chromatogr. A*, 666 (1994) 617-625.
- [100] M. Juza, E. Braun, V. Schurig, Preparative enantiomer separation of the inhalation anesthetics enflurane, isoflurane and desflurane by gas chromatography on a derivatized  $\gamma$ -cyclodextrin stationary phase, *J. Chromatogr. A*, 769 (1997) 119-127.
- [101] M. Juza, O. Di Giovanni, G. Biressi, V. Schurig, M. Mazzotti, M. Morbidelli, Continuous enantiomer separation of the volatile inhalation anesthetic enflurane with a gas chromatographic simulated moving bed unit, *J. Chromatogr. A*, 813 (1998) 333-347.
- [102] G. Biressi, F. Quattrini, M. Juza, M. Mazzotti, V. Schurig, M. Morbidelli, Gas chromatographic simulated moving bed separation of the enantiomers of the inhalation anesthetic enflurane, *Chemical Engineering Science*, 55 (2000) 4537-4547.
- [103] G. Biressi, A. Rajendran, M. Mazzotti, M. Morbidelli, The GC-SMB separation of the enantiomers of isoflurane, *Separation Science and Technology*, 37 (2002) 2529-2543.
- [104] J. Jänchen, J.B. Brückner, H. Stach, Adsorption of desflurane from the scavenging system during high-flow and minimal-flow anaesthesia by zeolites, *Eur. J. Anaesthesiol.*, 15 (1998) 324-329.
- [105] J. Doyle, R. Byrick, D. Filipovic, F. Cashin, Silica zeolite scavenging of exhaled isoflurane: A preliminary report, *Canadian Journal of Anesthesia*, 49 (2002) 799-804.
- [106] R. Ortmann, C. Pasel, M. Luckas, R. Heimböckel, S. Kraas, J. Bentgens, M. Fröba, D. Bathen, Adsorption and Desorption of Isoflurane on Carbonaceous Adsorbents and Zeolites at Low Concentrations in Gas Phase, *Journal of Chemical and Engineering Data*, 61 (2016) 686-692.

- [107] Y. Hua, N. Gargiulo, A. Peluso, P. Aprea, M. Eić, D. Caputo, Adsorption Behavior of Halogenated Anesthetic and Water Vapor on Cr-Based MOF (MIL-101) Adsorbent. Part II. Multiple-Cycle Breakthrough Tests, *Chem Ing Tech*, 88 (2016) 1739-1745.
- [108] D. Bucher, C. Pasel, M. Luckas, J. Bentgens, D. Bathen, Adsorption of Inhalation Anesthetics (Fluranes and Ethers) on Activated Carbons and Zeolites at Trace Level Concentrations, *Journal of Chemical & Engineering Data*, 62 (2017) 1832-1841.
- [109] T. Munkelt, I. Mutavdžin, C. Hamel, A. Seidel-Morgenstern, C. Kuester, D. Enke, Gas phase separation and recovery of volatile chiral anesthetics based on porous glass supports of different modifications, In preparation, 2018.
- [110] R.B. Bird, W.E. Stewart, E.N. Lightfoot, *Transport phenomena*, 2. ed. ed., Wiley, New York, NY u.a., 2002.
- [111] M.P. Wirth, W.A. See, D.G. McLeod, P. Iversen, T. Morris, K. Carroll, Bicalutamide 150 mg in addition to standard care in patients with localized or locally advanced prostate cancer: Results from the second analysis of the early prostate cancer program at median followup of 5.4 years, *Journal of Urology*, 172 (2004) 1865-1870.
- [112] M. Wirth, C. Tyrrell, K. Delaere, M. Sánchez-Chapado, J. Ramon, D.M.A. Wallace, J. Hetherington, F. Pina, C. Heyns, T. Borchers, T. Morris, J. Armstrong, Bicalutamide ('Casodex') 150mg in addition to standard care in patients with nonmetastatic prostate cancer: Updated results from a randomised double-blind phase III study (median follow-up 5.1y) in the early prostate cancer programme, *Prostate Cancer and Prostatic Diseases*, 8 (2005) 194-200.
- [113] B.J.A. Furr, B. Valcaccia, B. Curry, A novel non-steroidal, peripherally selective antiandrogen, *Journal of Endocrinology*, 113 (1987) R7-R9.
- [114] Casodex® (bicalutamide) Tablets:  
[http://www.accessdata.fda.gov/drugsatfda\\_docs/label/2005/020498s016lbl.pdf](http://www.accessdata.fda.gov/drugsatfda_docs/label/2005/020498s016lbl.pdf), Accessed on March 23, 2017.
- [115] National Center for Biotechnology Information. PubChem Compound Database; CID=2375: Bicalutamide: <https://pubchem.ncbi.nlm.nih.gov/compound/2375>, Accessed on March 30, 2017.
- [116] D. McKillop, G.W. Boyle, I.D. Cockshott, D.C. Jones, P.J. Phillips, R.A. Yates, Metabolism and enantioselective pharmacokinetics of casodex in man, *Xenobiotica*, 23 (1993) 1241-1253.
- [117] I.D. Cockshott, E.A. Sotaniemi, K.J. Cooper, D.C. Jones, The pharmacokinetics of Casodex enantiomers in subjects with impaired liver function, *British Journal of Clinical Pharmacology*, 36 (1993) 339-343.
- [118] H. Tucker, G.J. Chesterson, Resolution of the nonsteroidal antiandrogen 4'-cyano-3-[(4-fluorophenyl)sulfonyl]-2-hydroxy-2-methyl-3'- (trifluoromethyl)-propionanilide and the determination of the absolute configuration of the active enantiomer, *Journal of Medicinal Chemistry*, 31 (1988) 885-887.
- [119] B.J. Furr, "Casodex" (ICI 176,334)--a new, pure, peripherally-selective anti-androgen: preclinical studies, *Hormone research*, 32 Suppl 1 (1989) 69-76.
- [120] I.D. Cockshott, Bicalutamide: Clinical pharmacokinetics and metabolism, *Clinical Pharmacokinetics*, 43 (2004) 855-878.
- [121] A. Mukherjee, L. Kirkovsky, X.T. Yao, R.C. Yates, D.D. Miller, J.T. Dalton, Enantioselective binding of Casodex to the androgen receptor, *Xenobiotica*, 26 (1996) 117-122.
- [122] K.D. James, N.N. Ekwuribe, Syntheses of enantiomerically pure (R)- and (S)-bicalutamide, *Tetrahedron*, 58 (2002) 5905-5908.
- [123] R. Török, Á. Bor, G. Orosz, F. Lukács, D.W. Armstrong, A. Péter, High-performance liquid chromatographic enantioseparation of bicalutamide and its related compounds, *J. Chromatogr. A*, 1098 (2005) 75-81.
- [124] R. Nageswara Rao, A. Narasa Raju, D. Nagaraju, An improved and validated LC method for resolution of bicalutamide enantiomers using amylose tris-(3,5-dimethylphenylcarbamate) as a chiral stationary phase, *Journal of Pharmaceutical and Biomedical Analysis*, 42 (2006) 347-353.

- [125] D. Sadutto, R. Ferretti, L. Zanitti, A. Casulli, R. Cirilli, Analytical and semipreparative high performance liquid chromatography enantioseparation of bicalutamide and its chiral impurities on an immobilized polysaccharide-based chiral stationary phase, *J. Chromatogr. A*, 1445 (2016) 166-171.
- [126] H. Kaemmerer, M.J. Jones, H. Lorenz, A. Seidel-Morgenstern, Selective crystallisation of a chiral compound-forming system-Solvent screening, SLE determination and process design, *Fluid Phase Equilibria*, 296 (2010) 192-205.
- [127] M. Bohnet, F. Ullmann, Ullmann's encyclopedia of industrial chemistry, 6th, compl. rev. ed., Wiley-VCH, Weinheim, 2003.
- [128] P.L. Polavarapu, A.L. Cholli, G. Vernice, Absolute configuration of isoflurane, *Journal of the American Chemical Society*, 114 (1992) 10953-10955.
- [129] V. Schurig, M. Juza, B.S. Green, J. Horakh, A. Simon, Absolute Configurations of the Inhalation Anesthetics Isoflurane and Desflurane, *Angewandte Chemie (International Edition in English)*, 35 (1996) 1680-1682.
- [130] National Center for Biotechnology Information. PubChem Compound Database; CID=3763: Isoflurane: <https://pubchem.ncbi.nlm.nih.gov/compound/3763>, Accessed on March 30, 2017.
- [131] National Center for Biotechnology Information. PubChem Compound Database; CID=42113: Desflurane: <https://pubchem.ncbi.nlm.nih.gov/compound/42113>, Accessed on March 30, 2017.
- [132] D.A. Sidebotham, S.A. Schug, Stereochemistry in anaesthesia, *Clinical and Experimental Pharmacology and Physiology*, 24 (1997) 126-130.
- [133] N.P. Franks, W.R. Lieb, Stereospecific effects of inhalational general anesthetic optical isomers on nerve ion channels, *Science*, 254 (1991) 427-430.
- [134] B. Harris, E. Moody, P. Skolnick, Isoflurane anesthesia is stereoselective, *Eur. J. Pharmacol.*, 217 (1992) 215-216.
- [135] R. Dickinson, I. White, W.R. Lieb, N.P. Franks, Stereoselective loss of righting reflex in rats by isoflurane, *Anesthesiology*, 93 (2000) 837-843.
- [136] A.C. Hall, W.R. Lieb, N.P. Franks, Stereoselective and non-stereoselective actions of isoflurane on the GABAA receptor, *British Journal of Pharmacology*, 112 (1994) 906-910.
- [137] E.J. Moody, B.D. Harris, P. Skolnick, The potential for safer anaesthesia using stereoselective anaesthetics, *Trends in Pharmacological Sciences*, 15 (1994) 387-391.
- [138] H.Y. Aboul-Enein, J. Bojarski, J. Szymura-Oleksiak, The impact of chirality of the fluorinated volatile inhalation anaesthetics on their clinical applications, *Biomed. Chromatogr.*, 14 (2000) 213-218.
- [139] L.A. Rozov, C.G. Huang, D.F. Halpern, G.G. Vernice, K. Ramig, Enantioselective synthesis of the volatile anesthetic desflurane, *Tetrahedron Asymmetry*, 8 (1997) 3023-3025.
- [140] H.A. Haerberle, H.G. Wahl, G. Aigner, K. Unertl, H.J. Dieterich, Release of S(+) enantiomers in breath samples after anaesthesia with isoflurane racemate, *Eur. J. Anaesthesiol.*, 21 (2004) 144-150.
- [141] R. Schmidt, H.G. Wahl, H. Häberle, H.J. Dieterich, V. Schurig, Headspace gas chromatography-mass spectrometry analysis of isoflurane enantiomers in blood samples after anesthesia with the racemic mixture, *Chirality*, 11 (1999) 206-211.
- [142] M. Juza, H. Jakubetz, H. Hettesheimer, V. Schurig, Quantitative determination of isoflurane enantiomers in blood samples during and after surgery via headspace gas chromatography-mass spectrometry, *Journal of Chromatography B: Biomedical Sciences and Applications*, 735 (1999) 93-102.
- [143] C.G. Huang, L.A. Rozov, D.F. Halpern, G.G. Vernice, Preparation of the isoflurane enantiomers, *Journal of Organic Chemistry*, 58 (1993) 7382-7387.
- [144] K. Ramig, Synthesis and reactions of fluoroether anesthetics, *Synthesis*, DOI (2002) 2627-2631.

- [145] V. Schurig, H. Grosenick, B.S. Green, Preparative Enantiomer Separation of the Anesthetic Enflurane by Gas Inclusion Chromatography, *Angew. Chem. Int. Ed. Engl.*, 32 (1993) 1662–1663.
- [146] W. Saenger, Cyclodextrin Inclusion Compounds in Research and Industry, *Angew. Chem. Int. Ed. Engl.*, 19 (1980) 344–362.
- [147] V. Schurig, H.P. Nowotny, Gas chromatographic separation of enantiomers on cyclodextrin derivatives, *Angewandte Chemie - International Edition in English*, 29 (1990) 939-957.
- [148] A. Shitangkoon, D.U. Staerk, G. Vigh, Gas chromatographic separation of the enantiomers of volatile fluoroether anesthetics using derivatized cyclodextrin stationary phases. Part I, *J. Chromatogr. A*, 657 (1993) 387-394.
- [149] J. Meinwald, W.R. Thompson, D.L. Pearson, W.A. König, T. Runge, W. Francke, Inhalational anesthetics stereochemistry: Optical resolution of halothane, enflurane, and isoflurane, *Science*, 251 (1991) 560-561.
- [150] D.U. Staerk, A. Shitangkoon, G. Vigh, Gas chromatographic separation of the enantiomers of volatile fluoroether anesthetics by derivatized cyclodextrins II. Preparative-scale separations for isoflurane, *J. Chromatogr. A*, 663 (1994) 79-85.
- [151] D.U. Staerk, A. Shitangkoon, G. Vigh, Gas chromatographic separation of the enantiomers of volatile fluoroether anesthetics by derivatized cyclodextrins. III. Preparative-scale separations for enflurane, *J. Chromatogr. A*, 677 (1994) 133-140.
- [152] K. Ramig, A. Krishnaswami, L.A. Rozov, Chiral interactions of the fluoroether anesthetics desflurane, isoflurane, enflurane, and analogues with modified cyclodextrins studied by capillary gas chromatography and nuclear magnetic resonance spectroscopy: A simple method for column-suitability screening, *Tetrahedron*, 52 (1996) 319-330.
- [153] H. Grosenick, V. Schurig, Enantioselective capillary gas chromatography and capillary supercritical fluid chromatography on an immobilized  $\gamma$ -cyclodextrin derivative, *J. Chromatogr. A*, 761 (1997) 181-193.
- [154] T. Munkelt, C. Küster, C. Hamel, D. Enke, A. Seidel-Morgenstern, Rückgewinnung und Enantiomerentrennung chiraler Anästhetika mittels modifizierter poröser Gläser, *Chemie Ingenieur Technik*, 85 (2013) 1686-1693.
- [155] V. Schurig, Separation of enantiomers by gas chromatography, *J. Chromatogr. A*, 906 (2001) 275-299.
- [156] W.A. König, R. Krebber, P. Mischnick, Cyclodextrins as chiral stationary phases in capillary gas chromatography. Part V: Octakis(3-O-butyryl-2,6-di-O-pentyl)- $\gamma$ -cyclodextrin, *Journal of High Resolution Chromatography*, 12 (1989) 732-738.
- [157] F. Janowski, D. Enke, Porous Glasses, in: F. Schüth, K.S.W. Sing, J. Weitkamp (Eds.) *Handbook of Porous Solids*, Wiley-VCH Verlag GmbH 2008, pp. 1432-1542.
- [158] V. Schurig, M. Schleimer, S. Mayer, Immobilised CHIRASIL-DEX for separation or detection processes - having cyclodextrin bonded to polymer chain and immobilised on smooth or porous carrier, Patent No. DE4324636, 1994.
- [159] J.L. Anderson, A. Berthod, V. Pino, A.M. Stalcup, *Gas chromatography, sub- and supercritical fluid chromatography*, First edition ed., Wiley-VCH Verlag GmbH & Co. KGaA, Weinheim, 2015.
- [160] W.E. Schiesser, *The numerical method of lines: integration of partial differential equations*, Acad. Press, San Diego u.a., 1991.
- [161] P. Rouchon, M. Schonauer, P. Valentin, G. Guiochon, Numerical Simulation of Band Propagation in Nonlinear Chromatography, *Separation Science and Technology*, 22 (1987) 1793-1833.
- [162] Q. Huang, A. Malekian, M. Eić, Optimization of PSA process for producing enriched hydrogen from plasma reactor gas, *Separation and Purification Technology*, 62 (2008) 22-31.

- 
- [163] R. Haghpanah, R. Nilam, A. Rajendran, S. Farooq, I.A. Karimi, Cycle synthesis and optimization of a VSA process for postcombustion CO<sub>2</sub> capture, *AIChE Journal*, 59 (2013) 4735-4748.
- [164] P.A. Webley, J. He, Fast solution-adaptive finite volume method for PSA/VSA cycle simulation; 1 single step simulation, *Computers and Chemical Engineering*, 23 (2000) 1701-1712.
- [165] Q. Huang, M. Eić, Commercial adsorbents as benchmark materials for separation of carbon dioxide and nitrogen by vacuum swing adsorption process, *Separation and Purification Technology*, 103 (2013) 203-215.
- [166] S.P. Reynolds, A. Mehrotra, A.D. Ebner, J.A. Ritter, Heavy reflux PSA cycles for CO<sub>2</sub> recovery from flue gas: Part I. Performance evaluation, *Adsorption*, 14 (2008) 399-413.
- [167] S. Khattabi, D.E. Cherrak, J. Fischer, P. Jandera, G. Guiochon, Study of the adsorption behavior of the enantiomers of 1-phenyl-1-propanol on a cellulose-based chiral stationary phase, *J. Chromatogr. A*, 877 (2000) 95-107.
- [168] D.E. Cherrak, S. Khattabi, G. Guiochon, Adsorption behavior and prediction of the band profiles of the enantiomers of 3-chloro-1-phenyl-1-propanol - Influence of the mass transfer kinetics, *J. Chromatogr. A*, 877 (2000) 109-122.
- [169] A. Felinger, G. Guiochon, Optimization of the experimental conditions and the column design parameters in overloaded elution chromatography, *J. Chromatogr. A*, 591 (1992) 31-45.
- [170] I. Mutavdžin, T. Munkelt, A. Seidel-Morgenstern, Shortcut procedure for estimating performance and scale-up of gas chromatographic enantioseparation of fluorinated anaesthetics, In preparation, 2018.



## Appendix

### A. Derivation of the overall and component mass balance equations for a pressure swing adsorption process

Here the detailed derivation of the mass balance equations for a PSA process (eq. (2.50) and (2.54)) will be presented. The starting equation for the overall mass balance is:

$$-D_L \frac{\partial^2 C}{\partial z^2} + \frac{\partial C}{\partial t} + \frac{\partial(uC)}{\partial z} + \frac{1-\varepsilon}{\varepsilon} \sum_{i=1}^n \frac{\partial q_i}{\partial t} = 0 \quad (\text{A.1})$$

This equation is the same as eq. (2.49) from Chapter 2. For the ideal gas flow it can be written  $C = P/(RT)$ , as also stated in eq. (2.48), so each of the terms of eq. (A.1) can be derived as follows:

$$\begin{aligned} -D_L \frac{\partial^2 C}{\partial z^2} &= -\frac{D_L}{R} \frac{\partial}{\partial z} \left[ P \frac{\partial}{\partial z} \left( \frac{1}{T} \right) + \frac{1}{T} \frac{\partial}{\partial z} (P) \right] = \\ &= -\frac{D_L}{R} \left[ P \frac{\partial^2 (1/T)}{\partial z^2} + \frac{\partial(1/T)}{\partial z} \frac{\partial P}{\partial z} + \frac{1}{T} \frac{\partial^2 P}{\partial z^2} + \frac{\partial P}{\partial z} \frac{\partial(1/T)}{\partial z} \right] \end{aligned} \quad (\text{A.2})$$

$$\frac{\partial(uC)}{\partial z} = \frac{\partial}{\partial z} \left( \frac{uP}{RT} \right) = \frac{1}{R} \left[ uP \frac{\partial(1/T)}{\partial z} + \frac{u}{T} \frac{\partial P}{\partial z} + \frac{P}{T} \frac{\partial u}{\partial z} \right] \quad (\text{A.3})$$

$$\frac{\partial C}{\partial t} = \frac{\partial}{\partial t} \left( \frac{P}{RT} \right) = \frac{1}{R} \left[ P \frac{\partial(1/T)}{\partial t} + \frac{1}{T} \frac{\partial P}{\partial t} \right] \quad (\text{A.4})$$

With this, the overall mass balance becomes:

$$\begin{aligned} -\frac{D_L}{R} \left[ P \frac{\partial^2 (1/T)}{\partial z^2} + 2 \frac{\partial(1/T)}{\partial z} \frac{\partial P}{\partial z} + \frac{1}{T} \frac{\partial^2 P}{\partial z^2} \right] + \frac{1}{R} \left[ uP \frac{\partial(1/T)}{\partial z} + \frac{u}{T} \frac{\partial P}{\partial z} + \frac{P}{T} \frac{\partial u}{\partial z} \right] + \\ + \frac{1}{R} \left[ P \frac{\partial(1/T)}{\partial t} + \frac{1}{T} \frac{\partial P}{\partial t} \right] + \frac{1-\varepsilon}{\varepsilon} \sum_{i=1}^n \frac{\partial q_i}{\partial t} = 0 \end{aligned} \quad (\text{A.5})$$

By multiplying this equation by  $(RT/P)$ , we get the following expression:

$$\begin{aligned}
-D_L \left[ T \frac{\partial^2(1/T)}{\partial z^2} + \frac{2T}{P} \frac{\partial(1/T)}{\partial z} \frac{\partial P}{\partial z} + \frac{1}{P} \frac{\partial^2 P}{\partial z^2} \right] + \frac{\partial u}{\partial z} + \frac{u}{P} \frac{\partial P}{\partial z} + Tu \frac{\partial(1/T)}{\partial z} + \\
+ T \frac{\partial(1/T)}{\partial t} + \frac{1}{P} \frac{\partial P}{\partial t} + \frac{RT}{P} \frac{1-\varepsilon}{\varepsilon} \sum_{i=1}^n \frac{\partial q_i}{\partial t} = 0
\end{aligned} \quad (\text{A.6})$$

When the terms containing  $\partial(1/T)$  are transformed as

$$\frac{\partial(1/T)}{\partial X} = -\frac{1}{T^2} \frac{\partial(T)}{\partial X} \quad (\text{A.7})$$

where  $X$  can be either time ( $t$ ) or space ( $z$ ) coordinate, the following form of the overall mass balance is obtained:

$$\begin{aligned}
-D_L \left[ \frac{2}{T^2} \left( \frac{\partial T}{\partial z} \right)^2 - \frac{1}{T} \frac{\partial^2 T}{\partial z^2} + \frac{1}{P} \frac{\partial^2 P}{\partial z^2} - \frac{2}{TP} \frac{\partial T}{\partial z} \frac{\partial P}{\partial z} \right] + \frac{\partial u}{\partial z} + \frac{u}{P} \frac{\partial P}{\partial z} - \frac{u}{T} \frac{\partial T}{\partial z} - \\
- \frac{1}{T} \frac{\partial T}{\partial t} + \frac{1}{P} \frac{\partial P}{\partial t} + \frac{RT}{P} \frac{1-\varepsilon}{\varepsilon} \sum_{i=1}^n \frac{\partial q_i}{\partial t} = 0
\end{aligned} \quad (\text{A.8})$$

The eq. (A.8) represents the final expression for the overall mass balance of a PSA process and is identical to eq. (2.50).

Component mass balance equation is derived in the same way as the one for the overall mass balance. The starting expression is eq. (2.51), here denoted as (A.9):

$$-D_L \frac{\partial^2 c_i}{\partial z^2} + \frac{\partial c_i}{\partial t} + \frac{\partial(uc_i)}{\partial z} + \frac{1-\varepsilon}{\varepsilon} \frac{\partial q_i}{\partial t} = 0 \quad (\text{A.9})$$

On the other hand, using the overall mass balance (eq. (A.1)), for component  $i$ , we get:

$$-D_L y_i \frac{\partial^2 C}{\partial z^2} + y_i \frac{\partial C}{\partial t} + y_i \frac{\partial(uC)}{\partial z} + \frac{1-\varepsilon}{\varepsilon} y_i \sum_{i=1}^n \frac{\partial q_i}{\partial t} = 0 \quad (\text{A.10})$$

As equations (A.9) and (A.10) are equal, it is:

$$\begin{aligned}
-D_L \left( \frac{\partial^2 c_i}{\partial z^2} - y_i \frac{\partial^2 C}{\partial z^2} \right) + \left( \frac{\partial c_i}{\partial t} - y_i \frac{\partial C}{\partial t} \right) + \left( \frac{\partial(uc_i)}{\partial z} - y_i \frac{\partial(uC)}{\partial z} \right) + \\
+ \frac{1-\varepsilon}{\varepsilon} \left( \frac{\partial q_i}{\partial t} - y_i \sum_{i=1}^n \frac{\partial q_i}{\partial t} \right) = 0
\end{aligned} \quad (\text{A.11})$$



By introducing the relations  $c_i = y_i C$  and  $C = P/(RT)$  (from eq. (2.52) and (2.48)), some of the terms of the previous equation can be transformed as follows:

- 1) Transformation of the term  $\frac{\partial^2 c_i}{\partial z^2} - y_i \frac{\partial^2 C}{\partial z^2}$ :

By knowing:

$$\frac{\partial^2 c_i}{\partial z^2} = \frac{\partial}{\partial z} \left( \frac{\partial(y_i C)}{\partial z} \right) = \left( y_i \frac{\partial^2 C}{\partial z^2} + \frac{\partial C}{\partial z} \frac{\partial y_i}{\partial z} \right) + \left( C \frac{\partial^2 y_i}{\partial z^2} + \frac{\partial y_i}{\partial z} \frac{\partial C}{\partial z} \right) \quad (\text{A.12})$$

we can obtain the following expression for this term:

$$\begin{aligned} \frac{\partial^2 c_i}{\partial z^2} - y_i \frac{\partial^2 C}{\partial z^2} &= 2 \frac{\partial C}{\partial z} \frac{\partial y_i}{\partial z} + C \frac{\partial^2 y_i}{\partial z^2} = 2 \frac{\partial y_i}{\partial z} \frac{\partial}{\partial z} \left( \frac{P}{RT} \right) + \frac{P}{RT} \frac{\partial^2 y_i}{\partial z^2} = \\ &= \frac{2}{R} \frac{\partial y_i}{\partial z} \left( P \frac{\partial(1/T)}{\partial z} + \frac{1}{T} \frac{\partial P}{\partial z} \right) + \frac{P}{RT} \frac{\partial^2 y_i}{\partial z^2} \end{aligned} \quad (\text{A.13})$$

- 2) Transformation of the term  $\frac{\partial C_i}{\partial t} - y_i \frac{\partial C}{\partial t}$ :

After deriving the single parts of the term as follows:

$$\frac{\partial c_i}{\partial t} = \frac{\partial}{\partial t} \left( \frac{P y_i}{RT} \right) = \frac{1}{R} \left( \frac{y_i}{T} \frac{\partial P}{\partial t} + P y_i \frac{\partial(1/T)}{\partial t} + \frac{P}{T} \frac{\partial y_i}{\partial t} \right) \quad (\text{A.14})$$

and

$$y_i \frac{\partial C}{\partial t} = y_i \frac{\partial}{\partial t} \left( \frac{P}{RT} \right) = \frac{y_i}{R} \left( \frac{1}{T} \frac{\partial P}{\partial t} + P \frac{\partial(1/T)}{\partial t} \right) \quad (\text{A.15})$$

it can be obtained:

$$\frac{\partial C_i}{\partial t} - y_i \frac{\partial C}{\partial t} = \frac{P}{RT} \frac{\partial y_i}{\partial t} \quad (\text{A.16})$$

- 3) Transformation of the term  $\frac{\partial(uc_i)}{\partial z} - y_i \frac{\partial(uC)}{\partial z}$ :

When the two parts of the term are derived as

$$\frac{\partial(uc_i)}{\partial z} = \frac{\partial}{\partial z} \left( \frac{uP}{RT} y_i \right) = \frac{1}{R} \left( \frac{u y_i}{T} \frac{\partial P}{\partial z} + u P y_i \frac{\partial(1/T)}{\partial z} + \frac{P y_i}{T} \frac{\partial u}{\partial z} + \frac{P u}{T} \frac{\partial y_i}{\partial z} \right) \quad (\text{A.17})$$

and

$$y_i \frac{\partial(uC)}{\partial z} = y_i \frac{\partial}{\partial z} \left( \frac{uP}{RT} \right) = \frac{y_i}{R} \left( \frac{u}{T} \frac{\partial P}{\partial z} + uP \frac{\partial(1/T)}{\partial z} + \frac{P}{T} \frac{\partial u}{\partial z} \right) \quad (\text{A.18})$$

the resulting expression is:

$$\frac{\partial(uc_i)}{\partial z} - y_i \frac{\partial(uC)}{\partial z} = \frac{uP}{RT} \frac{\partial y_i}{\partial z} \quad (\text{A.19})$$

When the derivations in 1)-3) are introduced into eq. (A.11), the component mass balance becomes:

$$\begin{aligned} -D_L \left[ \frac{2}{R} \frac{\partial y_i}{\partial z} \left( P \frac{\partial(1/T)}{\partial z} + \frac{1}{T} \frac{\partial P}{\partial z} \right) + \frac{P}{RT} \frac{\partial^2 y_i}{\partial z^2} \right] + \frac{uP}{RT} \frac{\partial y_i}{\partial z} + \frac{P}{RT} \frac{\partial y_i}{\partial t} + \\ + \frac{1-\varepsilon}{\varepsilon} \left( \frac{\partial q_i}{\partial t} - y_i \sum_{i=1}^n \frac{\partial q_i}{\partial t} \right) = 0 \end{aligned} \quad (\text{A.20})$$

By multiplying this equation by  $(RT/P)$ , it can be written:

$$\begin{aligned} -D_L \left( 2T \frac{\partial y_i}{\partial z} \frac{\partial(1/T)}{\partial z} + \frac{2}{P} \frac{\partial y_i}{\partial z} \frac{\partial P}{\partial z} + \frac{\partial^2 y_i}{\partial z^2} \right) + u \frac{\partial y_i}{\partial z} + \frac{\partial y_i}{\partial t} + \\ + \frac{RT}{P} \frac{1-\varepsilon}{\varepsilon} \left( \frac{\partial q_i}{\partial t} - y_i \sum_{i=1}^n \frac{\partial q_i}{\partial t} \right) = 0 \end{aligned} \quad (\text{A.21})$$

Finally, by transforming of the terms containing  $\partial(1/T)$  in the same ways as given previously in eq. (A.7), the following form of the component mass balance is obtained:

$$\begin{aligned} -D_L \left( \frac{\partial^2 y_i}{\partial z^2} - \frac{2}{T} \frac{\partial y_i}{\partial z} \frac{\partial T}{\partial z} + \frac{2}{P} \frac{\partial y_i}{\partial z} \frac{\partial P}{\partial z} \right) + \frac{\partial y_i}{\partial t} + u \frac{\partial y_i}{\partial z} + \\ + \frac{RT}{P} \frac{1-\varepsilon}{\varepsilon} \left( \frac{\partial q_i}{\partial t} - y_i \sum_{i=1}^n \frac{\partial q_i}{\partial t} \right) = 0 \end{aligned} \quad (\text{A.22})$$

This equation is the same as eq. (2.54) and represents the final expression for the component mass balance for a PSA process.

## B. Derivation of the equations for the new binary-mixture ECP method from the analytical solution of the ideal model of chromatography

The analytical solution of the ideal model of chromatography (equilibrium theory) is taken from the literature [11, 87]. Here it will be used to derive the expressions for the binary-mixture ECP method that is described in Chapter 3, section 3.1.2. First the equations from the literature that describe the continuous parts of the elution profile shown in Figure 3.3 will be given.

The first arc of the component 1 represents the part of the elution profile of the component 1 in the zone I (defined in Figure 3.3). It cannot be expressed as a concentration function of time. There is available only the equation that gives the retention time depending on the concentration of the first component ( $c_1$ ):

$$t = t_{inj} + t_0 + (t_{R,1}^0 - t_0) \left[ \frac{1}{(1 + b_1 c_1)^2} - L_{f,2} \frac{\alpha_{2,1} - 1}{\alpha_{2,1}} \cdot \frac{1}{\left( \frac{\alpha_{2,1} - 1}{\alpha_{2,1}} + b_1 c_1 \right)^2} \right] \quad (\text{A.23})$$

The second arc of the component 1 (part of the elution profile of component 1 in the zone II) is expressed as:

$$c_1 = \frac{1}{b_1 + b_2 / (\alpha_{2,1} r_1)} \left( \sqrt{\frac{\gamma}{\alpha_{2,1}} \cdot \frac{t_{R,1}^0 - t_0}{t - t_{inj} - t_0}} - 1 \right) \quad (\text{A.24})$$

The equations for the component 2 are given as a function of concentration ( $c_2$ ) from the retention time ( $t$ ). The first and second arc of the component 2 (i.e. the parts of the elution profiles of the component 2 in the zone II and III, respectively) are described with equations (A.25) – first arc, and (A.26) – second arc:

$$c_2 = \frac{1}{b_2 + \alpha_{2,1} b_1 r_1} \left( \sqrt{\gamma \frac{t_{R,2}^0 - t_0}{t - t_{inj} - t_0}} - 1 \right) \quad (\text{A.25})$$

$$c_2 = \frac{1}{b_2} \left( \sqrt{\frac{t_{R,2}^0 - t_0}{t - t_{inj} - t_0}} - 1 \right) \quad (\text{A.26})$$

In the previous equations  $b_1$  and  $b_2$  are Langmuir isotherm parameters,  $t_0$  column hold-up time,  $t_{inj}$  injection time and  $\alpha_{2,1} = H_2/H_1$  the selectivity (eq. (2.37)). Without going into detailed derivations (which are given e.g. in [11, 87]) the expressions for the used parameters  $r_1$ ,  $\gamma$  and  $L_{f,2}$  are briefly presented here. The parameter  $r_1$  is the positive root of the following equation:

$$\alpha_{2,1}b_1c_2^{feed}r_{1,2}^2 - (\alpha_{2,1} - 1 + \alpha_{2,1}b_1c_1^{feed} - b_2c_2^{feed})r_{1,2} - b_2c_1^{feed} = 0 \quad (\text{A.27})$$

The two roots of this equation,  $r_{1,2}$ , can be therefore calculated as:

$$r_{1,2} = \frac{(\alpha_{2,1} - 1 + \alpha_{2,1}b_1c_1^{feed} - b_2c_2^{feed}) \pm \sqrt{(\alpha_{2,1} - 1 + \alpha_{2,1}b_1c_1^{feed} - b_2c_2^{feed})^2 + 4\alpha_{2,1}b_1c_2^{feed}b_2c_1^{feed}}}{2\alpha_{2,1}b_1c_2^{feed}} \quad (\text{A.28})$$

The variable  $\gamma$  is expressed as a function of isotherm parameters and the already defined  $r_1$ :

$$\gamma = \frac{\alpha_{2,1}b_1r_1 + b_2}{b_1r_1 + b_2} \quad (\text{A.29})$$

$L_{f,2}$  represents the loading factor calculated for the single second component:

$$L_{f,2} = \frac{b_2c_2^{feed}t_{inj}}{t_{R,2}^0 - t_0} \quad (\text{A.30})$$

The times  $t_{R1}^0$  and  $t_{R2}^0$  are retention times under linear conditions for components 1 and 2, and can be derived from the equation for Henry constant given in section 2.4 (eq. (2.36) and (2.1)), by taking into account the definition of phase ratio,  $F$  (eq. (2.7)):

$$t_{R,1}^0 = t_0(1 + H_1F) \quad (\text{A.31})$$

$$t_{R,2}^0 = t_0(1 + H_2F) \quad (\text{A.32})$$

By taking all the previous expressions, the equations that describe the ideal elution profile in the form  $t = f(c)$  can be derived.

From the equation (A.23) by implementing the definitions of the parameters  $t_{R1}^0$ ,  $L_{f,2}$  and  $\alpha_{2,1}$  we get the following expression for the retention time of the component 1 in the zone I (denoted as  $t_{R,1}^1(c_1)$ ):

$$t_{R,1}^I(c_1) = t_{inj} + t_0 + \left[ t_0(1 + H_1F) - t_0 \right] \left[ \frac{1}{(1 + b_1c_1)^2} - \frac{b_2c_2^{feed}t_{inj}}{t_0(1 + H_2F) - t_0} \cdot \frac{\frac{H_2/H_1 - 1}{H_2/H_1}}{\left( \frac{H_2/H_1 - 1}{H_2/H_1} + b_1c_1 \right)^2} \right] \quad (A.33)$$

which after additional rearrangements becomes:

$$t_{R,1}^I(c_1) = t_{inj} + t_0 + t_0H_1F \left( \frac{1}{(1 + b_1c_1)^2} - \frac{b_2c_2^{feed}t_{inj}(H_2 - H_1)}{t_0H_2^2F \left( \frac{H_2 - H_1}{H_2} + b_1c_1 \right)^2} \right) \quad (A.34)$$

The equation (A.34) represents the form that can be used for the binary-mixture ECP method and is repeated in Chapter 3 as eq. (3.8). When the retention time of the second arc of the component 1 ( $t_{R,1}^{II}(c_1)$ ), in the zone II, is expressed as a function of the concentration ( $c_1$ ) from eq. (A.24), we get the following:

$$t_{R,1}^{II}(c_1) = t_{inj} + t_0 + \frac{t_{R,1}^0 - t_0}{\frac{\alpha_{2,1}}{\gamma} \left[ 1 + c_1 \left( b_1 + \frac{b_2}{\alpha_{2,1}r_1} \right) \right]^2} \quad (A.35)$$

By implementing the definitions of the parameters  $t_{R,1}^0$ ,  $\alpha_{2,1}$  and  $\gamma$ , we get the next equation (for the sake of simplicity the expression for  $r_1$  was not introduced here, as well as later in the equation for component 2 in the zone II):

$$t_{R,1}^{II}(c_1) = t_{inj} + t_0 + \frac{t_0(1 + H_1F) - t_0}{\frac{\frac{H_2/H_1}{(H_2/H_1)b_1r_1 + b_2}}{b_1r_1 + b_2} \left[ 1 + c_1 \left( b_1 + \frac{b_2}{(H_2/H_1)r_1} \right) \right]^2} \quad (A.36)$$

The final equation (equal to eq. (3.9) in Chapter 3) is:

$$t_{R,1}^{II}(c_1) = t_{inj} + t_0 + \frac{t_0H_1F \left( b_1r_1 + \frac{H_1b_2}{H_2} \right)}{(b_1r_1 + b_2) \left( 1 + b_1c_1 + \frac{H_1b_2c_1}{r_1H_2} \right)^2} \quad (A.37)$$

For the second component the expressions are derived in the same way. The retention time of the first arc, in the zone II ( $t_{R,2}^{\text{II}}(c_2)$ ) resulting from eq. (A.25) is:

$$t_{R,2}^{\text{II}}(c_2) = t_{inj} + t_0 + \frac{\gamma(t_{R,2}^0 - t_0)}{(1 + b_2 c_2 + \alpha_{2,1} b_1 c_2 r_1)^2} \quad (\text{A.38})$$

By introducing the expressions for  $\gamma$ ,  $t_{R,2}^0$  and  $\alpha_{2,1}$ , this equation becomes:

$$t_{R,2}^{\text{II}}(c_2) = t_{inj} + t_0 + \frac{\frac{(H_2/H_1)b_1 r_1 + b_2}{b_1 r_1 + b_2} [t_0(1 + H_2 F) - t_0]}{\left(1 + b_2 c_2 + \frac{H_2 b_1 c_2 r_1}{H_1}\right)^2} \quad (\text{A.39})$$

$$t_{R,2}^{\text{II}}(c_2) = t_{inj} + t_0 + \frac{t_0 H_2 F \left(\frac{b_1 r_1 H_2}{H_1} + b_2\right)}{(b_1 r_1 + b_2) \left(1 + b_2 c_2 + \frac{H_2 b_1 c_2 r_1}{H_1}\right)^2} \quad (\text{A.40})$$

The previous equation is the final expression for  $t_{R,2}^{\text{II}}(c_2)$  and is equal to eq. (3.10). The time function of the component 2 in the zone III ( $t_{R,2}^{\text{III}}(c_2)$ ), derived from eq. (A.26) is:

$$t_{R,2}^{\text{III}}(c_2) = t_{inj} + t_0 + \frac{t_{R,2}^0 - t_0}{(1 + b_2 c_2)^2} \quad (\text{A.41})$$

With the definition of  $t_{R,2}^0$  the next equations are obtained:

$$t_{R,2}^{\text{III}}(c_2) = t_{inj} + t_0 + \frac{t_0(1 + H_2 F) - t_0}{(1 + b_2 c_2)^2} \quad (\text{A.42})$$

$$t_{R,2}^{\text{III}}(c_2) = t_{inj} + t_0 + \frac{t_0 H_2 F}{(1 + b_2 c_2)^2} \quad (\text{A.43})$$

The last expression is the one used for the binary-mixture ECP for determining the adsorption isotherm of the second component. This equation is shown also in Chapter 3 as eq. (3.11).

## List of symbols

### *Latin symbols*

|            |  |
|------------|--|
| $A$        | Parameter in the van Deemter equation that shows the eddy diffusion contribution   |
| $a_p$      | External surface area of the particles   |
| $B$        | Parameter in the van Deemter equation that shows the effects of longitudinal diffusion   |
| $b$        | Langmuir isotherm parameter which depends on the adsorption energy   |
| $b_0$      | Constant parameter in the Langmuir isotherm model, when parameter $b$ depends on temperature   |
| $C$        | Total concentration  |
| $c$        | Concentration in the mobile phase  |
| $C$        | Parameter in the van Deemter equation that shows the mass transfer kinetics  |
| $c^0$      | Initial concentration  |
| $C_{A,1}$  | Concentration of the first component on the front side of the second shock in the analytical solution of the ideal model of chromatography |
| $C_{B,2}$  | Concentration of the component 2 plateau in the analytical solution of the ideal model of chromatography                                   |
| $c^{calc}$ | Calculated concentration   |
| $c^{eq}$   | Equilibrium concentration in the mobile phase (Frontal analysis)   |
| $c^{exp}$  | Experimental concentration   |
| $CF$       | Calibration factor   |
| $c_{feed}$ | Feed concentration   |
| $c^{init}$ | Initial concentration in the mobile phase (Frontal analysis)   |
| $C_{M,1}$  | Maximum concentration of the component 1 in the analytical solution of the ideal model of chromatography                                   |
| $C_{M,2}$  | Maximum concentration of the second component in the analytical solution of the ideal model of chromatography                              |
| $C_{M',1}$ | Concentration of the first component on the rear side of the second shock in the analytical solution of the ideal model of chromatography  |
| $c_{max}$  | Maximal mobile phase concentration of a peak   |
| $c_p$      | Stagnant mobile phase concentration  |
| $C_{pg}$   | Gas heat capacity  |
| $C_{ps}$   | Solid (adsorbent) heat capacity  |
| $d$        | Column inner diameter  |
| $D_{app}$  | Apparent dispersion coefficient  |

---

|                 |   |
|-----------------|---|
| $D_{eff}$       | Effective diffusion coefficient in porous media                                   |
| $D_L$           | Axial dispersion coefficient  |
| $D_{mol}$       | Molecular diffusion coefficient   |
| $d_p$           | Particle diameter   |
| $D_p$           | Pore diffusion coefficient  |
| $D_s$           | Surface diffusion coefficient   |
| $ee$            | Enantiomeric excess   |
| $F$             | Phase ratio   |
| $H$             | Henry constant  |
| $\Delta H$      | Isosteric heat of adsorption  |
| $h$             | Overall heat transfer coefficient   |
| $HEPT$          | Height equivalent to a theoretical plate  |
| $i$             | Solute $i = 1, 2, \dots, n$   |
| $j$             | James-Martin compressibility factor   |
| $J$             | Diffusion flux  |
| $k_e$           | Mass transfer coefficient from fluid to particle                                  |
| $K_L$           | Thermal dispersion coefficient  |
| $k_m$           | Mass transfer resistance  |
| $L$             | Column length   |
| $L_{(test)}$    | Length of the test capture column   |
| $L_{f,2}$       | Loading factor calculated for the single second component                         |
| $M$             | Molar mass of the solute (in kg/mol)  |
| $m_{ads}$       | Adsorbent mass  |
| $m_{coll}$      | Collected mass  |
| $m_{feed}$      | Feed mass   |
| $m_z$           | Dimensionless flowrate ratios ( $m_z$ ) for each SMB zone ( $z = I, II, II, IV$ ) |
| $n$             | Number of components  |
| $n_{cycles}$    | Number of cycles  |
| $n_{elut}$      | Number of the elution profiles  |
| $n_i$           | Amount of a component ( $i$ )   |
| $n_{inj}$       | Number of injections  |
| $n_{inj(test)}$ | Number of injections that can be “parked” into a test capture column              |
| $n_p$           | Number of points  |
| $NTP$           | Number of theoretical plates ( $NTP$ )  |
| $OF$            | Objective function  |
| $P_{ads}$       | Adsorption step pressure (high pressure in the pressure swing adsorption process) |
| $P_{des}$       | Desorption step pressure (low pressure in the pressure swing adsorption process)  |



---

|                 |   |
|-----------------|---|
| $P_{drop}$      | Pressure drop   |
| $P_i$           | Partial pressure of a component ( $i$ )   |
| $P_{in}$        | Inlet pressure  |
| $P_{out}$       | Outlet pressure   |
| $PR$            | Normalized productivity, given as amount per cycle time and adsorbent volume                        |
| $PR^*$          | Productivity given as amount per cycle time   |
| $PU$            | Purity  |
| $Q$             | Volumetric flowrate   |
| $q^*$           | Equilibrium concentration in the stationary phase   |
| $q_0$           | Saturation capacity of the stationary phase (Langmuir isotherm parameter)                           |
| $Q_{eluent}$    | Flowrate in the eluent stream   |
| $q^{eq}$        | Equilibrium concentration in the stationary phase (Frontal analysis)                                |
| $Q_{extract}$   | Flowrate in the extract stream  |
| $Q_{feed}$      | Flowrate in the feed stream   |
| $q^{init}$      | Initial concentration in the stationary phase (Frontal analysis)                                    |
| $Q_I-Q_{IV}$    | Flowrates in the zones I-IV of SMB  |
| $Q_m$           | Mass flowrate   |
| $q_{max}$       | Stationary phase concentration in equilibrium with the maximal mobile phase concentration of a peak |
| $Q_{raffinate}$ | Flowrate in the raffinate stream  |
| $Q_{solid}$     | Virtual solid phase flow in SMB   |
| $r$             | Radial coordinate   |
| $R$             | Universal gas constant  |
| $r_{1,2}$       | Variable used in the analytical solution of the ideal model of chromatography                       |
| $R_b$           | Column (bed) radius   |
| $RE$            | Recovery or yield   |
| $R_p$           | Particle radius   |
| $T$             | Temperature   |
| $t$             | Time coordinate   |
| $\Delta t$      | Interval between the ending and starting cut time   |
| $t_0$           | Column hold-up time (dead time) i.e. the retention time of a non-adsorbing species                  |
| $\Delta t_0$    | Hold-up time of the section of the column required for one injection                                |
| $t_{ads}$       | Adsorption step time  |
| $t_{ads-s,1}$   | Time when the first component start eluting during the adsorption step of a PSA process             |
| $t_{ads-s,2}$   | Time when the second component start eluting during the adsorption step of a PSA process            |

---

|                      |  |
|----------------------|--|
| $t_B$                | End of the component 2 concentration plateau in the analytical solution of the ideal model of chromatography   |
| $t_{blow}$           | Blowdown step time   |
| $t_{BT}$             | Breakthrough time  |
| $t^{calc}$           | Calculated time  |
| $t_{cycle}$          | Cycle time   |
| $T_{des}$            | Desorption temperature   |
| $t_{des}$            | Desorption step time   |
| $t_{des-e,1}$        | Time when the first component completely leaves the column during the desorption step of a PSA process   |
| $t_{des-e,2}$        | Time when the second component completely leaves the column during the desorption step of a PSA process  |
| $t_{diff}$           | Duration of the diffusion process  |
| $t_{e,1}$            | End of the first component band, ending cut time of the component 1 (complete elution of the component 1)  |
| $t_{e,2}$            | End of the second component band, ending cut time of the component 2 (complete elution of the component 2)   |
| $t^{exp}$            | Experimentally measured time   |
| $T_{feed}$           | Feed temperature   |
| $t_{inj}$            | Injection time   |
| $t_{press}$          | Pressurization step time   |
| $t_R$                | Retention time   |
| $t_R^0$              | Retention time under linear conditions   |
| $t_{R,1}$            | Retention time of the first shock in the analytical solution of the ideal model of chromatography  |
| $t_{R,1}^I(c_1)$     | Retention time function for the first component in the zone I of the elution profile for the analytical solution of the ideal model of chromatography    |
| $t_{R,1}^{II}(c_1)$  | Retention time function for the first component in the zone II of the elution profile for the analytical solution of the ideal model of chromatography   |
| $t_{R,2}$            | Retention time of the second shock in the analytical solution of the ideal model of chromatography   |
| $t_{R,2}^{II}(c_2)$  | Retention time function for the second component in the zone II of the elution profile for the analytical solution of the ideal model of chromatography  |
| $t_{R,2}^{III}(c_2)$ | Retention time function for the second component in the zone III of the elution profile for the analytical solution of the ideal model of chromatography |
| $t_{s,1}$            | Starting cut time of the component 1 (start of the elution of component 1)   |
| $t_{s,2}$            | Starting cut time of the component 2 (start of the elution of component 2)   |
| $t_{shift}$          | Time between port shifts in SMB  |
| $t_{step}$           | Step time (duration of a step in the process)  |
| $T_{wall}$           | Column wall temperature  |

---

|                       |   |
|-----------------------|---|
| $u$                   | Interstitial linear mobile phase velocity   |
| $u_0$                 | Superficial mobile phase velocity   |
| $u_{des}$             | Desorption velocity   |
| $u_{feed}$            | Feed velocity   |
| $V$                   | Column total volume   |
| $V_0$                 | Total void volume of the column, available for the fluid phase  |
| $V_{ads}$             | Adsorbent volume  |
| $V_f$                 | Total void volume of the column, available for the fluid phase  |
| $V_{feed}$            | Feed volume   |
| $V_g$                 | Gaseous mixture volume  |
| $\Delta V_{id}$       | Volume of the column segment needed for storing one injection for the ideal case including only convection and no molecular diffusion |
| $V_{inj}$             | Injected volume   |
| $V_p$                 | Total particle volume   |
| $V_{pore}$            | Total pore volume   |
| $V_R$                 | Retention volume  |
| $V_s$                 | Volume of the solid phase   |
| $w_{1/2}$             | Peak width at its half-height   |
| $\Delta x_{diff}$     | Additional width on each side of the peak due to molecular diffusion  |
| $\Delta x_{diff,end}$ | Additional peak-width due to molecular diffusion behind the firstly "parked" injection (in the capture column)                        |
| $\Delta x_{id}$       | Length of the column segment needed for storing one injection for the ideal case including only convection and no molecular diffusion |
| $\Delta x_{MTZ}$      | Width of the mass transfer zone due to molecular diffusion  |
| $\Delta x_{real}$     | Length of the column segment needed for storing one injection for the real case including convection and molecular diffusion          |
| $y$                   | Mole fraction   |
| $y_{des}$             | Mole fraction in the desorption mixture   |
| $y_{feed}$            | Mole fraction in the feed   |
| $z$                   | Space coordinate  |

### **Greek symbols**

|                 |   |
|-----------------|---|
| $\alpha$        | Separation factor (selectivity)   |
| $\gamma$        | Variable used in the analytical solution of the ideal model of chromatography |
| $\varepsilon$   | Total column porosity   |
| $\varepsilon_e$ | External porosity   |

|                 |                   |
|-----------------|-------------------|
| $\varepsilon_i$ | Internal porosity |
| $\varepsilon_p$ | Particle porosity |
| $\mu_g$         | Gas viscosity     |
| $\rho_b$        | Bed density       |
| $\rho_g$        | Bulk gas density  |
| $\rho_p$        | Particle density  |
| $\tau$          | Tortuosity factor |

### ***Subscripts***

|            |                |
|------------|----------------|
| <i>ads</i> | Adsorption     |
| <i>des</i> | Desorption     |
| <i>l</i>   | Larger column  |
| <i>R</i>   | R-enantiomer   |
| <i>S</i>   | S-enantiomer   |
| <i>s</i>   | Smaller column |

### ***Superscripts***

|            |   |
|------------|---|
| <i>cap</i> | Capture column                                      |
| <i>GC</i>  | Corrected parameters used in the gas chromatography |
| <i>sep</i> | Separation column                                   |

### ***Abbreviations***

|      |  |
|------|--|
| CD   | Cyclodextrin                                   |
| ECP  | Elution by characteristic point                |
| EDM  | Equilibrium-dispersive model of chromatography |
| GC   | Gas chromatography                             |
| GRM  | General rate model of chromatography           |
| HPLC | High performance liquid chromatography         |
| IM   | Ideal model of chromatography                  |
| LC   | Liquid chromatography                          |
| LDF  | Linear driving force model                     |

---

|      |  |
|------|--|
| PSA  | Pressure swing adsorption                    |
| PVSA | Pressure-vacuum swing adsorption             |
| SFC  | Supercritical fluid chromatography           |
| SMB  | Simulated moving bed                         |
| TDM  | Transport-dispersive model of chromatography |
| TTBB | 1,3,5-tri-tert-butylbenzene                  |
| VSA  | Vacuum swing adsorption                      |



## List of Tables

|   |     |
|---|-----|
| Table 2.1. Different models used for describing a chromatographic process with the effects that they take into account. ....  | 15  |
| Table 2.2. Characteristics of the most commonly used methods for determination of adsorption isotherms. ....  | 23  |
| Table 2.3. An example of boundary conditions for the 4-step PSA shown in Figure 2.13. Here pressurization is applied to the feed mixture of the same content as in the adsorption step. ....  | 40  |
| Table 5.1. Some of the chemical and physical properties of bicalutamide. ....   | 74  |
| Table 5.2. Some of the chemical and physical properties of isoflurane and desflurane. ....  | 76  |
| Table 5.3. Overview of the previous publications on enantioseparation of the fluorinated anaesthetics: The used separation processes are listed followed by indications if experiments, modelling and simulations were performed (the sign “✓” stands for the performed actions and “-“ for the non-performed ones). ....                           | 79  |
| Table 5.4. Selected characteristics of $\alpha$ -, $\beta$ - and $\gamma$ -cyclodextrins. ....  | 80  |
| Table 5.5. Overview of the previous publications on enantioseparation of the fluorinated anaesthetics: Applied stationary and mobile phases are shown. ....   | 81  |
| Table 5.6. Overview of the previous publications on enantioseparation of the fluorinated anaesthetics: Indicated if thermodynamic parameters and process performance characteristics were determined and calculated (the sign “✓” stands for the determined parameters and “-“ for the non-determined ones). ....                                   | 84  |
| Table 6.1. Experimental data for bicalutamide injections (S-enantiomer – component 1, R-enantiomer – component 2). ....   | 88  |
| Table 6.2. Experimental data for isoflurane and desflurane injections provided from SPP1570 Subproject II [14]. ....  | 93  |
| Table 6.3. Calculated parameters for isoflurane and desflurane (S-enantiomer – component 1 and R-enantiomer – component 2) using the small injection amounts, based on mean retention times. ....   | 94  |
| Table 7.1. Data used for the simulation study to evaluate the binary-mixture ECP method. These data do not originate from any experimental system and therefore the substances are denoted as hypothetical. ....  | 100 |
| Table 7.2. Competitive Langmuir adsorption isotherm parameters of the hypothetic substances (simulation study, $NTP = 1500$ ): Comparison of the original data used for the simulation and those determined by the binary-mixture ECP method using three different combinations of the larger data sequences, defined in the previous text. ....    | 103 |
| Table 7.3. Competitive Langmuir adsorption isotherm parameters of the hypothetic substances (simulation study, $NTP = 1500$ ): Comparison of the original data used for the simulation and those determined with the binary-mixture ECP method using three different combinations of the smaller data sequences, defined in the previous text. .... | 104 |
| Table 7.4. Competitive Langmuir adsorption isotherm parameters of the hypothetic substances (simulation study): Comparison of the original data used for the simulation and those determined with the binary-mixture ECP method using elution profiles generated by simulations with different number of theoretical plates ( $NTP$ ). ....         | 106 |
| Table 7.5. Adsorption isotherm parameters of bicalutamide, isoflurane and desflurane enantiomers determined using the binary-mixture ECP method. ....   | 108 |
| Table 7.6. Competitive Langmuir adsorption isotherm (eq. (2.33)) parameters of bicalutamide enantiomers at 25 °C determined with the peak-fitting method. ....  | 111 |

|  |     |
|--|-----|
| Table 7.7. Competitive Langmuir adsorption isotherm parameters of isoflurane and desflurane enantiomers at 28 °C determined by the peak-fitting method. ....   | 113 |
| Table 8.1. Process performance characteristics (productivity - $PR$ , recovery - $RE$ and purity - $PU$ ) of bicalutamide enantiomers (S-enantiomer – component 1 and R-enantiomer – component 2) for three typical cases: touching bands (recovery of both components is close to 100 % i.e. 1), when the maximal productivity of S- enantiomer is achieved and when the maximal productivity of R-enantiomer is achieved. ....               | 122 |
| Table 8.2. Process performance characteristics (productivity - $PR$ , recovery - $RE$ and purity - $PU$ ) of isoflurane enantiomers (S-enantiomer – component 1 and R-enantiomer – component 2) for three typical cases: touching bands (recovery of both components is close to 100 % i.e. 1), when the maximal productivity of S- enantiomer is achieved and when the maximal productivity of R-enantiomer is achieved. ....                 | 126 |
| Table 8.3. Process performance characteristics (productivity - $PR$ , recovery - $RE$ and purity - $PU$ ) of desflurane enantiomers (S-enantiomer – component 1 and R-enantiomer – component 2) for three typical cases: touching bands (recovery of both components is close to 100 % i.e. 1), when the maximal productivity of S- enantiomer is achieved and when the maximal productivity of R-enantiomer is achieved. ....                 | 126 |
| Table 8.4. Comparison of process performance parameters of S- (component 1) and R-enantiomer (component 2) of isoflurane achieved in this work (batch GC when maximal production of S-enantiomer was obtained) and the examples from the literature where the same chiral selector was used (three batch GC processes and one GC-SMB). The values for the case done in this thesis are extracted from Table 8.2. ....                          | 130 |
| Table 8.5. Comparison of process performance parameters of S- (component 1) and R-enantiomer (component 2) of desflurane achieved in this work (batch GC when maximal production of S-enantiomer was obtained) and the example available in the literature (batch GC process). The values for the case done in this thesis are extracted from Table 8.3. ....  | 130 |
| Table 8.6. Scale-up results for bicalutamide enantiomers obtained from eq. (4.17) and by performing simulations with the data for the larger-scale columns. The operation and performance parameters are presented for the three examined column sizes (referred as small, intermediate and large). ....   | 132 |
| Table 8.7. Scale-up results for isoflurane enantiomers obtained from eq. (4.17) and by performing simulations with the data for the larger-scale columns. The operation and performance parameters are presented for the three examined column sizes (referred as small, intermediate and large). ....   | 133 |
| Table 8.8. Scale-up results for desflurane enantiomers obtained from eq. (4.17) and by performing simulations with the data for the larger-scale columns. The operation and performance parameters are presented for the three examined column sizes (referred as small, intermediate and large). ....   | 134 |
| Table 8.9. Data of the scale-up validation procedure for isoflurane and desflurane (shown in Figure 8.17 and Figure 8.18). Presented are the volumetric flowrates ( $Q$ ) and injected volumes ( $V_{inj}$ ) for the small column, while for the intermediate and large column the values, which are required according to the scale-up rule (eq. (4.17)), are compared to those applied in the experiments carried out in Subproject II. .... | 136 |
| Table 8.10. Parameters of the Langmuir adsorption isotherms of desflurane racemic mixture at 10 °C on the non-selective controlled porous glass beads (prepared by the research groups of Prof. Enke, Leipzig University and Prof. Fröba, University of Hamburg) used as adsorbent in the capture columns (data obtained from the parallel SPP1570 Subproject II). ...   | 138 |
| Table 8.11. Parameters of the capture columns required for storing at least one gram of desflurane enantiomers: Calculated column length ( $L^{cap}$ ), its volume ( $V^{cap}$ ) and adsorbent amount ( $V_{ads}^{cap}$ ) together with the needed additional parameters (notation given in the text) for the three capture columns (I, II and III) used to collect desflurane fractions after   |     |



---

|   |     |
|---|-----|
| the separation process. The volumetric flowrate (160.7 ml/min) and the diameter (1.66 cm) of all the three columns is equal to those of the large separation column. The number of the cycles to be stored in each of the columns is 52. The cycle time is 11.7 min. ....   | 139 |
| Table 8.12. The times when elution of the components starts during the adsorption step of the PSA process ( $t_{ads-s,1}$ and $t_{ads-s,2}$ ) and when the components exit the column during the desorption step ( $t_{des-e,1}$ and $t_{des-e,2}$ ). The values are given as time intervals from the start of the corresponding step until elution (as explained in the text above). Flowrate is 541.5 ml/min for isoflurane and 160.7 ml/min for desflurane, temperature 28 °C, high pressure 500 kPa. .... | 141 |
| Table 8.13. Parameters selected for the PSA simulations of the isoflurane and desflurane enantioseparation. The other data are the same as for the batch GC systems (Table 6.2 and Table 6.3). ....   | 142 |
| Table 8.14. Process performance characteristics for the 4-step PSA separation of isoflurane and desflurane enantiomers at two different adsorption pressures. The other operating parameters are given in Table 8.13. The comparison of the PSA to the batch GC process with 1 microliter injection of racemic mixture is also presented. ....  | 147 |



## List of Figures

|  |    |
|--|----|
| Figure 1.1. Spatial representation of molecules of enantiomers: C - chiral centre (mostly carbon atom), 1,2,3,4 - different groups attached to the centre. ....  | 2  |
| Figure 1.2. Determination of R- and S- configuration of enantiomers. The arrows around the molecules show the direction of decreasing priority (from 1 to 3) of the groups attached to the chiral centre (C). ....   | 2  |
| Figure 1.3. Some of the ways to produce single enantiomers (R and S represent single target enantiomers, R2 and S2 are intermediate enantiomers, and X and Y include one or more starting non-chiral substance(s)).....  | 3  |
| Figure 1.4. Chromatographic separation of a binary mixture. At the column inlet the narrow rectangular pulse of the mixture is injected resulting at the outlet in dispersed peaks of the two separated substances. ....   | 4  |
| Figure 1.5. Schematic overview of the study presented in this thesis, including the investigated substances and processes performed for their analysis and chromatographic separation. ....  | 8  |
| Figure 2.1. A typical chromatogram of a binary mixture with marked retention times of both components ( $t_{R1}$ – for the first eluting component and $t_{R2}$ – for the second eluting component) and the dead time ( $t_0$ )......  | 12 |
| Figure 2.2. Scheme of a chromatographic column with marked different volumes used for defining porosity.....   | 13 |
| Figure 2.3. Van Deemter curve (denoted as Total curve) with effects of single terms used in van Deemter equation (2.12). ....  | 14 |
| Figure 2.4. Most typical shapes of adsorption isotherms. In the first figure the most often encountered Langmuir-type isotherm is shown. ....  | 21 |
| Figure 2.5. Adsorption step in frontal analysis. Adsorbed amount corresponds to the integral in eq. (2.38). The term $t_{BT}$ represents the breakthrough time. ....   | 25 |
| Figure 2.6. Typical curve recorded when applying perturbation method for single component adsorption isotherm determination. ....  | 26 |
| Figure 2.7. Example of column inlet (dashed line) and outlet (solid line) concentration change analysed by nonlinear frequency response method in order to calculate the adsorption isotherm parameters.....   | 26 |
| Figure 2.8. Elution profiles for different feed concentrations used for determination of adsorption isotherms with peak maxima method. ....  | 28 |
| Figure 2.9. Process of isotherm parameter determination using peak-fitting method. The diagram shows the large number of recorded iterations before reaching the shape of the original experimental peak. ....   | 28 |
| Figure 2.10. Representation of a 4-zone SMB process with two columns in each zone and marked direction of the mobile-phase flow. The dashed arrows show the discrete shifting of the port positions. ....  | 30 |
| Figure 2.11. SMB triangle diagram with defined separation regions (where pure both components, only pure raffinate, pure extract, or no pure substances can be collected) for linear isotherm range. $H_1$ and $H_2$ represent the Henry constants of the first and second eluting component, respectively, while $m_{II}$ and $m_{III}$ are dimensionless flowrate ratios in the zones II and III, respectively. .... | 31 |
| Figure 2.12. Representation of pressure and temperature swing on the adsorption isotherm diagram. $P$ and $T$ represent the pressure and the temperature, and the subscripts $ads$ and   |    |

|   |    |
|---|----|
| <i>des</i> stand for adsorption and desorption process. The asterisk (*) shows the value of the stationary phase concentration in equilibrium with the mobile phase pressure. ....  | 32 |
| Figure 2.13. Demonstration of four steps (pressurization, adsorption or feed, blowdown or depressurization and desorption or regeneration) for a 1-column PSA. The up- and down-arrows ( $\uparrow$ and $\downarrow$ ) show that the pressure is increasing or decreasing, respectively. The thin arrows at column inlet and outlet show the flow direction, while the thick ones represent the sequence of the process steps. ....   | 34 |
| Figure 2.14. Pressure change in a 4-step PSA process. The increase and decrease of the pressure in the pressurization and blowdown step are represented by simplified linear functions. ....  | 34 |
| Figure 2.15. Skarstrom cycle representation (1 and 2 in the inlet and outlet streams stand for the first and second eluted component that are contained in the corresponding streams). ....   | 35 |
| Figure 2.16. Example of a typical four-step VSA cycle for a process with one column. ....   | 36 |
| Figure 2.17. PSA process showing the direction of $z$ -coordinate (with marked $z = 0$ and $z = L$ positions). ....   | 41 |
| Figure 3.1. Schematic representation of direct methods (simulation of a chromatogram by knowing the adsorption isotherm) and inverse methods (estimation of adsorption isotherm from the recorded chromatogram). ....   | 44 |
| Figure 3.2. An example of elution profile (one component, Langmuir-type isotherm) that can be used for the elution by characteristic point method. ....   | 45 |
| Figure 3.3. Schematic representation of the solution of the ideal model of chromatography for pulse injection of a binary mixture with Langmuir isotherms. Three separation zones (I, II and III) explained in the previous text are marked. The symbols used for defining the specific concentration and time points are given in the upcoming paragraphs. ....  | 47 |
| Figure 3.4. Elution profiles with indicated parts for which the analytical expressions – equations (3.8)-(3.11) – are derived (in the form of time as a function of concentration) and marked segments that are used for application of the binary-mixture ECP method (dash-dotted-line ellipses): a) Ideal profile characteristic for the very efficient columns (with more than 10,000 theoretical plates); b) More realistic profile, typical for less efficient columns. ....   | 50 |
| Figure 3.5. Three examples of binary-mixture elution profiles resulting from different injected volumes: a) Very small injection amount, which provides almost complete separation of the components and gives the profile that could only be used for providing the single component information; b) Proper injection amount for determining the competitive isotherms of both components with peak-fitting method; c) Too large injection amount that cannot provide correct data for the first eluting component. .... | 52 |
| Figure 4.1. Trade-off between productivity, purity and recovery to provide the optimal process performance. ....  | 56 |
| Figure 4.2. Representation of a binary-mixture elution profile with defined cycle time and the cut times ( $t_s$ – starting cut time, and $t_e$ – ending cut time), between which the pure substances (C. 1 – first and C. 2 – second eluted component) can be collected. ....  | 58 |
| Figure 4.3. Representation of the scale-up procedure when the same column length ( $L$ ) is kept and the diameter ( $d$ ) is increased. Accordingly, the volumetric flowrate through the column ( $Q$ ) and the injected amount ( $m_{feed}$ ) have to be increased as well. ....   | 60 |
| Figure 4.4. Schematically presented complete coupled production unit. It consists of one separation column and three capture columns for storing the three fractions resulting from the separation process. Here the inlet mixture is a racemate containing the E1 and E2 enantiomers. ....   | 63 |
| Figure 4.5. Procedure of capturing the three fractions (pure component 1, mixed fraction and pure component 2) which are resulting from the separation. For the separation column the outlet stream is presented, while for the capture columns I, II and III the inlet streams are depicted. The dash-dotted lines represent the cut times that separate the collected fractions   |    |

|  |    |
|--|----|
| at the outlet of the separation column. This example shows the first three consecutive injections that enter the capture columns. ....   | 65 |
| Figure 4.6. "Parking" of the fractions into a capture column for an ideal case without including the effect of the molecular diffusion. The rectangular shape of the fractions is assumed due to the self-sharpening effect. $L^{cap}$ and $\Delta x_{id}^{cap}$ are the length of the capture column and the length needed for one injection (one fraction), respectively. ....   | 66 |
| Figure 4.7. Process of the peak broadening with time due to molecular diffusion. At the beginning ( $t = 0$ ) the peak has ideal rectangular shape, while after time intervals $\Delta t_1$ and $\Delta t_2$ , the dispersed shapes can be observed. The meaning of the $\Delta x$ parameters is explained in the text. ....   | 68 |
| Figure 4.8. Schematic representation of the process of "parking" several peaks (5 peaks in the part e)) into the capture column, including the convection and diffusion effects (the solid line shows the overall concentration profile, dashed lines – the single profiles for each injection and the dotted lines – the rectangular shape of the injections that corresponds to the ideal case without diffusion effects): a) The first injection (injection 1) after the one-injection interval ( $\Delta t^{cap}$ ); b) The injection 1 after the cycle time interval ( $t_{cycle}$ ); c) Two injections at the time $t_{cycle} + \Delta t^{cap}$ ; d) Injections 1 and 2 after the time interval $2t_{cycle}$ ; e) The situation after the time interval $5t_{cycle}$ (the larger influence of the peak broadening on the injections that are longer time in the capture column can be observed)..... | 70 |
| Figure 4.9. The broadening effect due to molecular diffusion of the "parked" injections in the capture column represented for the example of five injections. The lengths required for storing the peaks due to convection ( $\Delta x_{id}$ ) and diffusion ( $\Delta x_{diff}$ and $\Delta x_{diff,end}$ ) are marked. The superscript <i>cap</i> denotes the capture column, solid line shows the overall concentration profile, dashed lines – the single profiles for each injection and the dotted lines – the ideal rectangular shape of the injections that correspond to the ideal case without diffusion effects included. The arrows show the positions where each injection has started.....   | 71 |
| Figure 5.1. Molecules of bicalutamide enantiomers. The chiral carbon atom is marked by an asterisk (*). ....   | 73 |
| Figure 5.2. Molecules of isoflurane (left) and desflurane (right) enantiomers. The chiral carbon atom is marked by an asterisk (*). ....   | 76 |
| Figure 5.3. Molecules of $\alpha$ -, $\beta$ - and $\gamma$ -cyclodextrin suggested in [147] (The figure is adapted from [147]). ....  | 79 |
| Figure 5.4. The molecule of Octakis(3-O-butyryl-2,6-di-O-pentyl)- $\gamma$ -Cyclodextrin, used as a chiral selector. ....  | 82 |
| Figure 6.1. HPLC unit used for separation of bicalutamide enantiomers. ....  | 86 |
| Figure 6.2. Elution profile with no interference between peaks used to calculate Henry constants of bicalutamide enantiomers and <i>NTP</i> (injected volume 5 $\mu$ l, injected mass of racemic mixture 0.192 mg and concentration 9.7 g/l, flowrate 1 ml/min, signal recorded at wavelength of 230 nm). ....   | 87 |
| Figure 6.3. Van Deemter curves for bicalutamide enantiomers. ....  | 88 |
| Figure 6.4. Dependency of peak area from the injected mass, used for detector calibration for bicalutamide experiments, done with racemic mixture: a) Wavelength 300 nm, injected amounts 0.1-5 $\mu$ l; b) Wavelength 320 nm, injected amounts 10-100 $\mu$ l. ....   | 89 |
| Figure 6.5. Staircase function recorded at the wavelength of 320 nm used for detector calibration for bicalutamide experiments done with racemic mixture. The maximal concentration (in the last step) was 17.86 g/l and the flowrate 0.5ml/min.....   | 90 |
| Figure 6.6. Elution profiles of bicalutamide for different injection volumes (in the brackets the feed mass of one enantiomer is given): 1 $\mu$ l (0.019 mg), 10 $\mu$ l (0.192 mg), 30 $\mu$ l (0.576 mg), 70 $\mu$ l (1.34 mg), 90 $\mu$ l (1.73 mg), 100 $\mu$ l (1.92 mg). The lowest-concentration profile corresponds to the smallest injected amount and higher-concentration profiles to larger   |    |

|   |     |
|---|-----|
| amounts injected. Feed concentration is 19.2 g/l (of racemic mixture), and mobile phase flowrate 2.5 ml/min. ....   | 90  |
| Figure 6.7. Four columns placed in the gas chromatograph used for the first tests and successful separation of isoflurane and desflurane enantiomers (The image is provided together with the data from SPP1570 Subproject II). ....  | 92  |
| Figure 6.8. Elution profiles used to calculate Henry constants and <i>NTP</i> of: a) Isoflurane (Injected volume 0.04 $\mu$ l of racemate, injected mass 0.060 mg of racemate, flowrate 71 ml/min); b) Desflurane (Injected volume 0.04 $\mu$ l of racemate, injected mass 0.076 mg of racemate, flowrate 21 ml/min). ....  | 93  |
| Figure 6.9. Elution profiles of isoflurane for different injection volumes of pure isoflurane racemate (in the brackets the feed mass of one enantiomer is given): 0.04 $\mu$ l (0.030 mg), 0.4 $\mu$ l (0.30 mg), 1 $\mu$ l (0.75 mg), 2 $\mu$ l (1.50 mg), 3 $\mu$ l (2.15 mg), 4 $\mu$ l (2.98 mg), 5 $\mu$ l (3.84 mg); Volumes are given for the samples in the liquid phase. The lowest-concentration profile corresponds to the smallest injected amount and higher-concentration profiles to larger amounts injected. Flowrate is 71 ml/min. .... | 94  |
| Figure 6.10. Elution profiles of desflurane for different injection volumes of pure desflurane racemate (in the brackets the feed mass of one enantiomer is given): 0.04 $\mu$ l (0.038 mg), 0.4 $\mu$ l (0.382 mg), and 1 $\mu$ l (0.70 mg); Volumes are given for the samples in the liquid phase. The lowest-concentration profile corresponds to the smallest injected amount and higher-concentration profiles to larger amounts injected. Flowrate is 21 ml/min. ....   | 95  |
| Figure 6.11. Repetitive injections of isoflurane (Injected volume 4 $\mu$ l, flowrate 71 ml/min). ....  | 95  |
| Figure 7.1. Comparison of an approximately theoretical elution profile of the binary mixture of the hypothetical substances ( <i>NTP</i> = 10000) to the one representing pseudo-experimental data ( <i>NTP</i> = 1500). ....   | 100 |
| Figure 7.2. Different data ranges used for estimating the adsorption isotherms of the hypothetical substances by binary-mixture ECP method. Thicker parts of the lines represent the data sequences used for component 1 (those are the sequences in the higher concentration range) and component 2 (sequences in the lower concentration range). The sequences, which are defined in the previous text, are presented as follows: a) W1 and W2; b) L1 and L2; c) M1 and M2; d) S1 and S2. ....  | 102 |
| Figure 7.3. An example of the function of the retention times from the concentration presented for the component 1 (the data in the higher concentration range) and component 2 (the data in the lower concentration range) of the hypothetical mixture: The original values (pseudo-experimental data) are compared to those calculated using isotherm parameters obtained by binary-mixture ECP method. The sequences of the pseudo-experimental data used for the component 1 and 2 are S1 and S2 regions (defined in Figure 7.2), respectively. ....  | 102 |
| Figure 7.4. Isotherm of the first eluting component of the hypothetic system (simulation study) determined with the binary-mixture ECP method. It is calculated using the parameters from different cases, defined in the previous text. The two insets show the zoomed parts of the isotherm. ....   | 105 |
| Figure 7.5. Isotherm of the second eluting component of the hypothetic system (simulation study) determined with the binary-mixture ECP method. It is calculated using the parameters from different cases, defined in the previous text. The two insets show the zoomed parts of the isotherm. ....  | 105 |
| Figure 7.6. Elution profiles of the hypothetic system (simulation study): Comparison of the profile simulated with the original isotherm parameters and two profiles where the isotherms were determined with the binary-mixture ECP method. The cases B and C are defined in the previous text. ....   | 106 |
| Figure 7.7. Elution profiles of the hypothetic system (simulation study): Comparison of the profiles simulated with the original isotherm parameters, by applying different number of theoretical plates (as defined in the sub-figures), to those where the isotherms were   |     |

|   |     |
|---|-----|
| determined from the corresponding original chromatograms using the binary-mixture ECP method. Solid lines represent original profiles and dashed lines – simulated profiles with the estimated parameters. ....   | 107 |
| Figure 7.8. Comparison of the experimental elution profiles to those simulated with the adsorption isotherm parameters (Table 7.5) determined using the binary-mixture ECP method for: Left – Bicalutamide ( $V_{inj} = 90 \mu\text{l}$ , $Q = 2.5 \text{ ml/min}$ ); Middle – Isoflurane ( $V_{inj} = 5 \mu\text{l}$ , $Q = 71 \text{ ml/min}$ ); Right – Desflurane ( $V_{inj} = 1 \mu\text{l}$ , $Q = 21 \text{ ml/min}$ ). ....   | 109 |
| Figure 7.9. Adsorption isotherms of bicalutamide enantiomers (S and R) at 25 °C determined for a Chiralpak AD stationary phase. The isotherms are described by the competitive Langmuir model (eq. (2.33)) with the parameters given in Table 7.6. ....   | 111 |
| Figure 7.10. Comparison of experimental (dotted line) and simulated (solid line) elution profiles of bicalutamide racemate for different injection volumes: a) 50 $\mu\text{l}$ , b) 70 $\mu\text{l}$ , c) 90 $\mu\text{l}$ , d) 100 $\mu\text{l}$ . Feed concentration was 19.2 g/l of racemic mixture and flowrate 2.5 ml/min. ....   | 112 |
| Figure 7.11. Comparison of experimental (dotted line) and simulated (solid line) elution profiles of S-bicalutamide for different injection volumes: a) 50 $\mu\text{l}$ , b) 70 $\mu\text{l}$ , c) 90 $\mu\text{l}$ , d) 100 $\mu\text{l}$ . Feed concentration was 20 g/l and flowrate 2.5 ml/min. ....   | 112 |
| Figure 7.12. Adsorption isotherms of isoflurane (left) and desflurane (right) enantiomers (S – component 1 and R – component 2 for both substances) at 28 °C on stationary phase based on modified $\gamma$ -cyclodextrin (defined in section 6.1.2.1). The isotherms are described by the competitive Langmuir model (eq. (2.33)) with the parameters given in Table 7.7. ....   | 113 |
| Figure 7.13. Comparison of experimental (dotted line) and simulated (solid line) elution profiles of isoflurane for different injection volumes: a) 1 $\mu\text{l}$ , b) 3 $\mu\text{l}$ , c) 4 $\mu\text{l}$ , d) 5 $\mu\text{l}$ . Injected pure racemic mixture in liquid phase. Flowrate was 71 ml/min. ....  | 114 |
| Figure 7.14. Comparison of experimental (dotted line) and simulated (solid line) elution profiles of desflurane for injection volume of 1 $\mu\text{l}$ . Injected pure racemic mixture in liquid phase. Flowrate was 21 ml/min. ....   | 115 |
| Figure 8.1. Dependency of the values of the cut times and the cycle time (defined in Figure 4.2) for the bicalutamide enantioseparation on the injection amount of one enantiomer. Volumetric flowrate is 2.5 ml/min. ....  | 119 |
| Figure 8.2. Elution profiles of the first (S-enantiomer, left diagram) and the second (R-enantiomer, right diagram) eluting components of bicalutamide for Increasing injection amounts: 1.4 mg, 1.9 mg, 5.7mg and 14.5 mg. Volumetric flowrate is 2.5 ml/min ....  | 119 |
| Figure 8.3. Dependency of productivity of bicalutamide enantiomers on the injection amount of one enantiomer. Volumetric flowrate is 2.5 ml/min. Lines represent the results from the simulation study and symbols the values estimated from the experiments. ....  | 120 |
| Figure 8.4. Dependency of recovery of bicalutamide enantiomers on the injection amount of one enantiomer. Volumetric flowrate is 2.5 ml/min. Lines represent the results from the simulation study and symbols the values estimated from the experiments. ....  | 120 |
| Figure 8.5. Elution profiles of bicalutamide given for the cases when maximum productivity of the first component – S-enantiomer (left, injected volume 76 $\mu\text{l}$ , injected mass 1.46 mg of each enantiomer) and second component – R-enantiomer (right, injected volume 101 $\mu\text{l}$ , injected mass 1.94 mg of each enantiomer) is achieved (flowrate 2.5 ml/min). Dashed lines show single component profiles and solid lines the total concentration. .... | 121 |
| Figure 8.6. Dependency of the values of cut times and the cycle time (defined in Figure 4.2) for the isoflurane (left) and desflurane (right) enantioseparation on the amount of one enantiomer injected at the column inlet. Volumetric flowrate is 71 ml/min for isoflurane and 21 ml/min for desflurane. ....  | 123 |
| Figure 8.7. Dependency of productivity of isoflurane (left) and desflurane (right) enantiomers on the amount of one enantiomer injected at the column inlet. Volumetric flowrate is 71  |     |

|  |     |
|--|-----|
| ml/min for isoflurane and 21 ml/min for desflurane. Lines represent the results from the simulation study and symbols the values estimated from the experiments.....   | 123 |
| Figure 8.8. Dependency of recovery of isoflurane (left) and desflurane (right) enantiomers on the amount of one enantiomer injected at the column inlet. Volumetric flowrate is 71 ml/min for isoflurane and 21 ml/min for desflurane. Lines represent the results from the simulation study and symbols the values estimated from the experiments.....  | 124 |
| Figure 8.9. Elution profiles of isoflurane given for the cases when maximum productivity of the first component – S-enantiomer (left, injected volume 5.8 $\mu$ l, injected mass 4.34 mg of each enantiomer) and of the second component – R-enantiomer (right, injected volume 5.1 $\mu$ l, injected mass 3.81 mg of each enantiomer) is achieved (flowrate 71 ml/min). Dashed lines show single component profiles and solid lines the total concentration. ....   | 125 |
| Figure 8.10. Elution profiles of desflurane given for the cases when maximum productivity of the first component – S-enantiomer (left, injected volume 6.8 $\mu$ l, injected mass 4.98 mg of each enantiomer) and of the second component – R-enantiomer (right, injected volume 5.6 $\mu$ l, injected mass 4.10 mg of each enantiomer) is achieved (flowrate 21 ml/min). Dashed lines show single component profiles and solid lines the total concentration. ....  | 125 |
| Figure 8.11. Dependency of productivity (left) and recovery (right) on required purity of isoflurane enantiomers (flowrate 71 ml/min, injected volume 5.8 $\mu$ l, injected mass 4.34 mg of each of the enantiomers). ....   | 127 |
| Figure 8.12. Dependency of productivity (left) and recovery (right) on required purity of desflurane enantiomers (flowrate 21 ml/min, injected volume 6.8 $\mu$ l, injected mass 4.98 mg of each of the enantiomers). ....   | 127 |
| Figure 8.13. Dependency of HETP (column efficiency) on the mobile phase flowrate (upper horizontal axis) and at the same time on velocity (lower horizontal axis) – Van Deemter curves, for isoflurane (left) and desflurane (right) enantiomers. Diagrams are constructed from the data provided from the parallel SPP1570 Subproject II. ....  | 128 |
| Figure 8.14. Dependency of productivity of S- (left) and R-enantiomer (right) of isoflurane from injected mass of one enantiomer and volumetric flowrate. ....   | 129 |
| Figure 8.15. Decrease of the time needed to collect 1 g of pure bicalutamide enantiomers by increasing the column diameter. Column length is kept constant (5 cm). Volumetric flowrate and the injected amount are changed with the column diameter according to eq. (4.17).....   | 132 |
| Figure 8.16. Decrease of the time needed to collect 1 g of pure enantiomers of isoflurane (left) and desflurane (right) by increasing the column diameter. Column length is kept constant (40 cm). Volumetric flowrate and the injected amount are varied with the column diameter according to eq. (4.17).....  | 135 |
| Figure 8.17. Experimental validation of the scale-up procedure for isoflurane illustrated by comparison of the experimental elution profiles for the small (diameter 0.6 cm, flowrate 71 ml/min, injected volume 5 $\mu$ l), intermediate (diameter 1 cm, flowrate 191 ml/min, injected volume 20 $\mu$ l) and the large column (diameter 1.66 cm, flowrate 492 ml/min, injected volume 40 $\mu$ l). The elution profiles originate from the experiments carried out in SPP1570 Subproject II.....   | 136 |
| Figure 8.18. Experimental validation of the scale-up procedure for desflurane illustrated by comparison of the experimental elution profiles for: a) Small column (diameter 0.6 cm, flowrate 21 ml/min, injected volume 0.4 $\mu$ l) and intermediate column (diameter 1 cm, flowrate 54 ml/min, injected volume 1 $\mu$ l); b) Small column (diameter 0.6 cm, flowrate 21 ml/min, injected volume 0.04 $\mu$ l) and large column (diameter 1.66 cm, flowrate 152 ml/min, injected volume 0.4 $\mu$ l). The elution profiles resulted from the experiments done in SPP1570 Subproject II. .... | 137 |
| Figure 8.19. Breakthrough curves of desflurane enantiomers at the end of the adsorption step (when elution of the second component begins). The elution of the S-enantiomer starts at $t_{ads-s,1} = 8.2$ min and for R-enantiomer it is at $t_{ads-s,2} = 13.0$ min – this time represents also   |     |



---

|  |     |
|--|-----|
| the end of the adsorption step. Flowrate is 160.7 ml/min, temperature 28 °C, high pressure 500 kPa. ....   | 142 |
| Figure 8.20. Influence of the adsorption step time variation on the productivity of desflurane enantiomers in the 4-step PSA process. ....                       | 143 |
| Figure 8.21. Influence of the adsorption step time variation on the purity (left) and recovery (right) of desflurane enantiomers in the 4-step PSA process. .... | 144 |
| Figure 8.22. Influence of the desorption step time variation on the productivity of desflurane enantiomers in the 4-step PSA process. ....                       | 145 |
| Figure 8.23. Influence of the desorption step time variation on the purity (left) and recovery (right) of desflurane enantiomers in the 4-step PSA process. .... | 146 |
| Figure 8.24. Influence of the high pressure variation during the adsorption step on the productivity of desflurane enantiomers in the 4-step PSA process. ....   | 146 |



# Curriculum Vitae

## Personal information

---

Name: **Ivana Mutavdžin**  
Date / place of birth: July 4, 1987, Pančevo, Serbia  
Address: Gustav-Adolf-Straße 2, 39104 Magdeburg



## Education

---

2012-2017 Max Planck Institute for Dynamics of Complex Technical Systems, Magdeburg and Faculty of Process and Systems Engineering, Otto von Guericke University, Magdeburg, Germany: Ph.D. in Chemical Process Engineering with the title “Contributions to develop enantioselective chromatographic processes”  
2010-2011 Faculty of Technology and Metallurgy, Chemical Engineering, University of Belgrade, Serbia: M.Sc. in Chemical Engineering, GPA: 10.00/10  
2006-2010 Faculty of Technology and Metallurgy, Chemical Engineering, University of Belgrade, Serbia: B.Sc. in Chemical Engineering, GPA: 9.74/10  
2002-2006 Gymnasium “Uroš Predić”, Mathematical-scientific branch, Pančevo, Serbia, GPA: 5.00/5

## Practical experience and study visits

---

10.-12.2013 University of New Brunswick, Faculty of Engineering, Department of Chemical Engineering, Fredericton, Canada  
04.-09.2011 Max Planck Institute for Dynamics of Complex Technical Systems, Magdeburg, Germany  
07.-08.2010 Aalto University School of Science and Technology, Department of Forest Products Technology, Espoo, Finland

## Other activities

---

Part of organizing committee of PhD Seminar on Adsorption, August 25-26, 2015, Magdeburg, Germany

Representing the International Max Planck Research School and Max Planck Institute Magdeburg at ACHEMA (World Exhibition Congress on Chemical Engineering, Environmental Protection and Biotechnology), 17-19.06.2015, Frankfurt, Germany

Member of International Adsorption Society (2017)

Member of Student Chapter of SIAM Magdeburg (2015-2017)

Member of International Max Planck Research School, Magdeburg (2012-2017)

Member of Serbian Chemical Society (2012-2014)

---

A handwritten signature in blue ink, reading "Ivana Mutavdžin".

Magdeburg, 30.06.2017